Development of an *in vitro* rat proximal tubule cell model as a platform for drug transporter and drug-drug interaction studies

Git Weng Chung

Thesis submitted for the degree of

Doctor of Philosophy

Institute for Cell and Molecular Biosciences

Newcastle University, UK

September 2014

Abstract

The kidney plays a vital role in the elimination of many endogenous metabolites and xenobiotics. Drug transporters expressed in the proximal tubule cells are key factors in the ability of the organ to successfully carry out its function. Previously, primary human proximal tubule cells have been shown to retain a remarkable degree of differentiation in culture and provide a realistic model of the proximal tubule. To address the challenge of extrapolation of drug transporter data from animal and human, this project was set out to develop a parallel rat proximal tubule cell model. This would allow direct comparison of the handling of candidate drugs in both species, and provide better understanding of the mechanisms of drug transport.

A technique to isolate primary rat proximal tubule cells (PTCs) was successfully developed using a collagenase digest/Percoll gradient approach. Rat PTCs cultured for 6 days were shown to exhibit cobberstone morphology, typical of many epithelial cells. A range of transport proteins including Mdr1a/b, Bcrp, Mrp2, Oat1, Oct2, Oatp4c1, Slc2a9, Urat1, Mate1, and Mct1 were detected at the mRNA level in these cells. Functional expression of Mdr1a/b, Bcrp, Mrp2, Oct2 and Mct1 was also detected using fluorescence substrate retention assays. In addition, Mdr1a/b, Bcrp and Mrp2 transporters were found localised on the apical membrane of polarised rat PTC monolayer, and Oct2 was found on the basolateral membrane.

The handling of urate by rat PTC monolayers was investigated. The monolayers showed absorptive and secretory pathways for urate, although the absorptive pathway was 3.2-fold higher in magnitude. Similarly, 3.4-times more urate was predominant across the apical than across the basolateral membrane. Oat1 and Bcrp were deduced as the transporters responsible for the secretory pathway, and Urat1 and Slc2a9 in the absorptive pathway. This was in accordance with the human PTC monolayers, and both models were representative of urate transport *in vivo*.

Digoxin transport exhibited a net absorptive flux in rat PTC monolayers; absorptive flux was 1.7-fold higher in magnitude than the secretory flux. In contrast, in human PTC monolayers, digoxin secretory flux was 4.2-fold higher than the absorptive flux. In human PTC monolayers, digoxin secretion consisted of OATP4C1-mediated digoxin uptake by the basolateral membrane and MDR1-mediated efflux across the apical membrane. In rat PTC monolayers in addition to these pathways, a significant Oatp-mediated absorptive flux of digoxin located on the apical membrane of rat PTC monolayer was identified as the difference between rat and human digoxin handling, resulting in a dominant absorptive flux of digoxin in rat compared to net secretion in human PTC monolayers.

These data alone highlight the importance of developing realistic *in vitro* human and rat PTC models to understand species difference in renal drug handling.

For my grandmother

Table of Contents

Acknowledgement

List of Abbreviation

ABC	ATP-binding cassette
ANOVA	Nonparametric One-way Analysis of Variance
ASP$^+$	4-(4-(dimethylamino)styryl)-N-methylpyridinium iodide
BCRP/Bcrp	Breast cancer resistance protein
cDNA	Complementary DNA
ciPTEC	Conditionally immortalized proximal tubular epithelial cell
CMFDA	5-chloromethylfluorescein-diacetate
CsA	Cyclosporine A
DMSO	Dimethyl sulphoxide
EDTA	Ethylenediaminetetraacetic acid
EGF	Epithelial growth hormone
FCS	Foetal calf serum
GSMF	Glutathione methylfluorescein
HBSS	Hank's balanced salt solution
HEPES	4-(2-hydroxyethyl)-1-piperazineethanesulfonic acid
HG-DMEM	High glucose Dulbecco's modified eagles medium
HK-2	Human kidney proximal tubule epithelial cells
Ko143	(3S,6S,12aS)-1,2,3,4,6,7,12,12a-Octahydro-9-methoxy-6-(2-methylpropyl)-1,4-dioxopyrazino[1′,2′:1,6]pyrido[3,4-b]indole-3-propanoic acid 1,1-dimethylethyl ester hydrate
LLC-PK1	Lilly Laboratories Cell-Porcine kidney 1
MATE1/Mate1	Multidrug and toxin extrusion protein 1
MCT1/Mct1	Monocarboxylate transporter 1
MDCK	Madin-Darby canine kidney
MDR1/Mdr1	Multidrug resistance protein 1
MK-571	5-(3-(2-(7-Chloroquinolin-2-yl)ethenyl)phenyl)-8-dimethylcarbamyl-4,6-dithiaoctanoic acid
mRNA	Messenger RNA
MRP/Mrp	Multidrug resistance-associated protein

MTS	3-(4,5-dimethylthiazol-2-yl)-5-(3-carboxymethoxyphenyl)-2-(4-sulfophenyl)-2H-tetrazolium
OAT/Oat	Organic anion transporter
OATP/Oatp	Organic anion transporting polypeptide
OCT/Oct	Organic cation transporter
OCTN/Octn	Organic cation transporter, novel
PBS	Phosphate-buffered saline
PTC	Proximal tubule cell *(In this thesis, PTC refers to the isolated primary proximal tubule cells)*
RPMI	Roswell Park Memorial Institute-1640 medium
RPTEC	Renal cortex, proximal tubule epithelial cell
rRNA	Ribosomal RNA
RT	Reverse transcript/Reverse transcriptase
SEM	Standard error of the mean
SLC	Solute carrier
T_3	Triiodothyronine
TEER	Transepithelial electrical resistance

List of Figures

Chapter 4

Chapter 5

Chapter 6

List of Tables

List of Publications

Articles:

G W Chung, S F Billington, N Soomro, C D A Brown (2014). Regulation of drug transporters by HIF-1 in HK-2 human proximal tubule epithelial cells. Submitted to *Pflügers Archiv European Journal of Physiology.*

P M E Probert, G W Chung, S J Cockell, L Agius, S White, F Oakley, C D A Brown, M C Wright (2013). Metabolic and toxicity screening potential of B13 progenitor-derived hepatocyte cells in vitro. *Toxicological Sciences*, 137(**2**): 350-70

S E Jenkinson, G W Chung, E van Loon, N Bakar, A M Dalzell, C D A Brown (2012). The limitations of renal epithelial cell line HK-2 as a model of drug transporter expression and function in the proximal tubule. *Pflügers Archiv European Journal of Physiology*, 464(**6**): 601-11

Abstracts:

G W Chung, S F Billington, C D A Brown (2014). Marked species difference in the handling of digoxin by primary human and rat proximal tubule cells. In: AAPS Annual Meeting, San Diego, California, USA: *American Association of Pharmaceutical Scientists*

G W Chung, S F Billington, C D A Brown (2014). Screening in rat kidney is not an accurate predictor of digoxin handling in human kidney. In: Overcoming the Barriers to Wider Uptake of Human Tissue for Safety Assessment, London, UK: *National Centre for the Replacement, Refine and Reduction of Animals in Research*

G W Chung, S F Billington, C D A Brown (2013). Development and Characterisation of Rat Primary Proximal Tubule Cell Model. In: International Congress of Physiological Sciences meeting, Birmingham, UK: *Physiological Society*

G W Chung, S F Billington, C D A Brown (2013). Regulation of drug transporters by HIF-1 in HK-2 human proximal tubule epithelial cells. In: Workshop on Drug Transporters ADME: From the Bench to the Bedside, Bethesda, Maryland, USA: *American Association of Pharmaceutical Scientists*

G W Chung, C D A Brown (2012). Regulation of ABC transporters by hypoxia in HK-2 human proximal tubule epithelial cells. In: Experimental Biology Meeting, San Diego, California, USA: *Federation of American Societies for Experimental Biology*

Chapter 1

Introduction and literature review

1.1 The kidney

The kidney is a bean-shaped organ located towards the back of the abdomen of mammals. The anatomy of a human kidney can be seen in Figure 1.1A. The kidney is highly perfused with around 20 % of cardiac output residing in the kidney. The renal artery enters the kidney at the hilus located on the medial surface of the kidney along with the ureter and renal vein of each kidney (Madsen and Tisher, 1976). The cortex and medulla are distinct regions visible on the surface of a bisected kidney. In humans, the medulla is divided into several renal pyramids, with the base of each pyramid positioned at the corticomedullary boundary and the apex towards the renal pelvis. The apexes have small openings which are the ends of the collecting ducts. These openings lead into the calyces of the renal pelvis which is responsible for draining the urine produced by the pyramidal units. The renal pelvis is lined with smooth muscles which enable it to propel urine out of the kidney into the ureter and ultimately into the bladder for excretion. In rats, and many other small mammals, the kidney consists of a single lobe of renal pyramid. In contrast, human kidney is multi-lobar with multiple renal pyramids. Apart from that, the gross appearance of the small animal kidneys resembles that of the human (Madsen and Tisher, 1976; Haley and Bulger, 1983).

The cortex of the kidney consists of nephrons, which are the functional units of the organ (Figure 1.1B). As many as 1 million nephrons are present in each human kidney, which contrasts with approximately 30,000 found in the rat kidney (Haley and Bulger, 1983; Nyengaard and Bendtsen, 1992). A unit of nephron comprises the Bowman's capsule that encases the glomerulus, the proximal tubule, the loop of Henle, and the distal tubule. Three kinds of nephrons are recognised in the kidney – ones with a very short loop of Henle (superficial nephrons), ones with a short loop of Henle (mid cortical nephrons) and ones with a long loop of Henle (juxtamedullary nephrons). Nephrons that possess long loops of Henle have their loops crossing the corticomedullary boundary and projecting deep into the medulla. In humans and rats only about 7 % of nephrons are juxtamedullary nephrons. In addition to the descending and ascending loops of Henle, collecting ducts are also found in the medulla of the kidney (Madsen and Tisher, 1976; Haley and Bulger, 1983).

The proximal tubule of the nephron is the main site of renal reabsorption and secretion of many endogenous metabolite and xenobiotics. The diameter of both rat and human proximal tubule cells is around 40 μm (Maunsbach, 1966; Helbert *et al.*, 1997). Three morphologically distinct segments (S1, S2 and S3) can be identified along the length of the proximal tubule as defined by the epithelial cells that form it. The S1 segment comprises the initial convoluted portion of the proximal tubule. The cells in this segment have tall brush border on the apical membrane, and the basolateral membrane forms extensive lateral invaginations with adjacent cells. The S2 segment consists of the rest of the convoluted proximal tubule and the initial portion of the straight tubule. The structure of the cells in this segment is similar to that of the S1, except for the shorter brush border. The S3 segment comprises the remainder of the proximal tubule. The cells in this segment have even shorter brush border, though that varies between species, and less basolateral invaginations (Bulger, 1965; Madsen and Tisher, 1976; Haley and Bulger, 1983). The mitochondria number is also lower in these cells than cells of the other two segments (Maunsbach, 1966).

All three segments play a major role in the reabsorption of a wide range of solutes including glucose, amino acids, small peptides and ions such as Na^+, K^+, Cl^-, HCO_3^- and PO_4^{3-} together with water. For some solutes, 100 % of filtered load is reabsorbed along the length of the proximal tubule. For others such as water and Na^+ approximately 70 % of the filtrate is reabsorbed in the proximal tubule. The proximal tubule is also the site of active secretion of many other compounds including a large number of xenobiotics (Madsen and Tisher, 1976; Moe *et al.*, 2004). Movement of this scale across the epithelium of the tubule requires membrane bound proteins to facilitate the transport of molecules. A large body of evidence supports the expression of a multitude of transporters at both apical and basolateral membrane face of the proximal tubule cells that serves this purpose (Beringer and Slaughter, 2005; Feng *et al.*, 2010). Whilst all transporters expressed in the proximal tubule cells are vital for maintaining renal homeostasis, in the context of drug transport, several families of transporters are more important. These drug transporters expressed in proximal tubule cells will be the focus of this thesis and reviewed in this chapter.

A
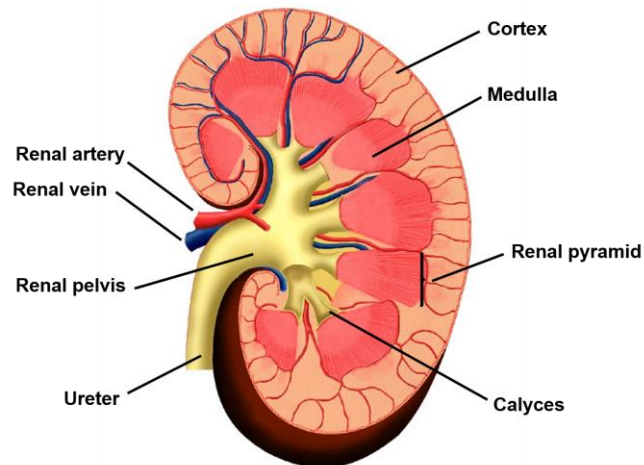
B
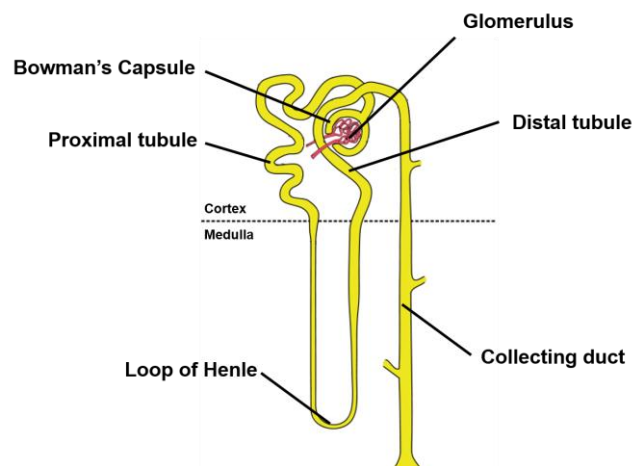
Figure 1.1: Anatomy of the human kidney and nephron.

(A) The cortex and medulla are distinct regions visible on the surface of a bisected human kidney. The medulla is divided into several renal pyramids. The apexes of the pyramids have small openings which lead into the calyces of the renal pelvis which is responsible for draining the urine produced into the bladder via the ureter. In rats, only single renal pyramids are found in the medulla of their kidneys. Apart from that, the gross appearance of a rat kidney resembles that of the human. (B) A unit of nephron comprises the Bowman's capsule that encases the glomerulus, the proximal tubule, the loop of Henle, and the distal tubule. They are found in the cortex of the kidney. In addition to the descending and ascending loops of Henle, collecting ducts are found in the medulla of the kidney.

1.2 Drug transporters

In its simplest form, transcellular renal transport of any compound is initiated via the sequential transfer of the compound by an uptake and then an efflux transporter. With its high expression of membrane transporters on the proximal tubule epithelial cells, it is widely acknowledged that the kidney can influence drug disposition and drug-drug interactions (Bonate *et al.*, 1998; Beringer and Slaughter, 2005; Consortium, 2010). As a result, considerable effort has been made to understand the impact these uptake and efflux transporters have on drug disposition and drug safety in the kidney (Bass *et al.*, 2009; Consortium, 2010).

1.2.1 OATs

Uptake transporters are so called because they facilitate the movement of substances primarily across the basolateral membrane into the cells. A well-characterised group of uptake transporter is that of the organic anion transporter (OAT) family, with members including OAT1, OAT2 and OAT3 found expressed on the basolateral membrane of the human proximal tubule cells (Kojima *et al.*, 2002; Wright and Dantzler, 2004; Consortium, 2010).

When transfected into *Xenopus* oocytes, OAT1 was found to mediate the transport of *p*-aminohippurate (PAH) (Sekine *et al.*, 1997; Sweet *et al.*, 1997), but was inhibited by a range of compounds such as anti-inflammatory drugs indomethacin and carprofen (Kuze *et al.*, 1999). PAH uptake by oocytes expressing OAT1 was enhanced by pre-treatment with glutarate, indicating that PAH uptake could be coupled to the efflux of internal glutarate (Sweet *et al.*, 1997). This set of data confirms OAT1 wide substrate specificity and its importance in drug-drug interactions. Whilst OAT1 is exclusively expressed in the kidney, OAT2 is found to express more abundantly in the liver than in the kidney (Cha *et al.*, 2001). OAT3, on the other hand, is almost exclusively found in the kidney in humans (Kusuhara *et al.*, 1999). Similar to OAT1, when expressed in oocytes, OAT2 also mediated the transport of PAH, and also salicylate and acetylsalicylate in drug interaction studies (Sekine *et al.*, 1998). In addition to that, OAT1 and OAT3 have been implicated in urate secretion by taking up urate from the blood across the basolateral membrane of the proximal tubule (Jutabha *et al.*, 2010). Although the OATs have overlapping substrate specificities, they differ in

affinities. PAH is also a substrate of OAT3 but it has a lower affinity for PAH when compared to OAT1 and OAT2 (Kusuhara *et al.*, 1999; Hasegawa *et al.*, 2002). Studies have also shown glutarate causing the same effect on PAH transport by OAT3 (Sweet *et al.*, 2003), which suggests OAT3 could function as a basolateral dicarboxylate/organic anion exchanger in the kidney. Rat orthologs of the human OATs also exhibit substrate specificities with different affinities. For instance, when LLC-PK1 cells were transfected with rat Oat3, the K_m for indoxyl sulphate was up to 15-fold higher when compared to Oat1 (Deguchi *et al.*, 2004).

Two other members of the OAT family (OAT4 and OAT5) have been identified. OAT4 is highly expressed in the human kidney (Sun *et al.*, 2001), and OAT5 is only expressed in the human liver but rat Oat5 is found in rat kidney and liver (Sun *et al.*, 2001; Youngblood and Sweet, 2004). Unlike the other OATs, OAT4 and OAT5 are expressed on the apical membrane of epithelial cells and have similar functions (Babu *et al.*, 2002). Uptake of estrone sulphate by cells transfected with OAT4 is enhanced by pre-treatment with glutarate and inhibited by high concentrations of external glutarate (Ekaratanawong *et al.*, 2004; Hagos *et al.*, 2007; Hagos *et al.*, 2008). Succinate also has the same impact on estrone sulphate transport by OAT5 (Anzai *et al.*, 2005). This has led some to believe apical absorption of organic anions by OAT4 and 5 may be coupled with carboxylate elimination from the kidney.

1.2.2 OATPs

Another group of organic anion transporters is the organic anion transporting polypeptide (OATP) family. All eleven members of OATP are solute carriers with the ability to transport a wide range of substrates. They are expressed in multiple tissues in rats and humans, but only a few members are found in the kidney (König, 2011). For example, OATP1A2/Oatp1a2 has been identified in human and rat kidneys as well as other tissues such as the brain (Jacquemin *et al.*, 1994; Bergwerk *et al.*, 1996; Lee *et al.*, 2005), although majority of it is found in the apical membrane of distal tubules. OATP1A2 substrates include estrone sulphate, estradiol-17β-glucuronide and methotrexate (Isern *et al.*, 2001; Badagnani *et al.*, 2006). Its localisation and substrate specificity indicates its role in xenobiotic reabsorption from the urine.

Another member of the OATP family found in the human kidney is OATP4C1. It is in fact the only OATP family member to be exclusively expressed in the human kidney (Yamaguchi *et al.*, 2010). Unlike OATP1A2, OATP4C1 is located in the basolateral membrane in human proximal tubule cells, and found to transport thyroid hormone and cardiac glycosides such as digoxin and ouabain (Mikkaichi *et al.*, 2004; Yamaguchi *et al.*, 2010). OATP4C1 also transports estrone sulphate, which is inhibited by cyclosporine A and triiodothyronine. Interestingly, OATP4C1 mediated transport of estrone sulphate is not affected by digoxin even though digoxin is also a substrate of the transporter (Yamaguchi *et al.*, 2010), which could be ascribed to multiple recognition sites on the OATP4C1. Rat Oatpc41 has also been identified in rat kidney (Mikkaichi *et al.*, 2004). In contrast to human OATP4C1, a recent publication shows the localisation of rat Oatp4c1 on the apical membrane of rat proximal tubule cells, which had the authors suggesting the function of the rat Oatp4c1 may be mainly renal reabsorption of substrates instead of secretion (Kuo *et al.*, 2012).

Oatp1a3v1 and Oatp1a3v2 (previously known as OAT-K1 and OAT-K2 respectively) are the other members of the OATP family found exclusively in the rat kidney (Saito *et al.*, 1996; Masuda *et al.*, 1999b). Oatp1a3v1, situated on the apical membrane of the proximal tubule cells, was identified as a bidirectional transporter of methotrexate that could be inhibited by anti-inflammatory drugs such as indomethacin and ibuprofen (Masuda *et al.*, 1997a). Folinic acid, a derivative of folic acid, was also found to stimulate methotrexate efflux, which has led some to believe Oatp3a1v1 could function as a methotrexate/folinic acid exchanger (Takeuchi *et al.*, 2000). Oatp1a3v2 also transports methotrexate across the apical membrane and therefore may play the same role in the rat kidney as Oatp1a3v1 (Masuda *et al.*, 1999a). Most substrates of OATPs, such as thyroid hormones and conjugated steroids, are also transported by Oatp1a3v1 and v2 (Takeuchi *et al.*, 2001), indicating both transporters also function as multispecific transporters in rat kidneys and have the potential to induce drug-drug interactions.

1.2.3 OCTs

Transport of organic cations by members of the OCT family in the kidney is an important route of elimination from the blood to urine. Like several OATs, rat Oct1

and Oct2 were initially identified and cloned from rat kidneys before human versions were identified (Okuda *et al.*, 1996; Chun, 1997; Gorboulev *et al.*, 1997). Human OCT1 is predominantly found in the liver, whereas rat Oct1 is ubiquitous in the liver and kidney (Gorboulev *et al.*, 1997). OCT2/Oct2 is almost exclusively expressed in the kidney of both species, and little expression in other tissues (Okuda *et al.*, 1996; Gorboulev *et al.*, 1997). Another member of the transporter family (OCT3) has also been identified in human kidney (Wu *et al.*, 2000b). All three transporters are located in the basolateral membrane of proximal tubules (Urakami *et al.*, 1998; Karbach *et al.*, 2000; Wu *et al.*, 2000b).

Similar to the other solute carriers mentioned so far, all human OCTs appear to have overlapping substrate specificities but different affinities. They were shown to be able to transport organic cations such as tetraethyl ammonium (TEA), and were inhibited by other organic cations including cimetidine, procainamide and quinidine (Grundemann *et al.*, 1994; Okuda *et al.*, 1996). The drug metformin, which is used in type 2 diabetes, was transported with higher affinity by human OCT2 than OCT1 (Kimura *et al.*, 2005). Similarly, rat Oct2 showed lower K_m values for dopamine, serotonin and adrenaline compared to Oct1, but higher K_m than human OCT2 (Urakami *et al.*, 2001).

Variations within the human OCT2 gene itself also result in substrate affinity changes. Various sites with different sequences have been identified within the same gene in different people. Some of these changes can cause amino acid substitution during mRNA translation, while some have produced proteins that not only altered affinity for organic cation MPP^+ but also the potency of their inhibition by TEA (Leabman *et al.*, 2002). More recently, the variant 808G/T resulted in amino acid change A270S, which showed 1.5-fold higher uptake of metformin when compared to the control (Chen *et al.*, 2009). This variation in OCT2 affinity within the human population could result in differences in renal elimination of cation compounds by people who possess the genetic variations in the OCT2 gene. OCT2 is thus an important transporter to consider when examining the elimination of positively charged xenobiotics in the kidney.

1.2.4 OCTNs

In addition to the OCTs, another subfamily of human OCT has been identified. Members of the organic cation transporters novel (OCTN) family have been

known to interact with several drugs (Pochini *et al.*, 2013). OCTN1 was the first to be identified in human foetal liver. Its expression is ceased in adult liver but is highly expressed in the kidney (Tamai *et al.*, 1997). It mediates pH-dependent transport of TEA in transfected HEK293 cells but at lower affinity than the OCT family of transporters (Tamai *et al.*, 1997). Expression in *Xenopus* oocytes also showed transport of other organic cations such as verapamil and pyrilamine, indicating OCTN1 is a multi-specific organic cation transporter (Yabuuchi *et al.*, 1999). A second transporter OCTN2 is also identified in human kidney. Like OCTN1, it is not expressed in the liver and mediates transport of a broad spectrum of organic cations (Wu *et al.*, 1998; Wu *et al.*, 1999).

Rat Octn1 and 2 have also been found to be widely distributed in rat tissues (Wu *et al.*, 1999; Wu *et al.*, 2000a; Slitt *et al.*, 2002); Octn1 mRNA levels were detected at high levels in the rat kidney and moderate levels in the liver, intestine, heart and brain. The mRNA levels of rat renal Octn1 was also found to be increasing steadily with the age of the rat (Slitt *et al.*, 2002). The functions of rat Octn1 and 2 are similar to that of the human. Rat Octn1 is a bidirectional pH-dependent transporter with affinity for organic cations (Yabuuchi *et al.*, 1999). Octn2 also transports organic cations, and has a higher affinity for TEA compared to human OCTN2 (Wu *et al.*, 1999). Another transporter, rat Octn3, has also been found in the rat kidney (Tamai *et al.*, 2000; Cano *et al.*, 2010), which has the ability to mediate transport of L-carnitine in a Na^+-independent manner (Cano *et al.*, 2010).

A major difference between the OCTs and OCTNs is that in addition to organic cations, carnitines are also substrates of OCTN1 and 2 whereas OCTs are unable to transport this compound. This was observed in cells that were transfected with OCTN2 and showed Na^+-dependent uptake of L-carnitine, but inhibited by quinidine and verapamil (Tamai *et al.*, 1998; Ohashi *et al.*, 1999; Wu *et al.*, 1999). OCTN1 was also seen to transport L-carnitine in a Na^+-dependent manner but with lower affinity than OCTN2. OCTN1, however, a more efficient transporter of TEA than OCTN2 (Tamai *et al.*, 2000). It is possible that OCTN1 main role is as an organic cation transporter, whereas as OCTN2 favours carnitine.

OCTN1 and OCTN2 are both situated in the apical membrane of proximal tubules (Tamai *et al.*, 2001; Tamai *et al.*, 2003), in contrast to OCTs which are basolateral transporters. This provides an indication that OCTN may be important for the

reabsorption of carnitine and organic cations from urine rather than their elimination. However, due to the bidirectional nature of the OCTN transporters, it is hypothesised that they also help in the secretion of organic cations into the urine depending on the condition in the tubule (Slitt *et al.*, 2002). Regardless of the direction of transport by OCTNs, they are without a doubt involved in interactions of many organic cations and constitute potential pharmacologic targets in the kidney.

1.2.5 BCRP

ATP-binding cassette (ABC) superfamily of transporters is a class of membrane-bound transporters mainly responsible for the efflux of substrates (Schinkel and Jonker, 2003), of which the breast cancer resistance protein (BCRP) is a member. BCRP was first identified in breast cancer cell line MCF-7 where it appeared to play a role in multidrug resistance (Doyle *et al.*, 1998). BCRP is now known as an efflux transporter that prevents drugs from penetrating tissues and is important in drug disposition and distribution.

Screenings in human tissues revealed the transporter is expressed in all major organs, such as the brain, liver and the intestines (Allikmets *et al.*, 1998). Studies also confirmed moderate BCRP expression at the mRNA and protein level in normal human kidney (Doyle *et al.*, 1998), although levels of BCRP mRNA was found up-regulated several folds in renal carcinoma (Diestra *et al.*, 2002). Expression of functional BCRP was detected in cultures of primary tubule cells as Hoechst 33342 efflux from these cells could be specifically blocked by BCRP inhibitor fumitremorgin C (Huls *et al.*, 2008). Rat kidneys, on the other hand, have constitutively higher mRNA levels of the transporter compared to the human (Tanaka *et al.*, 2005).

Both human BCRP and rat Bcrp are found on the apical membrane of the proximal tubule cells (Huls *et al.*, 2006; Huls *et al.*, 2008), where it acts as an efflux pump by mediating the unidirectional transport of substrates into the tubule (Maliepaard *et al.*, 2001). BCRP substrates are diverse, ranging from drugs such as nitrofurantoin, dipyridamole and cimetidine, to endogenous compounds such as estrones and bile acids (Jani *et al.*, 2009; Kis *et al.*, 2009; Be *et al.*, 2012). BCRP mediated transport may be inhibited by highly potent and specific inhibitors such as fumitremorgin C or its analogue Ko143 (Haslam *et al.*, 2011). There is

overlap in substrate specificity between BCRP and another ABC transporter, MDR1. It is thought that MDR1 generally transports hydrophobic compounds whereas BCRP additionally transports hydrophillic conjugated organic anions, particularly sulphates, with high affinity (MacLean *et al.*, 2008).

1.2.6 MDR1

Multidrug resistance protein 1 (MDR1) is another member of the ABC transporter superfamily. It transports a wide variety of substrates including drug molecules and like BCRP, expression of MDR1 confers multidrug resistance in the cells (Gros *et al.*, 1986). In humans, MDR1 is encoded by one gene (Chen *et al.*, 1986; Ueda *et al.*, 1986), whereas in rats two isoforms of the gene exist; Mdr1a and Mdr1b (Croop *et al.*, 1989; Devault and Gros, 1990; Deuchars *et al.*, 1992). Human MDR1 can be found in various tissues, including the kidney where it is located in the apical surface of the proximal tubule cells (Thiebaut, 1987). Similarly, rat Mdr1a and b are widely distributed in all tissues. As no isoform is more prevalent than the other in rat kidney tissue (Gros *et al.*, 1986; Deuchars *et al.*, 1992), the transporters will be collectively addressed as Mdr1 in this thesis for simplicity.

There are various established proximal tubule cell lines that express MDR1/Mdr1. This has allowed extensive investigation into the functions of the transporter *in vitro*. For instance, rat cell lines NRK-52E and GERP demonstrated inhibition of Mdr1-mediated calcein efflux by PSC833 (van de Water *et al.*, 2007). Expression of functional human MDR1 has also been reported in human proximal tubule cell line HK-2 (Tramonti *et al.*, 2001; Romiti *et al.*, 2002). These immortalised cells lines provide insights to species differences in the transporters sensitivity to the same drug and the inhibitory effects of MDR1 inhibitors. For example, LLC-PK1 cells transfected with MDR1 from human or rat Mdr1 showed inhibition of digotoxin efflux by quinidine had far lower IC_{50} value for human MDR1 when compared with rat Mdr1 (Suzuyama *et al.*, 2007).

The abovementioned studies also indirectly implicated MDR1's involvement in drug-drug interaction. This happens when two or more concomitant drugs are substrates of a transporter that leads to the inadvertent inhibition of the transport of the other drug. Clinically, the most important substrate of MDR1 in the kidney is digoxin. Many drugs are co-administered with digoxin, and due to digoxin's

narrow therapeutic index, drugs that are inhibitors of MDR1 will require clinical assessment of their impact on digoxin pharmacokinetics (Koren, 1987). This highlights the importance of MDR1 as a renal efflux transporter.

1.2.7 MRPs

Another subgroup of the ABC family involved in efflux of substrates in the proximal tubule is the multidrug-resistance associated protein (MRP) family. The family is made up of nine structurally related members (MRP1-9), which have a wide tissue and species distribution (Keppler, 2011). All members function as lipophilic anion efflux transporters and are expressed on either the apical or basolateral membrane of epithelial cells (Belinsky and Kruh, 1999). MRP1 was first identified in the drug-resistant lung cancer cell line H69AR, suggesting that this transporter plays a role in drug resistance in cancer cells (Cole *et al.*, 1992). MRP2, MRP3, MRP4 and MRP5 have subsequently been identified in various cancer cell lines and tissue samples, and all MRPs have been shown to confer resistance to many drugs including anti-cancer and anti-viral agents (Kool *et al.*, 1997).

MRP1 and MRP2 are the most abundant MRPs in the human kidney (Kool *et al.*, 1997). MRP3-6 have also been detected in the kidney, but their expression other tissue are more abundant, for instance MRP3 expression is more in the liver (König *et al.*, 1999; Kool *et al.*, 1999; Belinsky *et al.*, 2002). mRNA of MRP7-9 have been detected, but functional expressions of these transporters have yet to be investigated (Hopper *et al.*, 2001; Yabuuchi *et al.*, 2001). A similar expression pattern has been observed in rat kidney with high expression of rat Mrp1, Mrp2 and Mrp4 but low expression of Mrp3 (Cherrington *et al.*, 2002; Chen and Klaassen, 2004). Expression in the kidney appears to be fairly consistent across species. MRP2 and MRP4 are located in the apical membrane of proximal tubule cells (Schaub *et al.*, 1997; Evers *et al.*, 1998; Schaub *et al.*, 1999; van Aubel *et al.*, 2002), whereas MRP5 and 6 are found in the basolateral membrane (Wijnholds *et al.*, 2000; Scheffer *et al.*, 2002). MRP1 is not greatly expressed in the proximal tubule and is predominantly found in glomeruli and distal tubule cells in the basolateral membrane (Peng *et al.,* 1999).

As with other drug transporters, transfected cells have been used to investigate the function and substrate specificity of many of the MRPs. Mammalian cells

transfected with MRP1, MRP2 or MRP6 transport glutathione S-conjugates such as GS-DNP (Evers *et al.*, 1996; Evers *et al.*, 1998; Belinsky *et al.*, 2002). MRP2 or MRP4 transfected into SF9 cells mediate ATP-dependent transport of PAH with MRP4 showing higher affinity than MRP2 (Van Aubel *et al.*, 2000; Smeets *et al.*, 2004). This is particularly significant as PAH is a well known substrate for OATs in proximal tubules. MRP4 and MRP5 are able to transport cyclic nucleotides such as cAMP and cGMP, and are the only members of the MRP family that do so (Jedlitschky *et al.*, 2000; Chen *et al.*, 2001; van Aubel *et al.*, 2002; Wielinga *et al.*, 2003).

MRPs also have an important role to play in multidrug resistance and are a major elimination pathway for anti-cancer and anti-viral drugs via the kidney. For example anti-cancer drugs such as daunorubicin and vinblastine are transported by MRP1 and MRP2 (Evers *et al.*, 1996; Evers *et al.*, 1998) and nucleotide analog anti-cancer drugs including thiopurine and 6-mercaptopurine are substrates for MRP4 and MRP5 (Wijnholds *et al.*, 2000; Wielinga *et al.*, 2002). Anti-viral drugs saquinavir, ritonavir and indinavir are transported by MRP2-expressing MDCK cells (Huisman *et al.*, 2002) and MRP4 has been shown to be vital for efflux of adefovir and tenofovir as high accumulation of these compounds was seen in MRP4-knockout mice (Imaoka, 2007). In contrast MRP6 shows low level resistance to anti-cancer drugs compared to MRP1 and MRP2 (Belinsky *et al.*, 2002) suggesting that it does not play a major role in drug resistance in the kidney and may function predominantly as a organic anion transporter.

1.2.8 URAT1 and SLC2A9

Several organic anion transporters capable of transporting urate in the kidney have just recently been identified and characterised. URAT1 (SLC22A12) was identified in the apical membrane of proximal tubule epithelial cells in humans (Enomoto *et al.*, 2002). Urat1 in rat kidney has been previously identified as renal-specific transporter but now acknowledged as the homologue of URAT1 (Hu *et al.*, 2001; Hosoyamada *et al.*, 2004; Sato *et al.*, 2011). When transfected into oocytes, URAT1 mediated the transport of urate but was inhibited by uricosuric drugs such as probenecid and benzbromarone (Enomoto *et al.*, 2002; Hosoyamada *et al.*, 2004; Sato *et al.*, 2011). Studies have also shown URAT1-mediated transport of urate was stimulated by high external Cl^- and lactate

concentrations (Enomoto *et al.*, 2002; Sato *et al.*, 2011). Its function is therefore likely to be reabsorption of urate into the proximal tubule from urine via the co-transport of another molecule. Recently, transport of orotate, a heterocyclic precursor of pyrimidine synthesis was also shown in HEK293 cells transfected with human URAT1. Transport of orotate is mediated by the same co-transport system as urate since it is dependent on Cl^- exchange and stimulated by lactate (Miura *et al.*, 2011).

Another important urate transporter has been found in the human kidney. SLC2A9 (also known as GLUT9), has been shown to transport urate in the kidney and is found in the basolateral membrane of proximal tubule cells (Vitart *et al.*, 2008). SLC2A9 is also a known glucose/fructose transporter, although the affinity of SLC2A9 for urate transport is far higher than for either glucose or fructose, and also higher than URAT1 for urate (Caulfield *et al.*, 2008; Vitart *et al.*, 2008). Urate transport is inhibited by benzbromarone suggesting that SLC2A9 may possess similar binding sites to URAT1 (Caulfield *et al.*, 2008). Uptake of urate by SLC2A9 is voltage driven and hence is also referred to as URATv1 (Anzai *et al.*, 2008). Its location in the basolateral membrane suggests a possible role as an efflux transporter in proximal tubules and forms part of a urate transport system with URAT1; urate taken up from the lumen by URAT1 is then secreted into the blood by SLC2A9 (Anzai *et al.*, 2008).

1.2.9 MATE1 and MATE2-K

Multidrug and toxic compound extrusion (MATE) proteins have a wide distribution amongst mammal tissues (Otsuka *et al.*, 2005). Bacterial MATE transporters have been well characterised as cationic/H^+ or Na^+ exchangers but it is only in recent years that mammalian MATE proteins have been identified (Omote *et al.*, 2006). Two MATE proteins are found highly expressed in the human kidneys – MATE1 and MATE2-K (Otsuka *et al.*, 2005; Masuda *et al.*, 2006). MATE2-K, which is unique to the human kidney, is an isoform of MATE2. Another isoform of MATE2 is found exclusively in the brain and is designated MATE2-B (Masuda *et al.*, 2006). Rat Mate1 is also abundantly expressed throughout rat tissues, but surprisingly not in the liver (Ohta *et al.*, 2006; Terada *et al.*, 2006). Also, while rat Mate1 is found in the kidney, no Mate2 mRNA has been detected (Lickteig *et al.*, 2008). Human MATE1, MATE2-K and rat Mate1 are located on the apical

membrane of the proximal tubule cells (Otsuka *et al.*, 2005; Ohta *et al.*, 2006), and are thus considered as important barriers to substrate toxicity.

Like the bacterial MATE transporters, human MATE1 and MATE2-K, and rat Mate1 are H^+-coupled organic cation transporters expressed in the apical membrane of proximal tubule cells. They can transport a range of organic cations and share similar substrates as OCT including TEA, MPP^+, metformin and cimetidine (Otsuka *et al.*, 2005; Masuda *et al.*, 2006; Ohta *et al.*, 2006; Terada *et al.*, 2006; Komatsu *et al.*, 2011). They also transport certain organic anions such as estrone sulphate (Tanihara *et al.*, 2007). As with the other transporters, MATE1 and MATE2-K show overlapping substrate specificity but different affinities. For example MATE1 K_m for acyclovir is lower than that of MATE2-K (Tanihara *et al.*, 2007). Inhibition of TEA transport by metformin is also far greater in MATE1 than MATE2-K (Tsuda *et al.*, 2009). These data suggest MATE1 and MATE2-K may represent high and low affinity transporters in the kidney respectively.

MATE1 and MATE2-K affinities for cationic substrates also differ from that of OCTs. For instance, when metformin was exposed to MDCK cells transfected with only OCT2, accumulation of metformin was higher when compared to doubly-transfected cells with OCT2 and MATE1. Furthermore there was no saturation of metformin in OCT2/MATE1 transfected cells over a range of concentrations, suggesting efficient efflux by MATE1 (Konig *et al.*, 2011). Cimetidine was also found to be a more potent inhibitor of metformin transport by MATE1 when compared to OCT2 (Tsuda *et al.*, 2009; Ito *et al.*, 2012). This drug interaction with cimetidine could result in accumulation of metformin in proximal tubule cells as the drug uptake by OCT2 is less efficiently inhibited than efflux by MATE across the apical membrane. OCTs and MATEs are thus assumed to form an organic cation transport system in renal proximal tubules.

1.3 *In vitro* renal models

Much of the information about the functions and substrate specificity of the renal transporters had been investigated using *in vitro* models (Consortium, 2010). The systems used in these studies include kidney slices, *Xenopus laevis* oocytes transfected with a transporter, and various established cell lines (Bonate *et al.*, 1998). The advantages and disadvantages of these systems are discussed in the following sections.

1.3.1 Kidney slices

Kidney slices can be used to evaluate drug transport *in vitro* (Vickers *et al.*, 2004). They are prepared from kidney cortex which contains many of the drug transporters and used to perform transporter experiments. For example, Nelson and co-workers used kidney slices to determine the transport systems involved in the secretion of cisplatin (Nelson *et al.*, 1984; Bonate *et al.*, 1998). Cisplatin was shown to competitively inhibit the uptake of TEA, indicating it was actively secreted by the OCT system. These data were in agreement with another set of data from *in vivo* experiments, suggesting kidney slices provided a good *in vitro-in vivo* correlation for cisplatin using this approach (Nelson *et al.*, 1984). Although kidney slices may have the potential to be a good *in vitro* model for renal drug-drug interaction studies, they have several drawbacks including short viability, difficulty handling the slices and obtaining enough kidneys for the slices. After isolation, the tubular lumens may collapse which makes characterising the efflux transporters in kidney slices impossible. These issues limit the usefulness of kidney slices as an efficient model system.

1.3.2 Transfected *Xenopus* oocytes

One of the earliest methods used to characterise individual renal transporters was to express the transporter of interest in an expression system (Grundemann *et al.*, 1994; Okuda *et al.*, 1996). An established method involves the microinjection of transporter cRNA into *Xenopus* oocytes and allowing the oocytes to express the protein (Gurdon *et al.*, 1971). This provided a platform for the study of only the transporter of interest without the influence of the others. Many of the OCTs and OATs functions have been elucidated using this technique (Grundemann *et al.*, 1994; Okuda *et al.*, 1996; Sekine *et al.*, 1997). Whilst the

oocytes are ideal for the study of individual transporters, there are drawbacks to the systems. For instance, *Xenopus* oocytes only provide transient expression of proteins with marked variation in expression levels between batches of oocytes. Also, data suggest that kinetic values derived from oocytes differ from those from mammalian expression systems (Goldin, 1992), perhaps due to the different lipid environments that the transporter sits in. Equally, oocytes do not recapitulate the complexity and interactions between transporters found in more complex models.

1.3.3 Immortalised cell lines

Transporters of interest have also been transfected in immortalised cell lines. Similar to the oocytes, these cell lines can be transfected with a vector, usually a plasmid containing cDNA of the transporter (Gründemann *et al.*, 1997). Also similar to the oocytes, the disadvantage of these models is that the cell line usually expresses a single transporter at a time, although doubly-transfected cells have been achieved by Konig *et al.* (2011). Cell lines provide invaluable data on the kinetics and substrate specificity of the transfected transporter, but they still lack the complexity and interactions between transporters found in more complex models. A further disadvantage is that the transfected cells also do not reflect the transporter physiological expression levels because they are driven by the vector promoters and the cell translation and transcription machinery.

Immortalised renal epithelial cell lines can inherently express transporters of interest without the need for transfection. For instance, LLC-PK1 cells derived from pig kidney express functional MDR1 and have been used to investigate the efflux of prototypic substrates (Ohtomo *et al.*, 1996). MDCK cells derived from dog kidney have been used to investigate a range of drugs and HK-2 cells, which are immortalised human proximal tubule cells, have been used to investigate MDR1-mediated efflux of many compounds (Ryan *et al.*, 1994). In addition, HK-2 cells also showed functional expression of some members of ABC transporter and have been used as a model of drug-induced nephrotoxicity (Tramonti *et al.*, 2001).

Again, these cell lines have several limitations – the most important of these is that the vast majority of cell lines have undergone substantial dedifferentiation and have lost most of the basic functions of the cells of their origins. For example, MDCKII cells do not express substrate transporters such as Na^+-P_i cotransporter

2, Na$^+$-glucose cotransporter 1 and 2, or amino acid transporters usually found in the proximal tubule. In addition they do not show expression of other key transporters that affect drug disposition and drug-drug interactions. The same is true for LLC-PK1 cells (Kuteykin-Teplyakov *et al.*, 2010). Recently it was shown that HK-2 cells lack many key transporters and are thus poor model for drug transporter studies (Jenkinson *et al.*, 2012). On the positive side, a number of immortalised human cell lines such as RPTEC and ciPTEC are becoming available (Wieser *et al.*, 2008; Jansen et al. 2014). The data on these is still limited and they may also suffer from lack of crucial transporter expression (ciPTEC do not express OATs) but they are welcome step forward in the search for realistic human renal cell models (Jansen *et al.*, 2014).

1.3.4 Primary cells

The need for a robust *in vitro* model of drug transport that describes the physiological profile of transporters in intact tissue is apparent. Primary cultures of tubular epithelial cells may be seen as one of the solutions to address this. Primary tubular cells are usually isolated from intact tissues. An enzymatic approach to isolate the proximal tubule cells from human has been successfully achieved (Lash *et al.*, 2006; Brown *et al.*, 2008). Human proximal tubule cells when grown *in vitro* express a range of functional transporters including members of the OAT and OCT families and ABC transporters including MDR1 and MRP2 (Lash *et al.*, 2006; Brown *et al.*, 2008), which are missing in many immortalised cell lines. These cells have been shown to mediate the transport of prototypic organic anion and cation substrates such as PAH and creatinine (Lash *et al.*, 2006; Brown *et al.*, 2008) and xenobiotics such as rosuvastatin (Verhulst *et al.*, 2008). A recent study has also shown that primary proximal tubule cells isolated from rat kidney express a similar range of transporters and are able to transport prototypic substrates of apical transporters OCTN1 and OCTN2 (Nakanishi *et al.*, 2011).

These discoveries make primary cell cultures particularly important as a cell model for renal transporter studies. Since there are already studies confirming their use as *in vitro* model for nephrotoxicity studies (Boogaard *et al.*, 1989; Boogaard *et al.*, 1990a; Boogaard *et al.*, 1990b), the primary cells' suitability as an *in vitro* model for drug transporter and drug-drug interaction studies is ever

more compelling. Indeed, recent findings show primary human proximal tubule cells as a useful tool to investigating renal drug handlings and identifying drug-drug interactions for a range of drug molecules; they can be used to establish *in vivo-in vitro* correlations for the disposition of the drugs (Brown *et al.*, 2008). With the human model in place, the next stage of the process is to develop a rat model to understand the renal handling and drug-drug interactions for the same array of drug molecules.

1.4 Robust *in vitro* models of human and rat renal drug transport

A major challenge faced in drug discovery and development is the extrapolation of drug safety information from animals to humans (Rasmussen, 1983; Lin, 1995). Although data from animal studies may be reasonably extrapolated to humans, there are certainly some limitations, not least because of the unpredictable differences in renal drug handling between the two species (Lin, 1995; Bass *et al.*, 2009). However, a rat proximal tubule cell model would provide transport data on the handling of candidate drug molecules in this animal. The data could then be used to compare, at an early stage, the handling of molecules in similar *in vitro* models derived from the human kidney. With the human and rat screening platforms in place, not only would there be a system to investigate drug handling in either species, but also direct comparison of the renal handling of a molecule between rat and human kidney and flag up any differences they may have. Because rat remains as the initial test species in drug development and safety determination (Bass *et al.*, 2009), this would provide invaluable data on the impact on drug safety and development.

With that in mind, this project is designed to develop and characterise a rat primary proximal tubule model as a platform for drug transporter and drug-drug interaction studies, understand which transporters at the apical and basolateral membranes of rat proximal tubule cells are key in determining the renal handling of drugs, and to compare the species differences in the drug transport. The outcome of this work will provide greater understanding of the mechanisms underlying the renal handling of drug molecules in both rat and man.

1.5 Project Aims

The aims of this PhD project are three-fold:

- To generate and characterise a primary rat proximal tubule model as a platform for drug safety studies;

- To determine which transporters are present in the apical and basolateral membranes of primary rat proximal tubule cells that are important in handling candidate drugs;

- To compare the species difference in the handling of the same candidate drugs between primary rat proximal tubule cells and primary human proximal tubule cells.

Chapter 2

Materials and Methods

2.1 Materials

Cell culture reagents including High-glucose Dulbecco's modified eagles medium (HG-DMEM), Ham's F-12 Nutrient Mixture, Roswell Park Memorial Institute-1640 medium (RPMI), foetal calf serum (FCS), penicillin, streptomycin, L-glutamine, trypsin (with 0.02 % EDTA), Dulbecco's phosphate-buffered saline (PBS), mouse epithelial growth hormone, and rat collagen were obtained from Sigma-Aldrich, UK. SingleQuot kit renal epithelial growth medium supplements and growth factors were purchased from Lonza, Switzerland. Percoll was bought from GE Healthcare, UK, type 2 collagenase from Worthington Biochemicals, USA, and 10X HBSS from Invitrogen, USA.

Cyclosporine A (CsA) was purchased from CalBioChem-Merck, Germany, 5-chloromethylfluorescein-diacetate (CMFDA) from Invitrogen, USA, and Coomassie Blue Dye reagent was from ThermoFisher Scientific, UK. [3-(4,5-dimethyl-2-yl) – 5 – (3-carboxymethoxyphenyl)-2-(4-sulfophenyl)-2H-tetrazolium salt (MTS) was purchased from Promega, UK. Hoescht 33342 dye, 5-(3-(2-(7-Chloroquinolin-2-yl)ethenyl)phenyl)-8-dimethylcarbamyl-4,6-dithiaoctanoic acid (MK-571) and all other chemicals were from Sigma-Aldrich, UK, and were of the highest quality available.

2.2 Cell culture

Primary human proximal tubule cells and primary rat proximal tubule cells (PTC) were used in this study. Primary human PTCs were isolated from human kidney donations that were not suitable for transplant, for which ethical approval for their use in this study was granted to the supplier of the kidneys (Scievita Ltd). These kidneys were kept on ice after removal from the body and processed within 18 hours. Rat PTCs were isolated from kidneys excised from 8-12 weeks old Sprague-Dawley rats. The rats were bought from Charles River, UK, and had access to chow and water. These rats were sacrificed in accordance with Schedule 1 of the Animals (Scientific Procedures) Act 1986. All cell culture work was performed in a class II vertical laminar flow hood to ensure sterility. The protocol for human and rat PTCs isolation was adapted from (Brown *et al.*, 2008)). The procedure was as follows:

The kidneys were decapsulated and cortex slices were taken. The cortex slices were then minced to approximately 1 mm^3 pieces before 1 g of tissue was suspended per 25 ml of isolation medium. The composition of the isolation medium can be found in Table 2.1. Type 2 collagenase (activity of ≈300 units/mg) was added to the cell suspension to initiate the digestion of the tissue to a single cell suspension. The working concentration of collagenase used was 1 µg/ml.

The suspension was kept shaken gently for 2.5 hours at 37 °C before cell separation. To separate the cells, the cell suspension was passed through a 40 µm nylon sieve (BD cell strainer) to remove undigested material before centrifuged at 1200 rpm for 10 minutes. In this and all subsequent centrifugation steps the temperature was maintained at 4 °C. The resulting cell pellet was resuspended in 25 ml isolation medium before the cells were pelleted again by centrifugation at 1200 rpm for 7 minutes (wash step). The cell pellet was then loosened and gently resuspended in 10 ml isolation medium.

To separate out the proximal tubule cells, the cell suspension was loaded on top of discontinuous Percoll gradients with densities of 1.04 g/ml and 1.07 g/ml, and centrifuged at 3000 rpm for 25 minutes. 1.04 g/ml density Percoll was made up with stock Percoll and isolation medium in 5:12 ratio, and 1.07 g/ml density Percoll was made up with stock Percoll and PBS in 5:4 ratio. To prevent saturation of the density gradients, only 5 ml of cell suspension was loaded onto every 7 ml of 1.04 g/ml and 7 ml of 1.07 g/ml density Percoll gradients. After centrifugation, PTCs at the intersection of the gradients were aspirated and washed as previously described. The cells were resuspended in 10 ml warm renal epithelial growth medium (REGM). The composition of REGM is shown in Table 2.2. The cell yield was estimated using a Coulter Counter (Coulter Electronics, UK) or a Cellometer Auto T4 Cell Counter (Nexcelom Bioscience LLC, USA) after passing the cell suspension through a large bore needle three times to separate aggregated cells.

The cells were then seeded into cell culture flasks or plates at a range of densities. 3 µg/cm^2 of rat collagen was coated on the surfaces of cell culture flasks and plates prior to rat PTC seeding to increase adherence. PTCs were maintained in a humidified incubator at 37 °C with 5 % CO2 and 95 % air. Medium was changed every 2 days and cells seeded on cell culture flasks and plates were cultured for

6 to 7 days or to confluency before experimentation. The adherence and growth of the epithelial cells were inspected visually under a phase contrast microscope. To determine the number of cells after a period of time in culture, 0.25 % trypsin-EDTA was added to the cells to dislodge them from the culture platform. The cells were then processed and counted as mentioned above.

Isolated PTCs were also cultured on 24-well format Transwell inserts (Corning Costar). 200 µl of medium containing PTCs were seeded into the insert's well (apical chamber) and 600 µl of medium was placed in the well of the plate that supported the insert (basolateral chamber). The opacity of the polycarbonate filter on the insert meant the growth of the cells could not be monitored visually. Instead, the transepithelial electrical resistance (TEER) was used as an indicator of monolayer formation and hence cell growth. The monolayer resistance, which was comprised of the resistance of the filter and cell monolayer, was measured using an electric voltohmeter (EVOM, World Precision Instruments, UK). The TEER of the monolayer, with the unit of $\Omega.cm^2$, was calculated by subtracting the base resistance created by the filter submerged in culture medium (90 Ω) and then dividing it by the surface area (0.33 cm^2) of the filter. Only monolayers with TEERs greater than 60 $\Omega.cm^2$ were used in experiments.

5ml Cell suspension

7ml 1.04 Percoll

7ml 1.07 Percoll

Layer of debris

Layer of PCT cells.
To be retreived without
disturbing top debris layer

Layer of clear 1.07
Percoll gradient

Red blood cells
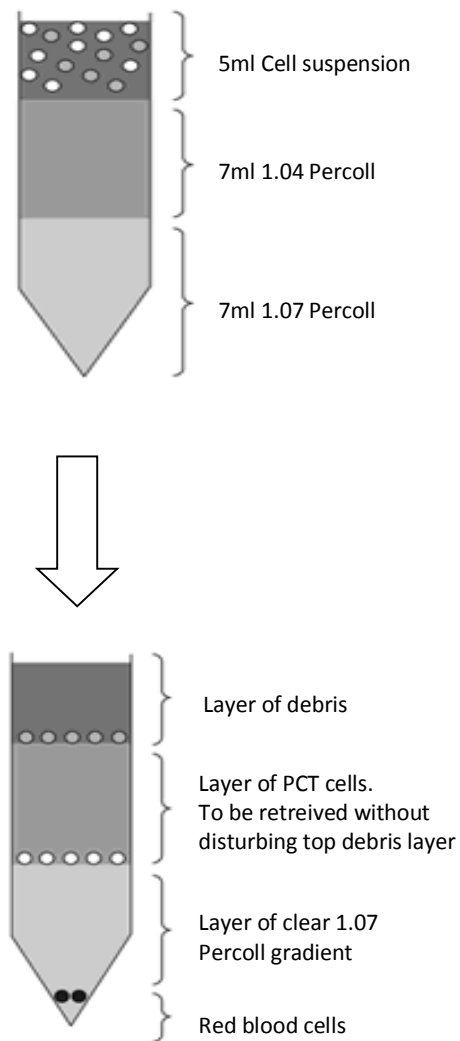
Figure 2.1: Percoll density gradients used in the separation of PTCs from the cellular debris.

5 ml of cell suspension was loaded onto every 7 ml of 1.04 g/ml and 7 ml of 1.07 g/ml density Percoll gradients. After centrifugation, PTCs at the intersection of the gradients were aspirated and washed. The other layers were discarded.

Supplements	Final concentration
RPMI (Basal medium)	-
FCS	5 %
Penicillin	200 units/ml
Streptomycin	200 µg/ml

Table 2.1: Composition of isolation medium used in the isolation of human and rat PTCs.

Supplements	Final concentration
DMEM/Ham's F-12 (Basal medium)	Ratio of 1:1
HEPES buffer	10 mM
Human epithelial growth factor	10 ng/ml
T_3	5 pM
Ascorbic acid	3.5 µg/ml
Transferrin	5 µg/ml
PGE	25 ng/ml
Sodium Selenite	8.65 ng/ml
G418	100 µg/ml
Insulin	5 µg/ml
L-glutamine	4 mM

Table 2.2: Composition of culture medium for human primary PTCs.

10 ng/ml of mouse epithelial growth factor was supplemented into the culture medium for rat primary PTCs instead the human epithelial growth factor.

2.3 Total cell RNA isolation and quality assessment

SV Total RNA Isolation System (Promega, UK) was used to isolate total cell RNA from freshly isolated and cultured rat PTCs according to the manufacturer's protocol. The yield and purity of the isolated RNA samples were then determined using NanoDrop ND-1000 UV-Vis Spectrophotometer (ThermoFisher Scientific, USA) where the absorbance at 260 nm and 280 nm (A260 and A280) were measured. The yield was calculated from A260, on the basis that an optical density reading of 1 is equivalent to 40 µg/ml. The purity of the samples was determined by calculating the A260/A280 ratio, where a value of 1.8 and above indicated good purity. The quality of the isolated RNA samples was assessed by measuring the 18S/28S rRNA ratio using the BioAnalyzer 2100 (Agilent Technologies, USA). In addition to the ribosomal RNA ratio, the BioAnalyzer also provided a RNA Integrity Number (RIN) software algorithm that took into account the entire electrophoretic trace of a sample and classified the RNA on a number scale of 1 to 10, with 1 being the most degraded and 10 being the most intact. Only RNA samples that had RIN of 8 or above were used in downstream applications.

2.4 Reverse transcription of isolated total cell RNA and endpoint PCR

Total cell RNA was reverse transcribed into cDNA using Moloney murine leukaemia virus reverse transcriptase (MMLV-RT) (Promega, UK). The reaction was carried out using 1 µg of total RNA mixed with 1 µl of 0.5 mg/ml random hexamers and heated for 5 minutes at 65 ˚C and then immediately cooled on ice in order to remove any secondary structure. The rest of the reaction mixture, which consisted of 0.5 µl MMLT-RT at 200 units/µl, 4 µl 5X RT buffer, 5 µl 2 mM dNTPs and 0.25 µl RNasin at 40 units/µl (Promega, UK) to a final reaction volume of 20 µl, were added and the samples incubated at 42 ˚C for 2 hours followed by 10 minutes at 70 degrees. RNasin is a ribonuclease inhibitor added to the reaction to prevent degradation of RNA by ribonuclease A.

Primers for genes of interest were designed using Primer-BLAST from the National Center for Biotechnology Information website (NCBI,

http://www.ncbi.nlm.nih.gov/tools/primer-blast/), unless otherwise stated. When designing the forward and reverse primer pairs, the following criteria were set: product size of around 100 base pairs should be amplified by a primer pair, individual primer was around 20 base pairs in length, the GC content of the primer should be 40-60 %, the melting temperature of individual primer should be between 58 and 64 °C and within 2 °C of each other in a primer pair, and either one of a primer pair should cross an exon-exon boundary. The retrieved primers by Primer-BLAST were analysed for hetero-dimer, homo-dimer, as well as hairpin formation, using the Netprimer software (http://www.premierbiosoft.com/netprimer/). The specificity of a primer pair to the intended gene was analysed by running the basic local alignment search tool (BLAST) on their sequences. HPLC purified primers were then ordered from IDT DNA (Belgium) using the checked and vetted sequences. The sequences of the primers are listed in Table 2.3.

Endpoint PCRs were carried out for genes of interest using GoTaq DNA polymerase (Promega, UK). A typical endpoint PCR consisted of 0.25 µl GoTaq DNA polymerase at activity of 5 units/µl, 2 µl 2 mM dNTPs, 0.5 µM of each primer of the gene of interest, 4 µl of 5X Green GoTaq buffer, 1.5 µl of cDNA template and molecular grade water to make up to a volume of 20 µl. The amplification protocol was as follows: 95 °C for 2 minutes, 35 cycles of 95 °C for 30 seconds, Ta °C for 30 seconds and 72 °C degree for 30 seconds, then an end stage of 72 °C for 10 minutes. T_a denotes the annealing temperature of a primer pair. An approximation of the T_a was determined as 5 °C below the melting temperature of the least stable primer. Reactions were carried out on a Px2 Thermo Cycler (Thermo Scientific, USA). The PCR products were separated by gel electrophoresis using 1.5 % agarose gels and visualised with 0.01 % (v/v) ethidium bromide. Products were excised and cleaned using the MinElute Gel Extraction kit (Qiagen, Hilden, Germany) and cloned using pGem T-easy vector system 2 (Promega, UK), according to the manufacturers' protocol. *E. coli* DH5$_\alpha$ was used as the competent cells. The cloned vector was extracted from the bacteria using the GenElute Plasmid Miniprep kit (Sigma, UK) and sequenced to verify that the correct product had been amplified. Sequencing was outsourced to Genevision (Newcastle upon Tyne, UK).

Gene		Sequence	Product Size	T_a (˚C)
Bcrp (NM_181381)	**F**	[836]TTG ACA GCC TCA CCT TAC TGG[856]	95	59
	R	[930]ACA GTG GTA ACC TGC TGA TGC[910]		
Mdr1 (M81855.1)	**F**	[1609]GTC AAG GAA GCC AAT GCC[1626]	148	59
	R	[1755]AAG GAT CTT GGG GTT GCG GAC[1735]		
Mrp2 (NM_012833)	**F**	[1063]GTT CTC GTC CTG GAA GAA GC[1082]	169	57
	R	[1232]TTC AGC AGC TGA GGA TTC AG[1213]		
Oat1 (NM_017224)	**F**	[1312]ATG CTG TGG TTT GCC ACT AGC[1332]	119	59
	R	[1431]AAC TTG GCA GGC AGG TCC AC[1411]		
Oct2 (NM_031584)	**F**	[1361]ATC CCT GAT GAT CTA CAG TGG[1381]	127	55
	R	[1487]CAA GAT TCC TGA TGT ATG TGG[1466]		
Oatp4c1 (NM_001002024)	**F**	[330]AGC CCT AAC GCA AGG TAT TGT[350]	101	57
	R	[430]ATA TCA GGC CGG TCA GGG AA[411]		
Slc2a9 (NM_001191551)	**F**	[288]CTC TGG TCT GTA ACT GTG TCC[309]	104	59
	R	[391]CAG CAG TGT GTA CTT CCT TCC[370]		
Urat1 (NM_001034943)	**F**	[1551]ACA GCC AGC CTC TTG ATG G[1570]	109	55
	R	[1659]ACA GCC AAC TGC AGC ATC C[1639]		
Mct1 (NM_012716)	**F**	[399]TAT GCC GGA GGT CCT ATC AGC[419]	157	59
	R	[555]GAC CTC CAA TGA CAC CAA TGC[535]		
Mate1 (NM_001014118)	**F**	[442]CCA GAT GTA TCC AGG CTC ACC[462]	123	59
	R	[564]AAC CTG AGG CAG AAC GAT GC[555]		

Table 2.3: Sequences of primers used in endpoint and qPCR for the amplification of drug transporters.

F and R denotes forward primer sequence and reverse primer sequence, respectively. The superscripted numbers are the position of the bases in the mRNA sequence. T_a denotes the annealing temperature of the primer pair. The number in brackets underneath the gene name is the NCBI reference number, from which the mRNA sequence of the gene was obtained.

2.5 Quantitative PCR

Changes in expression of mRNA levels in rat PTCs in different culture conditions were performed using quantitative PCR (qPCR). A reaction volume of 10 µl, comprising 2.5 µl one-in-three diluted RT as the cDNA template, 5 µl 2X SYBR-green Master Mix (Roche, UK), 0.5 µl of 10 µM primer mix and 2 µl water, was loaded on to a white 96-well format qPCR plate, and PCR run in a Roche LightCycler 480 (Roche, UK). The following protocol was used: 95 $^{\circ}$C for 10 minutes, 45 cycles of 95 $^{\circ}$C for 10 seconds, T_a $^{\circ}$C for 20 seconds and 72 $^{\circ}$C for 10 seconds, followed by melt curve step (cooling to 65 $^{\circ}$C followed by heating to 97 $^{\circ}$C), and a cooling step. Each PCR cycle and its corresponding fluorescence from each sample were logged by the software LightCycler 480 (version 1.5, Roche, UK). The software calculated the fluorescence baseline during the first 15 cycles of the PCR to create a common starting fluorescence intensity for all the samples. A threshold level of fluorescence intensity was also defined by an algorithm where it was significantly above the background fluorescence but still within the linear phase of amplification. The cycle at which a sample produces fluorescence intensity that crosses the threshold is termed the threshold cycle (C_t), and is correlated to the starting concentration of the cDNA template; the greater the amount of starting cDNA, the earlier the C_t. As such, for the purpose of analysis, samples that produced C_t of 35 and above were disregarded.

Serially diluted cloned PCR product of the gene of interest was also used as the DNA template and loaded on the same plate as the samples to produce a standard curve for quantification. Efficiency of the PCR was also determined from this standard curve. qPCR was also performed on the reference gene Gapdh, primers for which were purchased from PrimerDesign, UK. All data generated were normalised to the reference gene.

2.6 Fluorescence substrate retention assays

Fluorescence compounds, Hoechst 33342, 5-chloromethylfluorescein-diacetate (CMFDA), and 4-(4-(dimethylamino)styryl)-N-methylpyridinium (ASP$^+$) were used as tracer substrates to measure the affinity of drug transporters to the compounds and drug transporter-specific substrates. Hoechst 33342 is a cell-permeant nucleic acid stain that fluoresces when bound to double-stranded DNA. It is also

a substrate of Mdr1 and Bcrp. CMFDA is a non-fluorescent derivative of fluorescin, which easily permeates across the cell membrane. Inside the cells it is transformed via a 2-step process to glutathione methylfluorescein (GSMF). GSMF is fluorescent and hydrophilic; its only route of exit from the cell is via Mrp-mediated efflux. ASP$^+$ is an organic cation substrate specific to Oct2 that changes its fluorescence spectrum inside cells. The properties of the fluorescence dyes were utilised in determining the functional activity of drug transporters in rat PTC. The protocol was as set out by Jenkinson *et al.* (2012) and is described in brief here.

Modified-Krebs buffer was used as the cell medium in all drug transporter experiments. The composition of modified-Krebs buffer is shown in Table 2.4. Rat PTCs cultured on 96-well plates were prepared for experiment by aspirating the cell culture medium from the wells and the cells washed 3 times with warm modified-Krebs buffer. The cells were then incubated with an appropriate inhibitor substrate for 40 minutes. CsA and Ko143 were used to inhibit the efflux of Hoechst 33342 by Mdr1 and Bcrp, respectively, and MK-571 to inhibit GSMF efflux by Mrps. The appropriate dye was then co-incubated with the inhibitor and cells for a further 40 minutes. After which, the cells were washed with ice-cold modified-Krebs buffer and the intracellular accumulation of fluorescent dyes were determined by taking fluorescence reading at their respective excitation and emission wavelengths using FLUOstar Omega Microplate Reader (BMG Labtech, Germany). The wavelengths used are given in Table 2.5.

The microplate reader had the facility to read more than one fluorophore simultaneously. A novel technique was thus developed to investigate substrate specificity of efflux transporters to a range of inhibitor substrates simultaneously. As described above, rat PTCs cultured on 96-well plates were incubated with an inhibitor substrate for 40 minutes prior to the addition of Hoechst 33342 and CMFDA to the same cells and incubated for a further 40 minutes. Controls including rat PTCs exposed to Hoechst 33342 and CMFDA, Hoechst 33342 only, and CMFDA only, for 40 minutes were also performed to ensure the wavelengths of the fluorophores did not interfere with each other's excitation and emission readings. Cells were washed three times with ice-cold modified-Krebs buffer

before the fluorescence was read at Hoechst 33342 and GSMF wavelengths simultaneously.

The fluorescence intensity units produced were normalised to the amount of protein in the wells, which was assumed to be relative to the number of cells. The amount of protein in the wells was measured by adding 100 µl Coomassie blue reagent to the wells after fluorescence readings were taken, along with a standard curve created using known concentration of serially diluted BSA as the protein source. Absorbance of the Coomassie blue was measured at 595nm using the same microplate reader, 5 minutes after Coomassie blue introduction.

Salt	Concentration (mM)
NaCl	140
KCl	5.4
$MgSO_4$	1.2
NaH_2PO_4	0.3
KH_2PO_4	0.3
Glucose	5
$CaCl_2$	2
HEPES	10
Tris Base	ad hoc to pH 7.4

Table 2.4: Composition of modified-Krebs buffer used in all drug transporter experiments.

Sodium-free buffer was made by replacing sodium chloride with choline chloride. For buffer pH to be lower than 7, 10 mM MES was used instead of HEPES.

	Excitation wavelength (nm)	Emission wavelength (nm)
Hoechst 33342 (when bound to DNA)	350 (340)	461 (485)
GSMF	492 (485)	517 (540)
ASP^+	465	585

Table 2.5: Excitation and emission wavelengths of the fluorescence substrate used in the substrate retention experiments.

The excitation and emission wavelengths of the fluorescence compounds as recommended by the supplier. The numbers in brackets are the wavelength of the filters used in the microplate reader.

2.7 Efflux of CMFDA metabolite by Mrp

Rat PTCs cultured on 24-well Transwell filter support were used to investigate the differentiation and localisation of efflux transporters. Culture medium was first aspirated from the insert wells before sequential transfer of the inserts into three beakers of 100 ml warm modified-Krebs buffer. The inserts were then placed in a clean 24-well plate, each well containing 500 µl of warm modified-Krebs. 200 µl of modified-Krebs was added to each insert well and the cells were allowed to equilibrate for an hour. For the purpose of this study, the insert wells are referred to as the apical chamber and the plate wells are referred to as the basolateral chamber. Temperature was kept at 37 °C by placing the plates on a thermostat-controlled heated platform. Experiment was started when apical solution was replaced with 200 µl of 10 µM MK-571, 5 µM CsA or 1 µM Ko143 and incubated for 40 minutes. 1 µM Hoechst 33342 or 1 µM CMFDA was then introduced in the apical solution for a further 40 minutes, after which 100 µl and 250 µl were sampled from the apical and basolateral chambers, respectively, and transferred into a clean 96-well plate. The inserts were washed three times with ice-cold modified-Krebs buffer by passing them through three beakers of fresh buffer. The fluorescence of the solutions was measured to detect the presence of GSMF and the fluorescence per ml of solution calculated. Fluorescence reading was taken of the filters at Hoechst 33342 and GSMF wavelengths (Table 2.5).

2.8 Unidirectional transepithelial fluxes

Unidirectional transepithelial fluxes in both the apical to basolateral (J_{A-B}) and basolateral to apical (J_{B-A}) directions were carried out in PTCs cultured on 24-well format Transwell inserts. The schematics of the experiment is shown in Figure 2.2. The PTC monolayer TEERs were determined as described in Section 2.2 and they were paired according to their TEERs for J_{A-B} and J_{B-A} experiments prior to the start. Rat PTC monolayers were equilibrated as in Section 2.7. Fluxes were initiated when either the apical or basolateral solution was replaced with modified-Krebs buffer containing required concentration of the substrate of interest and the same concentration of mannitol. Radiolabelled forms of the substrate and mannitol were also included at activity of 1 µCi/ml and 0.1 µCi/ml, respectively,

as tracer. Different isotopes were used to distinguish the radioactivity of the substrate and mannitol.

Sampling of the opposite chamber was done at exactly 1 hour, or otherwise stated, after flux initiation by transferring half of the volume of buffer in a chamber into a scintillation vial. The insert was then washed by transferring it sequentially into three beakers containing 100 ml ice-cold modified-Krebs buffer and then allowed to dry. To measure the cellular substrate accumulation, the filter on which the cells were adhered to was cut from the insert and transferred to a clean scintillation vial.

2 ml of Optiphase Hisafe 2 scintillation solvent (Perkin Elmer, UK) was added to all the vials and mixed by vortexing. Radioactivities in the samples were determined by liquid scintillation spectrophotometery using Beckman LS5000 liquid scintillation counter, (Beckman-Coulter Ltd, UK). 100 µl of known concentration of the substrate and mannitol was also put through the scintillation counter to be used as standard. Background activity was counted using a vial containing only 2 ml scintillation fluid and this value was automatically deducted from the counts. The amount of substrate was calculated from the counts using the following equation:

$$\text{Amount of substrate} = \frac{A_{STD}}{DPM_{STD}} \times 2 \times 3 \times DPM_{SPL}$$

A_{STD} represents the amount of substrate in 100 µl of the standard, DPM_{STD} represents the average disintegration per minute of the radiolabelled substrate from 3 standards, and DPM_{SPL} represents the disintegration per minute of a sample. The constant 2 used in the equation was to double the count of a sample as only half the volume of the chamber was sampled, and the constant 3 was used to express the result in cm^2 (surface area of a Transwell insert was 0.33 cm^2).
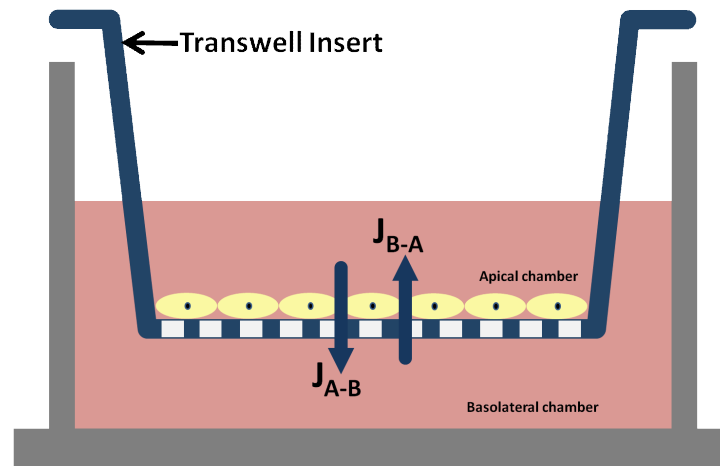
Figure 2.2: Schematic of unidirectional transepithelial flux carried out on cells cultured on Transwell inserts.

Unidirectional transepithelial fluxes in the apical to basolateral (J_{A-B}) and basolateral to apical (J_{B-A}) directions were carried out in PTCs cultured on 24-well format Transwell inserts. The PTC monolayer TEERs were determined as described in Section 2.2 and only monolayers with TEER greater than 60 $\Omega.cm^2$ were used in the experiment.

2.9 Expression of SLC2A9 and URAT1 in *Xenopus laevis* oocytes

Urate handling by human SLC2A9 and URAT1 was examined using *Xenopus* oocytes as the expression system for these transporters. Human cDNA clones of SLC2A9 and URAT1, inserted into the plasmid pCMV6-XL5, were purchased from Origene, USA. To prepare the cDNA for *in vitro* transcription to capped cRNA, the plasmid was linearised. The sequence of the plasmid and its cDNA insert was uploaded to the online software NEBcutter (version 2.0, http://tools.neb.com/NEBcutter2/index.php) to identify a suitable restriction endonuclease (RE) that would digest the plasmid only once, downstream of the insert. XBaI was identified as a suitable RE for both transporter cDNA. A reaction volume of 40 µl was created by mixing 10 µg of plasmid, 200 units of RE, 10 µl of 10X RE buffer and 0.01 µg of BSA, and incubated at 37 °C for 4 hours. The linearised plasmid was then purified by precipitation. This involved adding 10 µl of sodium acetate and 250 µl of 100 % ethanol to the reaction mixture, and incubated at -20 °C for 2 hours. The sample was then centrifuged at 18,000 rpm for 30 minutes at 4 °C, after which the supernatant was decanted gently to avoid dislodging the pelleted cDNA. The cDNA was washed with 70 % ethanol before being resuspended in water and the yield quantified using UV spectroscopy. Gel electrophoresis was performed with a small aliquot of the purified cDNA to ensure complete linearisation of the plasmid.

The cDNA was transcribed *in vitro* using the Ambion mMessenger mMachine T7 and Capped RNA Transcription Kit (Life Technologies, UK). The protocol for the transcription and recovery of the transcribed cRNA was followed as recommended by the manufacturer of the kit. The yield of the cRNA was quantified using UV spectroscopy before it was aliquoted and stored at -80 °C.

2.10 Collection and sorting of *Xenopus laevis* oocytes

Xenopus laevis was sacrificed in accordance with Schedule 1 of the Animals (Scientific Procedures) Act 1986 and the ovaries collected by manual dissection. Separation and defolliculation of the oocytes was achieved by incubation in 0.25 % (w/v) collagenase (Roches, USA) with continuous rotation for 2 hours. The

defollicullated oocytes were washed five times in calcium-free ORII buffer and five times in Barths buffer. These buffers were autoclaved before use and their compositions are shown in Table 2.6 and Table 2.7. Oocytes of stages V and VI were selected for microinjection and maintained at all times at 18 ˚C in Barths buffer. One day after isolation, the oocytes were microinjected with 50 ng of SLC2A9 or URAT1 cRNA at the vegetal pole of the oocytes. Water injected oocytes were used as controls. The oocytes were used two or three days post-microinjection.

Oocyte uptake experiments were carried out at room temperature (≈ 20˚C). The oocytes were equilibrated in uptake buffer (Table 2.8) for 5 minutes. The oocytes were then incubated for one hour with buffer containing 1 µCi/ml [^{14}C]-urate and non-radiolabelled urate, giving a final working concentration of 35 µM urate. Adding excess ice-cold uptake buffer to the oocytes stopped the uptake, and they were washed 3 times with fresh uptake buffer. The oocytes were then transferred to scintillation vials and lysed overnight with 200 µl 10 % (w/v) SDS. 2 ml scintillation fluid was then added and mixed by vortexing before radioactivity was quantified by liquid scintillation counts. 3 X 100 µl of 35 µM urate used in the experiment were also put through the scintillation counter to be used as standards. The amount of urate taken up by one oocyte was calculated from the counts using the following equation:

$$\text{Amount of urate} = \frac{350}{\text{DPM}_A} \times \text{DPM}_S$$

The constant 350 represents 350 pmol of urate present in 100 µl of standard, DPM$_A$ represents the average disintegration per minute of the radiolabelled substrate from 3 standards, and DPM$_S$ represents the disintegration per minute from one oocyte.

2.11 Statistics

Data are expressed as mean ± standard error of mean (SEM) of the specified number of replicates, where "N" denotes biological replicates, and "n" denotes technical replicates. In certain figures, the mean is taken from the all the technical replicates in separate experiments, and the most appopriate statistical test was performed to determine significant difference. Two-way Analysis of Variance (ANOVA) statistical test was performed to compare significance of difference in data between 3 or more conditions, as indicated. Two-way ANOVA was only used when the biological replicates (N) was used as the parameter. Student *t* test and nonlinear regression were also performed as indicated. GraphPad Prism 4.0 (GraphPad software Inc, USA) was used to perform the analysis.

Compound	Concentration (mM)
NaCl	88
KCl	1
$MgSO_4$	0.82
$CaCl_2$	0.41
$CaNO_3$	0.33
HEPES	10
$NaHCO_3$	2.4
Tris Base	ad hoc to pH 7.5

Table 2.6: Composition of Barths buffer.

Salt	Concentration (mM)
NaCl	82.5
KCl	2
$MgCl_2$	1
HEPES	10
Tris Base	ad hoc to pH 7.5

Table 2.7: Composition of calcium-free ORII buffer.

Compound	Concentration (mM)
NaCl	100
KCl	2
$MgCl_2$	1
$CaCl_2$	1
HEPES	10
Tris Base	ad hoc to pH 7.4

Table 2.8: Composition of oocyte uptake buffer.

Chapter 3

Isolation and Development of Rat PTCs

3.1 Chapter overview

This chapter describes the results of the isolation and development processes of the rat proximal tubule cells (PTCs). The outcome of the following is discussed:

- The optimal collagenase concentration used to isolate the rat PTCs from minced rat kidney cortex, which took into account the yield and cell viability.

- The morphology of cultured rat PTCs over a period of 7 days.

- The low adherence of rat PTCs and the use of collagen-coated cell culture platforms to increase adherence.

- The preservation of surplus rat PTCs using solid medium.

- The formation and assessment of tight junctions by rat PTCs when they were cultured on Transwells.

3.2 Collagenase concentration and cell yield

Collagenase was used to disaggregate rat PTCs. To determine the optimum conditions that produced the highest yield, different amounts of collagenase were tested in the isolation procedure. Figure 3.1 shows the yield of PTCs from different amount of collagenase, whose activity was 300 units/mg.

As expected, the yield of PTCs increased with the amount of collagenase used. The lowest concentration of collagenase used (20 μg of collagenase per gram of cortex tissue) yielded $5.04 \pm 0.59 \times 10^6$ cells. At the other extreme, the highest concentration of collagenase used was 35 μg of collagenase per gram of tissue, and that gave $14.32 \pm 0.77 \times 10^6$ cells. The other concentrations of collagenase used were 25 μg and 30 μg per gram of tissue. The number of cells retrieved was $10.65 \pm 0.54 \times 10^6$ and $13.46 \pm 0.76 \times 10^6$ cells, respectively.
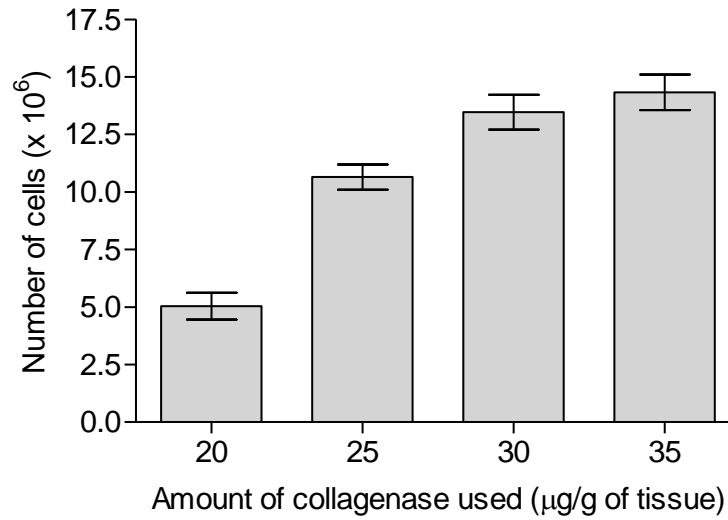
Figure 3.1: Yield of rat PTCs using the specified amount of collagenase to disaggregate minced rat kidney cortex.

The activity of collagenase used was 300 units/mg. 20 μg of collagenase per gram of cortex tissue yielded $5.04 \pm 0.59 \times 10^6$ cells. 25 μg and 30 μg collagenase per gram of tissue retrieved $10.65 \pm 0.54 \times 10^6$ and $13.46 \pm 0.76 \times 10^6$ cells, respectively. The highest concentration of collagenase used was 35 μg of collagenase per gram of tissue, and that gave $14.32 \pm 0.77 \times 10^6$ cells. Bars represent mean $\pm$ SEM of 3 independent rat PTC isolation procedures.

3.3 Collagenase concentration and cell viability

Whilst a high concentration of collagenase gave a high yield of PTCs, it was observed that the rate of propagation of cells decreased at high concentrations of collagenase. Figure 3.2 shows the number of cells propagated from PTCs isolated using a range of collagenase concentrations.

All concentrations of collagenase produced PTCs that propagated at an average of 4,900 ± 960 cells/cm^2 at day 3 of culture. PTCs gave a maximum propagation rate of 71,450 ± 10,440 cells/cm^2 at day 6 when 20 µg of collagenase was used to isolate them, decreased to 37,925 ± 6,980 cells/cm^2 at day 7, and 19,150 ± 7,570 cells/cm^2 at day 8. The propagation rates by PTCs isolated using 25 µg of collagenase were 6,1375 ± 13610 cells/cm^2 at day 6 before decreasing to 44,225 ± 6,980 cells/cm^2 and 15,050 ± 5,590 cells/cm^2 at day 7 and day 8, respectively.

The rates of propagation of isolated PTCs were lower in PTCs isolated with higher concentrations of collagenase. PTCs isolated with 35 µg of collagenase gave cell propagation rate of 20,850 ± 2,700 cells/cm^2 at day 5 of culture. The number of cells fell to 4,675 ± 690 cells/cm^2 at day 7, and 4,200 ± 240 cells/cm^2 at day 8. PTCs isolated with 30 µg of collagenase gave propagation rate of 38,410 ± 12,410 cells/cm^2 at day 6. The rate then decreased to 13,125 ± 2,660 cells/cm^2 and 4,875 ± 610 cells/cm^2 at day 7 and 8, respectively.
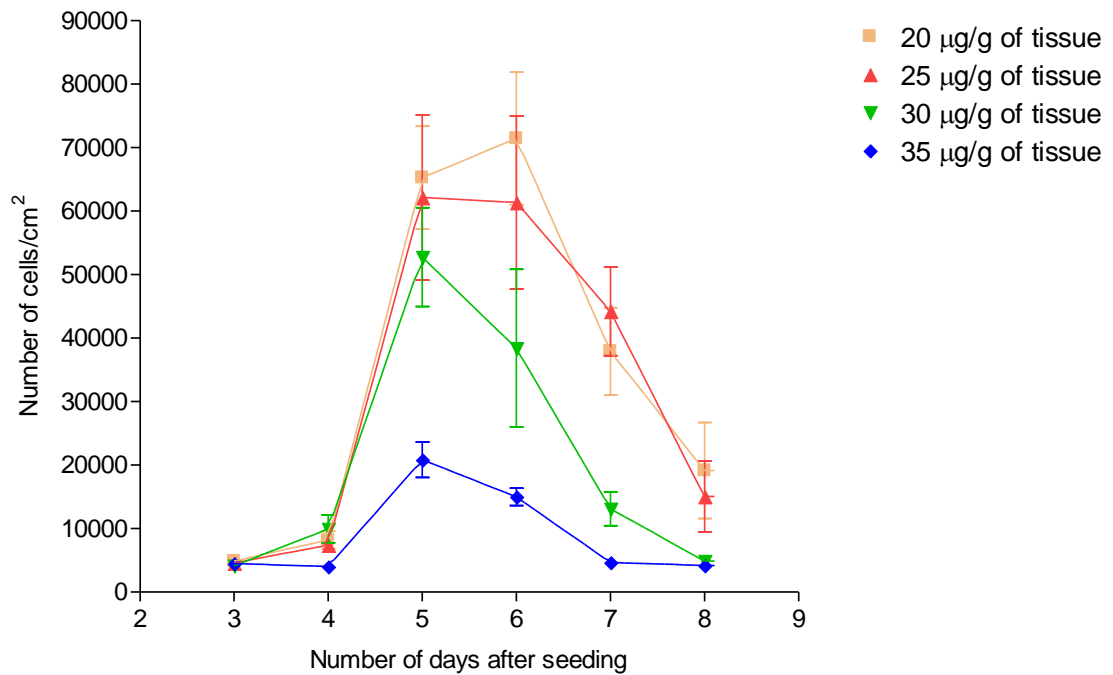
Figure 3.2: Number of cells propagated by rat PTCs over 8 days of culture isolated using a range of collagenase concentration.

An average of 4,900 ± 960 cells/cm² were produced by all conditions at day 3 of culture. PTCs gave a maximum propagation rate of 71,450 ± 10,440 cells/cm² at day 6 when 20 µg of collagenase was used to isolate them, and decreased to 37,925 ± 6,980 cells/cm² at day 7, and 19,150 ± 7,570 cells/cm² at day 8. PTCs isolated with 25 µg of collagenase per gram of tissue propagated to a peak of 61,375 ± 13,610 cells/cm² at day 6 before decreasing to 44,225 ± 6,980 cells/cm² and 15,050 ± 5,590 cells/cm² at day 7 and day 8, respectively. The rate of propagation of isolated PTCs was lower in PTCs isolated with higher concentrations of collagenase. PTCs isolated with 35 µg of collagenase gave cell propagation rate of 20,850 ± 2,700 cells/cm² at day 5 of culture. The number of cells fell to 4,675 ± 690 cells/cm² at day 7, and 4,200 ± 240 cells/cm² at day 8. PTCs isolated with 30 µg of collagenase gave propagation rate of 38,410 ± 12,410 cells/cm² at day 6. The rate then decreased to 13,125 ± 2,660 cells/cm² and 4,875 ± 610 cells/cm² at day 7 and 8, respectively. Each dot represents the mean ± SEM of 12 replicates obtained from 3 independent experiments. Each experiment was conducted using PTCs isolated from different rats.

3.4 Cell culture and morphology

Isolated PTCs from rat kidney cortex were seeded out on to various cell culture platforms. Figure 3.3 shows the cells that were grown on a T75 cell culture flask over a period of 8 days.

The morphology of freshly isolated rat PTCs were largely single cells of not more than 40 µm in diameter, although larger intact tubules can also be seen (Figure 3.3A). The optimal time for the attachment of isolated cells to the culture flasks was found to be 24 hours. During the first 24 hour, most of the cells adhered to the bottom of culture flask and lamellipodia on edges of cells can be identified (Figure 3.3B). Defined areas of flattened individual cells in loose contact can be seen in Figure 3.3C. In day 3 to 5 of culture, clusters of cuboidal shapes or islets of rounded cells were seen (Figure 3.3D). The cells then spread and the typical morphology of an almost confluent monolayer could be observed (Figure 3.3E and F). During this period the total number of cells on the culture plate doubled (Figure 3.2). Thereafter, the cell numbers dropped and the morphology was that of cell shrinkage.
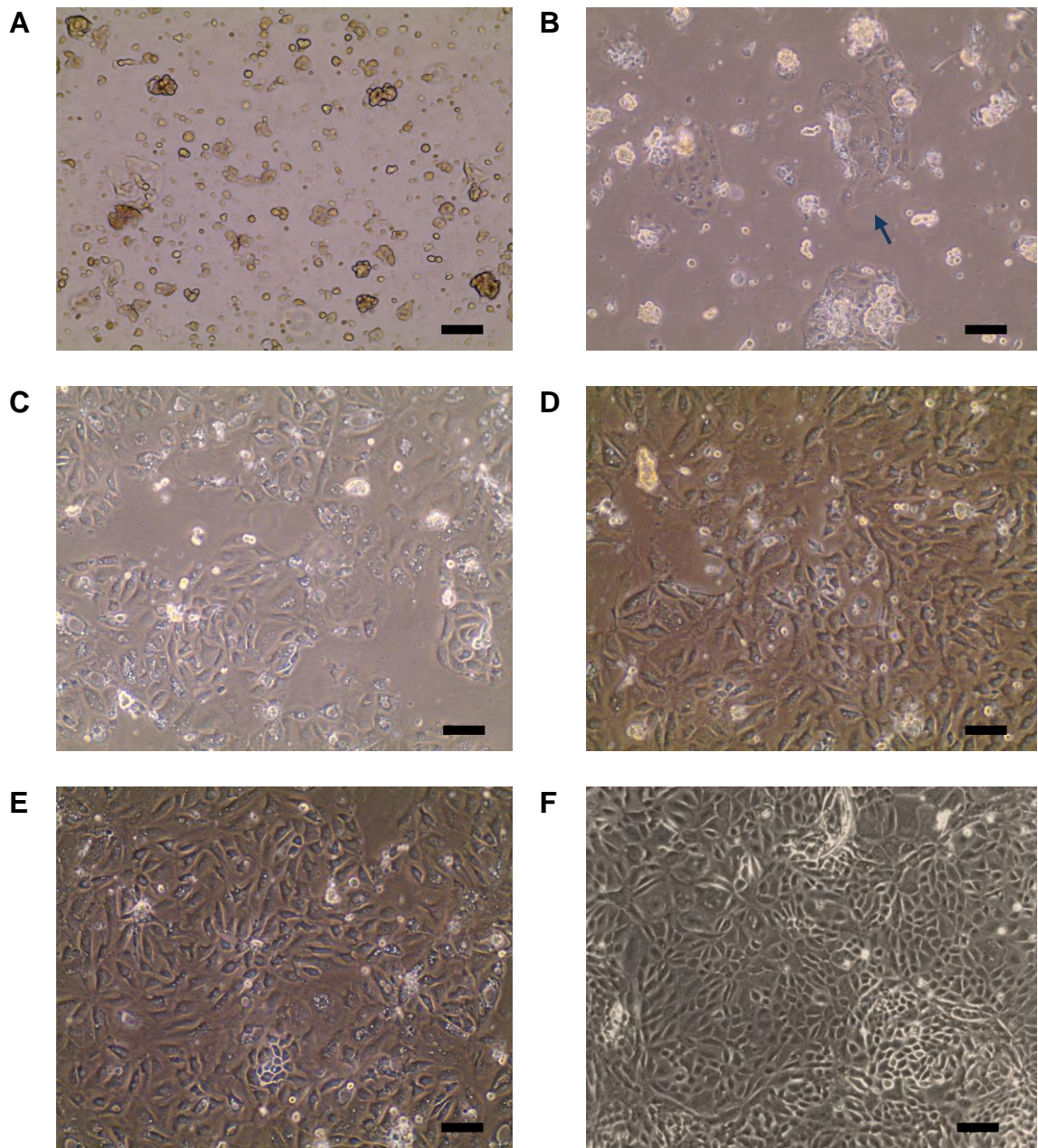
Figure 3.3: Images of T75 cell culture flask seeded with 3 million rat PTCs over 6 days of culture.

(A) The morphology of freshly isolated rat PTCs at day 1 of culture were still mainly single cells. (B) Most of the cells were seen adhered to the bottom of culture flasks and forming small lamellipodiae (arrow) at day 2. Clusters of cuboidal shapes or islets of rounded cells could also be seen. (C) Defined areas of flattened individual cells in contact with each other were seen at day 3. (D) Similar morphology was observed at day 4 but with more confluency. (E) The cell aggregates had spread on day 5 and the typical morphology of an almost confluent monolayer could be observed. (F) Confluent monolayer of rat PTCs was observed at day 6 of culture. The scale bar at the bottom right corner of images represents 200 µm.

3.5 Collagen coating of cell culture plates

Initial experiments showed low adherence of rat PTCs on 96-well plates, and collagen coating of wells was tested as a solution to address the problem. The amount of collagen used (1 µg/cm^2) to coat the wells did not cause a significant change in the absorbance of the Bradford reagent used to detect protein. To mimic a typical transporter experiment, Bradford reagent was added after the wells were washed with modified-Krebs buffer. A change in absorbance was assumed to be caused by cellular proteins only. Figure 3.4 shows the differences between the amount of protein in collagen-coated or non-coated wells at day 6 of culture. 13.86 ± 0.36 pmol/cm^2 of protein was detected in collagen-coated wells, whereas only 3.75 ± 0.95 pmol/cm^2 of protein was detected in non-coated wells.
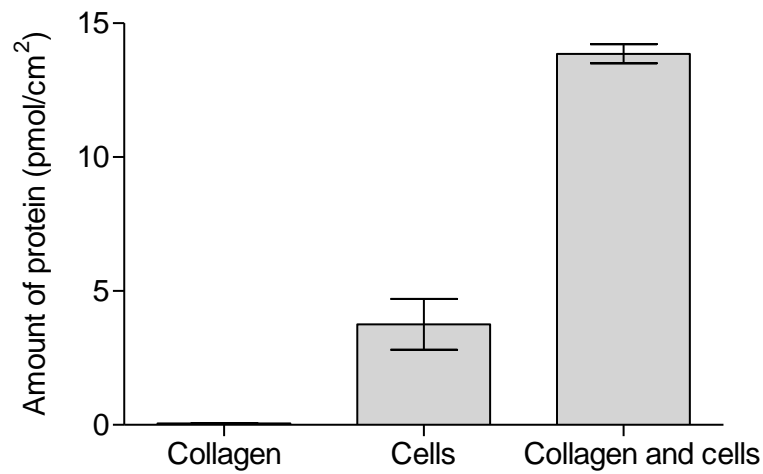
Figure 3.4: The amount of protein per cm² in collagen-coated and non-coated wells of a 96-well plate seeded with PTCs at day 6 of culture.

The amount of collagen used (1 µg/cm²) to coat the wells did not cause a significant change in the absorbance of the Bradford reagent used to detect protein. 13.86 ± 0.36 pmol/cm² of protein was detected in collagen-coated wells seeded with rat PTCs, whereas 3.75 ± 0.95 pmol/cm² of protein was detected in non-coated wells. Each bar represents the mean ± SEM of 18 replicates obtained from 3 separate rat PTC isolations.

3.6 Preservation of surplus isolated rat PTCs

Surplus freshly isolated rat PTCs were stored in SureTran, a proprietary solid medium, for up to 72 hours to find out if these cells could be preserved and thus decrease the number of animals sacrificed. Cell viability of stored PTCs was determined by MTS assay and Figure 3.5 shows the changes in viability over the period of storage.

Rat PTCs that were stored in SureTran for 24 hours showed no significant change in cell viability ($P > 0.05$). PTCs grown from cells stored for 48 hours had a 1.58-times decrease when compared to the control (63.4 ± 2.4 % of control, $P < 0.05$, $n = 8$). Similarly, PTCs grown from cells stored for 72 hours had a 1.61-times decrease (62.3 ± 4.1 % of control, $P < 0.05$, $n = 8$) in cell viability compared to control cells.

An initial experiment was then carried out to measure the retention of Hoechst 33342 in cultured cells of freshly isolated rat PTCs and PTCs stored in SureTran for 24 hours. Figure 3.6 shows the result of the drug transporter-dependent assay.

Cells cultured from fresh rat PTCs showed an apparent V_{max} of $25,472 \pm 4,035$ and K_m of 3.017 ± 0.96 µM. Cells cultured from rat PTCs that had been stored for 24 hours in SureTran showed an apparent V_{max} of $24,313 \pm 4,470$ and K_m of 4.97 ± 2.671 µM.
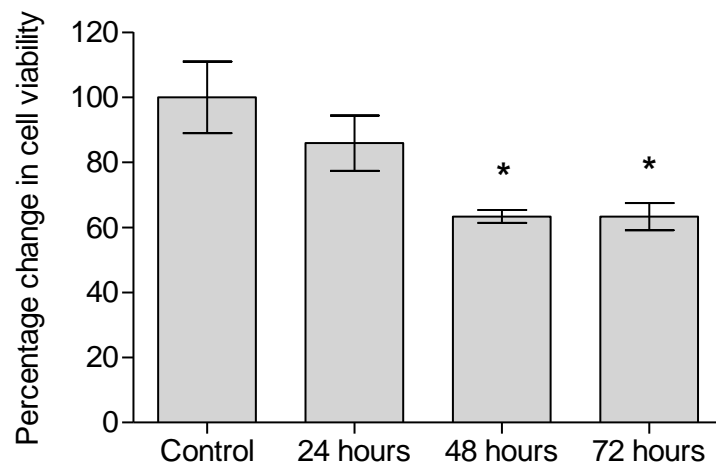
Figure 3.5: Percentage change in cell viability of culture rat PTCs that had been stored in SureTran.

Rat PTCs that were stored in solid medium for 24 hours showed no significant change in cell viability. PTCs grown from cells stored for 48 hours had 63.4 ± 2.4 % viability of the control. PTCs grown from cells stored for 72 hours had a 1.61-times decrease (62.3 ± 4.1 % of control) in cell viability compared to control cells. Each bar represents the mean ± SEM of 8 replicates obtained from 2 separate rat PTC isolations. Two-way ANOVA statistical test was performed to determine significance. *, P < 0.05.
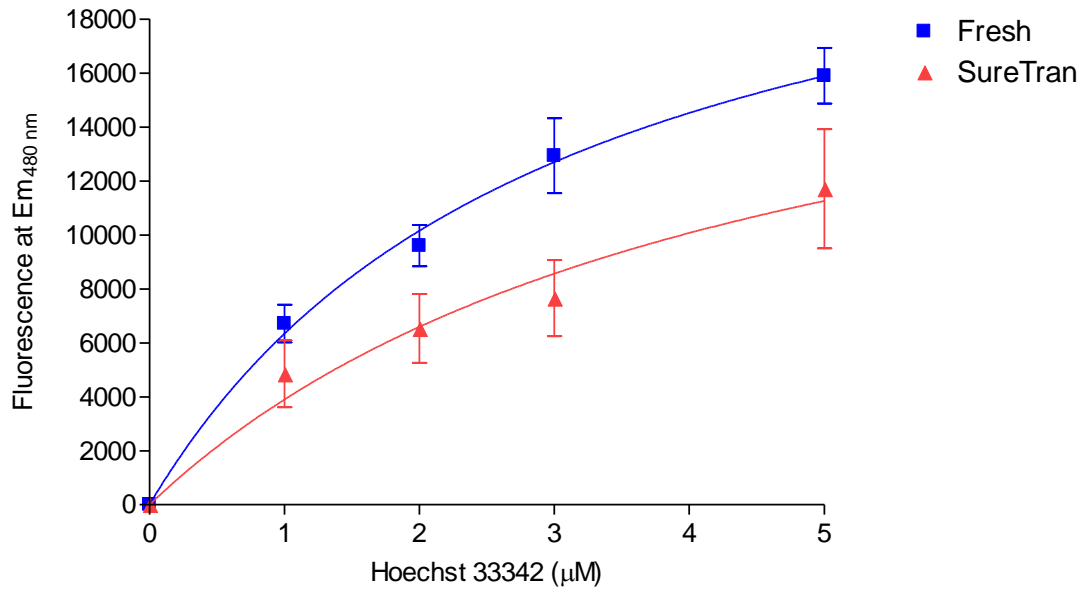
Figure 3.6: Fluorescence of intracellular Hoechst 33342 at 480 nm by rat PTCs.

Cells were cultured from freshly isolated rat PTCs or rat PTCs that had been stored in SureTran for 24 hours. Non-linear regression analysis performed on cells cultured from fresh rat PTCs showed an apparent V_{max} of 25,472 ± 4,035 and average K_m of 3.017 ± 0.96 µM. Cells cultured from rat PTCs that had been stored for 24 hours in SureTran showed an apparent V_{max} of 24,313 ± 4,470 and average K_m of 4.97 ± 2.671 µM. Each point represents the mean ± SEM of 6 replicates from one representative experiment. The K_m was the average from two separate experiments.

3.7 Transepithelial electrical resistance of rat PTC monolayers

To reinstate rat PTC monolayer formation, the isolated cells were cultured on Transwell filter support. Resistance of an empty Transwell filter support was found to be 90 Ω. The resistance of the Transwell filter support and PTC monolayer were measured over the culture period and the TEER of the monolayers calculated. The result is shown in Figure 3.7.

TEER of the rat PTC monolayer was negligible at day 1 of culture (result not shown), but an average of 12.01 ± 3.01 $\Omega.cm^2$ was measured at day 2. The TEER went up to 56.31 ± 7.61 $\Omega.cm^2$ at day 3 and 73.85 ± 9.71 $\Omega.cm^2$ at day 4, before peaking at day 5 with 77.48 ± 12.72 $\Omega.cm^2$. Day 6 saw a decrease in the TEER to 73.89 ± 6.51 $\Omega.cm^2$. Thereafter, the TEER decreased even further to 22.1 ± 5.47 $\Omega.cm^2$ and 1.1 ± 0.51 $\Omega.cm^2$ at day 7 and 8, respectively.
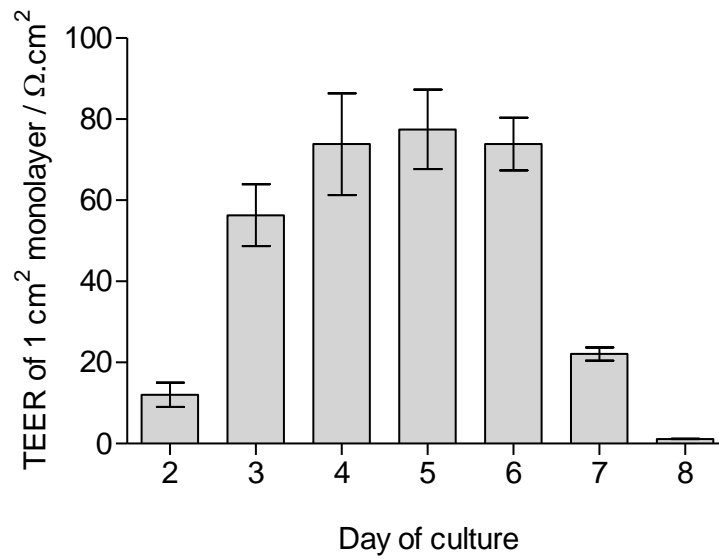
Figure 3.7: TEERs of rat PTC monolayer cultured on Transwell filter support.

Resistance of an empty Transwell filter support was found to be 90 Ω. TEER of the rat PTC monolayer was negligible at day 1 of culture (result not shown), but an average of 12.01 ± 3.01 $\Omega.cm^2$ was measured at day 2. The TEER went up to 56.31 ± 7.61 $\Omega.cm^2$ at day 3 and 73.85 ± 9.71 $\Omega.cm^2$ at day 4, before peaking at day 5 with 77.48 ± 12.72 $\Omega.cm^2$. Day 6 saw a decrease in the TEER to 73.89 ± 6.51 $\Omega.cm^2$. Thereafter, the TEER decreased even further to 22.1 ± 5.47 $\Omega.cm^2$ and 1.1 ± 0.51 $\Omega.cm^2$ at day 7 and 8, respectively. Each bar represents the mean ± SEM of 24 replicates. Figure is representative of 3 independent experiments using PTCs isolated from different rats.

3.8 TEER and mannitol paracellular permeability

TEERs of the rat PTC monolayers were correlated to the mannitol paracellular permeability (1 µM) to determine tight junction integrity of the monolayers. Figure 3.8 shows the relationship between the TEER and the mannitol appearance in a receiving chamber.

As expected, an inverse relationship between TEER and the amount of mannitol appearing in the receiving chambers was observed. Monolayers with TEER of 30 $\Omega.cm^2$ and under had poor integrity, which resulted in the large range of mannitol permeability (appearance of mannitol ranged from around 100 pmol/cm^2/hr to over 800 pmol/cm^2/hr). Monolayers with TEER of 50 $\Omega.cm^2$ and higher had a narrow range of mannitol permeability (around 20 pmol/cm^2/hr). This equated to mannitol paracellular flux of less than 10 % of the amount of mannitol used.
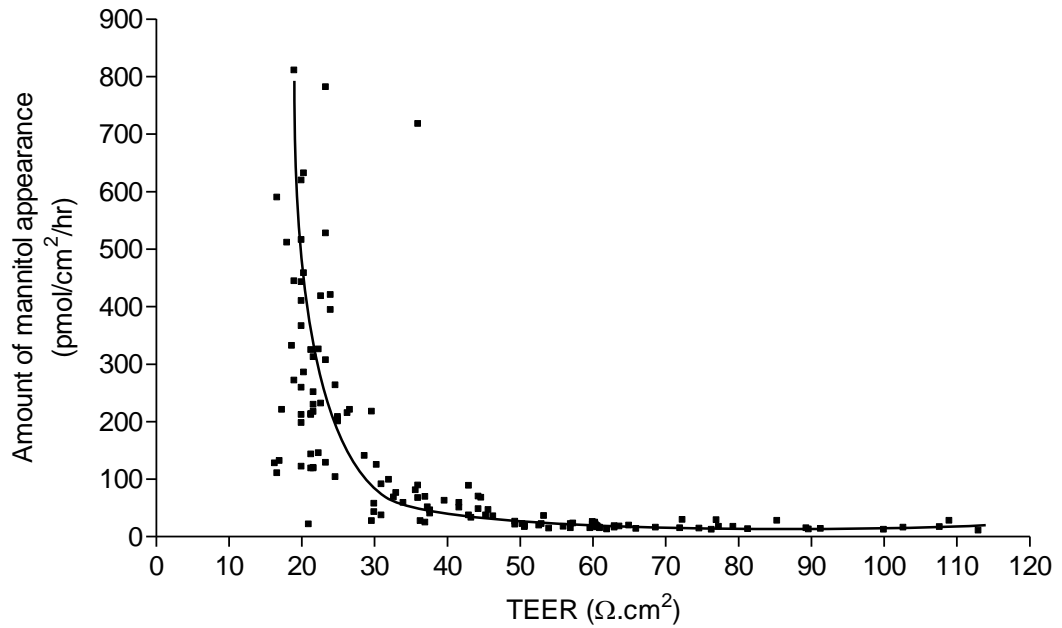
Figure 3.8: The relationship between TEER of the rat PTC monolayers and 1 μM mannitol paracellular permeability.

An inverse relationship between TEER and the amount of mannitol appearing the in receiving chamber was observed. Monolayers with TEER of 30 $\Omega.cm^2$ and under had poor integrity, which resulted in the large range of mannitol permeability (appearance of mannitol ranged from around 100 $pmol/cm^2/hr$ to over 800 $pmol/cm^2/hr$). Monolayers with TEER of 50 $\Omega.cm^2$ and higher had a narrow range of mannitol permeability (around 20 $pmol/cm^2/hr$). This equated to mannitol paracellular flux of less than 10 % of the amount mannitol used. Each dot represents the TEER of the monolayer and corresponding amount of mannitol appearance in the receiving chamber. Non-linear regression curve fit was performed to determine the relationship, which produced an equation of $y = 69505x^{-1.811}$.

3.9 Discussion

3.9.1 Isolation and culture of rat PTCs

Primary monolayer cultures are generally accepted as an excellent experimental model for the investigation of metabolic and enzymatic regulation. Many problems are more accurately solved in this system because elementary cell properties become accessible to study without being masked by other factors.

The vital component of a successful *in vitro* system is the cells that are used to represent the system. In the case of renal drug transporter investigations, primary proximal tubule cells are the perfect candidates (Bonate *et al.*, 1998). The two main methods used in isolating primary tubular cells from intact kidneys are either through a mechanical or an enzymatic approach (Sharpe, 1988; Boogaard *et al.*, 1990a). The mechanical approach to obtain renal cells involves mincing the kidney into small pieces and sieving them through a cell strainer (Boogaard *et al.*, 1990a). Although this method is ideal for the isolation of the glomeruli, the yield of other cell types, especially proximal tubule cells, is low and this technique is rarely used (Boogaard *et al.*, 1990a). A more effective way for acquiring tubule cells is via enzymatic digestion using collagenase (Boogaard *et al.*, 1989). An amalgamation of the two methods is used to isolate tubular cells from rat kidneys in this project; renal cortex is broken by mechanical means into small renal tissue fragments before they are subjected to collagenase digest.

Whilst this approach has been published (Brown *et al.*, 2008), the protocol was optimised for the isolation of human PTCs, and it needed to be adapted to the isolation of rat PTCs to ensure good yield and cell viability. The first consideration was the amount of collagenase to be used and the exposure time of the tissue to the collagenase. A range of concentrations of collagenase were tested in the isolation process to identify a concentration along with an incubation time that would provide a good yield. As expected, the more collagenase was used and longer the period of incubation, the higher the cell yield. Figure 3.1 shows that when 35 µg of collagenase for every gram of rat kidney cortex tissue was incubated for one and a half hours, the yield was over 14 million cells. However, when these cells were cultured, their abilities to propagate were not as great as cells isolated using lower concentrations of collagenase (Figure 3.2). PTCs that

propagated most after 6 days of culture those isolated with the lowest concentration of collagenase at fixed incubation time. This suggests that cell viability, by proxy of the ability to propagate, had an inverse relationship with the amount of collagenase it was exposed to.

The collagenase used in the isolation process contained a mixture of proteases, and high concentrations have been known to affect cell viability (Boogaard *et al.*, 1990a). This may explain why using concentrations of above 30 µg/g of tissue produced fewer viable cells. The solution to the problem was to use the lowest concentration of collagenase that would give the highest yield of viable cells. Based on the initial experiments, collagenase concentration of 25 µg/g of tissue at exposure time of one and a half hours gave the highest yield of viable cells, and was selected as the concentration for all subsequent isolation of rat PTCs.

This process of cell isolation would produce a mixture of cell types and a method of cell separation and purification was needed. This project used the technique of equilibrium or isopycnic centrifugation (Sharpe, 1988) to separate intact renal cells from denser erythrocytes and leukocytes, and cellular debris. Isopycnic centrifugation is a form of density gradient centrifugation that works on the principle that a cell will sediment to an equilibrium position in the gradient where the gradient density is equal to the density of the cell when a cell mixture is loaded on top of a discontinuous density gradient and centrifuged (Pertoft *et al.*, 1977; Sharpe, 1988). Although this allowed effective separation of tubule cells from cellular debris, the population of isolated cells are not pure PTCs as they would contain proximal tubule, distal tubules and collecting ducts (Curthoys and Bellemann, 1979; Boogaard *et al.*, 1990a). However, the proportion of tubule cells could be maximised by selecting only the kidney cortex for the isolation process. It had also been shown that PTCs were among the first cells to adhere to culture flaks and this fact could be used to further select for these alone (Curthoys and Bellemann, 1979; Gesek *et al.*, 1987). Indeed, media on cell culture platforms seeded with freshly isolated rat PTCs were changed after 24 hours of seeding, with which unadhered cells were removed, leaving a higher proportion of proximal tubule cells. Should the need for pure PTCs arise, immunomagnetic separation developed by Baer *et al.* could be used to separate the different cell type culture (Baer *et al.*, 1997).

Freshly isolated PTCs in the form of single cells of around 40 µm in diameter were grown on various cell culture platforms. Their growth was monitored visually using a phase contrast microscope where possible. The culture medium used was a recognised renal epithelial growth medium which comprised of several supplements and growth factors in the basal medium of DMEM/Ham's F-12 (Ltd, 2014). The composition of the supplements had been optimised for primary renal cell lines, and upon recommendation by the industry sponsor of this project, mouse epithelial growth hormone was used to tailor to the species of rat.

As mentioned in Chapter 3.4, the different stages of the isolated rat PTC growth were observed in culture over a period of eight days. Cobblestone-like morphology characteristic of many epithelial cells was evident in the rat PTCs after five days of culture. Soon after day 6, the cell number dropped and the morphology exhibited was that of apoptotic cells. Apoptosis of the cells occurred regardless of how many times the culture medium was changed. While overcrowding of the PTCs was suggested as a cause for the programmed cell death, lowering of the seeding density of rat PTCs did not see improvement in longevity of the cells; the cells still exhibited an apparent apoptotic morphology after day 6 or 7 before confluency was achieved (data not shown). Further tests would need to be carried out to verify apoptosis. Nonetheless, this initial study still suggested an inherent property of the rat PTCs that prevented it from proliferating after 6 or 7 days in culture. Because of this, rat PTCs older than day 6 were not used in experiments to ensure robustness of the data generated.

Another inherent property of the isolated rat PTC was poor adherence to plastic. The reason behind rat PTC poor adherence is still poorly understood, though poor adherence of this and other cell types has been documented in several publications (Hynes, 1987; Mendrick *et al.*, 1990; Knaggs, 1992). The mechanism of cell adherence by freshly isolated rat PTCs were investigated by Mendrick *et al.* (Mendrick *et al.*, 1990). It was found that glycoprotein gp330 on the surface of rat epithelial cells played an important role in the attachment of the cell to extracellular matrix such as collagen and fibronectin. On collagen-coated plastic surfaces, adherence of rat PTCs were significantly increased (Figure 3.4), suggesting the limiting factor was not the lack of expression of cell surface glycoprotein gp330, but the absence of a matrix for the anchoring of the cells via

the glycoprotein. All cell culture platforms were thus coated with collagen prior to rat PTCs seeding.

3.9.2 Preservation of rat PTC

Preservation of surplus rat PTCs was considered in this project. The clear advantage to preserving surplus rat PTCs was the creation of a stock allowing these cells to be used as and when needed. This would save on costs as the number of rats and amount of reagents and materials used during cell isolation would be lowered. In addition to lowering the cost, the use of fewer rats is in line with the principles of 3Rs and should be encouraged (Russell and Burch, 1959).

Of the several methods of cell preservation, cryopreservation and storing of cells in solid medium were investigated. Cryopreservation involves suspending cells in a serum rich medium containing a cryoprotectant, usually DMSO, to protect the cells from rupture by the formation of ice crystals, before controlled freezing to temperatures below -135 ˚C. In theory, the cells could be kept in this state of suspension for an indefinite period of time. However, when performed on isolated rat PTCs, the cells were unable to proliferate after thawing. The reduction in rat PTC viability may be due to the harshness of the cryopreservation techniques; the process uses cytotoxic organic solvent (DMSO) at high concentration. Indeed, unsuitability of cryopreservation of primary cells has been documented. The thawed cells often have reduced viability, and at times lose drug transporter expression altogether (Alexandre *et al.*, 2002; Badolo *et al.*, 2011).

The other method of preservation considered was the use of solid medium to suspend isolated rat PTCs. SureTran is the proprietary medium used and its components remain undisclosed by its manufacturer, Abcellute Ltd. The medium is known to be gelatinous at temperatures below 10 ˚C and cells stored in this medium could be considered quiescent at this phase. (Palmgren *et al.*, 2013) published a study in which they found SureTran to be ideal in storing freshly isolated hepatocytes for a short period of time. They were able to prepare and maintain hepatocytes in SureTran reasonably well for up to 4 days post cell isolation, but cell viability declined thereafter. Rat PTC viability, on the other hand, decreased significantly after 48 hours (Figure 3.5). Cells cultured from freshly isolated rat PTCs and PTCs stored for 24 hours in SureTran were used in experiments to examine any changes in cell functions. Substrate kinetic

experiments using Hoechst 33342 as the fluorescence substrate of Mdr1 showed saturable kinetics in both sets of cells with similar V_{max} values (Figure 3.6). However, a difference in K_m was evident which suggests variability in the expression of Mdr1 transporter between the two sets of cells. From these initial data, it was decided that preservation of freshly isolated rat PTCs may not yet be feasible, and for robustness of the data for the project, isolation of rat PTCs as and when the cells were needed was more pragmatic.

3.9.3 Rat PTC monolayer layer and its integrity

Ex vivo primary epithelial cells are known to dedifferentiate. A well known example is exhibited in human primary epithelial airway cells. When cultured on flat plastics, these cells assume a poorly differentiated state with a "squamous" phenotype. However, when these cells were allowed to grow under a polarised condition, such as on a Transwell filter support, the morphology and functions were more representative of *in vivo* conditions (Fulcher *et al.*, 2005; Randell *et al.*, 2011). Other studies have also shown proximal tubular cells grown on Transwell filter support maintained a differentiated state with expression of an array of functional drug transporters. For instance, Lash *et al.* showed better protein expression and functional activity of many drug transporters when human primary tubule cells were cultured on Transwell filter support (Lash *et al.*, 2006). It is reckoned the polycarbonate filter allows the cells to be polarised and bathed in medium from the apical and basolateral sides, replicating the physiology of the cells *in vivo*, and hence allowing maintaining their differentiated state (Fulcher *et al.*, 2005). With that in mind, to reinstate the formation of rat PTC epithelial barrier characteristics, the cells were cultured on Transwell filter support.

A good indicator of the integrity of the monolayer, and indirectly the viability of the cells, was the TEER of the monolayer (Gochoco *et al.*, 1994). TEER is a well-recognised parameter to examine cell monolayer integrity (Bonsdorff *et al.*, 1985). The TEER of rat PTCs grown on Transwell filter support increased from 12.01 ± 3.01 $\Omega.cm^2$ on day 2 of culture, to a plateau of around 77 $\Omega.cm^2$ for several days, an indication of monolayer formation. Thereafter, the TEER decreased rapidly, with negligible resistance after day 8 (Figure 3.7). The resistance did not improve with a change of medium, with which TEER of Caco-2 monolayers were shown to be revived (Mukherjee *et al.*, 2004). The pattern of the TEER values exhibited

by the cells corresponded with results that show the short life span of these rat PTCs, further supporting the stance of not using these cells after 6 days in culture. TEER of around 70 $\Omega.cm^2$ are typical of proximal tubule epithelium, though *in vivo* the TEER of more distal segments of the nephron is sometimes several folds higher (Seely, 1973; Bello-Reuss, 1986).

To investigate the "leakiness" of the epithelium, mannitol paracellular permeability across the rat PTC monolayers was performed. 1 µM of mannitol was added on one side of a rat PTC monolayer and its appearance on the receiving side was measured after an hour, and the amount of mannitol correlated to the TEER (Figure 3.8). As expected, a general trend of the higher the TEER, the lower the permeability was observed.

The permeability properties of the rat PTC monolayers have been primarily determined by the patterns of expression of cell adhesion proteins at the junctions between cells. It was shown that N-cadherin and claudin-2 were the predominant tight junction proteins in the proximal tubule *in vivo* (Hirsch and Noske, 1993), and there was evidence to indicate that the leaky phenotype of the proximal epithelium may be due to the latter (Furuse *et al.*, 1999).While there was leakage of mannitol in rat PTC monolayers, the monolayer was deemed, to a certain extent, to be able to act as a barrier to restrict the paracellular movement of solutes. Depending on the nature of the experiments with which these rat PTC monolayers were used, their TEER values and mannitol paracellular permeability were assessed together to determine if the monolayers were suitable for said experiment. A criterion for disregarding a monolayer's inclusion in the experiment was if its TEER was below 60 $\Omega.cm^2$. For transepithelial transport experiments, concomitant administration of mannitol with the substrate of interest would provide an indication of monolayer "leakiness" and use information could be used to correct for true transport of substrate across the monolayer.

3.10 Summary

The isolation and culture of rat PTCs has been optimised, with the basic parameters of growth and viability assessed. Further characterisation of the rat PTCs was needed to determine its suitability as a robust model for drug-drug interaction studies, which will be addressed in Chapter 4.

Chapter 4

Characterisation of Rat PTCs

4.1 Chapter overview

This chapter highlights the results from the characterisation of rat proximal tubule cells (PTCs) at the mRNA level and function level. The following is discussed:

- The specificity of ten pairs of in-house designed primers to ten different membrane transporters that are deemed important in drug transporter studies.

- The quantification of the changes in mRNA expression levels of the ten transporters between freshly isolated rat PTCs, rat PTCs cultured on plastics, and rat PTCs cultured on Transwells.

- The functional expression of Mdr1, Bcrp and Mrps in rat PTCs cultured on plastics.

- The functional expression of Oct2 in rat PTCs cultured on plastics.

- The functional expression of lactate in rat PTCs cultured on Transwells.

- The development of a novel technique to measure the activity of Mdr1 and Mrps simultaneously.

4.2 Total cell RNA purity and integrity

Total cell RNA was isolated from freshly isolated rat PTCs, rat PTCs that had been cultured on plastics, and rat PTCs that had been cultured on Transwell filter support. The purity of all the isolated RNA samples were assessed and only those that exhibited A_{260}/A_{280} of at least 1.8 and A_{260}/A_{230} of 2.1 were used in downstream applications. All RNA samples also had a concentration of at least 100 μg/ml. The integrity of all the RNA samples was assessed before use in downstream applications. Figure 4.1 shows the electropherograms produced when 1 μl RNA samples were run on a BioAnalyzer chip.

The peak on the left of the trace of the electropherogram represents the 28S ribosomal subunit from total cell RNA, and the peak on the right represents the 18S rRNA subunit. All RNA samples contained ribosomal subunits that elute at the same time of around 45 seconds and 50 seconds for the 18S and 28S subunits, respectively. The ratio of 28S/18S gave at least 2.1 in all RNA samples. Proprietary software algorithm was also performed to give a RNA integrity number on all the samples (Schroeder *et al.*, 2006). All samples had RIN of 8 and above.
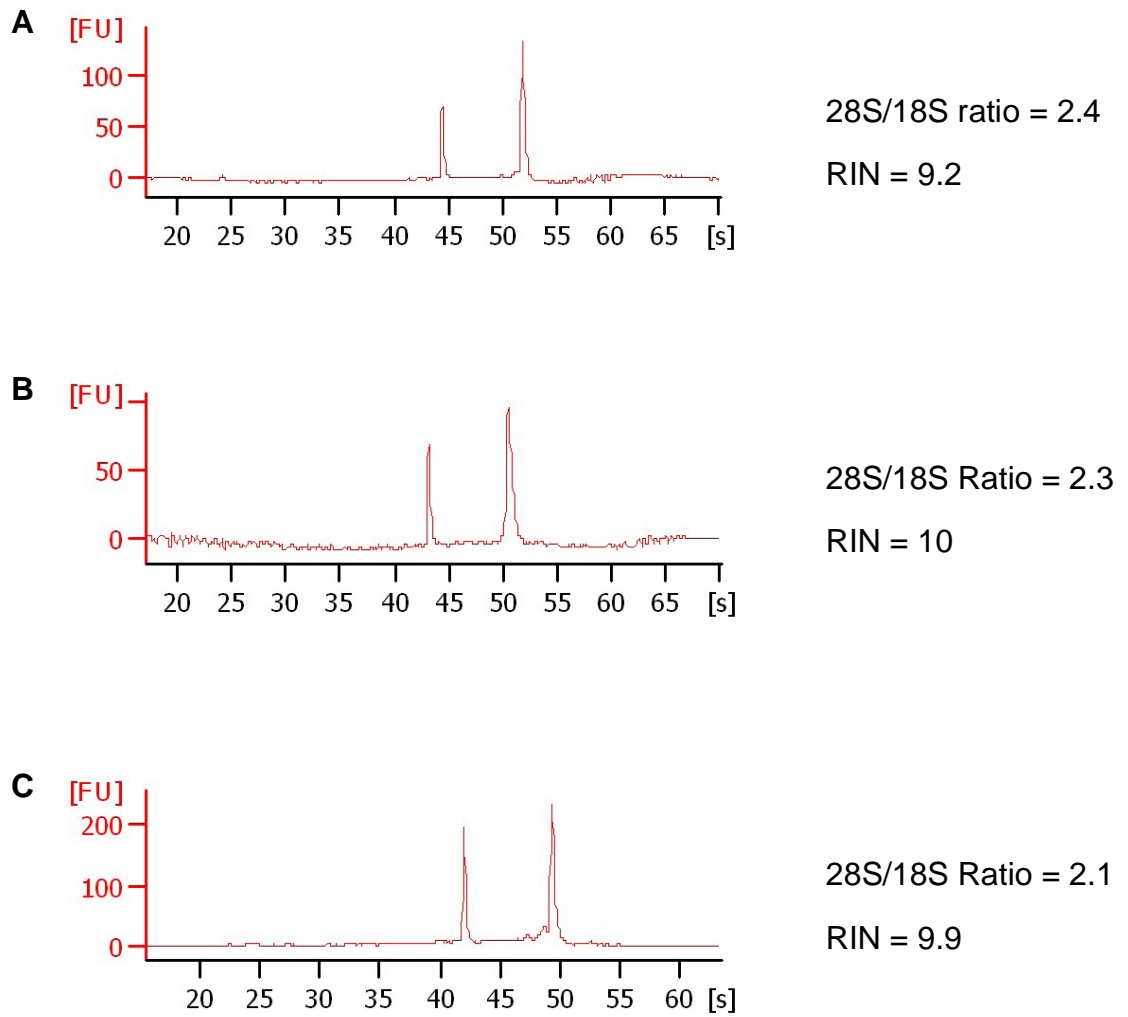
Figure 4.1: Representative electropherograms produced by Agilent BioAnalyzer 2100 with 1 μl RNA samples.

RNA samples were from (A) freshly isolated rat PTCs, (B) rat PTCs cultured on Transwell insert supports for 6 days, and (C) rat PTCs cultured on plastic for 6 days. All RNA samples used in downstream applications had 28S/18S ratio of 2.1 and above, and RNA integrity number of at least 8.

4.3 PCR screening of drug transporters in rat PTCs

The expression of several key transporters was investigated using endpoint PCR. The PCR products were visualised on 1.5 % agarose gels stained with ethidium bromide.

Figure 4.2 shows the separation of PCR products on the gels. Lane 1 of each of the gel was loaded with DNA ladder. Lane 2 was loaded with PCR product amplified using cDNA template from freshly isolated rat PTCs. Lanes 3 and 4 was loaded with PCR product amplified using cDNA template from rat PTCs cultured for 6 days on Transwell filter support, and rat PTCs cultured for 6 days on plastic, respectively. Lane 5 shows the negative control for the PCR. Endpoint PCR was also performed using Gapdh primers. The gel for Gapdh shows one band in each of the lanes with equal intensity, indicating the amount of cDNA template used was comparable across all samples.

4.3.1 Mdr1

Figure 4.2A shows the gel with PCR products amplified using primers designed to amplify both Mdr1a and Mdr1b cDNA (collective referred to as Mdr1 in this thesis). A band of approximately 148 base pairs was detected in lanes 2, 3 and 4, but the intensities between different samples are different. This band was of the expected size for the Mdr1 specific primers used. Sequencing of the products showed 100 % identity to Mdr1. No bands were detected in the negative control.

4.3.2 Bcrp

Figure 4.2B shows the gel with PCR products amplified using Bcrp specific primers. A band of the expected size for Bcrp (95 base pairs) was detected in all the sample lanes. Sequencing of the products showed 100 % identity to Bcrp. The intensity of each of the band in lanes 2, 3 and 4 was similar. No bands were detected in the negative control.

4.3.3 Mrp2

Figure 4.2C shows the gel with PCR products amplified using Mrp2 specific primers. A band of approximately 169 base pairs was detected in lanes 2, 3 and 4, which was the expected size of the PCR product. Sequencing of the products

showed 100 % identity to Mrp2. The intensity of the band in lane 2 was greater than in lane 3 or 4. The intensity of each of the band in lanes 3 and 4 was similar and no bands were detected in the negative control.

4.3.4 Oat1

Figure 4.2D shows the agarose gel with PCR products amplified using Oat1 specific primers. Lanes 2, 3 and 4 had a band of approximately 119 base pairs. Sequencing of the products showed 100 % identity to Oat1. The intensity of each of the band in lanes 2, 3 and 4 was similar. No bands were detected in the negative control.

4.3.5 Oct2

Figure 4.2E shows the gel with PCR products of approximately 127 base pairs amplified using Oct2 specific primers in all the sample lanes. Sequencing of the products showed 100 % identity to Oct2. The intensity of the band was greatest in lane 2 and similar between lanes 3 and 4. No bands were detected in the negative control.

4.3.6 Oatp4c1

Figure 4.2F shows the gel with PCR products amplified using Oapt4c1 specific primers. A band of approximately 101 base pairs was detected in lanes 2, 3 and 4, which was the expected size for the Oatp4c1 specific primers used. Sequencing of the products showed 100 % identity to Oatp4c1. The intensity of the band in lane 2 was greater than in lane 3, which in turn was greater than lane 4. No bands were detected in the negative control.

4.3.7 Slc2a9

Figure 4.2G shows the gel with PCR products of around 151 base pairs in lanes 2, 3 and 4 amplified using Slc2a9 specific primers. The size of the product was the expected size for of primers used and sequencing of the products showed 100 % identity to Slc2a9. The intensity of each of the band in lanes 2, 3 and 4 was similar. No bands were detected in the negative control.

4.3.8 Urat1

Figure 4.2H shows the gel with PCR products amplified using Urat1 specific primers. A band of approximately 109 base pairs was detected in lanes 2, 3 and 4, but no band was detected in the negative control. The band was of the expected size for the Urat1 specific primers used and sequencing of the products showed 100 % identity to Urat1. The intensity of the band in lane 2 was greater than in lane 3, which in turn was greater than lane 4.

4.3.9 Mate1

Figure 4.2I shows the gel with PCR products amplified using Mate1 specific primers with similar intensity bands on all sample lanes. The size of the band was around 123 base pairs. That was the expected size for the PCR product. Sequencing of the products showed 100 % identity to Mate1. No bands were detected in the negative control.

4.3.10 Mct1

Figure 4.2J shows the gel with PCR products amplified using Mct1 specific primers. A band of approximately 157 base pairs was detected in lanes 2, 3 and 4, but no band was detected in lane 5 (negative control). This band was of the expected size for the Mct1 specific primers used. Sequencing of the products showed 100 % identity to Mct1. The intensity of band in lanes 2 and 3 was greater than lane 4.
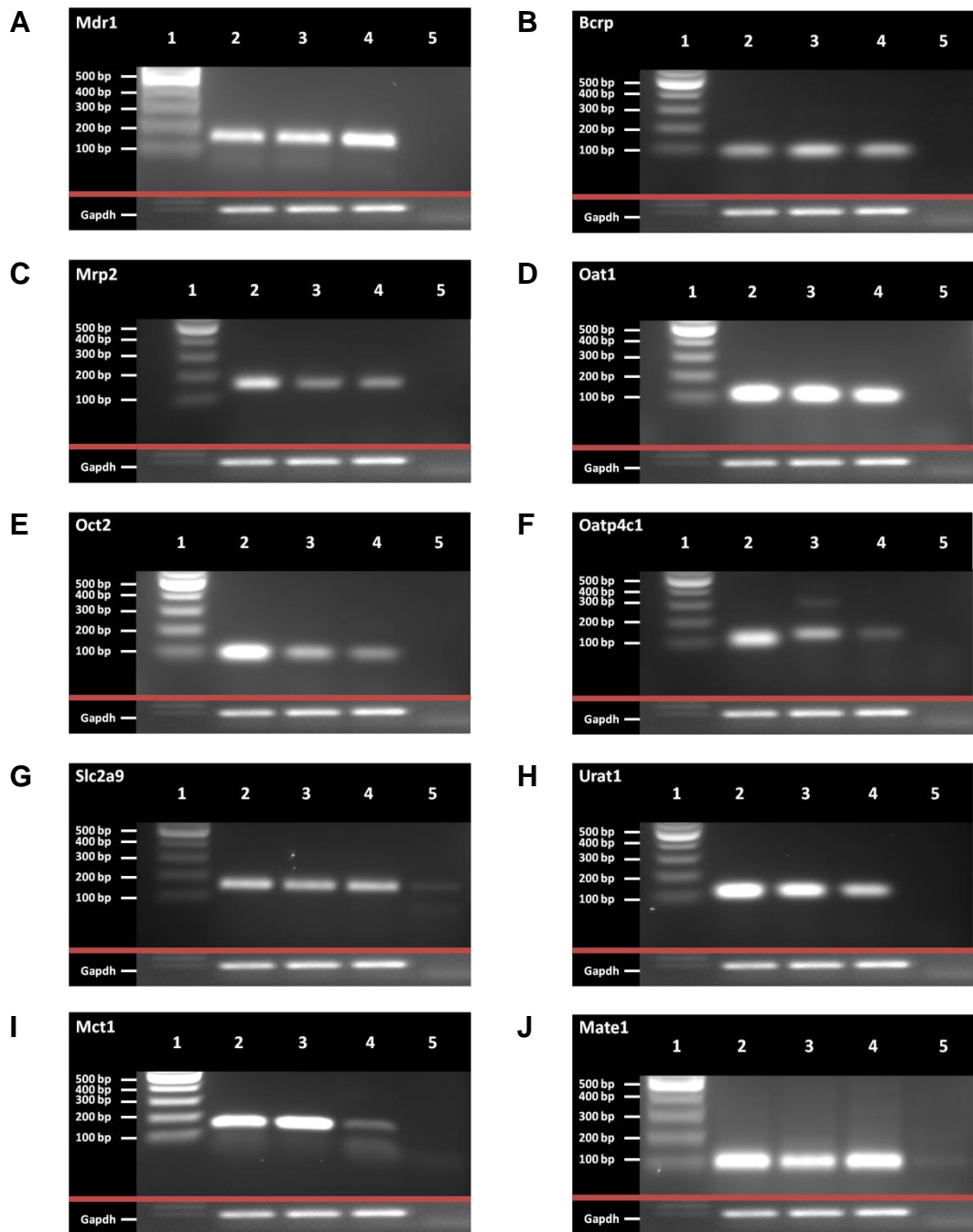
Figure 4.2: 1.5 % agarose gel showing separation of PCR products amplified using primers specific to the transporter.

The primers used were specific to (A) Mdr1, (B) Bcrp, (C) Mrp2, (D) Oat1, (E) Oct2, (F) Oatp4c1, (G) Slc2a9, (H) Urat1, (I) Mct1, and (J) Mate1. DNA ladder (lane 1), PCR products amplified using cDNA template from freshly isolated rat PTCs (lane 2), rat PTCs cultured on Transwell filter support for 6 days (lane 3), rat PTCs cultured for 6 days on plastic (lane 4), and PCR negative control (lane 5) were loaded on to the gel. Endpoint PCR was also performed for Gapdh using the same samples to ensure amount of starting cDNA template was comparable across all the samples.

4.4 Quantifying drug transporter expression changes between culture conditions

qPCR was performed to determine the change in relative mRNA expression levels of key drug transporters by rat PTCs in different culture conditions. Figure 4.3 to Figure 4.12 shows the percentage change in expression levels of drug transporters between rat PTCs cultured on Transwell filter support and rat PTCs cultured on plastic, compared with the mRNA levels of freshly isolated rat PTCs, which had been assigned as the control. The expression levels had been normalised to reference gene Gapdh expression level prior to comparison. Table 4.1 shows the summary of the percentage change in expression level when compared to the control. The data are presented as the mean percentage change in expression levels from three separate batches of RNA.

4.4.1 Mdr1

Rat PTCs cultured on Transwell filter support showed Mdr1 mRNA level was expressed at 72.81 ± 5.39 % of control, giving a 1.37-times decrease in expression (Figure 4.3, $P < 0.05$, N = 3). Mdr1 mRNA level in rat PTCs cultured on plastic was expressed at 60.25 ± 7.07 % of control, which was a 1.66-times down-regulated ($P < 0.05$, N = 3). No statistical difference was observed between Mdr1 mRNA levels of rat PTCs cultured on Transwell filter support and rat PTCs cultured on plastic.

4.4.2 Bcrp

Rat PTCs cultured on Transwell filter support showed a decrease in Bcrp mRNA level when compared to the control (24.98 ± 20.23 % of control, $P < 0.01$, N = 3, Figure 4.4). Bcrp mRNA level in rat PTCs cultured on plastic was decreased further when compared to the control (20.23 ± 6.32 %, $P < 0.05$, N = 3). No statistical difference was observed between Bcrp mRNA levels of rat PTCs cultured on Transwell filter support and rat PTCs cultured on plastic.

4.4.3 Mrp2

Rat PTCs cultured on Transwell filter support showed Mrp2 mRNA level at 37.71 ± 21.19 % of control (Figure 4.5, $P < 0.01$, N = 3). Mrp2 mRNA level in rat PTCs cultured on plastic was at 21.19 ± 10.33 % of control (4.71-times decrease, P <

0.01, N = 3) while no statistical difference was observed between Mrp2 mRNA levels of rat PTCs cultured on Transwell filter support and rat PTCs cultured on plastic.

4.4.4 Oat1

At 24.97 ± 7.51 % of control, Oat1 mRNA level of rat PTCs cultured on Transwell filter support was decreased almost 4-times (Figure 4.6, P < 0.001, N = 3). Oat1 mRNA level in rat PTCs cultured on plastic was also decreased by almost 6-times when compared to the control (16.50 ± 4.93 % of control, P < 0.001, N = 3). No statistical difference was observed between Oat1 mRNA levels of rat PTCs cultured on Transwell filter support and rat PTCs cultured on plastic.

4.4.5 Oct2

Oct2 mRNA levels of rat PTCs cultured on Transwell filter support was down-regulated to 36.98 ± 17.71 % of control (Figure 4.7, P < 0.01, N = 3). Mrp2 mRNA level in rat PTCs cultured on plastic was also down regulated to 27.68 ± 16.88 % of control (P < 0.01, N = 3). No statistical difference was observed between Oct2 mRNA levels of rat PTCs cultured on Transwell filter support and rat PTCs cultured on plastic.

4.4.6 Oatp4c1

Oatp4c1 mRNA level of rat PTCs cultured on Transwell filter support and rat PTCs cultured on plastic were at 22.81 ± 10.68 % (Figure 4.8, P < 0.01, N = 3) and 12.46 ± 7.57 % of control (P < 0.01, N = 3), respectively. No statistical difference was observed between Oatp4c1 mRNA levels of rat PTCs cultured on Transwell filter support and rat PTCs cultured on plastic.

4.4.7 Slc2a9

Rat PTCs cultured on Transwell filter support showed Slc2a9 mRNA level was expressed at 23.25 ± 5.61 % of freshly isolated rat PTCs, giving a 4.30-times decrease in expression (Figure 4.9, P < 0.05, N = 3). Slc2a9 mRNA level in rat PTCs cultured on plastic was shown to express at 35.74 ± 16.91 % of freshly isolated rat PTCs. No statistical difference was observed between Slc2a9 mRNA levels of rat PTCs cultured on Transwell filter support and rat PTCs cultured on plastic.

4.4.8 Urat1

Rat PTCs cultured on Transwell filter support showed Urat1 mRNA level was expressed at 19.05 ± 6.20 % of control (Figure 4.10, $P < 0.001$, N = 3). Urat1 mRNA level in rat PTCs cultured on plastic was expressed at 25.17 ± 4.53 % of control, which equated to a 3.97-times decrease when compared to the control ($P < 0.001$, N = 3). No statistical difference was observed between Urat1 mRNA levels of rat PTCs cultured on Transwell filter support and rat PTCs cultured on plastic.

4.4.9 Mate1

Rat PTCs cultured on Transwell filter support showed Mate1 mRNA level was expressed at 28.09 ± 6.00 % of control (Figure 4.11, $P < 0.01$, N = 3), whereas Mate1 mRNA level in rat PTCs cultured on plastic was expressed at 18.93 ± 9.44 % of the control ($P < 0.01$, N = 3). No statistical difference was observed between Mate1 mRNA levels of rat PTCs cultured on Transwell filter support and rat PTCs cultured on plastic.

4.4.10 Mct1

At 26.39 ± 11.77 % of control, Mct1 mRNA level in rat PTCs cultured on Transwell filter support showed a 3.79-times decrease in expression (Figure 4.15, $P < 0.05$, N = 3). Similar, Mrp2 mRNA level in rat PTCs cultured on plastic was down-regulated by 4.15-times (18.93 ± 9.44 % of control, $P < 0.05$, N = 3). No statistical difference was observed between Mct1 mRNA levels of rat PTCs cultured on Transwell filter support and rat PTCs cultured on plastic.
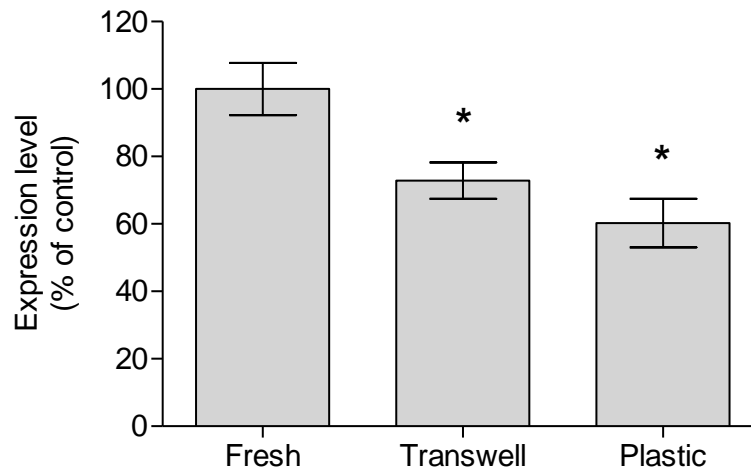
Figure 4.3: Percentage change in relative expression levels of Mdr1 by freshly isolated rat PTCs, rat PTCs cultured on Transwell filter support for 6 days, and rat PTCs cultured on plastic for 6 days.

Rat PTCs cultured on Transwell filter support showed Mdr1 mRNA level was expressed at 72.81 ± 5.39 % of control, down-regulated by 1.37-times. Mdr1 mRNA level in rat PTCs cultured on plastic was expressed at 60.25 ± 7.07 % of control. No statistical difference was observed between Mdr1 mRNA levels of rat PTCs cultured on Transwell filter support and rat PTCs cultured on plastic. The expression levels had been normalised to reference gene Gapdh. Each bar represents the mean ± SEM percentage change from three batches of RNA. One-way ANOVA statistical test was performed on the data set to determine significance. $*, P < 0.05$.
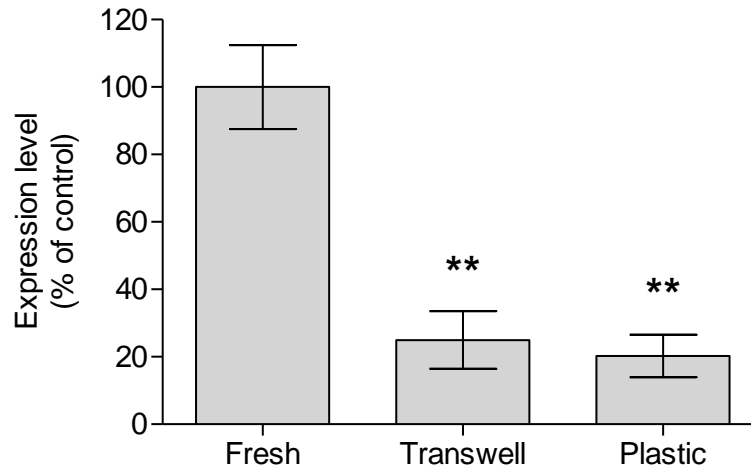
Figure 4.4: Percentage change in relative expression levels of Bcrp by freshly isolated rat PTCs, rat PTCs cultured on Transwell filter support for 6 days, and rat PTCs cultured on plastic for 6 days.

Rat PTCs cultured on Transwell filter support showed Bcrp mRNA level was at 24.98 ± 20.23 % of the control. Bcrp mRNA level in rat PTCs cultured on plastic was expressed at 20.23 ± 6.32 % of control. No statistical difference was observed between Bcrp mRNA levels of rat PTCs cultured on Transwell filter support and rat PTCs cultured on plastic. The expression levels had been normalised to reference gene Gapdh. Each bar represents the mean ± SEM percentage change from three batches of RNA. One-way ANOVA statistical test was performed on the data set to determine significance. **, P < 0.01.
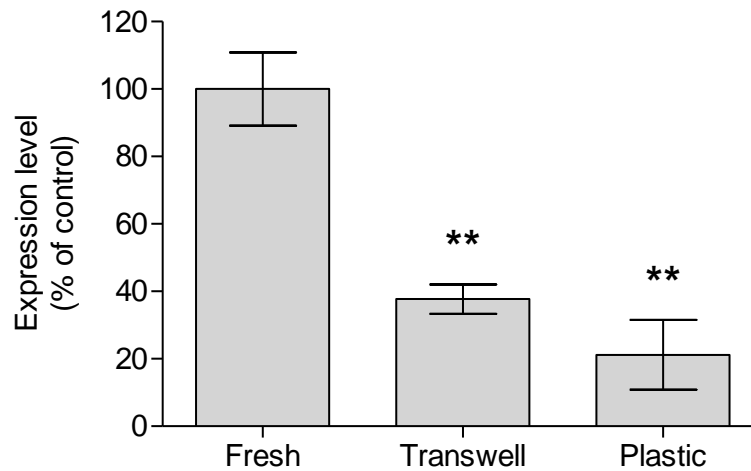
Figure 4.5: Percentage change in relative expression levels of Mrp2 by freshly isolated rat PTCs, rat PTCs cultured on Transwell filter support for 6 days, and rat PTCs cultured on plastic for 6 days.

Rat PTCs cultured on Transwell filter support showed Mrp2 mRNA level was 2.65-times less when compared to the control (37.71 ± 21.19 %). Mrp2 mRNA level in rat PTCs cultured on plastic was also down-regulated by 4.71-times when compared to the control (21.19 ± 10.33 %). No statistical difference was observed between Mrp2 mRNA levels of rat PTCs cultured on Transwell filter support and rat PTCs cultured on plastic. The expression levels had been normalised to reference gene Gapdh. Each bar represents the mean $\pm$ SEM percentage change from three batches of RNA. One-way ANOVA statistical test was performed on the data set to determine significance. **, P < 0.01.
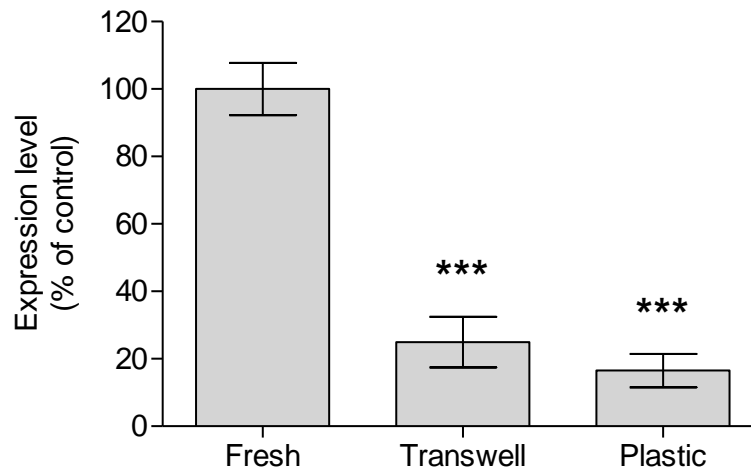
Figure 4.6: Percentage change in relative expression levels of Oat1 by freshly isolated rat PTCs, rat PTCs cultured on Transwell filter support for 6 days, and rat PTCs cultured on plastic for 6 days.

Oat1 mRNA level in rat PTCs cultured on Transwell filter support showed down-regulation of 4.00-times (24.97 ± 7.51 % of control). Oat1 mRNA level in rat PTCs cultured on plastic was also down regulated to 16.50 ± 4.93 % of control. No statistical difference was observed between Oat1 mRNA levels of rat PTCs cultured on Transwell filter support and rat PTCs cultured on plastic. The expression levels had been normalised to reference gene Gapdh. Each bar represents the mean ± SEM percentage change of three batches of RNA. One-way ANOVA statistical test was performed on the data set to determine significance. ***, P < 0.001.
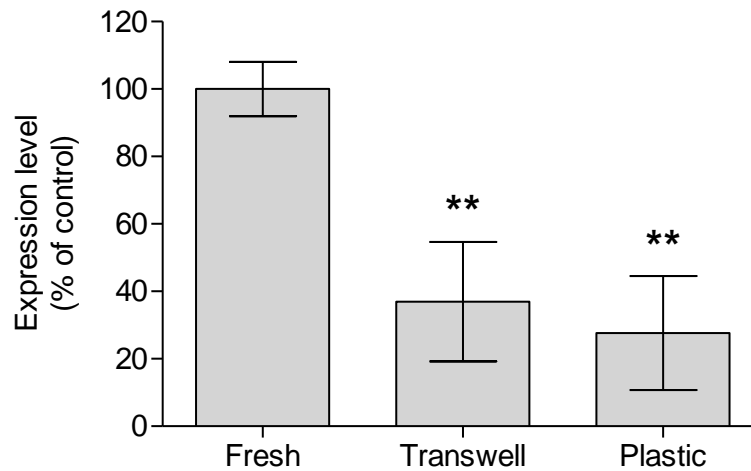
Figure 4.7: Percentage change in relative expression levels of Oct2 by freshly isolated rat PTCs, rat PTCs cultured on Transwell filter support for 6 days, and rat PTCs cultured on plastic for 6 days.

At 36.98 ± 17.71 % of control, Oct2 mRNA level in rat PTCs cultured on Transwell filter support was down-regulated. Oct2 mRNA level in rat PTCs cultured on plastic was also down-regulated to 27.68 ± 16.88 % of control. No statistical difference was observed between Oct2 mRNA levels of rat PTCs cultured on Transwell filter support and rat PTCs cultured on plastic. The expression levels had been normalised to reference gene Gapdh. Each bar represents the mean ± SEM percentage change of three batches of RNA. One-way ANOVA statistical test was performed on the data set to determine significance. **, $P < 0.01$.
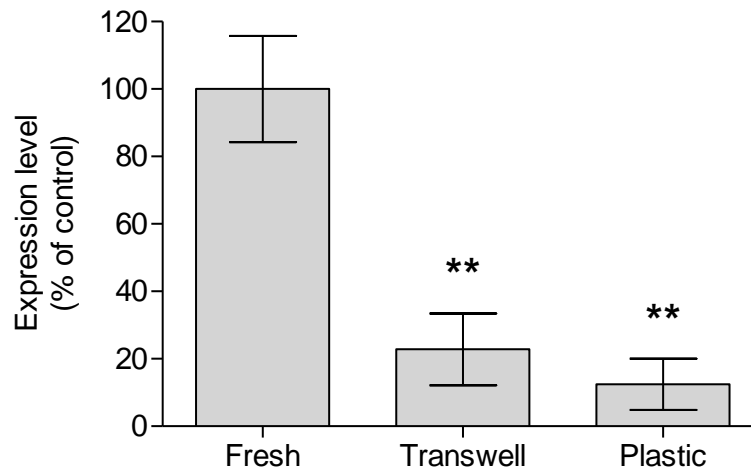
Figure 4.8: Percentage change in relative expression levels of Oatp4c1 by freshly isolated rat PTCs, rat PTCs cultured on Transwell filter support for 6 days, and rat PTCs cultured on plastic for 6 days.

Rat PTCs cultured on Transwell filter support showed Oatp4c1 mRNA level was expressed at 22.81 ± 10.68 % of control. Oatp4c1 mRNA from Rat PTCs cultured on plastic was even lower at 12.46 ± 7.57 % of control, though no statistical difference was observed between two culture conditions. The expression levels had been normalised to reference gene Gapdh. Each bar represents the mean ± SEM percentage change of three batches of RNA. One-way ANOVA statistical test was performed on the data set to determine significance. **, $P < 0.01$.
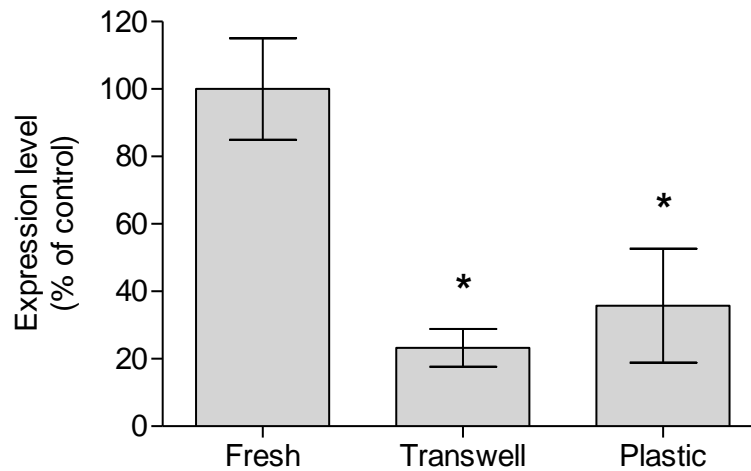
Figure 4.9: Percentage change in relative expression levels of Slc2a9 by freshly isolated rat PTCs, rat PTCs cultured on Transwell filter support for 6 days, and rat PTCs cultured on plastic for 6 days.

Rat PTCs cultured on Transwell filter support showed Slc2a9 mRNA level was expressed at 23.25 ± 5.61 % of control, giving a 4.30-times decrease in expression. Slc2a9 mRNA level in rat PTCs cultured on plastic also decreased, but only to 35.74 ± 16.91 % of control. No statistical difference was observed between Slc2a9 mRNA levels of rat PTCs cultured on Transwell filter support and rat PTCs cultured on plastic. The expression levels had been normalised to reference gene Gapdh. Each bar represents the mean ± SEM percentage change of three batches of RNA. One-way ANOVA statistical test was performed on the data set to determine significance. *, $P < 0.05$.
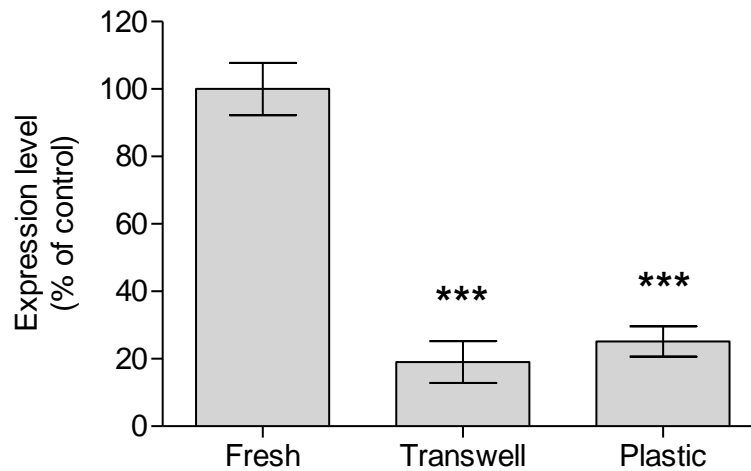
Figure 4.10: Percentage change in relative expression levels of Urat1 by freshly isolated rat PTCs, rat PTCs cultured on Transwell filter support for 6 days, and rat PTCs cultured on plastic for 6 days.

Rat PTCs cultured on Transwell filter support showed Urat1 mRNA level was down-regulated 5.25-times when compared to the control (19.05 ± 6.20 % of control). Urat1 mRNA level in rat PTCs cultured on plastic was also down-regulated by 3.97-times (25.17 ± 4.53 % of control). No statistical difference was observed between Urat1 mRNA levels of rat PTCs cultured on Transwell filter support and rat PTCs cultured on plastic. The expression levels had been normalised to reference gene Gapdh. Each bar represents the mean ± SEM percentage change of three batches of RNA. One-way ANOVA statistical test was performed on the data set to determine significance. ***, $P < 0.001$.
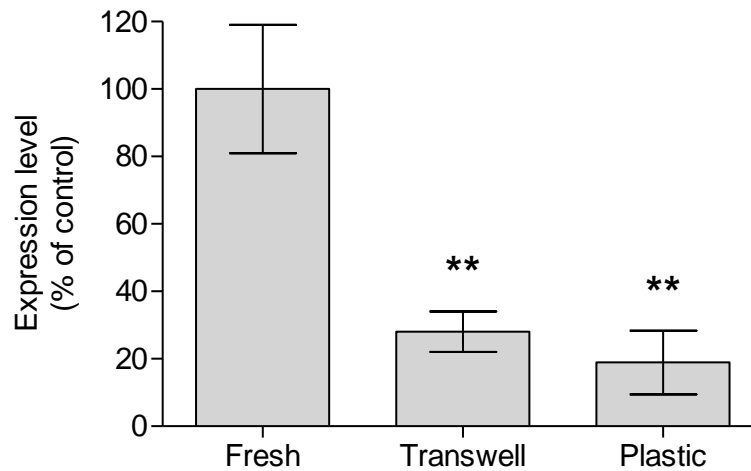
Figure 4.11: Percentage change in relative expression levels of Mate1 by freshly isolated rat PTCs, rat PTCs cultured on Transwell filter support for 6 days, and rat PTCs cultured on plastic for 6 days.

Rat PTCs cultured on Transwell filter support showed Mate1 mRNA level was expressed at 28.09 ± 6.00 % of control. Mate1 mRNA level in rat PTCs cultured on plastic was expressed at 18.93 ± 9.44 % of control. No statistical difference was observed between Mate1 mRNA levels of rat PTCs cultured on Transwell filter support and rat PTCs cultured on plastic. The expression levels had been normalised to reference gene Gapdh. Each bar represents the mean ± SEM percentage change of three batches of RNA. One-way ANOVA statistical test was performed on the data set to determine significance. **, P < 0.01.
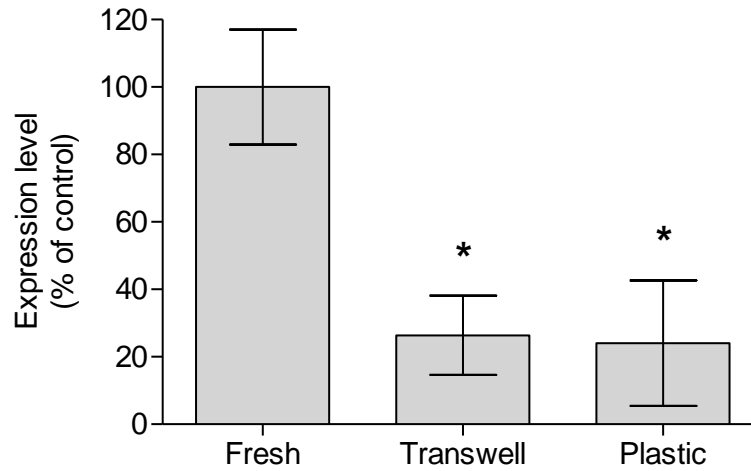
Figure 4.12: Percentage change in relative expression levels of Mct1 by freshly isolated rat PTCs, rat PTCs cultured on Transwell filter support for 6 days, and rat PTCs cultured on plastic for 6 days.

Rat PTCs cultured on Transwell filter support showed Mct1 mRNA level was expressed at 26.39 ± 11.77 % of control, and rat PTCs cultured on plastics showed mRNA level at 18.93 ± 9.44 % of control. No statistical difference was observed between Mct1 mRNA levels of rat PTCs cultured on Transwell filter support and rat PTCs cultured on plastic. The expression levels had been normalised to reference gene Gapdh. Each bar represents the mean ± SEM percentage change of three batches of RNA. One-way ANOVA statistical test was performed on the data set to determine significance. *, $P < 0.05$.

Gene	Percentage of control expression (fold difference)	
	Transwell	**Plastic**
Mdr1	72.8 ± 5.4 (1.4)	60.2 ± 7.2 (1.7)
Bcrp	24.9 ± 8.5 (4.0)	20.2 ± 6.3 (4.9)
Mrp2	37.7 ± 4.3 (2.7)	21.2 ± 10.3 (4.7)
Oat1	24.9 ± 7.5 (4.0)	16.5 ± 4.9 (6.1)
Oct1	36.9 ± 17.7 (2.7)	27.7 ± 16.9 (3.6)
Oatp4c1	22.8 ± 10.7 (4.4)	12.5 ± 7.6 (8.02)
Slc2a9	23.2 ± 5.6 (4.3)	35.7 ± 16.9 (2.8)
Urat1	19.1 ± 6.2 (5.2)	25.2 ± 4.5 (3.9)
Mate1	28.1 ± 6.0 (3.6)	18.9 ± 9.4 (5.3)
Mct1	26.4 ± 11.8 (3.8)	24.1 ± 18.6 (4.2)

Table 4.1: Summary of the change in mRNA expression levels of drug transporters in rat PTCs cultured on plastics and Transwell filter support compared to freshly isolated rat PTCs.

Expression levels are expressed as a percentage of the control. Numbers in brackets are the fold difference in expression when compared to the control. Expression levels have been normalised to Gapdh expression levels. Data are the mean ± SEM of 3 batches of RNA.

4.5 Functional expression of ABC transporters

The functional expression of ABC transporters (Mdr1, Bcrp and Mrps) was examined using fluorescent substrate retention assays. The differences in fluorescence of retained Hoechst 33342 or GSMF by rat PTCs cultured on plastic for 6 days, in the absence or presence of transporter specific inhibitors, are shown in Figure 4.13 to Figure 4.16. The figures in this section are representative of three independent experiments, and the concentrations that caused half maximal fluorescent intensity (K_m or IC_{50}) given are the mean of the three experiments.

4.5.1 Mdr1 activity

Intracellular retention of Hoechst 33342, a substrate of Mdr1, by rat PTCs was measured over a range of Hoechst 33342 concentrations. The results showed mean apparent K_m of 4.04 ± 0.60 µM (Figure 4.13A). In the presence of 5 µM CsA, an Mdr1 inhibitor, the maximum level of intracellular fluorescence remained similar, but the mean apparent K_m was significantly lower at 0.42 ± 0.06 µM (P < 0.01, N = 3). The concentration curves generated using a range of CsA concentrations upon the inhibition of 1 µM Hoechst 33342 gave mean IC_{50} value of 2.13 ± 0.48 µM (Figure 4.13B).

Another inhibitor of Mdr1 used to determine its function was GF120918. In the absence of GF120918, the mean K_m was 3.16 ± 0.36 µM. In the presence of 2 µM GF120918, the mean K_m decreased to 0.48 ± 0.05 µM (Figure 4.14A, P < 0.01, N = 3). The inhibition of Hoechst 33342 efflux by GF120918 showed mean IC_{50} of 0.19 ± 0.04 µM (Figure 4.14B).

4.5.2 Bcrp activity

Hoechst 33342 is also a substrate of Bcrp. The mean K_m of Hoechst 33342 retention by rat PTCs was 4.04 ± 0.60 µM in the absence of Ko143, a Bcrp specific inhibitor. But in the presence of 1 µM Ko143, the mean K_m was 0.23 ± 0.04 µM (Figure 4.15A, P < 0.01, N = 3). The inhibition of Hoechst 33342 efflux by Ko143 showed a mean IC_{50} of 5.48 ± 1.09 µM (Figure 4.15B).

4.5.3 Mrps activity

CMFDA metabolite, GSMF, is a substrate of Mrps. Figure 4.16A shows a linear relationship between the intracellular fluorescence intensity and the external concentration of CMFDA (mean slope of 9,728 ± 258 units/µM, r^2 = 0.62, N = 3). Intracellular fluorescence intensity was significantly increased in the presence of 10 µM MK-571 (mean slope of 15420 ± 376.7 units/µM, r^2 = 0.71, P < 0.01, N = 3). The linear increase in intracellular fluorescence relative to extracellular dye concentration was maintained with no evidence of saturation of intracellular fluorescence. In contrast, GSMF retention was dependent on MK-571 concentration. Inhibition of GSMF efflux by a range of MK-571 concentrations gave mean IC_{50} value of 1.05 ± 0.34 µM for the ability of MK-571 to inhibit GSMF efflux by Mrps (Figure 4.16B).

A

B
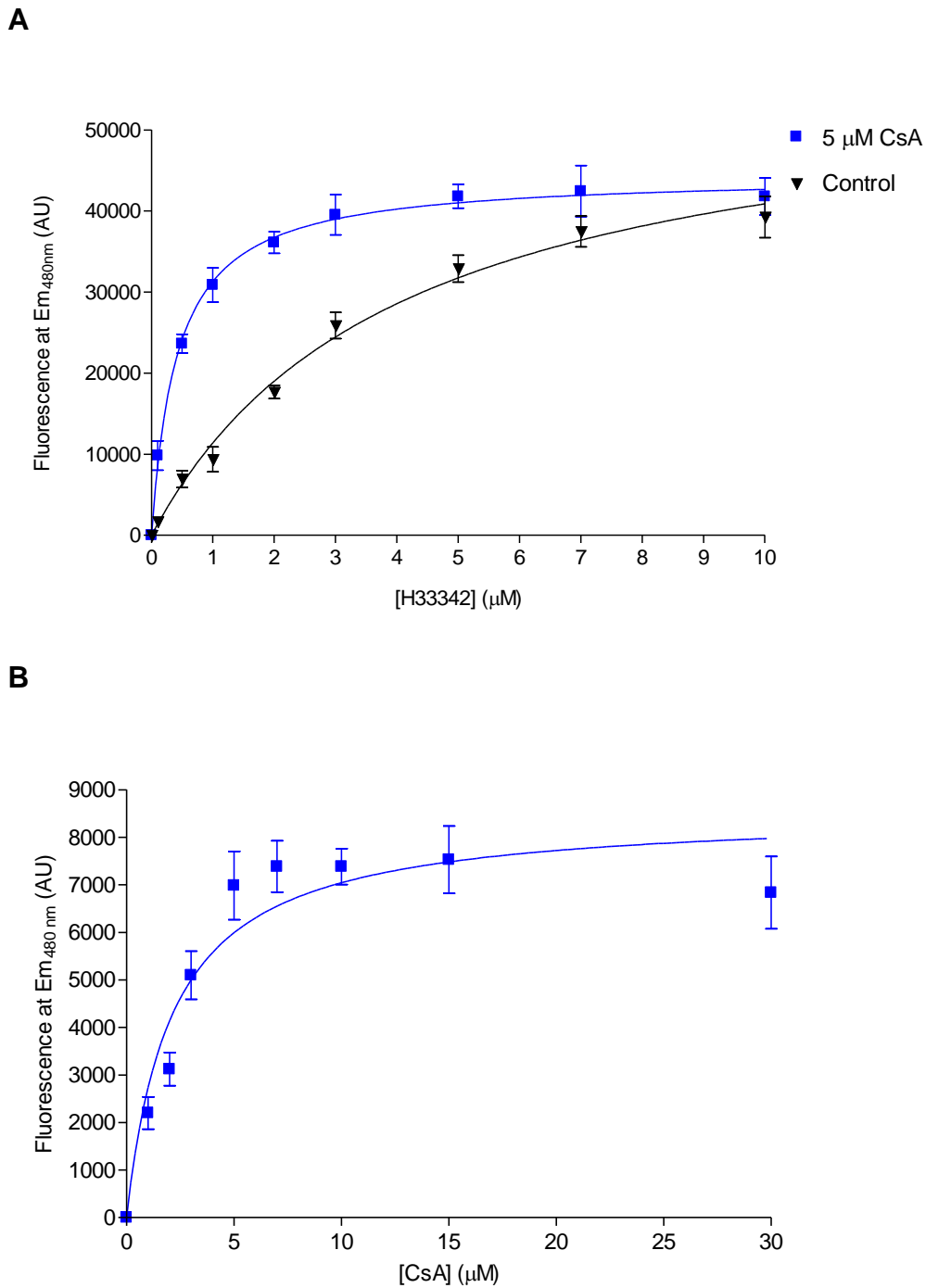
Figure 4.13: Fluorescence of retained Hoechst 33342 by rat PTCs cultured on plastic in the presence of CsA.

*(**A**) Intracellular retention of Hoechst 33342 showed a saturable kinetic with mean K_m at 4.04 ± 0.60 μM. In the presence of 5 μM CsA, the maximum level of intracellular fluorescence remained similar, but K_m was significantly lower with mean of 0.42 ± 0.06 μM. (**B**) The concentration curve for the inhibition of Hoechst 33342 efflux by CsA had a mean IC_{50} of 2.13 ± 0.48 μM. Each point represents the mean ± SEM of 6 replicates. Each figure is a representative of 3 independent experiments, and the K_m and IC_{50} values are the mean of the three experiments. Non-linear regression analysis was performed to obtain the K_m and IC_{50}.*

A
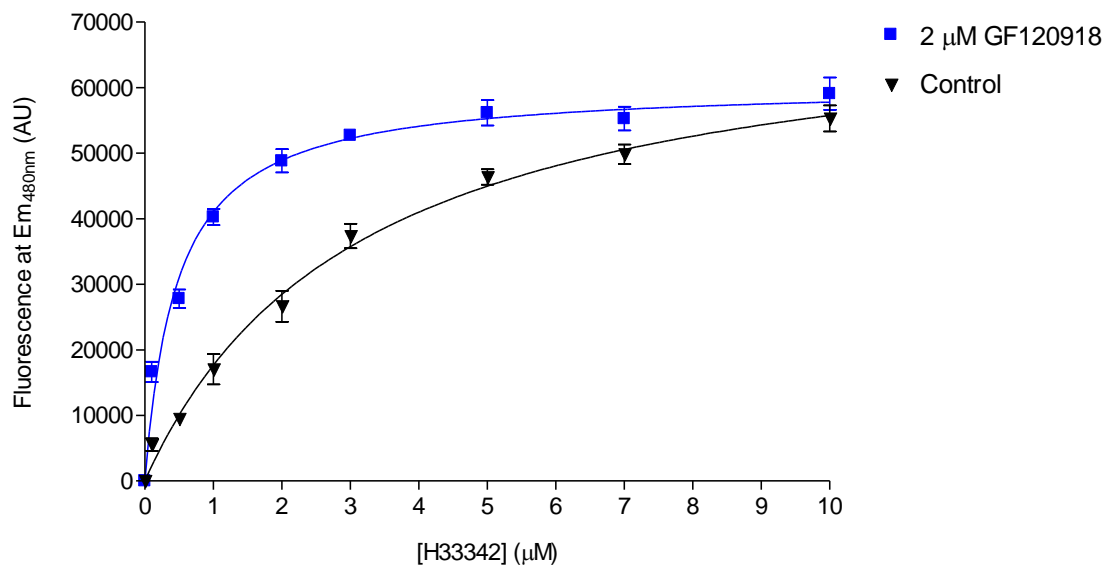
B
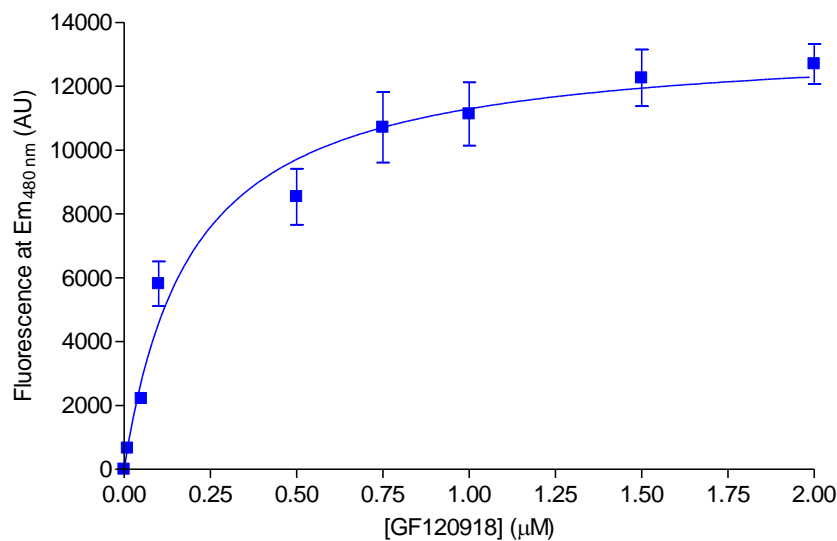
Figure 4.14: Fluorescence of retained Hoechst 33342 by rat PTCs cultured on plastic in the presence of GF120918.

(A) In the absence of GF120918, intracellular retention of Hoechst 33342 showed a saturable kinetic with K_m of 3.16 ± 0.36 µM. In the presence of 2 µM GF120918, the K_m decreased to 0.48 ± 0.05 µM. (B) The concentration curve for the inhibition of Hoechst 33342 efflux by GF120918 showed apparent IC_{50} of 0.19 ± 0.04 µM. Each dot represents the mean ± SEM of 6 replicates. Each figure is a representative of 3 independent experiments, and the K_m and IC_{50} values are the mean of the three experiments. Non-linear regression analysis was performed to obtain the K_m and IC_{50}.

A
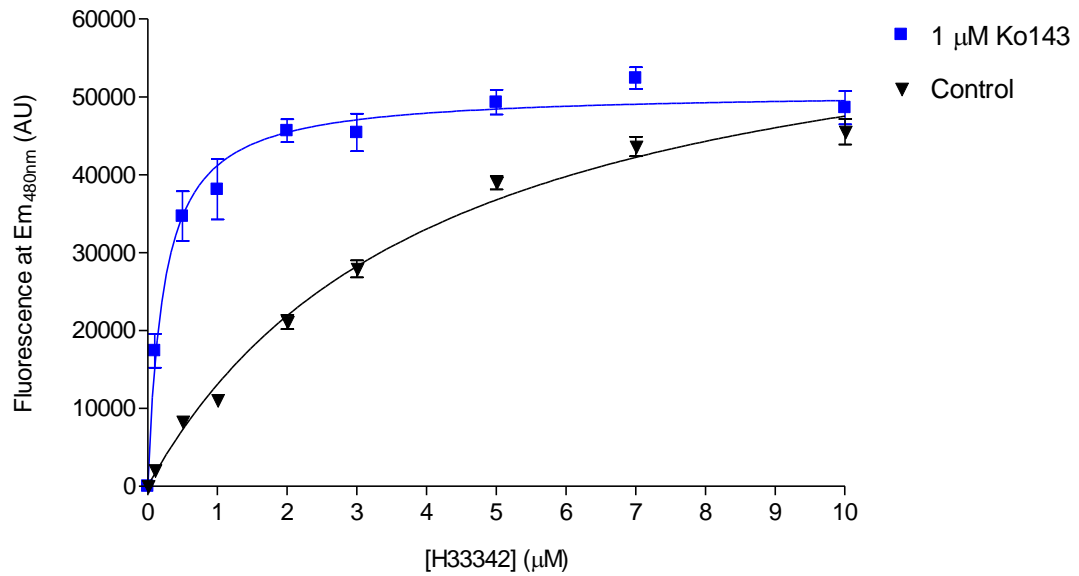
B
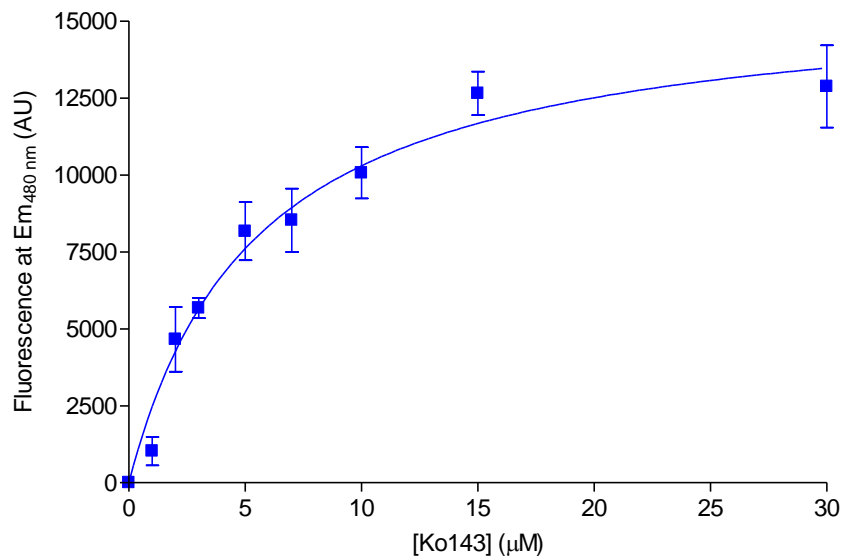
Figure 4.15: Fluorescence of retained Hoechst 33342 by rat PTCs cultured on plastic in the presence of Ko143.

(A) In the absence of Ko143, intracellular retention of Hoechst 33342 showed a saturable kinetic with mean K_m of 4.13 ± 0.37 μM. In the presence of 1 μM Ko143, the mean K_m decreased to 0.23 ± 0.04 μM. (B) The concentration curve for the inhibition of Hoechst 33342 efflux by Ko143 showed mean IC_{50} of 5.48 ± 1.09 μM. Each dot represents the mean ± SEM of 6 replicates. Each figure is a representative of 3 independent experiments, and the K_m and IC_{50} values are the mean of the three experiments. Non-linear regression analysis was performed to obtain the K_m and IC_{50} values.

A
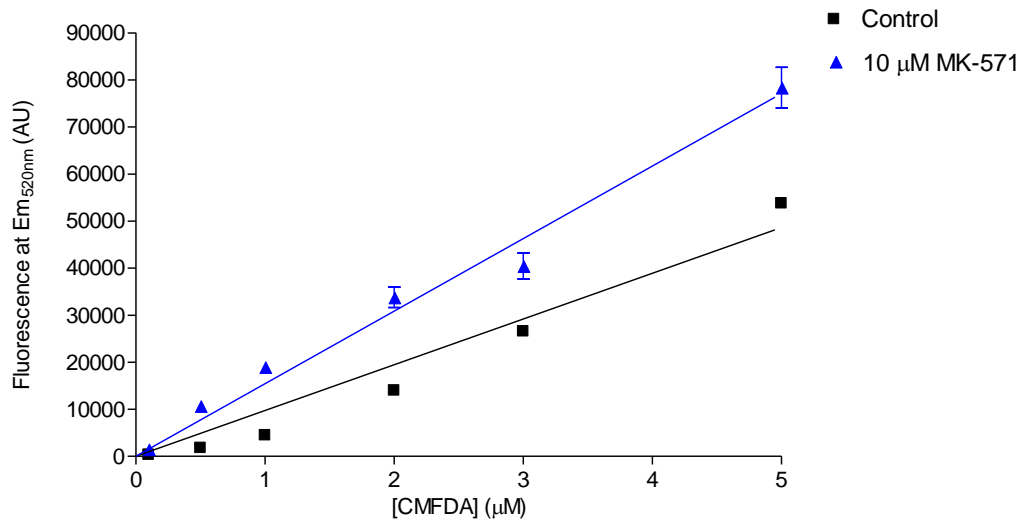
B
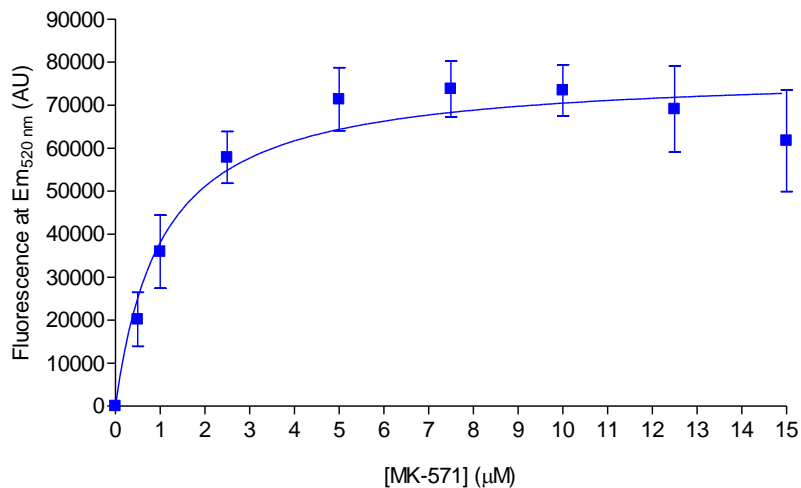
Figure 4.16: Intracellular fluorescence of retained GSMF by rat PTCs in the presence of MK-571.

(A) A linear relationship between the intracellular fluorescence intensity and the external concentration of CMFDA (mean slope of 9,728 ± 258 units/µM, $r^2 = 0.62$) was observed. Intracellular fluorescence intensity was significantly increased in the presence of 10 µM MK-571 (mean slope of 15420 ± 376.7 units/µM, $r^2 = 0.71$). (B) The linear increase in intracellular fluorescence relative to extracellular dye concentration was maintained with no evidence of saturation of intracellular fluorescence. Inhibition of GSMF efflux by a range of MK-571 concentrations gave mean IC_{50} value of 1.05 ± 0.34 µM. Each dot represents the mean ± SEM of 6 replicates. Each figure is a representative of 3 independent experiments, and the slope and IC_{50} values are the mean of the three experiments. Linear regression analysis was performed to obtain the slope, and non-linear regression analysis was performed to obtain the IC_{50}.

4.6 Functional expression of Oct2

Uptake of fluorescence substrate ASP$^+$ by rat PTCs cultured on plastic was carried out to measure the activity of Oct2. Figure 4.17A shows a representative uptake of ASP$^+$ by rat PTCs exhibiting a saturable kinetics, with mean K_m of 5.5 ± 1.05 µM (N = 3).

The effect of Oct2 specific substrates on ASP$^+$ uptake was also tested. Figure 4.17B shows the percentage change in uptake of ASP$^+$ in the presence of 100 µM TEA and 100 µM MPP$^+$, both substrates of Oct2. The uptake of ASP$^+$ was decreased in the presence of both TEA and MPP$^+$, with TEA exposed rat cells taking up 68.43 ± 9.43 % of ASP$^+$, and MPP$^+$ exposed rat PTCs taking up 44.0 ± 4.78 % of ASP$^+$, when compared to the control. That equated to 1.46-times (P < 0.05, n = 18, N = 3) and 2.27-times (P < 0.01, n = 18, N = 3) decrease in ASP$^+$ uptake.

A
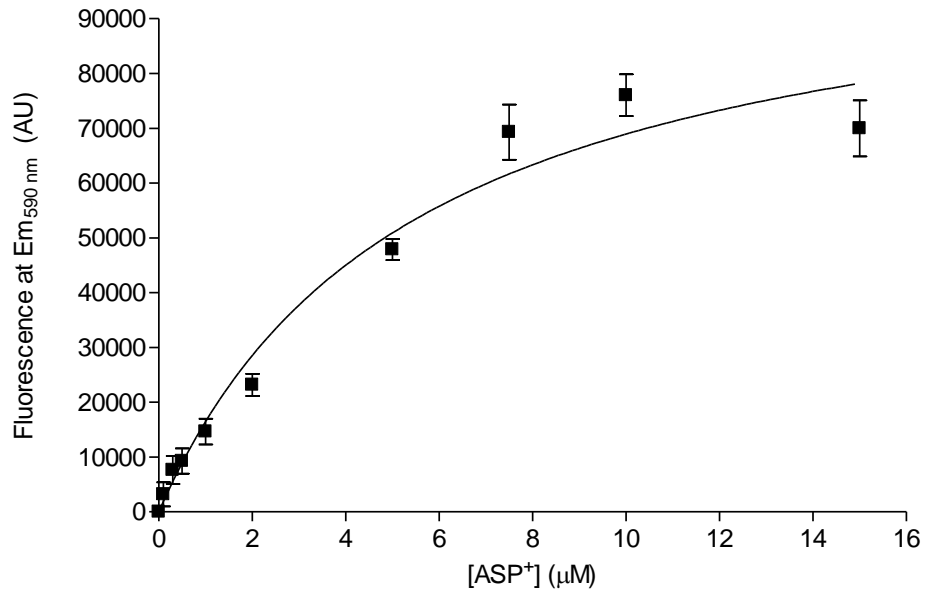
B
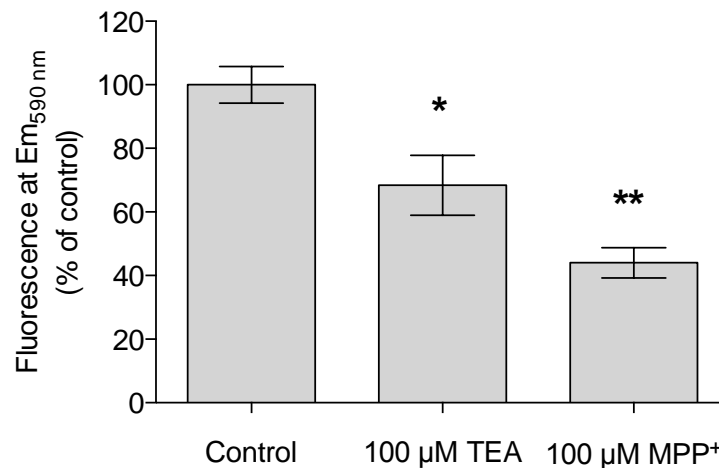
Figure 4.17: Uptake of fluorescence substrate ASP+ by rat PTCs cultured on plastic.

*(A) Uptake of ASP+ by rat PTCs exhibited a saturable kinetic with an average K_m of 5.5 ± 1.05 μM from three separate experiments. Each dot represents the mean ± SEM of 6 replicates. The figure is a representative of 3 independent experiments, and the K_m is the mean of the three experiments. Non-linear regression analysis was performed to obtain the K_m values. (B) The uptake of ASP+ was decreased in the presence of both TEA and MPP+, with TEA exposed rat cells taking up 68.43 ± 9.43 % of ASP+, and MPP+ exposed rat PTCs taking up 44.0 ± 4.78 % of ASP+, when compared to the control. Each bar represents the mean ± SEM of 18 replicates obtained from three separate experiments. One-way ANOVA statistical test was performed to determine significance. *, P < 0.05, ** P < 0.01.*

4.7 Simultaneous measurement of Hoechst 33342 and GSMF retention

A novel technique was developed to investigate the specificity of MK-571 and CsA as specific inhibitors of MRPs and MDR1 in HK-2 cells (Jenkinson *et al.*, 2012). This assay was repeated on rat PTCs.

Figure 4.18 shows that at Hoechst 33342 emission wavelength of 480 nm, only rat PTCs exposed to Hoechst 33342 generated the intracellular fluorescence signals. Similarly at GSMF emission wavelength of 520 nm, only rat PTCs exposed to CMFDA were fluorescent. More importantly, the magnitude of the fluorescent generated by individual substrate did not change significantly in the presence of the others.

To test the specificity of MK-571, CsA and Ko143 as inhibitors of Mrps, Mdr1, or Bcrp, respectively, the impact of incubation of cells with either compound, was measured upon GSMF and Hoechst 33342 retention. Figure 4.19 shows that the exposure of rat PTCs to 10 µM MK-571 resulted in 5.5-fold increase (550.2 ± 80.7 % of control, $P < 0.001$, n = 18, N = 3) in GSMF retention, but had not effect upon the level of fluorescent generated by Hoechst 33342. In contrast, incubation of the rat PTCs with 5 µM CsA was associated with a 2.2-fold increase (219.4 ± 30.9 % of control, $P < 0.01$, n = 18, N = 3) and 4.2-fold increase (419.7 ± 18.0 % of control, $P < 0.01$, n = 18, N = 3) in intracellular Hoechst 33342 and GSMF fluorescence, respectively. 1 µM Ko143 only caused Hoechst 33342 signal to increase significantly, 207.9 ± 31.7 % of control ($P < 0.01$, n= 18, N = 3).
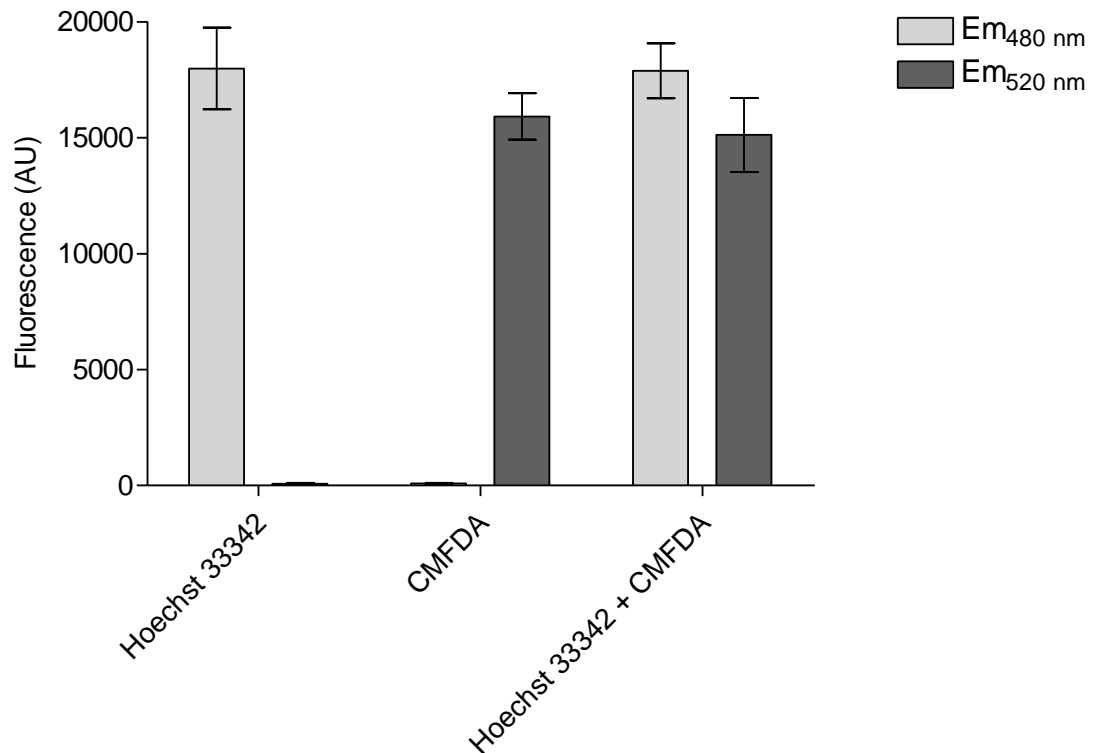
***Figure 4.18: Simultaneous measurement of Hoechst 33342 and GSMF fluorescence
retention in rat PTCs.***

*At Hoechst 33342 emission wavelength of 480 nm, only rat PTCs exposed to
Hoechst 33342 generated the intracellular fluorescence signals. Similarly at
GSMF emission wavelength of 520 nm, only rat PTCs exposed to CMFDA
were fluorescent. The magnitude of the fluorescent generated by individual
substrate did not change significantly in the presence of the others. Each bar
represents the mean ± SEM of 18 replicates obtained from three separate
experiments.*
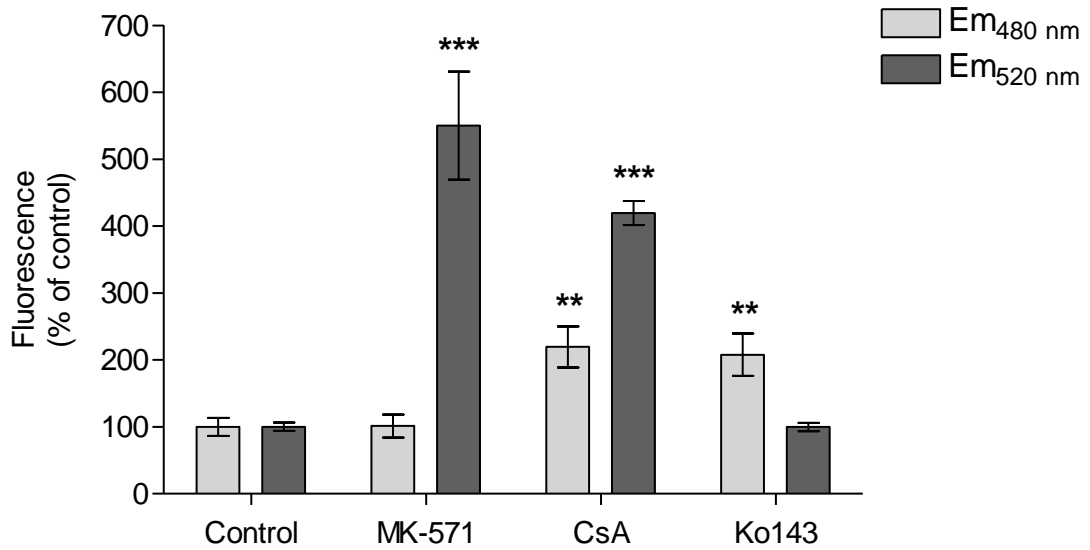
Figure 4.19: Simultaneous measurement of Hoechst 33332 and GSMF retention in rat PTCs to demonstrate substrate specificity.

The exposure of rat PTCs to 10 µM MK-571 resulted in 5.5-fold increase in GSMF retention, but had not effect upon the level of fluorescent generated by Hoechst 33342. Incubation of the rat PTCs with 5 µM CsA was associated with a 2.2-fold increase and 4.2-fold increase respectively in intracellular Hoechst 33342 and GSMF fluorescence. The presence of 1 µM Ko143 only saw 2.1-fold increase in Hoechst 33342 retention. Each bar represents the mean ± SEM of 18 replicates from three separate experiments. Two-way ANOVA statistical test was performed to determine significance. **, P < 0.01, *** P < 0.001.

4.8 Efflux of fluorescence substrates by rat PTC monolayer

Rat PTCs were cultured on Transwell filter support to reinstate the formation of the monolayer. They were then characterised functionally to identify efflux transporters. Figure 4.20 shows the percentage change in efflux of GSMF by rat PTC monolayers in the presence of 10 µM MK-571. Efflux of GSMF from the basolateral membrane of rat PTC monolayers was significantly lower (12.79 ± 6.17 %, $P < 0.001$, n = 12, N = 3) when compared to the efflux from the apical membrane. The presence of MK-571 caused a decrease (79.71 ± 8.65 %, $P < 0.05$, n = 12, N = 3) in GSMF efflux from the apical membrane when compared to the control.

Figure 4.21 shows the percentage change in intracellular retention of GSMF and Hoechst 33342 by rat PTC monolayer on the Transwell filters. Compared to the control, the presence of 10 µM MK-571 saw a 1.95-fold increase in GSMF retention (195.16 ± 15.32 % of the control, Figure 4.21A, $P < 0.01$, n = 12, N = 3).

Hoechst 33342 retention by rat PTC monolayers was also investigated. Figure 4.21B shows the percentage change in Hoechst 33342 retention by the monolayer on Transwell filters. At 202.2 ± 24.01 % (2.02-fold increase, $P < 0.01$, n = 12, N = 3), more Hoechst 33342 was significantly retained in the presence of 5 µM CsA when compared to the control. Similarly, 1 µM of Ko143 also caused Hoechst 33342 retention by the monolayer to increase to 184.1 ± 16.49 % (1.84-fold, $P < 0.01$, n = 12, N = 3) when compared to the control.
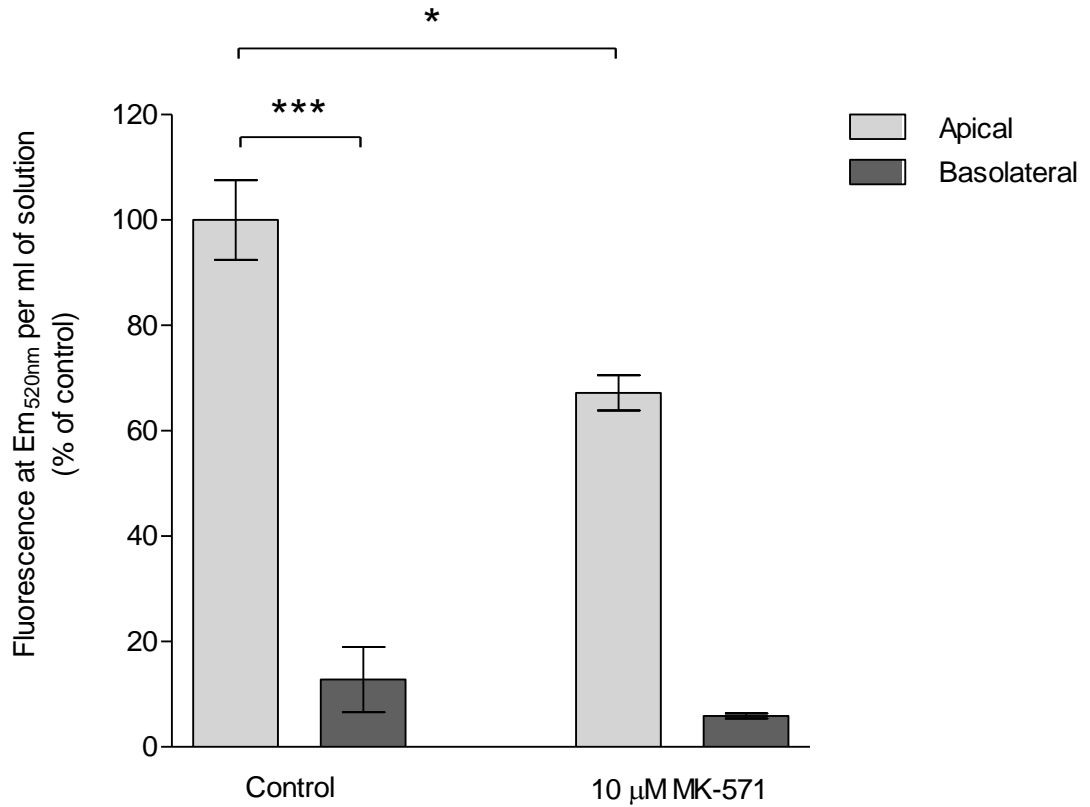
Figure 4.20: Percentage change in GSMF efflux by polarised rat PTC monolayers cultured on Transwell filters.

Efflux of GSMF from the basolateral membrane of rat PTC monolayers was significantly less (12.79 ± 6.17 %) compared to the efflux from the apical membrane. The presence of MK-571 caused a decrease (79.71 ± 8.65 %) in GSMF efflux from the apical membrane when compared to the control. Each bar represents the mean ± SEM of 12 replicates from three separate experiments. One-way ANOVA statistical test was performed to determine significance. *, P < 0.05, *** P < 0.001.

A
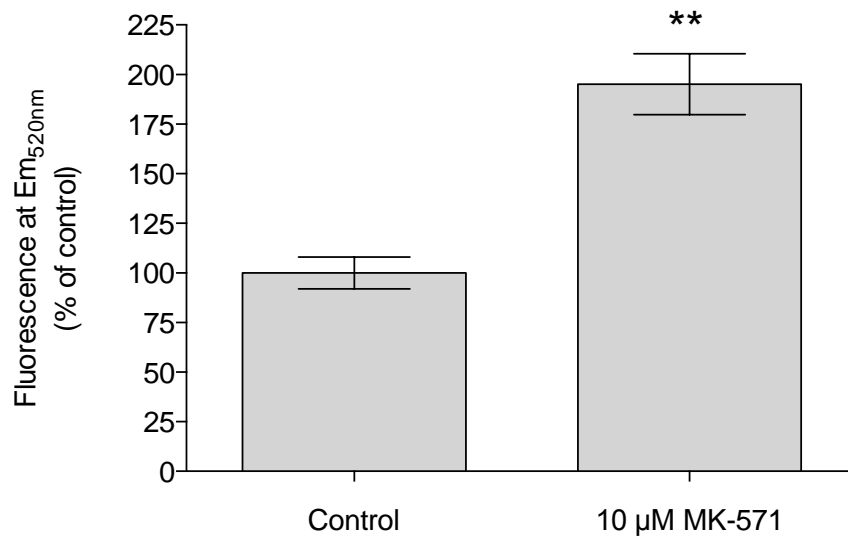
B
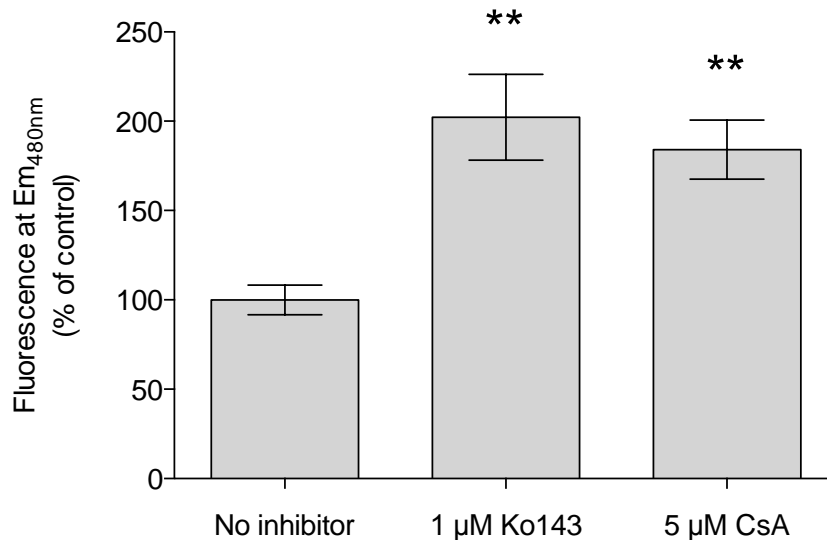
Figure 4.21: Percentage change in GSMF and Hoechst 33342 retention by rat PTC monolayers cultured on Transwell filters.

(A) Compared to the control, the presence of 10 μM MK-571 saw a 1.95-fold increase in GSMF retention (195.16 ± 15.32 % of the control). At 202.2 ± 24.01 % (2.02-fold), more Hoechst 33342 was retained in the presence of 5 μM CsA when compared to the control. (B) Similarly, 1 μM of Ko143 also caused Hoechst 33342 retention by the monolayer to increase to 184.1 ± 16.49 % (1.84-fold) when compared to the control. Each bar represents the mean ± SEM of 12 replicates from three separate experiments. One-way ANOVA statistical test was performed to determine significance. ** P < 0.01.

4.9 Uptake of ASP$^+$ by rat PTC monolayers

Along with fluorescence substrate efflux mentioned in Chapter 4.5, rat PTC monolayers were also used to determine the functional expression and localisation of Oct2. Figure 4.22 shows the percentage change in uptake of ASP$^+$ in the presence of 100 µM TEA and 100 µM MPP$^+$.

Uptake of ASP$^+$ was significantly lower from the apical membrane of the rat PTC monolayer (5.06-times lower, $P < 0.001$, $n = 12$, $N = 3$) when compared to the basolateral membrane. ASP$^+$ uptake from the basolateral membrane significantly decreased in the presence of TEA or MPP$^+$, giving 50.22 ± 4.42 % ($P < 0.001$, $n = 12$, $N = 3$) and 46.55 ± 4.99 % ($P < 0.01$, $n = 12$, $N = 3$) of the control, respectively.
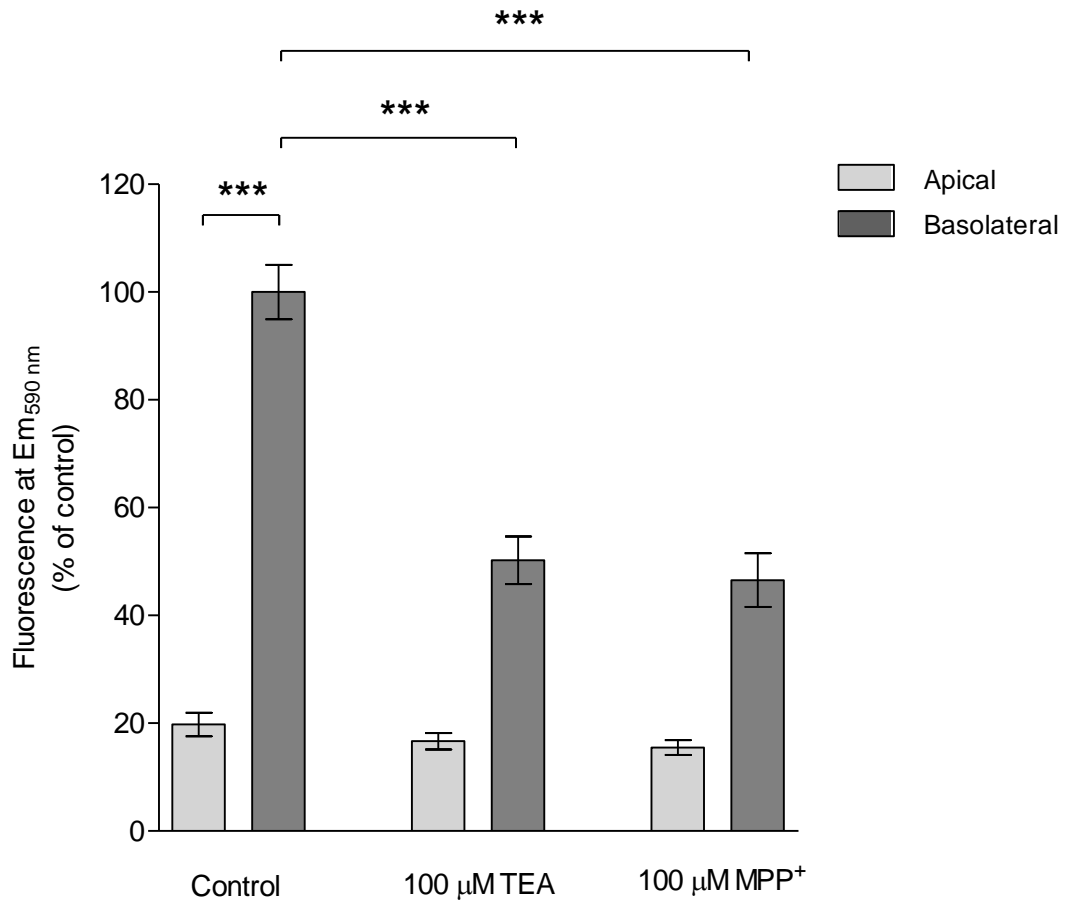
Figure 4.22: Percentage change in uptake of ASP+ by rat PTC monolayers cultured on Transwell filters in the presence of inhibitors.

Uptake of ASP+ was significantly lower from the apical membrane of the rat PTC monolayer (5.06-times lower) when compared to the basolateral membrane. ASP+ uptake from the basolateral membrane significantly decreased in the presence of TEA or MPP+, giving 50.22 ± 4.42 % and 46.55 ± 4.99 % of the control, respectively. Each bar represents the mean ± SEM of 12 replicates obtained from three separate experiments. Two-way ANOVA statistical test was performed to determine significance. *** P < 0.001.

4.10 Uptake of lactate by rat PTC monolayers

Functional expression and localisation of Mct1 was examined in polarised rat PTC monolayers. Figure 4.23 shows the amount of lactate taken up by rat PTC monolayers in different extracellular conditions. Uptake across the apical membrane was 0.55 ± 0.04 pmol/cm^2/min, which was 3.63-fold higher than uptake across the basolateral membrane (0.15 ± 0.03 pmol/cm^2/min, $P < 0.01$, n = 12, N = 3). In the presence of 500 μM phloretin, a Mct1 specific inhibitor, the apical uptake of lactate was decreased to 0.26 ± 0.02 pmol/cm^2/min (52.7 % of control, $P < 0.01$, n = 12, N = 3). However, the changing of external pH from 7.4 to 6.0 increased the apical uptake of lactate by 1.58-fold (0.88 ± 0.09 pmol/cm^2/min, $P < 0.05$, n = 12, N = 3) when compared to the control.
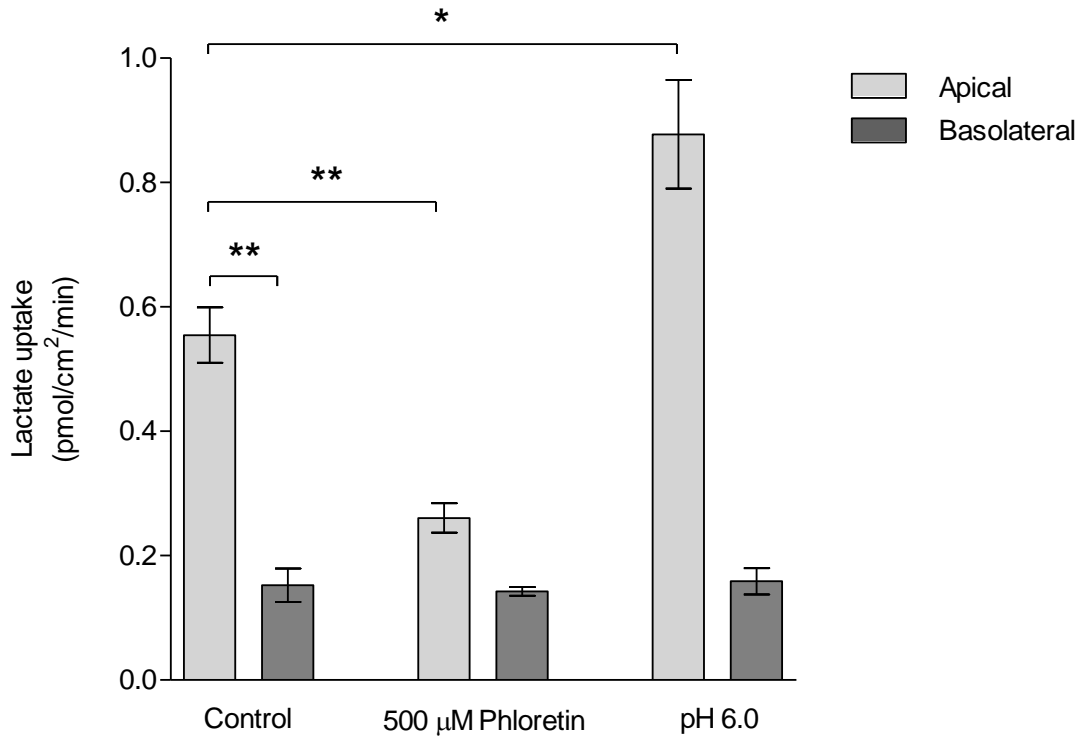
Figure 4.23: Amount of lactate uptake by rat PTC monolayers cultured on Transwell filters.

Uptake across the apical membrane was 0.55 ± 0.04 pmol/cm²/min, which was 3.63-fold higher than uptake across the basolateral membrane (0.15 ± 0.03 pmol/cm²/min). In the presence of 500 µM phloretin, the apical uptake of lactate was decreased to 0.26 ± 0.02 pmol/cm²/min. However, the change of external pH from 7.4 to 6.0 increased the apical uptake of lactate by 1.58-fold (0.88 ± 0.09 pmol/cm²/min) when compared to the control. Each bar represents the mean ± SEM of 12 replicates from three separate experiments. One-way ANOVA statistical test was performed to determine significance. *, P < 0.05, **, P < 0.01.

4.11 Discussion

One of the important properties of a renal cell model is the ability of the transport proteins expressed on the basolateral and apical membranes of the cells to function as it would *in vivo.* In this chapter, rat PTCs were cultured on plastics and filter support for the initial characterisation of the cells, which focused on transporter expression of a range of key proximal tubule transporters at the mRNA level and compared the expression patterns with the expression patterns found in freshly isolated PTCs. This was followed by a study of the functional expression and localisation of some transporters expressed in the proximal tubule.

Of all the transporters expressed in the proximal tubule, focus was given to Mdr1, Bcrp, Mrp2, Oat1, Oct2, Oatp4c1, Slc2a9, Urat1, Mate1 and Mct1 in this project. A paper published in 2010 by the International Transporter Consortium identified the importance of these 10 transporters in drug absorption and disposition in the human kidney (Consortium, 2010). Due consideration for the expression and function of these transporters are thus needed in the rat PTCs to identify its robustness as a model of drug interaction studies.

4.11.1 Differential mRNA expression of transporters in rat PTCs

The mRNA expression levels of several transporters in two different cell culture conditions were examined. Rat PTCs cultured on plastics for 6 days, and rat PTCs cultured on Transwell filter support also for 6 days were compared to freshly isolated rat PTCs. Freshly isolated rat PTCs refer to the cells from the isolation procedure prior to their growth on various platforms. These cells were considered to be representative of the native proximal tubule *in vivo* and thus used as the control.

Endpoint PCRs performed using cDNA template that was reverse transcribed from RNA isolated from the three rat PTC cultures detected the expression of all the transporters tested. Visualisation of the PCR products on the agarose gels showed the presence of only one product in each of the lanes. This indicated the specificity of the primers used as only the gene of interest was amplified. In addition, the size of the PCR products and their sequences also validated the specificity of the primers. However, even though mRNA expression of all the

transporters was detected using endpoint PCR, the difference in the intensity of the PCR products between the lanes in the same gel suggested there were differences in the level of expression between the two culture platforms and the native tissue. For instance, Mrp2 PCR product was amplified from freshly isolated rat PTCs, PTCs cultured on plastics, and PTCs cultured on filter support, but the intensities of the bands were lower in the latter two. The same pattern of expression was detected in Oat1, Oct2, Oatp4c1, Slc2a9, Urat1 and Mct1, although Mdr1, Bcrp and Mct1 showed equal PCR product intensity in all samples.

The intensity of a band on an agarose gel is a qualitative measure of the amount of PCR product. For a quantitative measure of the amount of starting PCR template, and indirectly the mRNA level, real-time quantitative PCR is a better suited technique. The relative mRNA expression levels of the ten transporters were determined using this method. The percentage change in expression levels between the culture conditions showed similar patterns to the results of the endpoint PCR. The expression levels of cultured cells were significantly lower than that of freshly isolated cells across the array of transporters tested; in the majority expression was down regulated more than 3-fold when compared to the native cells.

As mentioned in the Chapter 3, the decrease in expression of many transporters is expected when primary cells are cultured (Bens and Vandewalle, 2008; Nakanishi *et al.*, 2011). There is no data in the literature that provides an explanation for the phenomenon. However, dedifferentiation of epithelial cells may offer an inclination as to why cells lose transporter expression during culture. In the context of renal epithelial cells, dedifferentiation is defined as the loss of a cell's epithelial phenotype and acquisition of features of a mesenchymal cell, such as the expression of vimentin (Liu, 2004; Russ *et al.*, 2009). Vimentin is an intermediate filament protein found only in mesenchymal cytoskeleton (Herrmann *et al.*, 2009; Russ *et al.*, 2009), and increases in expression during kidney injury (Witzgall *et al.*, 1994). Zhuang *et al.* showed vimentin was detected in freshly isolated mouse PTCs, and the level of vimentin was elevated in culture over a period of 7 days (Zhuang *et al.*, 2012).

Mature renal tubular cells under normal conditions are tightly connected to each other via tight-junctions to form an integrated epithelial sheet. They are quiescent

and exhibit a differentiated phenotype (Bonventre, 2003). Alterations in the structure, for instance, during cell isolation, would destabilise the renal epithelium integrity and make cells dissociate from their neighbour and lose their polarity. It is this process that seemed to "injure" the cells and initiate the phenotypic switch of renal epithelial cells from the quiescent, differentiated state to a dedifferentiated one. And it is this dedifferentiation that could have caused the transition of these epithelial cells to mesenchymal and the subsequent loss of transporters.

Whilst dedifferentiation was a concern in the culture of the rat PTCs, there was general consensus that primary tubule cells do retain their proximal tubule phenotype better than other renal cell lines (Terryn *et al.*, 2007; Bens and Vandewalle, 2008; Nakanishi *et al.*, 2011). For example, Caki-1 cells lack mRNA of several organic anion and organic cation transporters, including OAT1, OAT2, OCT1 and OCT2 (Glube *et al.*, 2006; Hilgendorf *et al.*, 2007). Similarly, rat cell line NRK-52E, and swine cell line LLC-PK1 lack mRNA expression of these transporters (Fauth *et al.*, 1988; Lash, 2006). Furthermore, LLC-PK1, which is often used to evaluate renal drug transport, also lack proximal brush-border enzymes compared with those in primary cultured PTCs (Terryn *et al.*, 2007). Taking these findings together, expression of major transporters was still relatively well preserved in the rat PTCs, albeit at a lower expression level than the native cells.

It has been shown that maintenance of primary cells differentiated state, and incidentally their brush-border enzyme activity, was greatly influenced by the composition of the culture medium, and had been used in this project to encourage rat PTCs to differentiate (Taub *et al.*, 1989; Courjault-Gautier *et al.*, 1995). In addition, it has also been proven that bathing epithelial cells at both the apical and basolateral sides, thus replicating the *in vivo* physiology, enhances their ability to remain differentiated (Fulcher *et al.*, 2005).

4.11.2 Functional expression of ABC transporters and Oct2

Rat PTCs were examined for their transporter activity to describe the aptness of this cell model. Fluorescent substrates, which are removed from or taken up into cells by specific transporters, provide a method of measuring the functional expression of particular transporters. Hoechst 33342 and CMFDA have been

previously used for this purpose (Brown *et al.*, 2008; Jenkinson *et al.*, 2012), and were used in this project to characterise Mdr1, Bcrp and Mrps. Fluorescent substrate ASP$^+$ was utilised to determine functional expression of Oct1.

Hoechst 33342 is a cell-permeable nuclear stain that easily diffuses through cell membranes. Upon chelation with double stranded DNA, it emits a blue fluorescence when excited in the correct spectrum (Lalande *et al.*, 1981). When rat PTCs were exposed to a concentration of Hoechst 33342, a state of equilibrium was achieved between the amount of Hoechst 33342 inside the cell and the amount actively pumped out by Mdr1 and Bcrp. The concentration of extracellular Hoechst 33342 that would cause half the maximal amount of Hoechst 33342 (K_m) inside rat PTCs was approximately 4 µM. As would be expected, in the presence of an Mdr1 inhibitor (5 µM CsA) (Gupta *et al.*, 2006), efflux of Hoechst 33342 was hindered and the equilibrium shifted to decrease the K_m to approximately 0.4 µM (Figure 4.13). CsA was also found to inhibit Hoechst 33342 efflux in a concentration dependent manner, with IC_{50} of around 2 µM. These results provide evidence for the expression of functional Mdr1 by rat PTCs. Similarly, expression of functional Bcrp was surmised when the K_m of Hoechst retention decreased to approximately 0.2 µM when rat PTCs were exposed to 1 µM Ko143, a Bcrp inhibitor (Haslam *et al.*, 2011). Ko143 also inhibited Hoechst 33342 efflux with approximate IC_{50} of 5.5 µM (Figure 4.15).

GF120918 was also used as an inhibitor of Hoechst 33342 efflux by rat PTCs. GF120918 was originally developed as a MDR1 inhibitor (Tan *et al.*, 2000). However, it has been shown that GF120918 is also a potent human BCRP and rat Bcrp inhibitor in transfected cell lines (Pan *et al.*, 2007; Wang *et al.*, 2008a). When GF120918 was used to inhibit the efflux of Hoechst 33342 in rat PTCs, one would expect the IC_{50} to decrease significantly more than with just CsA or Ko143 alone. Indeed, that was observed in the rat PTCs when GF120918 was used; the IC_{50} was around 0.2 µM whereas it was 2 µM with CsA and 5 µM with Ko143 (Figure 4.14).

The CMFDA metabolite, GSMF, is another well established fluorescent substrate for the study of Mrp efflux transporters (Gutmann *et al.*, 1999). Treatment of rat PTCs with another Mrp substrate MK-517 resulted in an increase in the intracellular retention of GSMF when compared to the control (Figure 4.16),

suggesting GSMF efflux by Mrps had been blocked. MK-571 was also found to inhibit the efflux of GSMF in a concentration dependent manner with apparent IC_{50} of around 1 μM, confirming functional expression of Mrps.

Unlike the retention of Hoechst 33342 in rat PTCs that began to plateau at 2 μM, it appeared impossible to saturate the cells with GSMF even at high extracellular CMFDA concentration. The two-step process of CMFDA conversion to GSMF inside cells might explain why the relationship between extracellular CMFDA concentration and intracellular fluorescence was linear over the concentration range tested. Lipophilic CMFDA would easily diffuse across the cell membrane before being broken down by esterases to the hydrophilic intermediate 5-chloromethylfluorescein (CMF). In the second step, CMF reacts with intracellular glutathione via glutathione-S-transferase to form fluorescent GSMF (Müller *et al.*, 2007). This conversion would be rapid and allow more CMFDA to be taken up by the cells without saturation.

Along with ABC transporters, the functional expression of Oct2 was also demonstrated. APS^+ is a fluorescent organic cation and was first used by Pietruck *et al.* for organic cation transport measurements in rats *in vivo* (Peitruck and Ullrich, 1995). Since then, the use of ASP^+ as a fluorescent substrate has been carried out in human alveolar (A549), bronchial (Calu-3) and intestinal (Caco-2) epithelium, amongst others (Salomon *et al.*, 2012).The uptake of fluorescence substrate ASP^+ by rat PTCs cultured on plastic showed saturable kinetics with K_m of 5.5 μM (Figure 4.17A). In the presence of TEA or MPP^+, both high affinity substrates of Oct2, the uptake was significantly hindered by as much as over 2-fold when compared to the control. This result, along with the transcript for Oct2 detected, provides evidence for the expression of Oct2 in the rat PTCs.

4.11.3 Simultaneous measurement of ABC transporter activities

So far, publications featuring efflux assays had been looking at the action of one efflux transporter at a time (van den Berg van Saparoea *et al.*, 2005; Wang *et al.*, 2008b). A novel technique had been developed to perform simultaneous measurement of the activities of two transporters and proved to be advantageous (Jenkinson *et al.*, 2012). Figure 4.19 shows an increase in intracellular retention of GSMF relative to the control when either 5 μM CsA or 10 μM MK-571 were exposed to rat PTCs. However, increased Hoechst 33342 retention was only

observed in CsA-treated cells. MK-571 had no effect on the amount of Hoechst 33342 retained in rat PTCs. The data suggested that whilst MK-571 is a specific inhibitor of Mrps at the concentration used, CsA is less specific and inhibits efflux mediated by both Mdr1 and Mrps. Similar interactions between CsA and Mrps have previously been reported (Schinkel and Jonker, 2003). An advantage of this assay was that it used the same set of cells to measure the functional expression of two different transporters, thus providing a form of internal control. Another benefit of simultaneous measurement of transporter activities is the possibility of determining the effects, if any, of a range of compounds, in a quick and effective way, as demonstrated by the above.

4.11.4 Functional expression and localisation of Mrps and Oct2 on polarised rat PTCs

The experiments mentioned thus far had been performed on rat PTCs cultured on plastics, and demonstrated the functional expression of several ABC transporters and Oct2. To identify the localisation of these transporters, the experiments were repeated on rat PTCs cultured on filter support, where the apical and basolateral surfaces of the rat PTC monolayers could be compartmentalised.

GSMF is a fluorescent substrate of Mrps, and its appearance in a chamber would signify the presence of the transporter adjacent to that chamber. Figure 4.20 shows GSMF was effluxed 7.8 times more from the apical side. As expected, the efflux from the apical membrane was significantly inhibited by 10 µM MK-517, which caused the amount of GSMF present in the apical chamber to decrease by 1.2-fold. This data corresponded with the intracellular retention of GSMF by the same set of rat PTC monolayers, in that rat PTC monolayers retained 1.9-fold more GSMF in the presence of MK-571, thus confirming the functional expression of Mrps on the apical membrane of rat PTC monolayers (Figure 4.21A). This was also in accordance with other published works that shows Mrp localisation on the apical membrane of renal epithelial cells (Kool *et al.*, 1997; Schaub *et al.*, 1999).

The compartmentalised uptake of ASP^+ from the apical and basolateral membranes was also performed. ASP^+ was shown to be taken up significantly more from the basolateral membrane (5-fold) than the apical membrane, but significantly decreased in the presence of TEA or MPP^+ (1.99-fold and 2.1-fold

respectively), both high-affinity substrates of Oct2 (Figure 4.22). Once again, this signified the presence of basolaterally located Oct2 in rat PTC monolayers.

Unfortunately, Hoechst 33342 would not fluoresce unless bound to DNA. That meant its efflux into extracellular solutions by rat PTC monolayers was undetectable, though functional expression of Mdr1 and Bcrp could still be detected in the monolayers. Hoechst 33342 retention by rat PTC monolayers in the presence of CsA was almost up 2-fold when compared to the control (Figure 4.21B). Similarly, Hoechst 33342 retention was also up 1.8 fold in the presence of Ko143 when compared to the control.

4.11.5 Polarised lactate uptake by rat PTC monolayers

In agreement with previous studies, high expression of mRNA for Mct1 was observed in rat PTCs (Eladari *et al.*, 1999; Wang *et al.*, 2006). Functional expression of Mct1 was also performed on rat PTC monolayers. Lactate uptake by rat PTCs monolayers showed pH-dependency suggesting the presence of an H^+-dependent monocarboxylate transporter (Figure 4.23). A marked difference between the uptake of lactate from the apical membrane and basolateral membrane was also observed. Uptake of lactate from the apical membrane was 3.6-fold higher than from the basolateral side. Functional expression of Mct1 was confirmed when lactate uptake was significantly decreased in the presence of phloretin, a potent Mct1 inhibitor (Jackson and Halestrap, 1996).

The source and uptake route for monocarboxylates in rat PTCs have not been characterised in detail. However, initial studies have shown that Mct1 can mediate net lactate uptake or excretion depending on the intracellular and extracellular pH ratio, and on the relative concentrations of lactate inside or outside the cell (Garcia *et al.*, 1994). In the kidney, the proximal tubule is engaged in gluconeogenesis and oxidation, and Mct1 may be involved in taking up lactate or pyruvate for these processes. Conversely, Mct1 may act as an efflux pathway for lactate from glycolysis or from the reabsorption of filtered lactate that has been taken up from urine via other transporters (Jackson and Halestrap, 1996).

4.12 Summary

The expression of several important drug transporters by rat PTCs at the mRNA and functional levels has been demonstrated in this chapter. Transcripts for transporters including Bcrp, Mdr1, Mrp2, Oat1, Oct2, Oatp4c1, Slc2a9, Urat1, Mate1 and Mct1 were detected in rat PTCs. The functional expression and localisation of some of the transporters on polarised rat PTC monolayers has also been elucidated, and is summed up in Figure 4.24. While these data highlight the capacity of rat PTCs to reflect proximal tubules *in vivo*, their capacity as an *in vitro* model for renal drug handling would need to be investigated. The subsequent chapters investigate the differences in the renal handling of typical renal molecules urate and digoxin by rat and human PTCs.
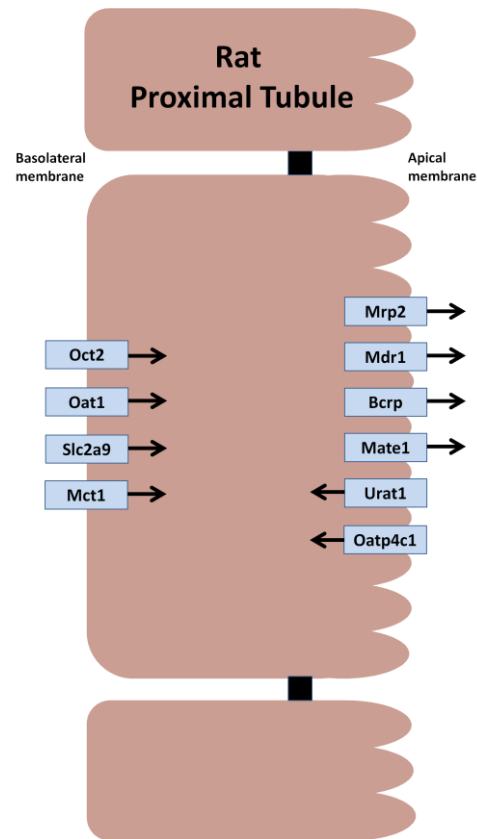
Figure 4.24: The key drug transporters in rat PTCs.

Of all the transporters expressed in the proximal tubule, focus was given Mdr1, Bcrp, Mrp2, Oat1, Oct2, Oatp4c1, Slc2a9, Urat1, Mate1 and Mct1 in this project. mRNA of all ten transporters were detected in freshly isolated and cultured rat PTCs. The localisations and functions of some of these transporters were based on data obtained in this project. Others were based on data from the literature.

Chapter 5

Urate Handling by Rat and Human PTC monolayers

5.1 Chapter overview

This chapter discusses the results of the mechanisms of urate handling by rat and human proximal tubule cell (PTC) monolayers cultured on Transwells. The data from the following experiments are highlighted in this chapter:

- Unidirectional urate fluxes and uptake by rat and human PTC monolayers.

- The effects of benzbromarone, an uricouric agent, on the unidirectional fluxes and uptake of urate by rat and human PTC monolayers.

- The effects of Ko143, a BCRP inhibitor, on the unidirectional fluxes and uptake of urate by rat and human PTC monolayers.

- The effects of OAT substrate, *p*-aminohippuric acid (PAH), on the unidirectional fluxes and uptake of urate by rat and human PTC monolayers.

- The effects of MK-571, an MRP inhibitor, on urate unidirectional fluxes and uptake up rat and human PTC monolayers.

- The uptake of urate by *Xenopus* oocytes transfected with human URAT1 and SLC2A9.

5.2 Urate handling by rat PTC monolayers

Rat PTC monolayers were used to investigate the renal handling of urate molecules by rat proximal tubule. Unidirectional urate transepithelial fluxes in the apical to basolateral direction (J_{A-B}), and in the basolateral to apical direction (J_{B-A}), were carried out using 35 µM urate in all urate experiments. The net flux (J_{Net}) was calculated from the difference between the two fluxes. Uptake of urate across the apical and basolateral membranes was also determined from the amount of intracellular urate in rat PTC monolayers after the flux.

Figure 5.1A shows urate in rat PTC monolayers exhibited a net absorption pathway. J_{A-B} (33.27 ± 3.29 pmol/cm^2/hr) was 3.21-fold higher than J_{B-A} (10.34 ± 2.95 pmol/cm^2/hr), which led to an absorptive J_{Net} of 22.93 ± 3.63 pmol/cm^2/hr ($P < 0.01$, n = 12, N = 3). The amount of urate taken up across the apical membrane and basolateral membrane of the rat PTC monolayers were 4.31 ± 0.91 pmol/cm^2/hr and 1.26 ± 0.42 pmol/cm^2/hr, respectively, which was 3.41-fold more urate uptake across the apical side ($P < 0.01$, n = 12, N = 3, Figure 5.1B).

A
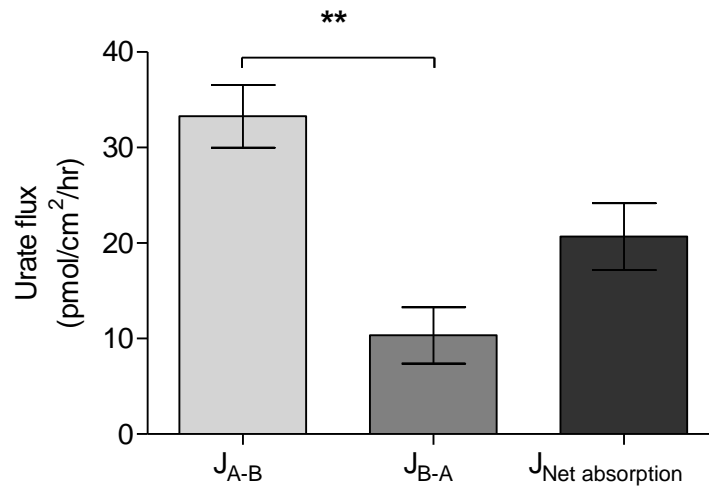
B
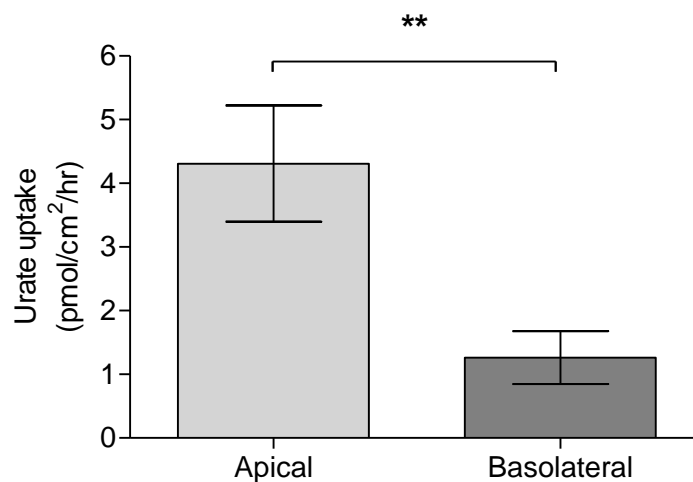
Figure 5.1: Unidirectional urate fluxes and uptake by rat PTC monolayers.

(*A*) Urate J_{A-B} was 33.27 ± 3.29 pmol/cm^2/hr, which was 3.21-fold higher than J_{B-A} (10.34 ± 2.95 pmol/cm^2/hr). This led to an absorptive J_{Net} of 22.93 ± 3.63 pmol/cm^2/hr. (*B*) The amount of urate taken up across the apical membrane and basolateral membrane of the rat PTC monolayers were 4.31 ± 0.91 pmol/cm^2/hr and 1.26 ± 0.42 pmol/cm^2/hr, respectively. Each bar represents the mean ± SEM of 12 replicates obtained from 3 separate experiments. Student t test was performed to determine statistical significance in the differences between the conditions. **, $P < 0.01$.

5.3 The effects of benzbromarone on urate transport by rat PTC monolayers

Urate unidirectional fluxes were carried out in the presence of an uricouric drug benzbromarone to determine the mechanism of urate transport in rat PTC monolayers. Either the apical or basolateral membranes of the rat PTC monolayers were exposed to 50 µM benzbromarone for 30 minutes prior and during urate fluxes. Figure 5.2 shows the results of urate J_{A-B} and J_{B-A} in the presence of benzbromarone.

Regardless of whether benzbromarone was on either the apical or basolateral membranes, rat PTC monolayers J_{A-B} was significantly decreased in the drug's presence when compared to the control. J_{A-B} had the sharpest decrease in magnitude when rat PTC monolayers were treated with benzbromarone on the apical membrane (a 72.7 % decrease, from 33.27 ± 3.29 pmol/cm^2/hr to 9.09 ± 3.15 pmol/cm^2/hr, $P < 0.01$, n = 10, N = 3, Figure 5.2A). When the monolayers were treated with benzbromarone on the basolateral membrane, J_{A-B} was 15.13 ± 3.32 pmol/cm^2/hr, a 54.5 % decrease ($P < 0.01$, n = 12, N = 3). Urate J_{B-A} was 16.73 ± 1.69 pmol/cm^2/hr and 15.94 ± 1.87 pmol/cm^2/hr when benzbromarone was present on the apical and basolateral membranes, respectively (Figure 5.2B), but when compared to the control J_{B-A} of 10.34 ± 2.95 pmol/cm^2/hr, no statistically significant difference was observed ($P > 0.05$, n = 12, N = 3).

Uptake of urate across the apical membrane showed marked differences as shown in Figure 5.3. When benzbromarone was treated from the apical membrane, the amount of urate uptake across the apical membrane was 2.29-times lower than control (1.88 ± 0.29 pmol/cm^2/hr, $P < 0.01$, n = 12, N = 3, Figure 5.3A). However, uptake of urate was 2.48-fold higher than control when benzbromarone was treated on the basolateral side (10.70 ± 1.44 pmol/cm^2/hr, $P < 0.01$, n = 11, N = 3). Uptake of urate across the basolateral membrane in the presence of apically-treated benzbromarone was 1.26 ± 0.42 pmol/cm^2/hr, which was not significantly different to the control of 1.50 ± 0.47 pmol/cm^2/hr (Figure 5.3B, $P > 0.05$, n = 11, N = 3). But when benzbromarone was on the basolateral membrane, basolateral uptake was increased in magnitude to 2.73 ± 0.37 pmol/cm^2/hr ($P < 0.05$, n = 11, N = 3).

A
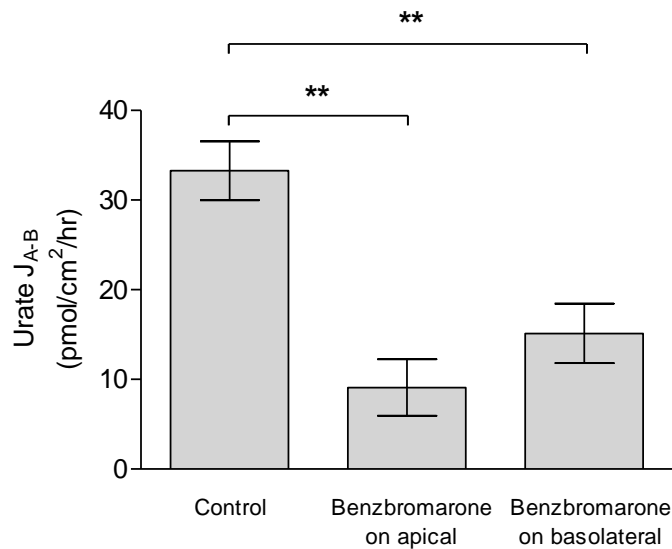
B
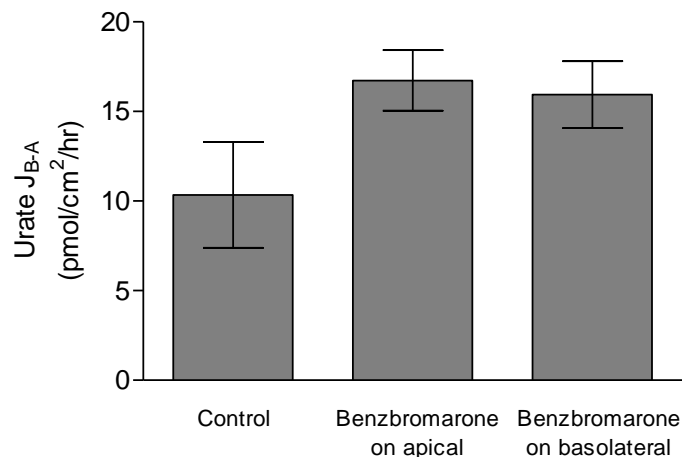
Figure 5.2: Unidirectional urate fluxes by rat PTC monolayers in the presence of 50 μM benzbromarone.

*(A) J_{A-B} saw a 72.7 % decrease in magnitude when benzbromarone was on the apical membrane (from 33.27 ± 3.29 pmol/cm^2/hr to 9.09 ± 3.15 pmol/cm^2/hr). When the monolayers were treated with benzbromarone on the basolateral membrane, J_{A-B} was 15.13 ± 3.32 pmol/cm^2/hr (54.5 % decrease) when compared to the control. (B) J_{B-A} was 16.73 ± 1.69 pmol/cm^2/hr and 15.94 ± 1.87 pmol/cm^2/hr when benzbromarone was present on the apical and basolateral membranes, respectively, but when compared to the control J_{B-A} of 10.34 ± 2.95 pmol/cm^2/hr, no statistically significant difference was observed between the conditions. Each bar represents the mean ± SEM of 10-12 replicates from three separate experiments. Two-way ANOVA was performed to determine significant difference between the conditions. **, $P < 0.01$.*

A
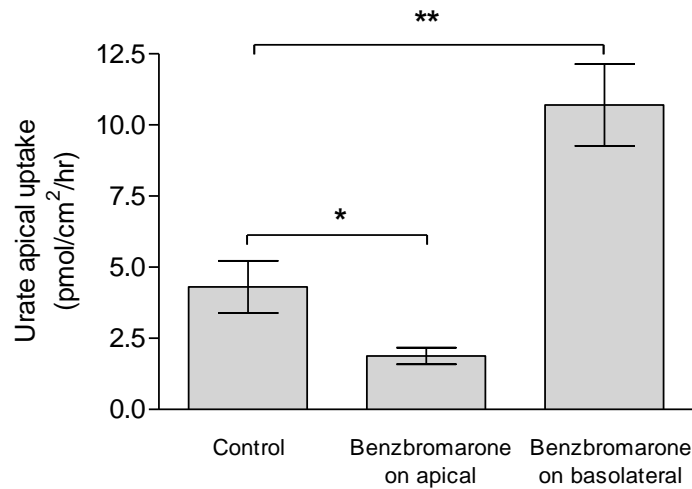
B
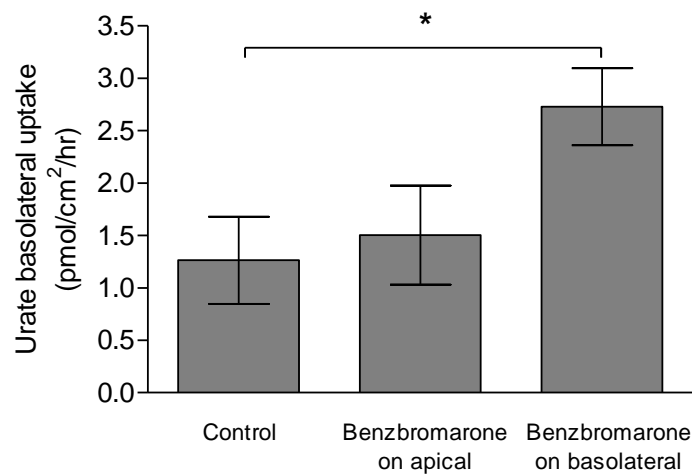
Figure 5.3: Uptake of urate by rat PTC monolayers in the presence of 50 μM benzbromarone.

(A) When benzbromarone was treated from the apical membrane, the amount of urate uptake across the apical membrane was 2.29-times lower than control (1.88 ± 0.29 pmol/cm^2/hr). However, uptake of urate was 2.48-fold higher than control when benzbromarone was treated on the basolateral side (10.70 ± 1.44 pmol/cm^2/hr). (B) Uptake of urate across the basolateral membrane was 1.50 ± 0.47 pmol/cm^2/hr and when benzbromarone was present on the apical membrane uptake was 1.26 ± 0.42 pmol/cm^2/hr, which was not significantly different. But when benzbromarone was on the basolateral membrane, basolateral uptake was increased in magnitude to 2.73 ± 0.37 pmol/cm^2/hr. Each bar represents the mean ± SEM of 10-12 replicates from three separate experiments. Two-way ANOVA was performed to determine significant difference between the conditions. *, P < 0.05, **, P < 0.01.

5.4 The effects of Ko143 on urate transport by rat PTC monolayers

The effects of Bcrp inhibitor, Ko143, in urate transport by rat PTC monolayers were also investigated. Unidirectional urate fluxes and uptake were carried out using rat PTC monolayers pre-treated with 1 µM Ko143. Ko143 was treated and present on either the apical or basolateral membrane of the monolayers during the experiments. Figure 5.4 and Figure 5.5 summarise the results.

Urate J_{A-B} exhibited no significant difference in magnitude between the control monolayers and monolayers treated with Ko143 (Figure 5.4A). The J_{A-B} values were: control, 33.27 ± 3.29 pmol/cm^2/hr, in the presence of apical Ko143, 34.25 ± 3.96 pmol/cm^2/hr, in the presence of basolateral Ko143, 35.68 ± 3.08 pmol/cm^2/hr ($P > 0.05$, n = 12, N = 3). However, J_{B-A} saw a 68.5 % decrease in magnitude when Ko143 was present in the apical membrane (from 10.34 ± 2.95 pmol/cm^2/hr to 3.26 ± 1.00 pmol/cm^2/hr, $P < 0.05$, n = 12, N = 3, Figure 5.4B). No significant difference was observed in J_{B-A} when Ko143 was present in the basolateral membrane (10.92 ± 2.14 pmol/cm^2/hr, $P > 0.05$, n = 12, N = 3).

No significant difference was also observed in urate uptake across the apical membrane of the rat PTC monolayers with Ko143 treatment (Figure 5.5A). Uptake across the basolateral membrane, however, saw a significant increase in magnitude when ko143 was treated on the apical membrane of the monolayer. Uptake of urate was up 2.58-fold when compared to the control (from 1.26 ± 0.42 pmol/cm^2/hr to 3.25 ± 0.64 pmol/cm^2/hr, $P < 0.05$, n = 12, N = 3, Figure 5.5B). No significant difference was observed in basolateral uptake when Ko143 was treated on the basolateral side of the monolayer (1.63 ± 0.67 pmol/cm^2/hr, $P > 0.05$, n = 12, N = 3).

A
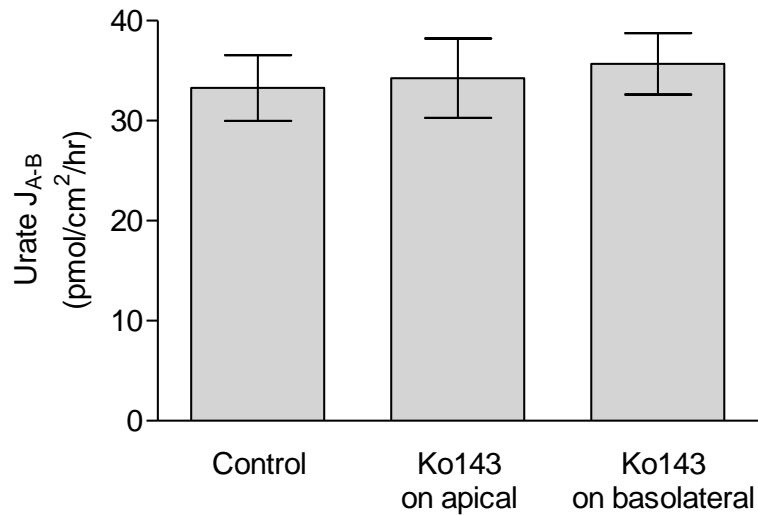
B
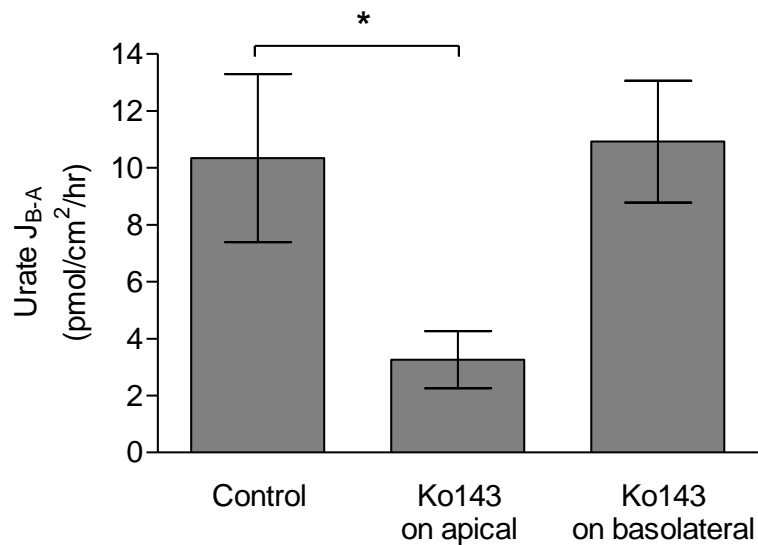
Figure 5.4: Unidirectional urate fluxes by rat PTC monolayers in the presence of 1 µM Ko143.

(A) J_{A-B} exhibited no significant difference in magnitude in the presence of Ko143 when compared to the control. (B) However, J_{B-A} saw a 68.47 % decrease in magnitude when Ko143 was present in the apical membrane (from 10.34 ± 2.95 pmol/cm^2/hr to 3.26 ± 1.00 pmol/cm^2/hr). No significant difference was observed in J_{B-A} when Ko143 was present in the basolateral membrane (10.92 ± 2.14 pmol/cm^2/hr). Each bar represents the mean ± SEM of 12 replicates obtained from three separate experiments. Two-way ANOVA was performed to determine statistical significant difference between the conditions. *, P < 0.05.

A
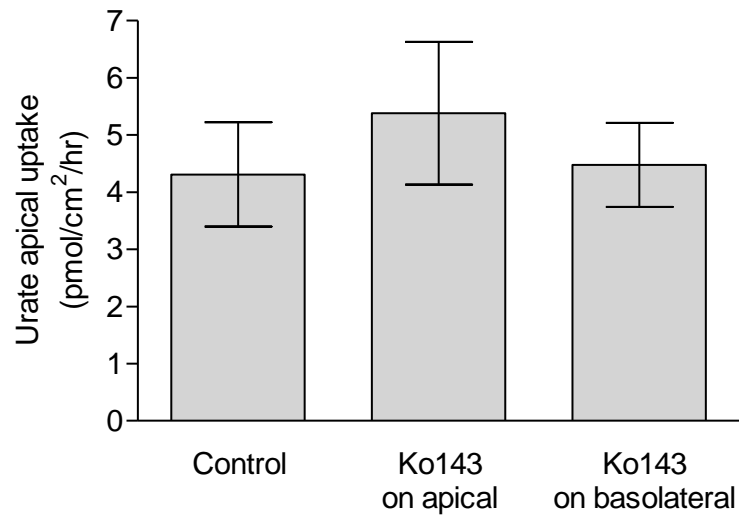
B
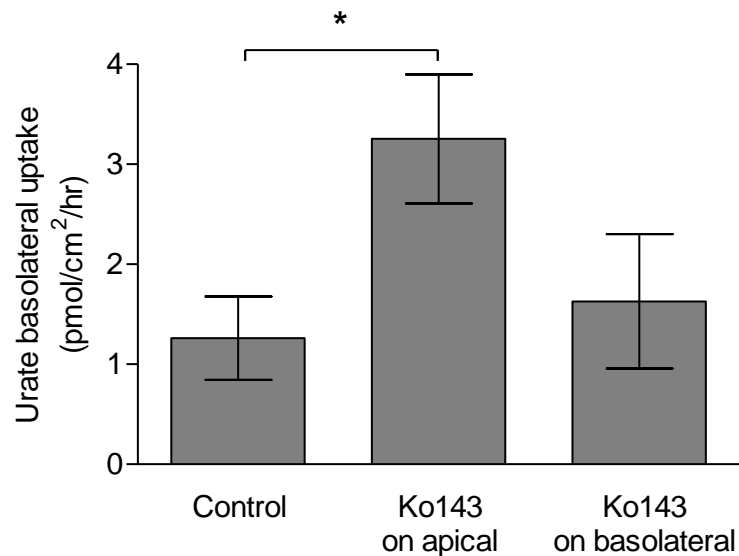
Figure 5.5: Urate uptake by rat PTC monolayers in the presence of 1 μM Ko143.

(A) No significant difference was observed in urate uptake across the apical membrane of the rat PTC monolayers with Ko143 treatment. (B) Uptake of urate across the basolateral membrane was up 2.58-fold when compared to the control (from 1.26 ± 0.42 pmol/cm²/hr to 3.25 ± 0.64 pmol/cm²/hr). No significant difference was observed in basolateral uptake when Ko143 was treated on the basolateral side of the monolayer (1.63 ± 0.67 pmol/cm²/hr). Each bar represents the mean ± SEM of 12 replicates obtained from three separate experiments. Two-way ANOVA was performed to determine significant difference between the conditions. *, P < 0.05.

5.5 The effects of PAH on urate transport by rat PTC monolayers

Unidirectional urate fluxes were repeated in the presence of 10 µM PAH to identify Oat1-mediated component of urate transport in rat PTC monolayers. PAH was treated only on the apical or basolateral side of the confluent monolayer. The results are shown in Figure 5.6 and Figure 5.7.

The presence of PAH on the apical or basolateral sides did not affect the magnitude of J_{A-B} significantly ($P > 0.05$, n = 9, N = 3). The values were not significantly different to the control (PAH on the apical side; 35.40 ± 3.29 pmol/cm^2/hr, PAH on the basolateral side; 30.66 ± 4.07 pmol/cm^2/hr, control; 33.27 ± 3.29 pmol/cm^2/hr, n = 9, N = 3). J_{B-A} was significantly lowered with treatment of PAH on the basolateral side of the monolayer when compared to the control. The magnitude fell from 10.34 ± 2.95 pmol/cm^2/hr to 4.15 ± 0.72 pmol/cm^2/hr, a 59.9 % decrease ($P < 0.05$, n = 9, N = 3).

Uptake of urate across the apical membrane did not change significantly with apical or basolateral treatment of PAH ($P > 0.05$, n = 9, N = 3). However, uptake of urate across the basolateral membrane saw a 65.9 % decrease in magnitude (from 1.26 ± 0.42 pmol/cm^2/hr to 0.43 ± 0.25 pmol/cm^2/hr, $P < 0.05$, n = 9, N = 3) when PAH was presence in the basolateral side of the rat PTC monolayers.

A
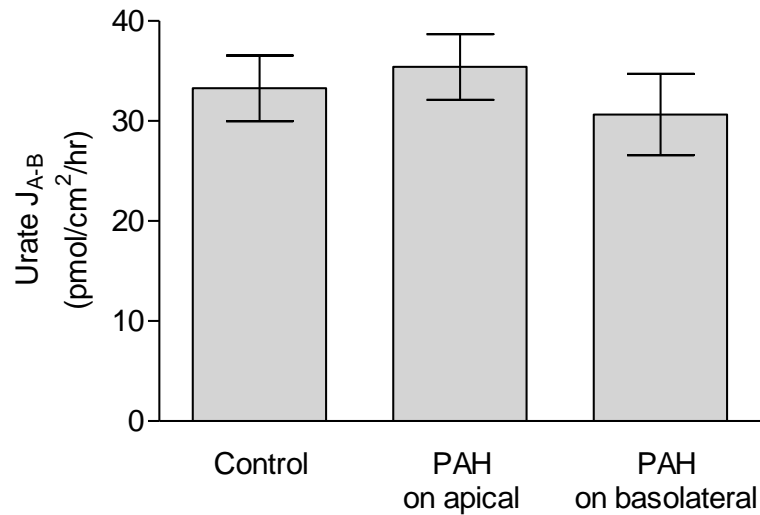
B
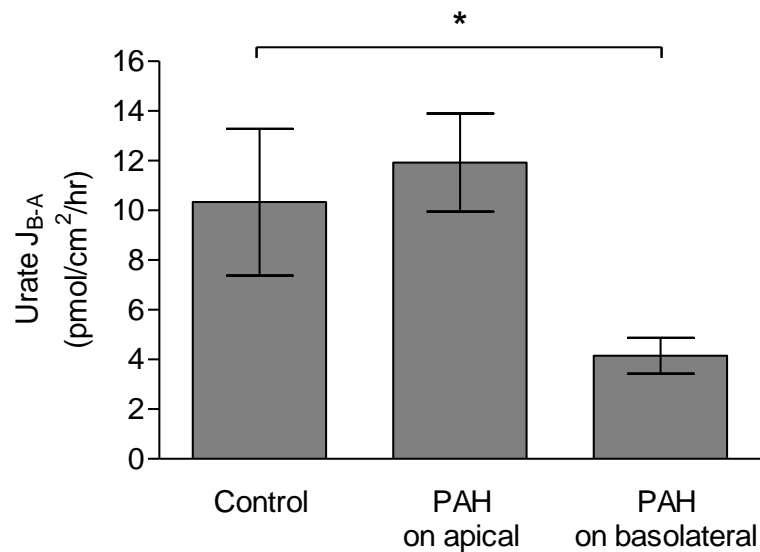
Figure 5.6: Unidirectional urate fluxes by rat PTC monolayers in the presence of 10 μM PAH.

(A) The presence of PAH on the apical or basolateral sides did not affect the magnitude of J_{A-B} significantly. (B) J_{B-A} was significantly lowered with treatment of PAH on the basolateral side of the monolayer when compared to the control. The magnitude fell from 10.34 ± 2.95 pmol/cm²/hr to 4.15 ± 0.72 pmol/cm²/hr, a 59.9 % decrease. Each bar represents the mean $\pm$ SEM of 9-10 replicates obtained from three separate experiments. Two-way ANOVA was performed to determine significant difference between the conditions. *, $P < 0.05$.

A
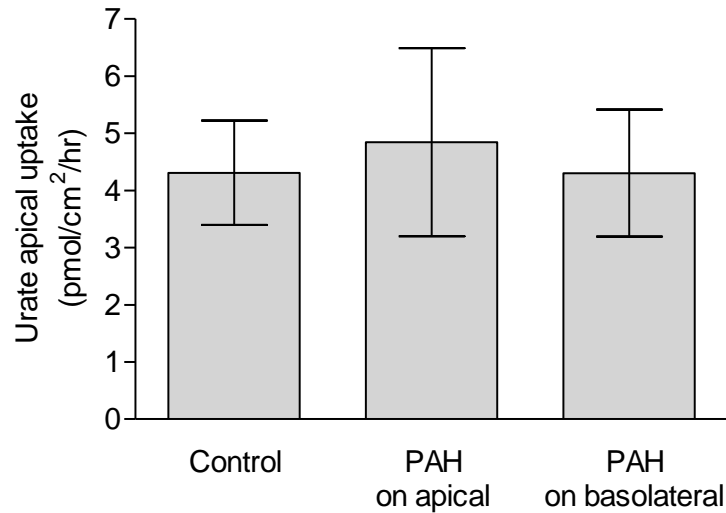
B
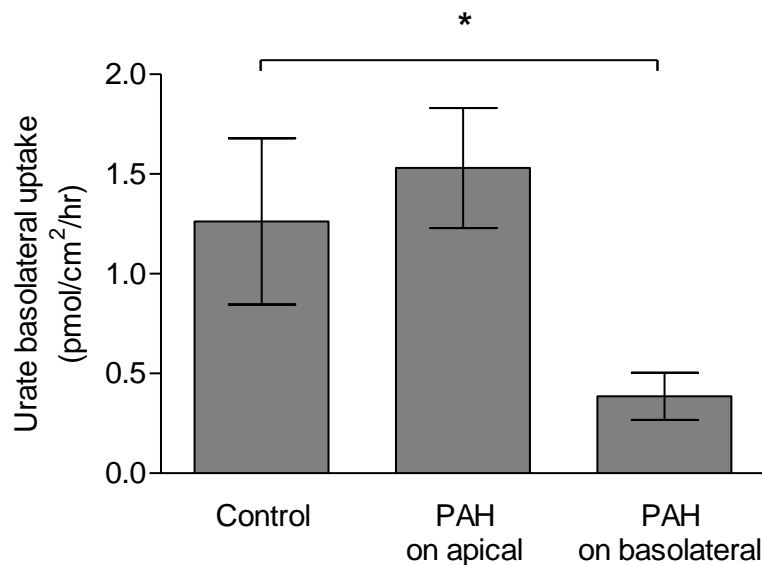
Figure 5.7: Urate uptake by rat PTC monolayers in the presence of 10 μM PAH.

(A) Uptake of urate across the apical membrane did not change significantly with apical or basolateral treatment of PAH. (B) However, uptake of urate across the basolateral membrane saw a 65.9 % decrease in magnitude (from 1.26 ± 0.42 pmol/cm^2/hr to 0.43 ± 0.25 pmol/cm^2/hr) when PAH was presence in the basolateral side of the rat PTC monolayers. Each bar represents the mean $\pm$ SEM of 9-10 replicates from three separate experiments. Two-way ANOVA was performed to determine significant difference between the conditions. *, $P < 0.05$.

5.6 The effects of MK-571 on urate transport by rat PTC monolayers

Mrp inhibitor, MK-571, was also used during urate fluxes to verify if urate transport by rat PTC monolayers had an Mrp-mediated component. Unidirectional urate fluxes were performed in rat PTC monolayers in the presence of 10 µM MK-571. The results are shown in Figure 5.8.

Urate J_{A-B} and J_{B-A} were 33.98 ± 3.34 pmol/cm^2/hr and 12.09 ± 2.81 pmol/cm^2/hr, respectively, in the presence of MK-571 (Figure 5.8). These values were not significantly different in magnitude when compared to the control J_{A-B} and J_{B-A} (P > 0.05, n = 12, N = 3). Similarly, uptake across the apical and basolateral membranes (4.13 ± 0.73 pmol/cm^2/hr and 1.75 ± 0.41 pmol/cm^2/hr, respectively) in the presence of MK-571 were not significantly different to the controls (P > 0.05, n = 12, N = 3).

A
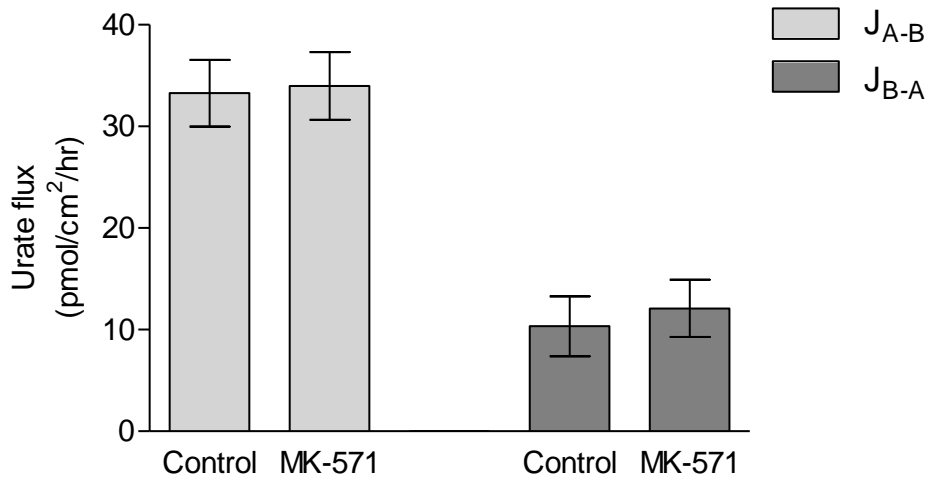
B
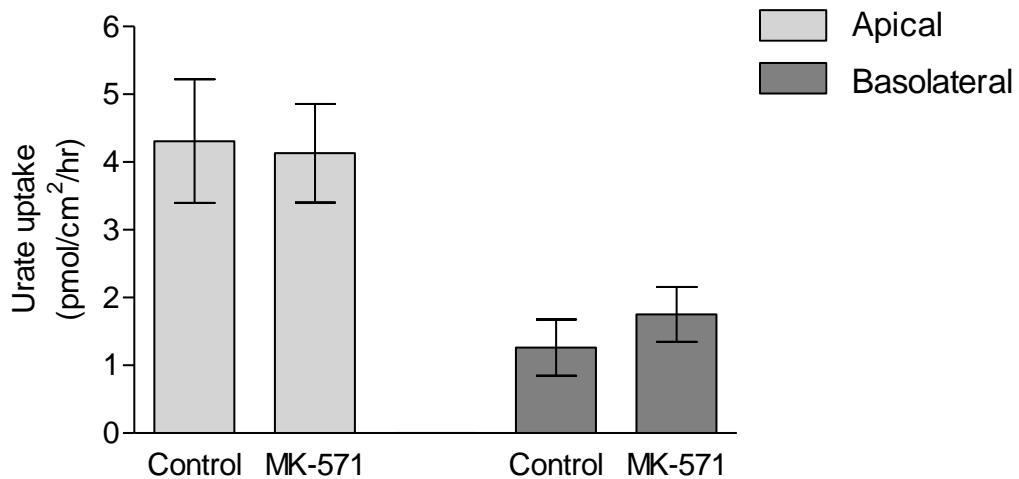
Figure 5.8: Unidirectional urate fluxes and uptake by rat PTC monolayers in the presence of 10 μM MK-571.

*(**A**) Urate J_{A-B} and J_{B-A} were 33.98 ± 3.34 pmol/cm^2/hr and 12.09 ± 2.81 pmol/cm^2/hr, respectively, in the presence of MK-571. These values were not significantly different in magnitude when compared to the controls. (**B**) Uptake across the apical and basolateral membranes were 4.13 ± 0.73 pmol/cm^2/hr and 1.75 ± 0.41 pmol/cm^2/hr, respectively, in the presence of MK-571. These values were not significantly different to the controls. Each bar represents the mean $\pm$ SEM of 12 replicates from three separate experiments. Student t test was performed to determine significant difference between the conditions.*

5.7 Urate handling by human PTC monolayers

Unidirectional urate fluxes and uptake were also carried out in human PTC monolayers to highlight any differences the rat and human PTC models may have. Similar to the experiments using rat PTC monolayers, this series of experiments were carried out using 35 µM of urate.

Like the rat PTC monolayers, human PTC monolayers also exhibit net urate absorption (Figure 5.9A). Urate J_{A-B} (47.59 ± 4.83 pmol/cm^2/hr) was 3.43-fold higher than J_{B-A} (13.87 ± 1.78 pmol/cm^2/hr), which gave an absorption J_{Net} of 33.72 ± 6.30 pmol/cm^2/hr ($P < 0.001$, n = 12, N = 3). Urate uptake was predominately across the apical side, which was 7.64 ± 1.16 pmol/cm^2/hr, compared to the across the basolateral side which was 2.60 ± 0.71 pmol/cm^2/hr (66.0 % decrease, $P < 0.01$, n = 12, N = 3, Figure 5.9B).

A
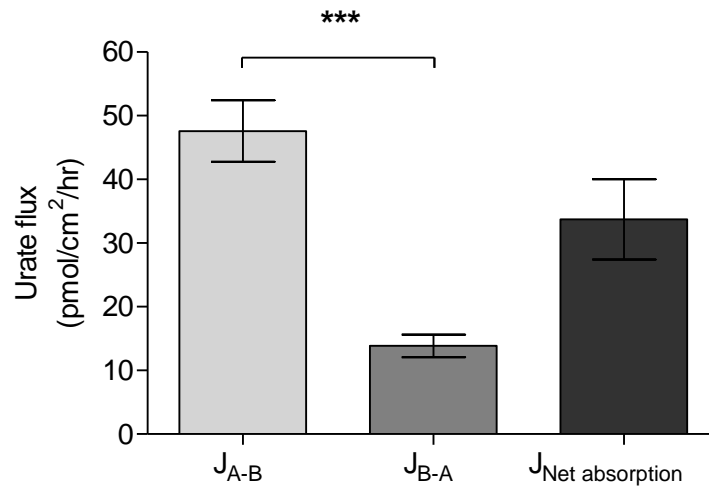
B
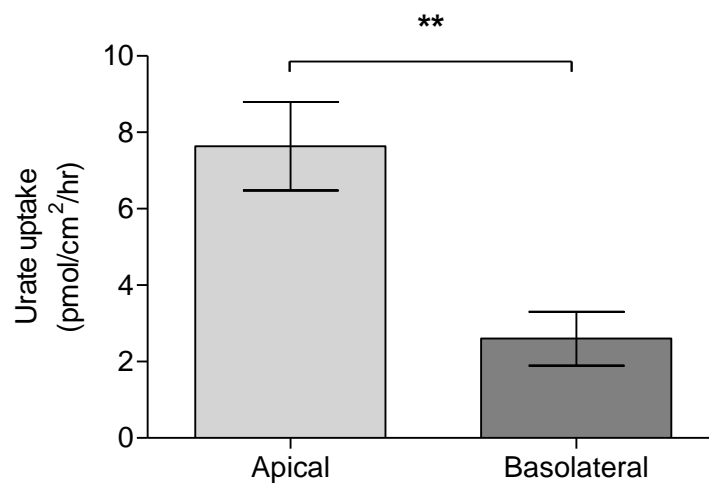
Figure 5.9: Unidirectional urate fluxes and uptake by human PTC monolayers.

*(A) Urate J_{A-B} (47.59 ± 4.83 pmol/cm^2/hr) was 3.43-fold more than J_{B-A} (13.87 ± 1.78 pmol/cm^2/hr), which gave a J_{Net} absorption of 33.72 ± 6.30 pmol/cm^2/hr. (B) Urate uptake was predominately across the apical side, which was 7.64 ± 1.16 pmol/cm^2/hr, compared to the across the basolateral side which was 2.60 ± 0.71 pmol/cm^2/hr, a 66.0 % decrease. Each bar represents the mean ± SEM of 12 replicates from three separate experiments. Student t test was performed to determine statistical significance. **, $P < 0.01$, ***, $P < 0.001$.*

5.8 The effects of benzbromarone on urate transport by human PTC monolayers

Unidirectional urate fluxes and uptake by human PTC monolayers were repeated in the presence of benzbromarone. 50 µM of benzbromarone was treated on either the apical or basolateral membranes of the human PTC monolayers prior to the initiation of urate fluxes. The results are presented in Figure 5.10 and Figure 5.11.

Urate J_{A-B} saw marked changes in the presence of benzbromarone (Figure 5.10A). When benzbromarone was treated on the apical side of the human PTC monolayers, J_{A-B} decreased 71.7 % when compared to the control (from 47.59 ± 4.83 pmol/cm^2/hr to 13.47 ± 3.46 pmol/cm^2/hr, P < 0.01, n = 11, N = 3). Similarly, when benzbromarone was treated on the basolateral side of the monolayer, J_{A-B} was decreased to 14.28 ± 4.46 pmol/cm^2/hr, a 70.0 % decrease (P < 0.01, n = 11, N = 3). Conversely, the presence of benzbromarone on the apical membrane caused the J_{B-A} to increase by 1.57-fold, from 13.86 ± 1.78 pmol/cm^2/hr to 21.81 ± 2.60 pmol/cm^2/hr (P < 0.05, n = 11, N = 3, Figure 5.10B). When compared to the control, J_{B-A} did not exhibit statistically significant change when benzbromarone was on the basolateral membrane.

Only urate uptake across the apical membrane was significantly different when compared to their respective controls. Apical uptake of urate was 2.46 times lower in magnitude when benzbromarone was treated on the apical membrane of the human PTC monolayer (from 7.64 ± 1.16 pmol/cm^2/hr to 3.11 ± 0.69 pmol/cm^2/hr, P < 0.05, n = 11, N = 3, Figure 5.11B). Urate uptake across the apical membrane was increased by 1.88-fold when benzbromarone was on the basolateral membrane (14.38 ± 1.54 pmol/cm^2/hr, P < 0.05, n = 12, N = 3). Basolateral uptake of urate was 3.22 ± 1.04 pmol/cm^2/hr and 3.35 ± 0.59 pmol/cm^2/hr when benzbromarone was on the apical and basolateral membrane of the monolayer, respectively. When compared to the control basolateral uptake of urate at 2.60 ± 0.71 pmol/cm^2/hr, no statistically significant differences were calculated (Figure 5.11B).

A
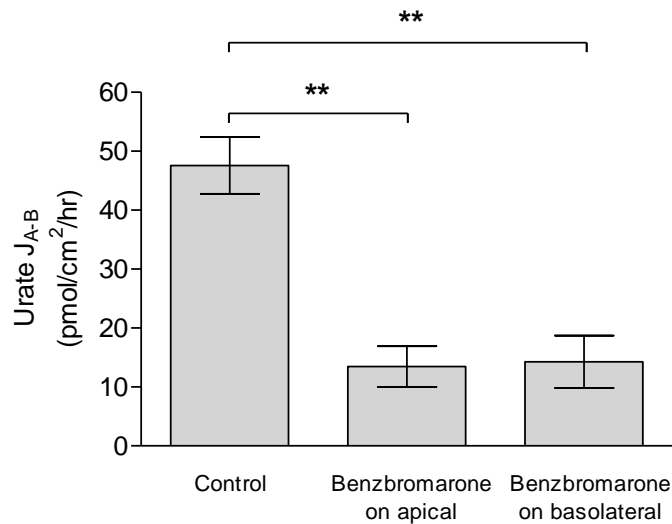
B
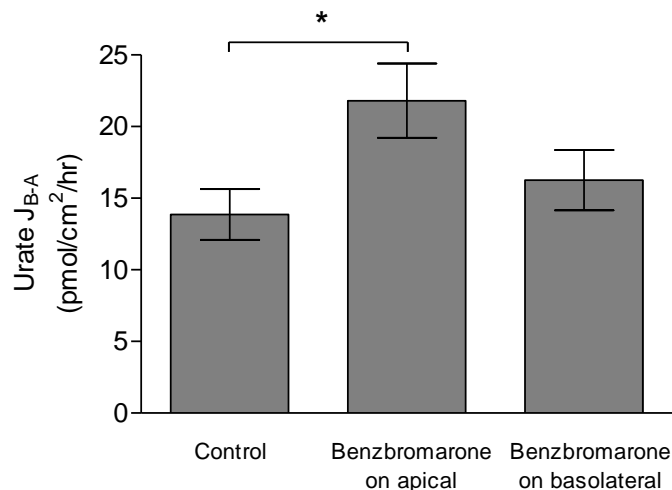
Figure 5.10: Unidirectional urate fluxes by human PTC monolayers in the presence of 50 μM benzbromarone.

*(A) J_{A-B} decreased 71.7 % in the presence of apically-treated benzbromarone when compared to the control (from 47.59 ± 4.83 pmol/cm^2/hr to 13.47 ± 3.46 pmol/cm^2/hr). When benzbromarone was treated on the basolateral side of the monolayer, J_{A-B} decreased to 14.28 ± 4.46 pmol/cm^2/hr (70.0 %). (B) Conversely, the presence of benzbromarone on the apical membrane caused J_{B-A} to increase by 1.57-fold, from 13.86 ± 1.78 pmol/cm^2/hr to 21.81 ± 2.60 pmol/cm^2/hr. When compared to the control, J_{B-A} did not exhibit statistically significant change when benzbromarone was on the basolateral membrane. Each bar represents the mean ± SEM of 11-12 replicates obtained from three separate experiments. Two-way ANOVA was performed to determine statistical significance. *, $P < 0.05$, **, $P < 0.01$.*

A
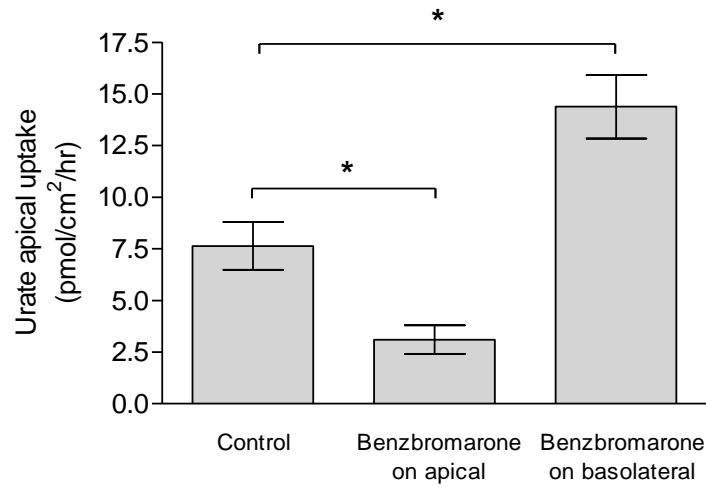
B
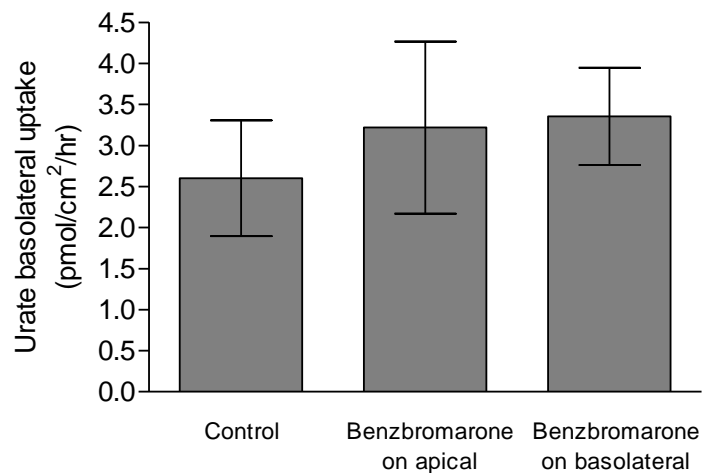
Figure 5.11: Uptake of urate by human PTC monolayers in the presence of 50 μM benzbromarone.

(A) Apical uptake of urate was 2.46 times lower in magnitude when benzbromarone was treated on the apical membrane of the human PTC monolayer (from 7.64 ± 1.16 pmol/cm^2/hr to 3.11 ± 0.69 pmol/cm^2/hr). Urate uptake across the apical membrane was increased by 1.88-fold when benzbromarone was on the basolateral membrane (14.38 ± 1.54 pmol/cm^2/hr). (B) Basolateral uptake of urate was 3.22 ± 1.04 pmol/cm^2/hr and 3.35 ± 0.59 pmol/cm^2/hr when benzbromarone was on the apical and basolateral membrane of the monolayer, respectively. When compared to the control basolateral uptake of urate at 2.60 ± 0.71 pmol/cm^2/hr, no statistically significant differences were calculated. Each bar represents the mean ± SEM of 11-12 replicates from three separate experiments. Two-way ANOVA was performed to determine statistical significance. *, $P < 0.05$.

5.9 The effects of Ko143 on urate transport by human PTC monolayers

A series of experiments were carried out where unidirectional urate fluxes and uptake were repeated with human PTC monolayers in the presence of human BCRP specific inhibitor, Ko143, to identify BCRP-mediated transport of urate. Similar to the previous experiment, 1 µM Ko143 was exposed to either the apical or basolateral membranes of the human PTC monolayers for 30 minutes prior to urate flux initiation. The results are presented in Figure 5.12 and Figure 5.13.

The presence of Ko143 did not change the magnitudes of urate J_{A-B} by the human PTC monolayers significantly. The values of J_{A-B} were 47. 59 ± 4.83 pmol/cm^2/hr by the control monolayers, 49.21 ± 3.76 pmol/cm^2/hr by the monolayers that were apically-treated with Ko143, and 50.66 ± 5.80 pmol/cm^2/hr by the monolayers that were basolaterally-treated with Ko143 ($P > 0.05$, $n = 12$, $N = 3$, Figure 5.12A). J_{B-A} was significantly decreased when the monolayer was treated with Ko143 from the apical membrane. Ko143 caused J_{B-A} to fall from 13.87 ± 1.78 pmol/cm^2/hr to 5.53 ± 1.38 pmol/cm^2/hr ($P < 0.01$, $n = 12$, $N = 3$, Figure 5.12B). J_{B-A} was not significantly changed when Ko143 was treated on from the basolateral membrane (15.22 ± 1.12 pmol/cm^2/hr, $P > 0.05$, $n = 12$, $N = 3$).

A similar pattern was observed in the uptake of urate by human PTC treated with Ko143. The presence of Ko143 did not change the magnitudes of urate uptake across the apical membrane significantly (Figure 5.13A). However, basolateral uptake of urate was increased in the presence of Ko143 in the apical membrane, from 2.60 ± 0.71 pmol/cm^2/hr to 5.25 ± 0.75 pmol/cm^2/hr, a 2-fold increase ($P < 0.05$, $n = 12$, $N = 3$, Figure 5.13B).

A
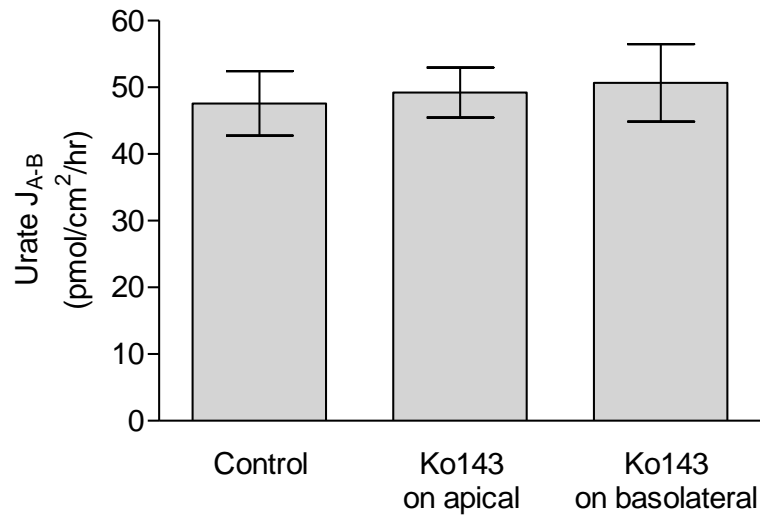
B
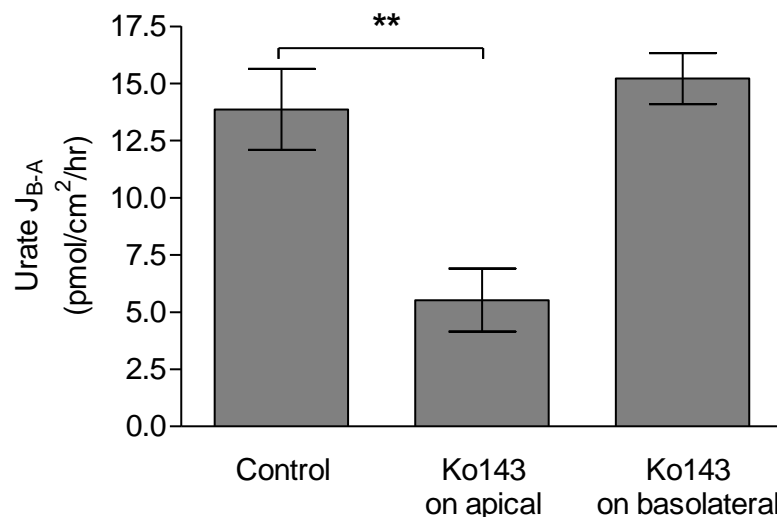
Figure 5.12: Unidirectional urate fluxes by human PTC monolayers in the presence of 1 μM Ko143.

(*A*) *The presence of Ko143 did not change the magnitudes of urate* J_{A-B} *in the human PTC monolayers significantly. (**B**)* J_{B-A} *was significantly decreased when the monolayer was treated with Ko143 from the apical membrane. Ko143 caused* J_{B-A} *to fall from* 13.87 ± 1.78 *pmol/cm^2/hr to* 5.53 ± 1.38 *pmol/cm^2/hr.* J_{B-A} *was not significantly changed when Ko143 was treated on from the basolateral membrane. Each bar represents the mean ± SEM of 12 replicates obtained from three separate experiments. Two-way ANOVA was performed to determine statistical significance. **, P < 0.01.*

A
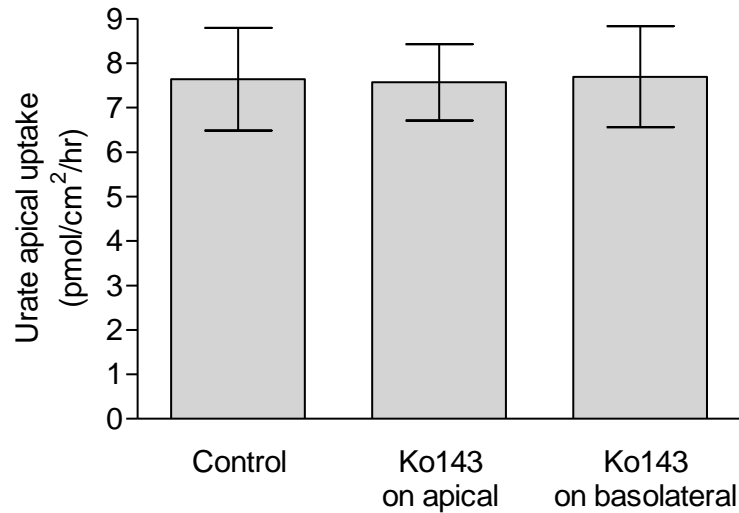
B
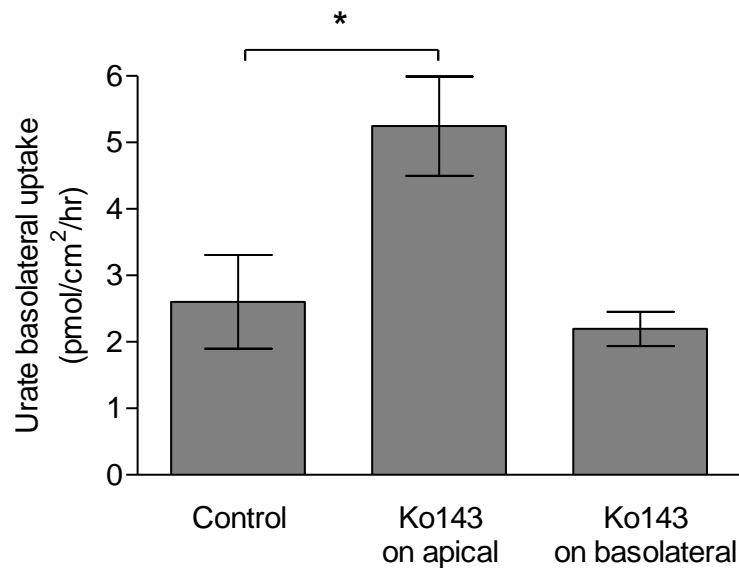
Figure 5.13: Uptake of urate by human PTC monolayers in the presence of 1 μM Ko143.

(**A**) The presence of Ko143 did not change the magnitudes of urate uptake across the apical membrane significantly. (**B**) Basolateral uptake of urate was increased in the presence of Ko143 in the apical membrane, from 2.60 ± 0.71 pmol/cm^2/hr to 5.25 ± 0.75 pmol/cm^2/hr, a 2-fold increase. The presence of Ko143 on the basolateral membrane did not alter the magnitude of basolateral uptake of urate significantly. Each bar represents the mean $\pm$ SEM of 12 replicates from three separate experiments. Two-way ANOVA was performed to determine statistical significance. *, $P < 0.05$.

5.10 The effects of PAH on urate transport by human PTC monolayers

Urate unidirectional fluxes by human PTC monolayers were performed in the presence of 10 µM PAH, which is an inhibitor of OAT1. PAH was treated to either the apical or basolateral side of the monolayers. This will elucidate OAT1's role in basolateral uptake of urate by PTCs. Figure 5.14 and Figure 5.15 show the results.

The magnitudes of J_{A-B} by the human PTC monolayers in the presence of PAH in the apical chambers and basolateral chambers were 50.40 ± 3.51 pmol/cm^2/hr and 53.41 ± 3.66 pmol/cm^2/hr, respectively. These values were not statistically different to the control ($P > 0.05$, n = 9, N = 3). Only J_{B-A} was significantly different to the control when PAH was present in the basolateral chamber, which saw the J_{B-A} decreased from 13.86 ± 1.78 pmol/cm^2/hr to 6.15 ± 1.85 pmol/cm^2/hr, a 55.6 % decrease ($P < 0.05$, n = 10, N = 3).

Uptake of urate across the apical membrane was not affected by the presence of PAH on either the apical or basolateral membrane. However, monolayers treated with PAH on the basolateral side saw a 60.0 % decrease in uptake across the basolateral membrane (from 2.60 ± 0.71 pmol/cm^2/hr to 1.04 ± 0.16 pmol/cm^2/hr, $P < 0.05$, n = 10, N = 3).

A
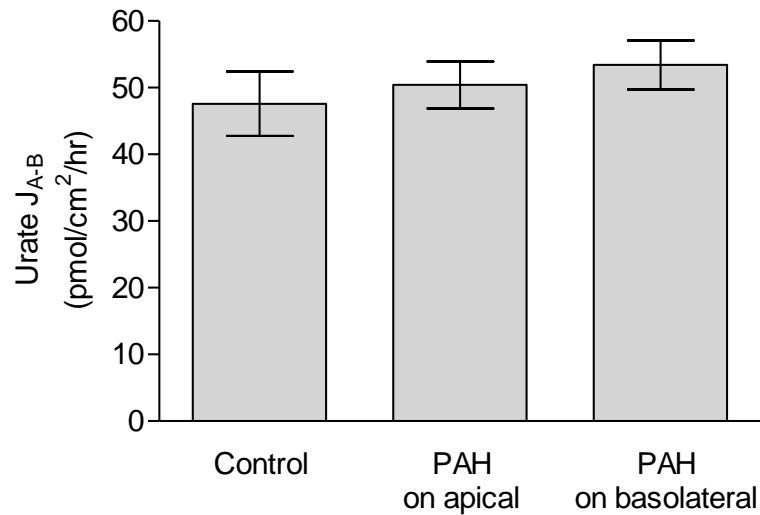
B
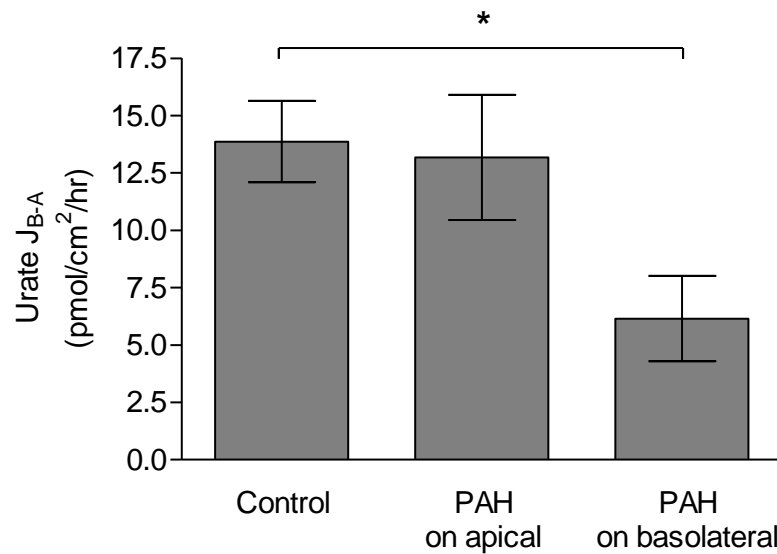
Figure 5.14: Unidirectional fluxes of urate by human PTC monolayers in the presence of 10 µM PAH.

*(A) J_{A-B} by the human PTC monolayers in the presence of PAH in the apical chambers and basolateral chambers were 50.40 ± 3.51 pmol/cm²/hr and 53.41 ± 3.66 pmol/cm²/hr, respectively. These values were not statistically different to the control. (B) Only J_{B-A} was significantly different to the control when PAH was present in the basolateral chamber, which saw the J_{B-A} fell to 6.15 ± 1.85 pmol/cm²/hr, a 55.6 % decrease. Each bar represents the mean ± SEM of 9-10 replicates from three separate experiments. Two-way ANOVA was performed to determine statistical significance. *, P < 0.05.*

A
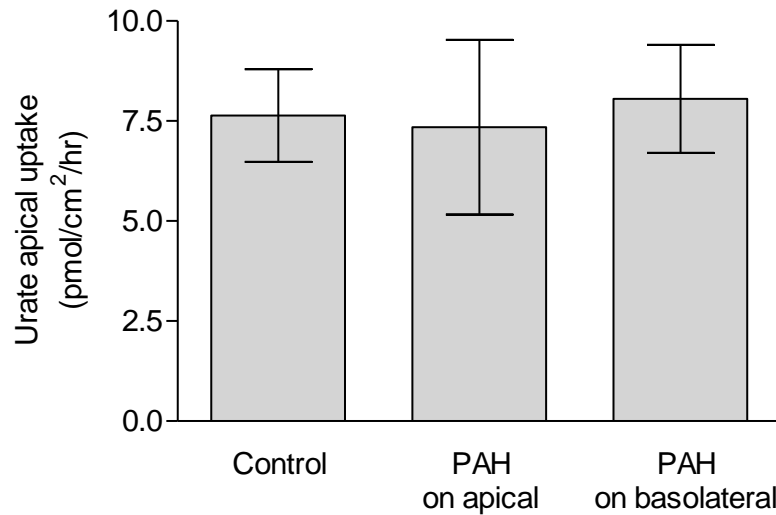
B
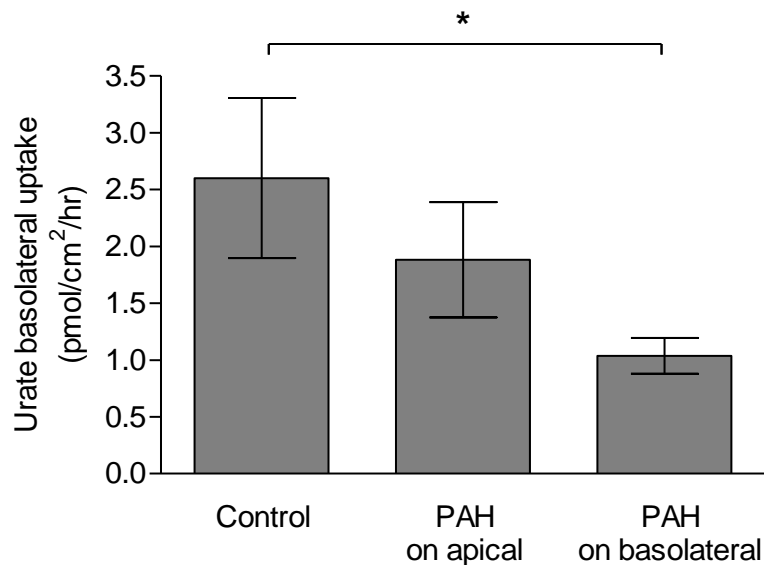
Figure 5.15: Uptake of urate by human PTC monolayers in the presence of 10 μM PAH.

(A) Uptake of urate across the apical membrane was not affected by the presence of PAH, which saw no significant changes in apical uptake of urate when PAH was treated either apically or basolaterally. (B) However, when PAH on the basolateral side of the monolayer, a 60.0 % decrease in uptake across the basolateral membrane was observed (from 2.60 ± 0.71 pmol/cm^2/hr to 1.04 ± 0.16 pmol/cm^2/hr). Each bar represents the mean $\pm$ SEM of 9-10 replicates from three separate experiments. Two-way ANOVA was performed to determine statistical significance. *, $P < 0.05$.

5.11 The effects of MK-571 on urate transport by human PTC monolayers

In addition to BCRP, the activity of human MRP in urate transport by human PTC monolayers was also examined by initiation urate fluxes in the presence of MK-571. Unidirectional urate fluxes and uptake were repeated in the presence of 10 µM MK-571. The results are summarised in Figure 5.16.

The presence of MK-571 did not alter urate J_{A-B} significantly (48.96 ± 4.30 pmol/cm^2/hr, P > 0.05, n = 12, N = 3, Figure 5.16A). Urate J_{B-A} in the presence of MK-571 was 13.78 ± 1.63 pmol/cm^2/hr, but was not significantly different to the control of 13.87 ± 1.78 pmol/cm^2/hr (P > 0.05, n = 12, N = 3).

Uptake of urate across the apical membranes of the monolayer was not affected by MK-571 (P > 0.05, n = 12, N = 3, Figure 5.16B), nor was uptake across the basolateral membrane when compared to the controls (P > 0.05, n = 12, N = 3).

A

B
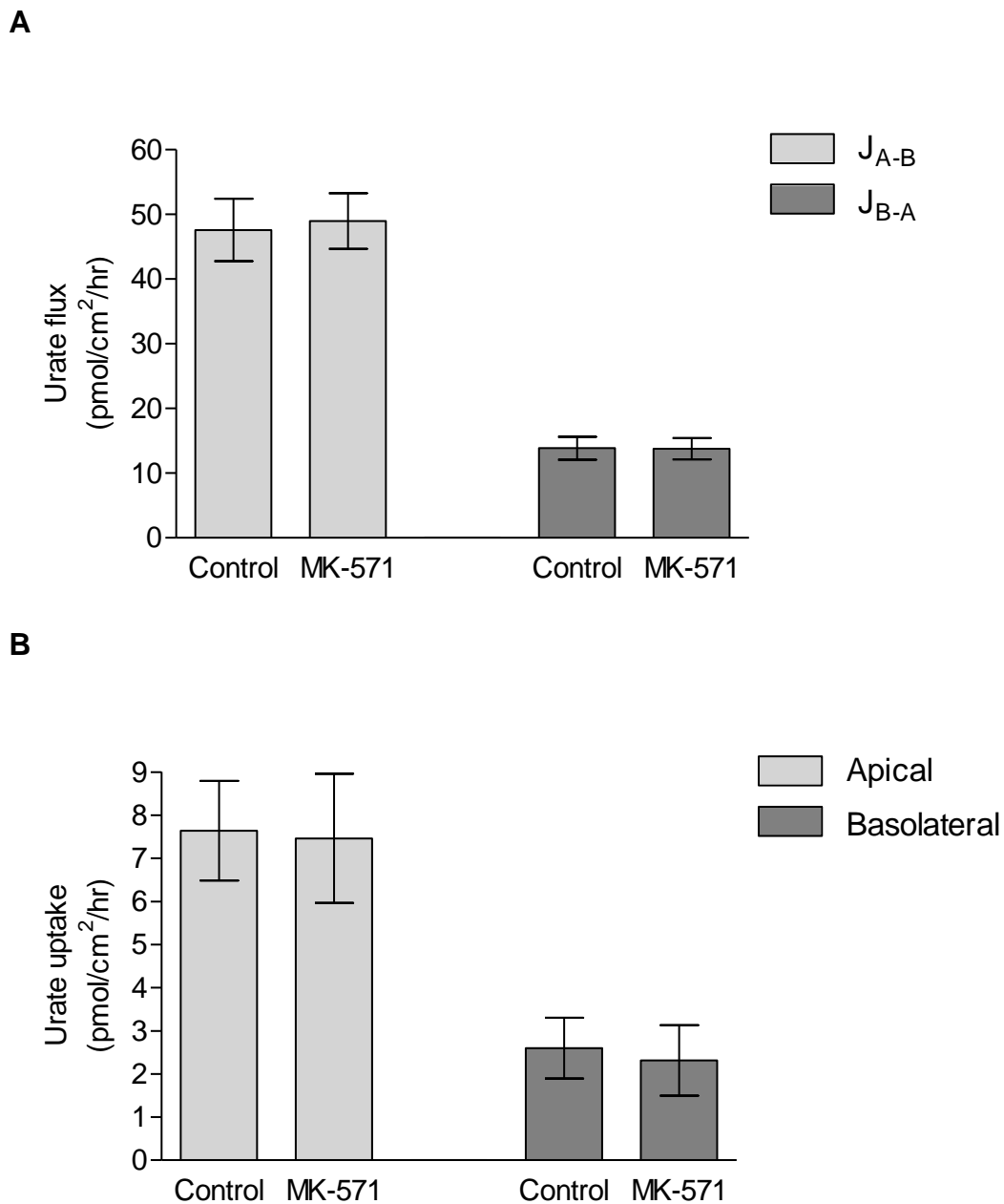
Figure 5.16: Unidirectional urate flux by human PTC monolayers in the presence of 10 μM MK-571.

(A) MK-571 did not alter urate J_{A-B} significantly (48.96 ± 4.30 pmol/cm^2/hr). Urate J_{B-A} in the presence of MK-571 was 13.78 ± 1.63 pmol/cm^2/hr, which was not significantly different to the control of 13.87 ± 1.78 pmol/cm^2/hr. (B) Uptake of urate across the apical membranes of the monolayer was not affected by MK-571, nor was uptake across the basolateral membrane, when compared to the controls. Each bar represents the mean ± SEM of 12 replicates from three separate experiments. Two-way ANOVA was performed to determine statistical significance.

5.12 Urate uptake by URAT1 and SLC2A9 expressing *Xenopus* oocytes

Xenopus oocytes were used as a model to investigate the mechanism of human URAT1 and SLC2A9 in urate transport. The effect of benzbromarone was tested on the transporters, along with a novel anti-gout drug, lesinurad. A representative of the results from 3 independent experiments is shown in Figure 5.17. The amount of transporter-mediated urate taken up by oocytes was calculated by subtracting away the urate amount in water-injected oocytes. Water-injected oocytes showed urate uptake of below 0.05 pmol/oocyte/hr in all instances (data not shown).

URAT1-injected oocytes showed the highest uptake of urate; in the absence of any inhibitor, URAT1-injected oocytes were taking up 3.54 ± 0.67 pmol/oocyte/hr. In the presence of 50 µM benzbromarone, the influx of urate decreased 84.7 % to 0.54 ± 0.07 pmol/oocyte/hr ($P < 0.001$, N = 10). Similarly, in the presence of 50 µM lesinurad, the influx of urate fell to 0.48 ± 0.11 pmol/oocyte/hr ($P < 0.001$, N = 10).

SLC2A9 injected oocytes also showed urate uptake, but the presence of 50 µM benzbromarone caused urate uptake by SLC2A9-injected oocytes to decrease 4.93-times (0.51 ± 0.12 pmol/oocyte/hr, $P < 0.01$, N = 12), and the presence of 50 µM lesinurad caused the urate uptake to decrease 2.60-times (0.95 ± 0.15 pmol/oocyte/hr, $P < 0.01$, N = 12).

A
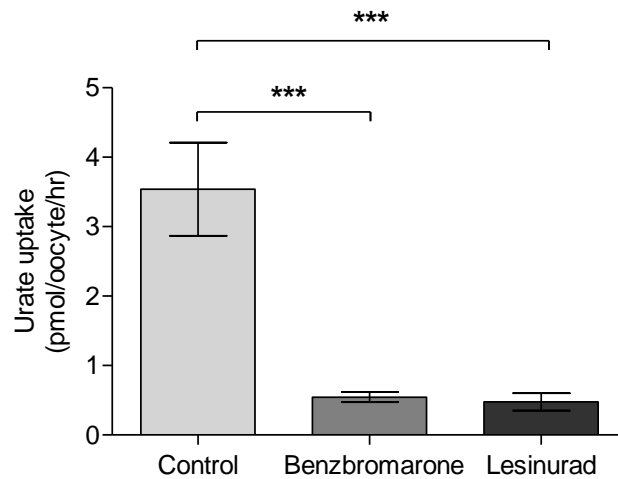
B
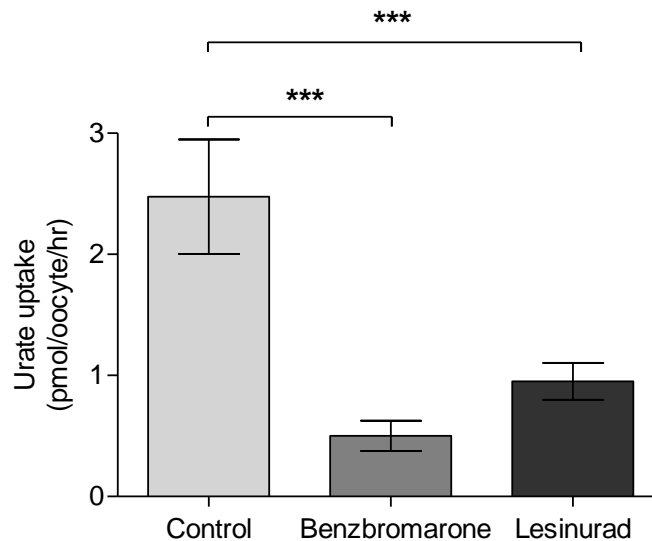
Figure 5.17: Uptake of urate by URAT1 and SLC2A9-injected oocytes.

(A) In the absence of any inhibitor, URAT1-injected oocytes were taking up urate at 3.54 ± 0.67 pmol/oocyte/hr. In the presence of 50 μM benzbromarone, the influx of urate decreased to 0.54 ± 0.07 pmol/oocyte/hr. Similarly, in the presence of 50 μM lesinurad, the influx of urate fell to 0.48 ± 0.11 pmol/oocyte/hr. (B) SLC2A9-injected oocytes also showed urate uptake, but the presence of 50 μM benzbromarone caused urate uptake to decrease 4.93-times (0.51 ± 0.12 pmol/oocyte/hr), and the presence of 50 μM lesinurad caused the urate uptake to decrease 2.60-times (0.95 ± 0.15 pmol/oocyte/hr). The amount of transporter-mediated urate taken up by oocytes was calculated by subtracting away the urate amount in water-injected oocytes. Water-injected oocytes showed urate uptake of below 0.05 pmol/oocyte/hr in all instances (data not shown). The experiments were performed using 3 batches of oocytes, and results from the representative experiment are expressed as mean ± SEM of 10-12 oocytes. Statistical significance was determined by two-way ANOVA.

5.13 Discussion

The rat PTCs' ability to retain mRNA and functional expressions of various transporters are highlighted in the previous chapters. The cells role as a robust *in vitro* model for drug transporter studies has yet to be validated. In this chapter, urate handling by rat PTC monolayers was investigated and compared with the handling of urate by human PTC monolayers. Renal transport of urate in humans has been extensively studied, which involves a complex interplay of absorption and secretory pathways (Guggino and Aronson, 1985; Enomoto *et al.*, 2002; Anzai *et al.*, 2005). This makes the use of urate as a candidate molecule to study how the two *in vitro* models reflect the *in vivo* setting particularly advantageous.

5.13.1 Mechanism of urate reabsorption

In humans, urate is filtered via glomerular filtration and enters the proximal tubule before more than 90 % is extensively reabsorbed (Roch-Ramel and Guisan, 1999). The initial transport mechanism predominantly occurs in the proximal tubules with the distal tubules and collecting ducts hardly permeable to urate (Roch-Ramel and Guisan, 1999). Reabsorption of the filtered urate is initiated by the urate/anion exchanger, URAT1. First cloned by Enomoto *et al.* in 2001, URAT1 is a member of the organic anion transporter family and is found on the apical membrane of the proximal tubule (Enomoto *et al.*, 2002). Its expression in *Xenopus* oocytes resulted in significant uptake of urate into the oocytes. Inactivated mutants of URAT1 were discovered in patients with idiopathic renal hypouricemia and hyperuricosuria (Enomoto *et al.*, 2002; Tanaka *et al.*, 2003). Taken together, these data suggest URAT1 as a major transporter for urate reabsorption.

Urate fluxes performed on the rat and human PTC monolayers were able to replicate the absorptive nature of the proximal tubule; J_{A-B} was significantly higher in magnitude than J_{B-A} in both models, resulting in an absorptive J_{Net}. The data also showed the amount of urate taken up across the apical membrane was significantly more than from across the basolateral membrane in both rat and human PTC monolayers. To further verify the handling of urate by both species of PTCs, in particular the functional expression of URAT1/Urat1, the fluxes were repeated in the presence of known URAT1 inhibitor, benzbromarone (Fox and

Sinclair, 1977). As expected, several folds decrease in magnitude of J_{A-B} in both species was observed when benzbromarone was present in the apical membrane of the monolayers. This was correlated with a decrease in urate uptake across the same membrane. The movement of urate from the basolateral to apical direction was increased in the human PTC monolayers. This could be explained by the tendency of the monolayer to reabsorb urate. Urate that had already been secreted from the basolateral to the apical chamber was reabsorbed by the monolayer. But inhibition of URAT1/Urat1 by benzbromarone led to significantly less urate being reabsorbed and the observed increase in J_{B-A}.

Interestingly, when benzbromarone was exposed only to the basolateral membrane of the monolayer, J_{A-B} was also decreased by as much as 3.3-fold. One could ascribe that to the uncontrollable leak of benzbromarone from the basolateral to the apical chamber during the course of the experiment, leading to the inadvertent inhibition of URAT1/Urat1 on the apical membrane. However, the uptake of urate across the apical membrane was now higher than the control, which should become lower in magnitude. This set of data was more likely the effects of the presence of a functional benzbromarone-sensitive transporter capable of urate efflux on the basolateral membrane.

Genome-wide association studies gave the first inclination that renal urate transport involved other important protein, which was later shown to be GLUT9, or SLC2A9, a member of the facilitative glucose transporter family (Li *et al.*, 2007; Vitart *et al.*, 2008; Bobulescu and Moe, 2012). Similar to the discovery of URAT1, these studies found loss-of-function mutations in the SLC2A9 gene locus were associated with massive hyperuricosuria (Anzai *et al.*, 2008; Matsuo *et al.*, 2008; Dinour *et al.*, 2010; Kawamura *et al.*, 2011; Dinour *et al.*, 2012). Its ubiquity in the basolateral membrane of proximal tubule cells and the subsequent expression in oocytes that showed strong urate transport activity have led many to accept SLC2A9 as the principle pathway of urate basolateral exit in the human kidney (Augustin *et al.*, 2004; Vitart *et al.*, 2008). SLC2A9 has been shown to be sensitive to benzbromarone as well (Caulfield *et al.*, 2008), and most likely the transporter involved in the efflux of urate across the basolateral membrane of the rat and human PTC monolayers.

J_{A-B} is a measure of the rate of urate appearance on the basolateral chamber when urate was added on the apical chamber. With the inhibition of SLC2A9 on the basolateral membrane by benzbromarone, the transition of urate from the intracellular space into the basolateral chamber was impeded, which resulted in the diminished appearance of urate in that chamber. Consequently, the amount of urate retained in the monolayer would increase as the uptake of urate by URAT1 across the apical membrane remained active. The presence of functioning rat ortholog of SLC2A9 as a urate efflux transporter can also be used to account for the higher basolateral uptake of urate in rat PTC monolayers when benzbromarone was treated on the basolateral side. Urate that had successfully been secreted was reabsorbed, but because of the inhibition of rat Slc2a9 by benzbromarone on the basolateral membrane, the amount of urate retained in the monolayer was increased compared to the control. mRNA of Slc2a9 had been detected in rat PTCs as shown in Chapter 4.

5.13.2 Mechanism of urate secretion

Studies have shown that urate is bi-directionally transported, and reabsorption and secretion happen at the same site in the proximal tubule (Hediger *et al.*, 2005; So and Thorens, 2010; Lipkowitz, 2012). Indeed, both pathways were observed in this study in the rat and human PTC monolayers as J_{A-B} and J_{B-A}. The mechanism of urate secretion is less established than urate reabsorption. Nonetheless, there are increasing data to suggest the involvement of several key transporters. For instance, human OAT1 and OAT3 are postulated as basolateral urate uptake transporters as they have been shown to transport urate (Bakhiya *et al.*, 2003), and human BCRP and MRP4 are seen as possible urate efflux transporter across the apical membrane of proximal tubule cells (Van Aubel *et al.*, 2005; Woodward *et al.*, 2009).

To show OAT1-mediated urate transport in human PTC monolayers, PAH was used to inhibit activity of OAT1. PAH has been used as an OAT1-specific inhibitor in the renal clearance of many drugs, most recently by Maeda *et al.* (Maeda *et al.*, 2014). PAH would compete with the urate for basolaterally located OAT1 and prevent the basolateral uptake, and hence J_{B-A}, of urate when PAH were treated on the basolateral membrane. This was indeed observed in the experiments,

where the uptake of urate and J_{B-A} was significantly decreased when compared to the controls.

BCRP's involvement in urate transport was tested in the human PTC monolayers as well. To identify BCRP-mediated urate transport, Ko143 was used to inhibit the activity of BCRP. The results show marked decrease in J_{B-A} only when Ko143 was present on the apical membrane of the monolayer. This would agree with the theory of BCRP acting as a urate efflux transporter on the apical membrane as Ko143 blocked the basolateral-to-apical passage. The corresponding effect of inhibiting apical secretion of urate by Ko143 would be an increased in urate retention in the cells of the monolayer, which was indeed detected in the human PTC monolayers. In addition to the functional expressional of BCRP by the cells, these data also provide further evidence of BCRP's involvement in renal urate secretion.

To date, there are no conclusive data on the mechanism of urate secretion by rat proximal tubules. A logical assumption would be that the mechanism of urate secretion in rats involved rat Oat1 and Bcrp. The functional expression of rat Oat1 and Bcrp had already been verified in Chapter 4. To substantiate these transporters' involvement in the excretion of urate, the fluxes of urate by rat PTC monolayers were repeated in the presence of PAH or Ko143. The rat monolayers showed stark similarities to the human PTC model in J_{B-A} and basolateral uptake of urate in the presence of the transporter-specific inhibitors. For instance, when PAH was present in the basolateral membrane of the rat PTC monolayer, basolateral uptake and J_{B-A} were significantly lower than the controls. And when Ko143 was present in the apical membrane, J_{B-A} was significantly decreased but apical retention of urate was up in rat PTC monolayers apically-treated with Ko143. This is evidence of Oat1 and Bcrp's role in the efflux of urate across the apical membrane of rat proximal tubule.

MK-571, previously shown to modulate the activity of MRPs (Gekeler *et al.*, 1995), was used to associate human MRPs and rat Mrps with urate transport in their respective PTC monolayers. The inhibition of MRPs/Mrps using MK-571 did not exert significant effects on J_{A-B} or J_{B-A}, nor did it affect the retention of urate by the monolayer. The role of MRPs/Mrps on renal urate transport was thus not conclusive in this instance.

5.13.3 The use of human and rat PTC monolayers as *in vitro* models for urate transport

The importance of renal transporters and their role in the handling of urate in the kidney have been highlighted in the previous sections. The transporters provide efficient vectorial transport of urate across the proximal tubules. Undoubtedly, drugs that regulate the activity of any of the transporters would affect urate homeostasis. It is thus surprising that there are still no suitable models for the assessment of the effects of novel drugs on urate reabsorption and secretion levels in the kidney. Until recently, benzbromarone was one of the common uricosuric agents prescribed to treat gout (Rider and Jordan, 2010). However, due to its hepatoxicity properties, benzbromarone is no longer prescribed (Lee *et al.*, 2008). With the incidence of gout increasing, the search for an alternative drug has intensified and so has the need for a tool to develop such a drug (Lee *et al.*, 2008; Rider and Jordan, 2010).

A model system with the ability to showcase urate transporters interactions with novel drugs is that of the *Xenopus* oocytes. To illustrate this, oocytes injected with human URAT1 or SLC2A9 cRNA transcripts were used to investigate the effect of an established URAT1/SLC2A9 inhibitor (benzbromarone) and a novel drug currently being developed for gout treatment (lesinurad). Both sets of oocytes showed marked increase in influx of urate compared to the controls, indicating the expression of urate transporters by the oocytes, although urate influx was 1.43-fold lower in SLC2A9-injected oocytes when compared to URAT1-injected oocytes. In the presence of benzbromarone, the magnitude of urate influx fell by more than 6.5-fold in URAT1-injected oocytes. Similarly, SLC2A9-injected oocytes were also decreased in the presence of benzbromarone. These observations were in agreement with published data (Witkowska *et al.*, 2012), which suggested the difference in magnitude between URAT1 and SLC2A9-mediated urate influx was due to the electrogenic nature of SLC2A9. Witkowska *et al.* found SLC2A9 showed symmetry of uptake and efflux of urate, and this balance was determined by the electrochemical gradient of the membrane on which the transporter was located (Witkowska *et al.*, 2012). Interestingly, in the presence of lesinurad, both URAT1 and SLC2A9-injected oocytes showed more than 1.5-fold decrease in urate influx, even though

lesinurad was developed as a URAT1-specific inhibitor (Bobulescu and Moe, 2012).

Another published model as a potential tool in urate transporter interaction studies are the URAT1 and SLC2A9-transfected cells (Shin *et al.*, 2011; Nakanishi *et al.*, 2013). Shin *et al.* stably transfected MDCK cells with URAT1 and used this system to study URAT1 interactions with drugs like benzbromarone (Shin *et al.*, 2011). With the understanding of SLC2A9's role in renal urate handling, Nakanishi *et al.* then improved on the model by doubly-transfecting MDCK cells with URAT1 and SLC2A9 (Nakanishi *et al.*, 2013). Both systems showed remarkable potential as *in vitro* models to demonstrate the interactions of the transporters with uricosuric drugs, especially the doubly-transfected MDCK system as it drew attention to the functional cooperation of the two transporters (Nakanishi *et al.*, 2013).

However, the drawback of the above mentioned systems lies in their simplicity – the systems did not take into account the urate transporters involved in the secretory pathway. Likewise, *Xenopus* oocytes do not fully elucidate the operations of the absorptive and secretory pathways and their transporters. On that aspect, the human and rat PTC monolayers developed in this project may be better suited for this aim. A series of experiments where the effects of lesinurad on urate handling by rat and human PTC monolayers were planned, but due to the limited supply of the drug the experiments were unable to be performed. Nonetheless, the monolayers were still able to demonstrate their value as a platform for drug development and drug-drug interaction studies using other candidate molecules and are discussed in Chapter 6.

5.13.4 Species differences in renal handling of urate

A major challenge faced in drug discovery and development is the extrapolation of drug safety information from animals to humans (Rasmussen, 1983; Lin, 1995). Although data from animal studies may be reasonably extrapolated to humans, there are still limitations, not least because of the differences in physiology of renal handling of molecules between the two species (Lin, 1995; Bass *et al.*, 2009).

Take the handling of urate for example: humans lack the enzyme that catalyses the breakdown of urate whereas rats do, consequently serum level of urate is much higher in humans than rats (Stavric and Nera, 1978). The amount of urate the kidneys handle will be different between the species. This is a serious limitation faced in the research of urate handling as the rat kidneys may not be equipped to handle the elevated amount of urate. Urate levels had been genetically manipulated by some to more closely resemble the human situation, but the rat kidneys were still not able to mimic the human model (Wu *et al.*, 1994).

However, when a fixed amount of urate was used to investigate its handling by the rat and human PTC monolayers development in this project, the models shared remarkable similarities in their magnitudes of urate flux and inhibition. For example, urate J_{A-B} produced by the human PTC was around 47 pmol/cm^2/hr, which was comparable to the value produced by rat PTC at 33 pmol/cm^2/hr as these values were not significantly different ($P > 0.05$, N = 12-18). The urate transporter sensitivities to inhibitors in both models were also similar, as indicated by their fold-changes in J_{A-B} in the presence of benzbromarone, amongst others.

Rodents are still the key species in drug development and safety determination (Bass *et al.*, 2009), and the relevance of studies using this species for human biology has to be interpreted with great caution. Findings from animal studies should not be directly extrapolated without some form of validation in humans, which makes the development of both the rat and human PTC as *in vitro* models more important. This is because a rat and human drug handling screening platform could be used to compare species differences. This will flag up any differences the two may have and provide invaluable data that have significant impact on drug safety and development.

5.14 Summary

The use of the rat PTC monolayer as an *in vitro* model for renal urate handling has been demonstrated in this chapter. The rat model exhibited a net absorptive pathway for urate, consistent with the physiology of urate handling *in vivo*. The transporters responsible for the absorption of urate were shown to be Urat1 and Slc2a9, found on the apical and basolateral membranes of the monolayer, respectively. Both transporters' transcript were detected and discussed in

Chapter 4. The secretory pathway of urate transport were also highlighted, in which Oat1 and Bcrp were proposed as the uptake and efflux transporters responsible for the movement of urate across the basolateral and apical membranes, respectively. The proposed mechanism of urate transport in rat PTC monolayers are summarised in Figure 5.18. The series of urate experiments were repeated in human PTC monolayers to compare the renal handling of urate between the two species. Similarities between the two models suggest the human and the rat PTC monolayers may contribute to information on drug safety and its development. The use of rat PTC monolayers as an *in vitro* model for studying drug interaction is discussed in Chapter 6.
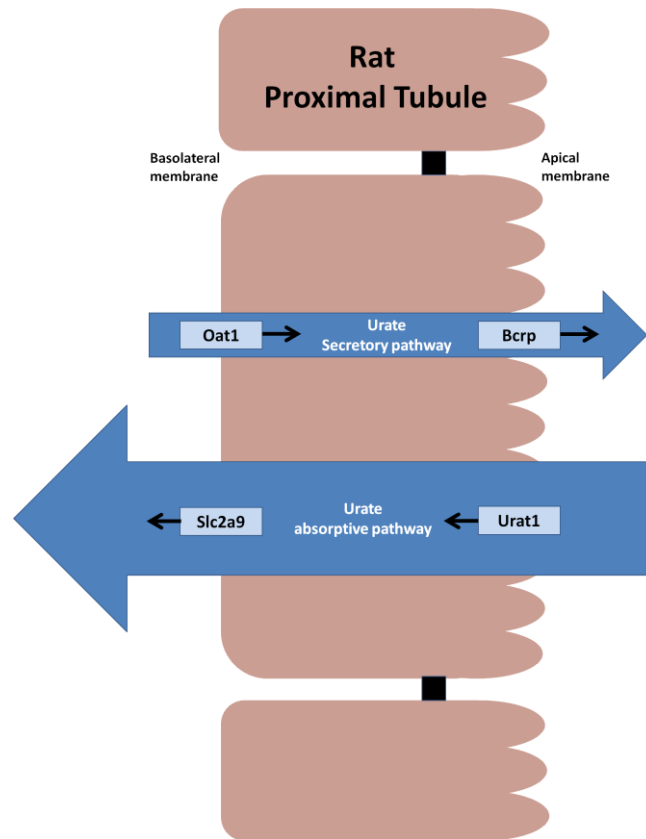
Figure 5.18: Mechanisms of urate transport in rat PTC monolayers.

Rat PTC monolayers exhibited secretory and absorptive pathways of urate transport, consistent with the physiology of urate handling in vivo. The transporters responsible for the absorption of urate were shown to be Urat1 and Slc2a9, found on the apical and basolateral membranes of the monolayer, respectively. Oat1 and Bcrp were proposed as the uptake and efflux transporters of the secretory pathway responsible for the movement of urate across the basolateral and apical membranes, respectively. The absorptive pathway dominates the movement of urate, resulting in net absorption of urate. The mechanisms of urate transport were similar in human PTC monolayers.

Chapter 6

Digoxin Handling by Rat and Human PTC monolayers

6.1 Chapter overview

This chapter contains the results from the investigation of digoxin handling by rat and human proximal tubule cell (PTC) monolayers. Data from the following experiments are discussed:

- Unidirectional digoxin fluxes and uptake by rat and human PTC monolayers.

- The effects of GF120918, an MDR1 inhibitor, on digoxin fluxes and uptake by rat and human PTC monolayers.

- The effects of T_3, a substrate of OATPs, on digoxin fluxes by rat and human PTC monolayers.

- The use of human PTC monolayers as an *in vitro* model for digoxin-drug interactions.

6.2 Digoxin handling by rat PTC monolayers

Rat PTC monolayers were used to investigate the renal handling of digoxin molecules by rat proximal tubule. Unidirectional transepithelial fluxes in the apical to basolateral direction (J_{A-B}), and in the basolateral to apical direction (J_{B-A}), were carried out using 1 µM of digoxin. The net flux (J_{Net}) was calculated from the difference between the two fluxes. Uptake of digoxin from across the apical and basolateral membrane was determined from the amount of intracellular digoxin in rat PTC monolayers after the flux.

Figure 6.1A shows the fluxes of digoxin by rat PTC monolayers. J_{A-B} (48.60 ± 6.20 pmol/cm^2/hr, n = 12, N = 3) was 1.65-fold higher than J_{B-A} (29.53 ± 3.55 pmol/cm^2/hr, P < 0.05, n = 12, N = 3) in rat PTC monolayers. This resulted in net digoxin absorption of 19.06 ± 6.07 pmol/cm^2/hr. Although intracellular digoxin showed uptake across the apical membrane was 0.80 ± 0.11 pmol/cm^2/hr, and across the basolateral membrane was 1.17 ± 0.15 pmol/cm^2/hr, these figures were not statistically different (P > 0.05, n = 12, N = 3, Figure 6.1B).

A
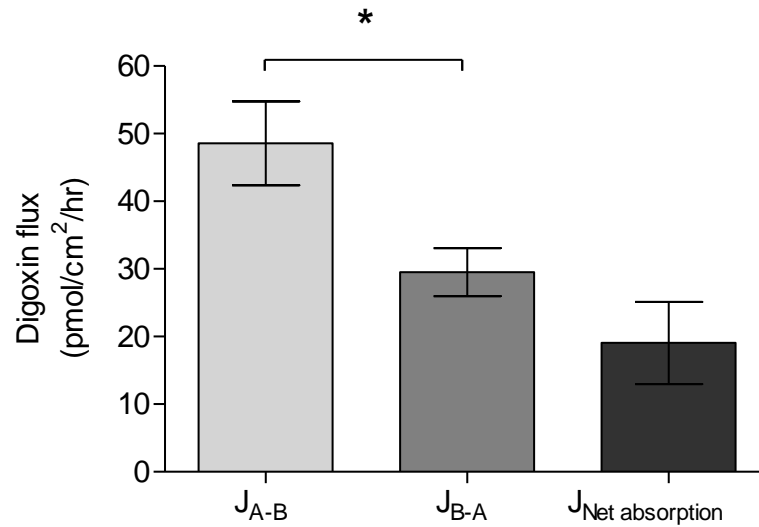
B
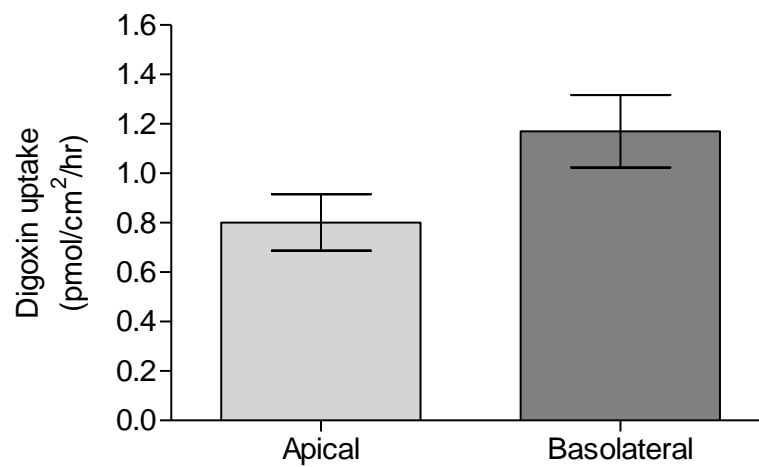
Figure 6.1: Unidirectional fluxes and uptake of digoxin by rat PTC monolayers.

Fluxes of digoxin by rat PTCs showed J_{A-B} at 48.60 ± 6.20 pmol/cm²/hr, which was 1.65-fold higher than J_{B-A}, which was 29.53 ± 3.55 pmol/cm²/hr. This resulted in digoxin J_{Net} absorption of 19.06 ± 6.07 pmol/cm²/hr. Intracellular digoxin showed uptake across the apical membrane was 0.80 ± 0.11 pmol/cm²/hr, and uptake across basolateral membrane was 1.17 ± 0.15 pmol/cm²/hr. Statistical test revealed there was no significant difference between the two values. Each bar represents the mean ± SEM of 12 replicates obtained from three separate experiments. Student t test was performed to assess statistical significance. *, P < 0.05.

6.3 The effects of GF120918 on digoxin fluxes and uptake by rat PTC monolayers

Digoxin J_{A-B} and J_{B-A} were repeated in the presence of an Mdr1 inhibitor, GF120918. Figure 6.2 shows the effect of the inhibitor on digoxin J_{A-B} and J_{B-A}, and the amount of intracellular digoxin in rat PTC monolayers.

In the presence of 2 µM GF120918, digoxin J_{A-B} saw no significant change in magnitude when compared to the control (Figure 6.2A). However, J_{B-A} was significantly decreased to 5.43 ± 1.75 pmol/cm^2/hr (81.6 % decrease, $P < 0.05$, n = 12, N = 3) when compared to the control. Figure 6.2B shows the amount of intracellular digoxin in the rat PTC monolayers after the flux experiment. The amount of digoxin taken up from the apical side was 1.04 ± 0.17 pmol/cm^2/hr in the presence of 2 µM GF120918. But when compared to the control value of 0.80 ± 0.11 pmol/cm^2/hr, no statistical difference was calculated ($P > 0.05$, n = 12, N = 3). However, in the presence of GF120918, the uptake of digoxin from the basolateral side was increased 1.73-fold (from 1.17 ± 0.15 pmol/cm^2/hr to 2.02 ± 0.27 pmol/cm^2/hr, $P < 0.05$, n = 12, N = 3), when compared to the control.

A
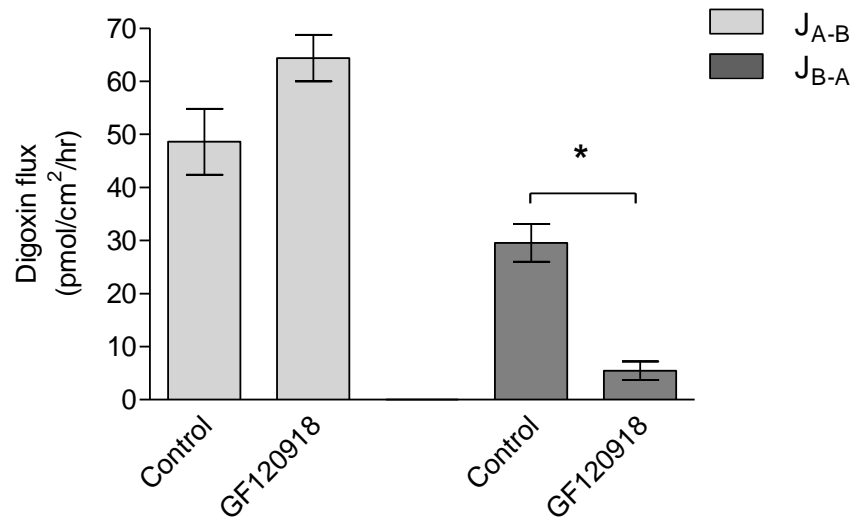
B
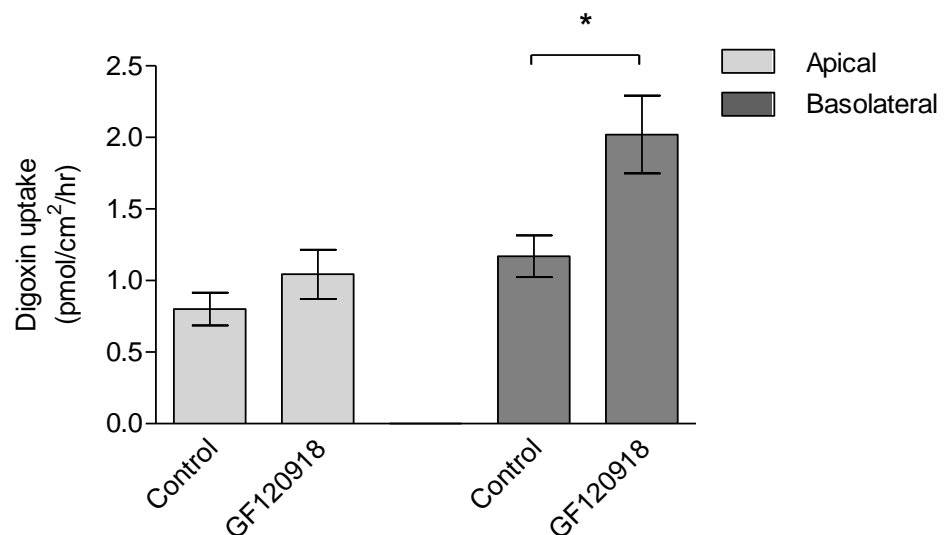
Figure 6.2: Unidirectional digoxin fluxes and uptake in the presence of 2 μM GF120918 by rat PTC monolayers.

*Digoxin J_{A-B} was not significantly different in magnitude between the presence and absence of 2 μM GF120918. However, J_{B-A} was significantly decreased to 5.43 ± 1.75 pmol/cm^2/hr (81.6 % decrease) when compared to the control (29.53 ± 3.55 pmol/cm^2/hr). The amount of intracellular digoxin taken up from the apical side was 1.04 ± 0.17 pmol/cm^2/hr in the presence of 2 μM GF120918. But when compared to the control value of 0.80 ± 0.11 pmol/cm^2/hr, no statistical difference was calculated. However, in the presence of GF120918, the uptake of digoxin from the basolateral side was increased 1.73-fold (from 1.17 ± 0.15 pmol/cm^2/hr to 2.02 ± 0.27 pmol/cm^2/hr). Each bar represents the mean ± SEM of 12 replicates obtained from three separate experiments. Student t test was performed to assess statistical significant. *, P < 0.05.*

6.4 The effects of T_3 on digoxin fluxes and uptake by rat PTC monolayers

Digoxin J_{A-B} and J_{B-A} were repeated in the presence of an Oatp inhibitor, T_3. 10 μM T_3 was exposed to either the apical or basolateral membrane of rat PTC monolayers prior to digoxin flux. Figure 6.3 shows the effect of the inhibitor on digoxin J_{A-B} and J_{B-A}, and Figure 6.4 shows the amount of intracellular digoxin in rat PTC monolayers in the presence of 10 μM T_3.

Rat PTC monolayers exposed to T_3 only on the apical membrane saw a 65.1 % decrease in J_{A-B} when compared to the control (from 48.60 ± 6.20 pmol/cm^2/hr to 16.98 ± 3.90 pmol/cm^2/hr, $P < 0.01$, n = 12, N = 3, Figure 6.3A), but saw a 1.56-fold increase in J_{B-A} (from 29.54 ± 3.55 pmol/cm^2/hr to 46.16 ± 4.80 pmol/cm^2/hr, $P < 0.05$, n = 12, N = 3, Figure 6.3B). The opposite happened when only the basolateral membranes of rat PTC monolayers were exposed to T_3; the magnitude of J_{A-B} increased significantly to 80.74 ± 6.71 pmol/cm^2/hr (1.66-fold increase, $P < 0.05$, n = 12, N = 3) when compared to the control, and J_{B-A} fell to 11.61 ± 2.95 pmol/cm^2/hr (60.1 % decrease, $P < 0.01$, n = 12, N = 3), when compare to the control.

Exposure of 10 μM T_3 to only the apical membranes of rat PTC monolayers saw a 58.8 % decrease in apical uptake of digoxin when compared to the control (from 0.80 ± 0.11 pmol/cm^2/hr to 0.33 ± 0.08 pmol/cm^2/hr, $P < 0.01$, n = 12, N = 3, Figure 6.4A), but no apparent change was observed in the basolateral uptake. Conversely, when rat PTC monolayers were exposed to 10 μM T_3 only on the basolateral membranes, no significant change in level of apical uptake was calculated, but basolateral uptake of digoxin was decreased 57.3 % (from 1.17 ± 0.15 pmol/cm^2/hr to 0.50 ± 0.09 pmol/cm^2/hr, $P < 0.05$, n = 12, N = 3, Figure 6.4B).

A
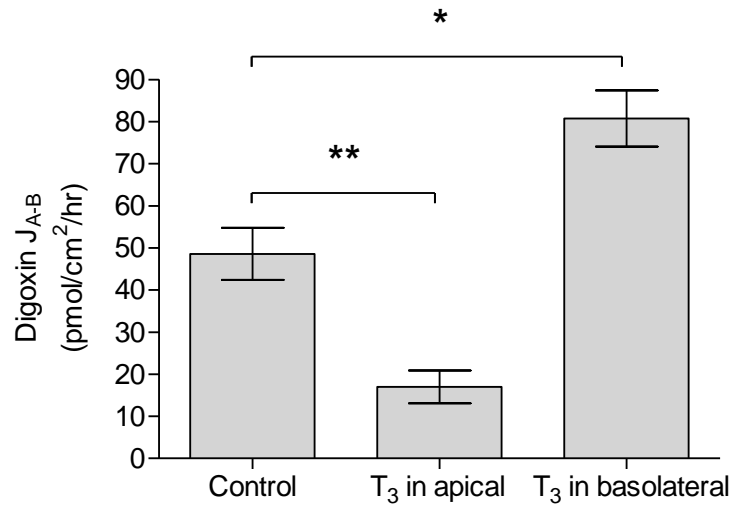
B
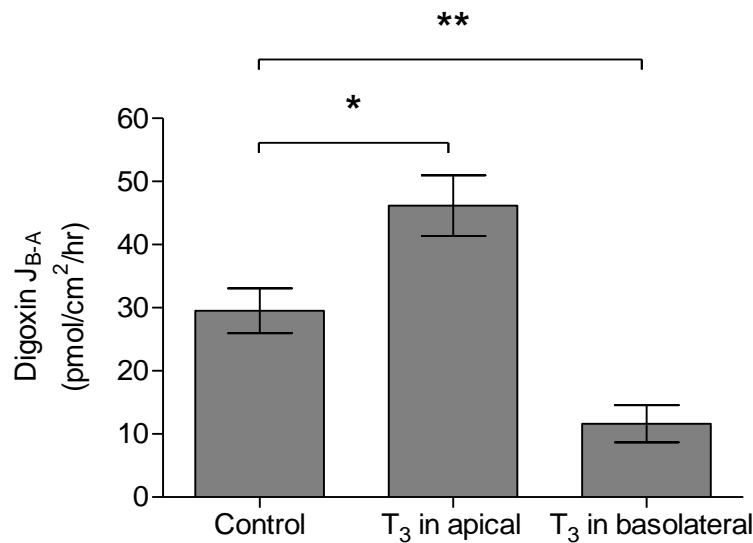
Figure 6.3: Unidirectional digoxin fluxes by rat PTC monolayers in the presence of 10 μM T₃.

*(**A**) J_{A-B} in the presence of T_3 on the apical membrane only was 16.98 ± 3.90 pmol/cm²/hr, a 65.1 % decrease when compared to the control (48.60 ± 6.20 pmol/cm²/hr), but increased 1.66-fold (80.74 ± 6.71 pmol/cm²/hr) when the T_3 was on the basolateral membrane. (**B**) Conversely, J_{B-A} saw a 1.56-fold increase from 29.54 ± 3.55 pmol/cm²/hr to 46.16 ± 4.80 pmol/cm²/hr when T_3 was on the apical membrane but decreased to 11.61 ± 2.95 pmol/cm²/hr (60.1 % decrease) when T_3 was on the basolateral membrane. Each bar represents the mean $\pm$ SEM of 12 replicates from three separate experiments. Two-way ANOVA was performed to assess statistical significance. *, $P < 0.05$, **, $P < 0.01$.*

A
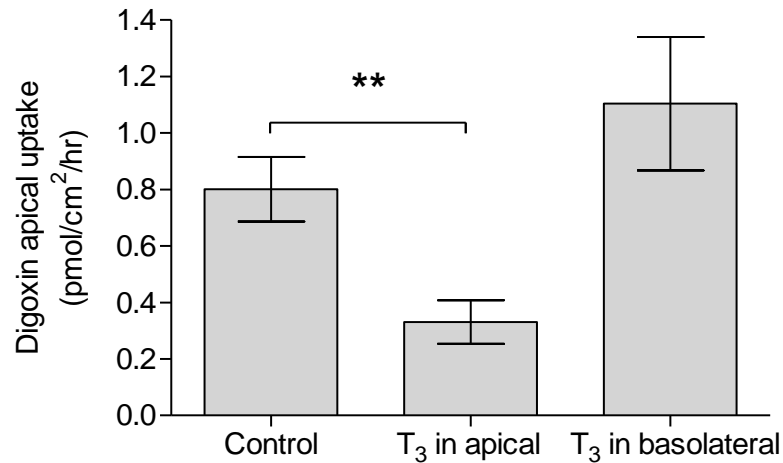
B
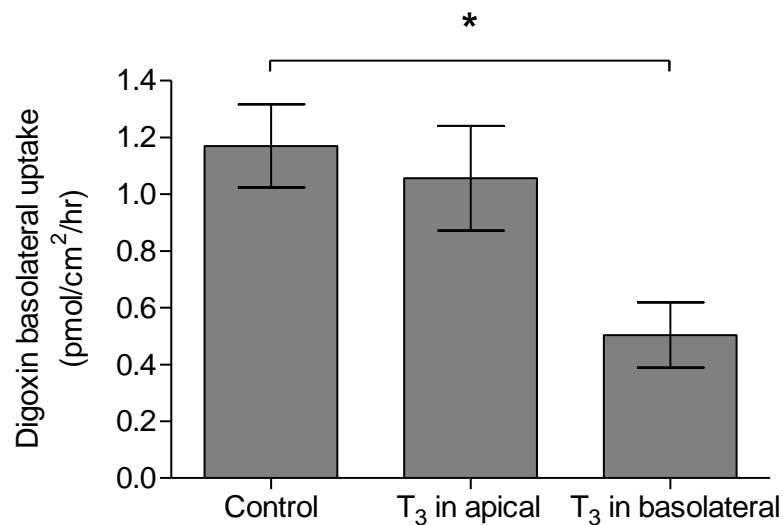
Figure 6.4: Uptake of digoxin by rat PTC monolayers in the presence of 10 μM T₃.

*(A) Exposure of T₃ to only the apical membranes saw a 58.8 % decrease in apical uptake of digoxin when compared to the control, from 0.80 ± 0.11 pmol/cm²/hr to 0.33 ± 0.08 pmol/cm²/hr, but no apparent change was observed in the basolateral uptake. (B) When rat PTC monolayers were exposed to T₃ only on the basolateral membranes, no significant change in level of apical uptake was calculated, but basolateral uptake of digoxin was decreased 57.2 %, from 1.17 ± 0.15 pmol/cm²/hr to 0.50 ± 0.09 pmol/cm²/hr. Each bar represents the mean ± SEM of 12 replicates from three separate experiments. Two-way ANOVA was performed to assess statistical significance. *, P < 0.05, **, P < 0.01.*

6.5 Handling of digoxin by human PTC monolayers

Unidirectional digoxin fluxes were also carried out in human PTC monolayers. Figure 6.5 shows J_{A-B} and J_{B-A} of 1 µM digoxin by human PTC monolayers, and the subsequent uptake of digoxin by the cells.

Digoxin fluxes by human PTC monolayers showed J_{B-A} (66.12 ± 6.71 pmol/cm^2/hr, n = 12, N = 3, Figure 6.5A) was significantly more than J_{A-B} (15.68 ± 3.92 pmol/cm^2/hr, P < 0.001, n = 12, N = 3), which resulted in a net secretion of digoxin (50.43 ± 5.16 pmol/cm^2/hr). Uptake of digoxin by the human PTC monolayers across the basolateral membrane (3.72 ± 0.51 pmol/cm^2/hr) was significantly higher than across the apical membrane (0.88 ± 0.32 pmol/cm^2/hr, P < 0.01, n = 12, N = 3, Figure 6.5B).

A
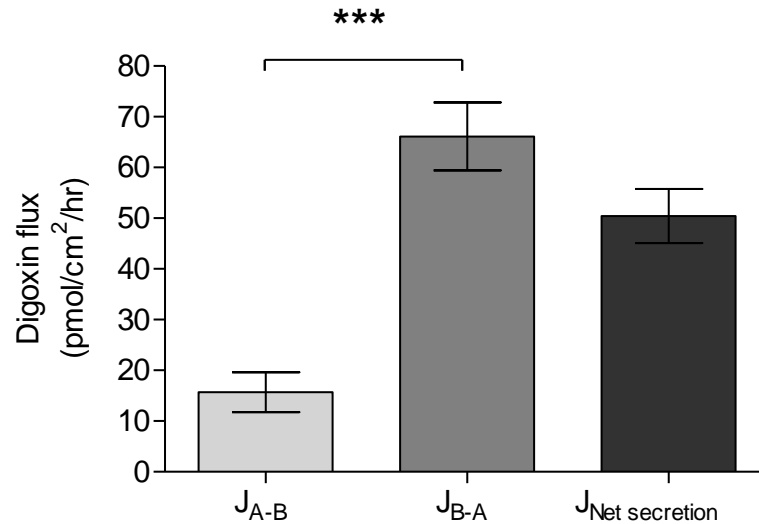
B
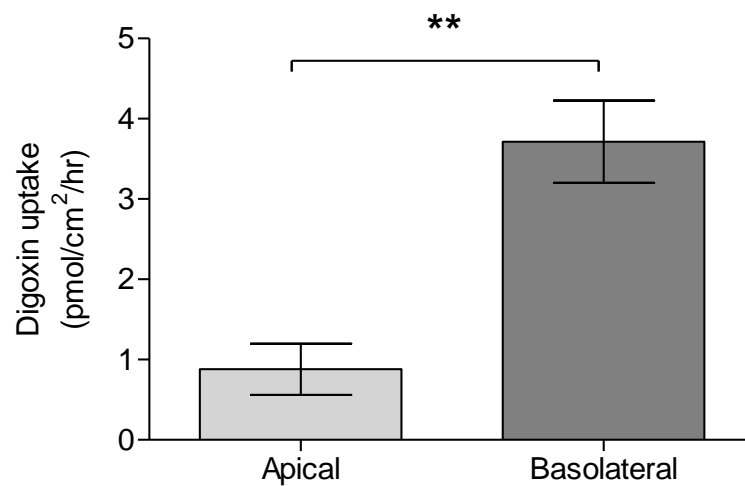
Figure 6.5: Unidirectional digoxin fluxes and uptake by human PTC monolayers.

*(**A**)At 66.12 ± 6.71 pmol/cm^2/hr, J$_{B-A}$ was significantly more than J$_{A-B}$ (15.68 ± 3.92 pmol/cm^2/h), which resulted in digoxin J$_{Net}$ secretion (50.43 ± 5.16 pmol/cm^2/hr). (**B**) Uptake of digoxin by the human PTC monolayers across the basolateral membrane (3.72 ± 0.51 pmol/cm^2/hr) was significantly higher than across the apical membrane (0.88 ± 0.32 pmol/cm^2/hr). Each bar represents the mean ± SEM of 12 replicates from three separate experiments. Two-way ANOVA was performed to assess statistical significance. **, P < 0.01, ***, P < 0.001.*

6.6 The effects of GF120918 on digoxin fluxes and uptake by human PTC monolayers

Digoxin fluxes by human PTC monolayers were repeated in the presence of 2 µM GF120918, a known MDR1 inhibitor. Figure 6.6 shows the effect of GF120918 had on digoxin J_{A-B} and J_{B-A}, and the uptake of digoxin by the human PTC monolayers.

In the presence of 2 µM GF120918, digoxin J_{A-B} was 23.38 ± 3.97 pmol/cm^2/hr, and when compared to the control (15.68 ± 3.92 pmol/cm^2/hr), there was no statistically significant difference between the two conditions (P > 0.05, n = 10, N = 3, Figure 6.6A). J_{B-A}, however, saw a 76.5 % decrease in magnitude in the presence of GF120918 when compared to the control (from 66.12 ± 6.71 pmol/cm^2/hr to 15.55 ± 3.74 pmol/cm^2/hr, P < 0.001, n = 10, N = 3). Similarly, there was no statistically significant difference in the apical uptake of digoxin by human PTC monolayers in the presence or absence of 2 µM GF120918 (Figure 6.6B). Basolateral uptake of digoxin, however, was 2.28-fold higher in the presence of GF120918 (8.47 ± 0.95 pmol/cm^2/hr, P < 0.05, n = 10, N = 3).

A
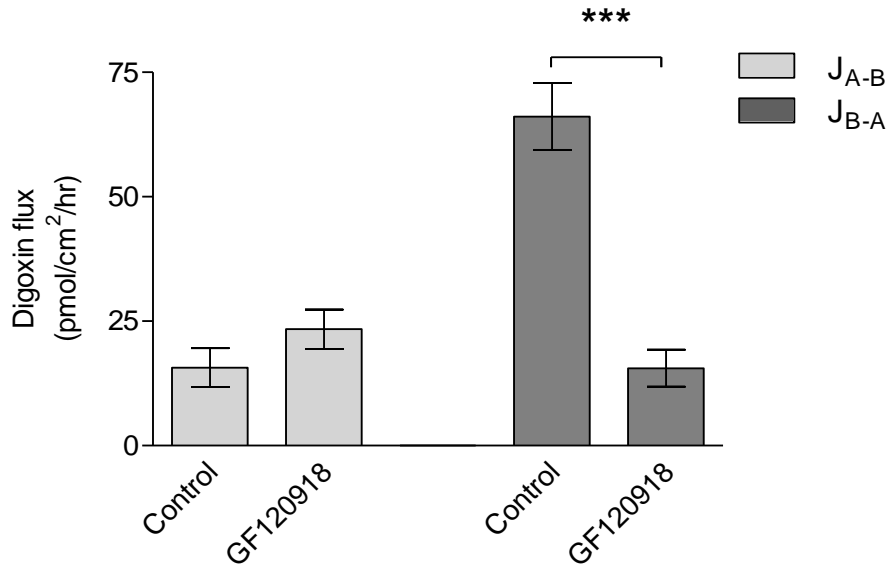
B
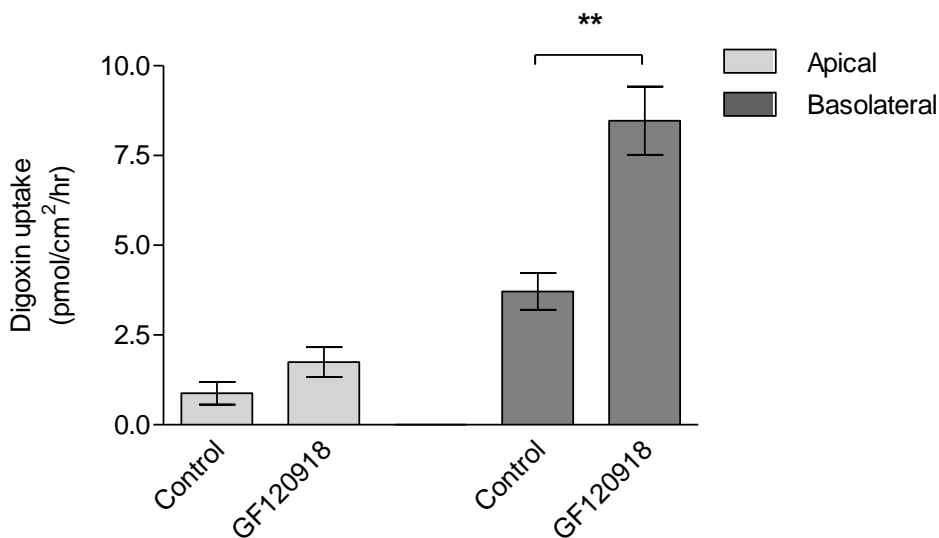
Figure 6.6: Unidirectional digoxin fluxes in the presence of 2 μM GF120918 by human PTC monolayers.

*(A) There was no statistically significant difference between J_{A-B} of the two conditions. J_{B-A}, however, saw a 76.5 % decrease in magnitude in the presence of GF120918 when compared to the control (66.12 ± 6.71 pmol/cm^2/hr to 15.55 ± 3.74 pmol/cm^2/hr). (**B**) Similarly, there was no statistically significant difference in the apical uptake of digoxin by human PTC monolayers in the presence or absence of 2 μM GF120918. Basolateral uptake of digoxin, however, was 2.28-fold higher in the presence of GF120918 (8.47 ± 0.95 pmol/cm^2/hr). Each bar represents the mean ± SEM of 10-12 replicates from three separate experiments. Student t test was performed to assess statistical significance. **, P < 0.01, ***, P < 0.001.*

6.7 The effects of T_3 on digoxin fluxes and uptake by human PTC monolayers

Digoxin J_{A-B} and J_{B-A} were repeated in the presence of 10 μM T_3. T_3 was exposed to either the apical or basolateral membrane of human PTC monolayers prior to digoxin flux. Figure 6.7 shows the effects of the inhibitor on digoxin J_{A-B} and J_{B-A}, and Figure 6.8 shows the amount of intracellular digoxin in the human PTC monolayers in the presence of T_3.

Digoxin J_{A-B} was 11.81 ± 4.04 pmol/cm^2/hr when T_3 was present in the apical membrane, which was not significantly different to the control (15.68 ± 3.92 pmol/cm^2/hr, $P > 0.05$, n = 9, N = 3, Figure 6.7A). No statistical significant change also was observed in J_{A-B} when T_3 was present in the basolateral membrane of the human PTC monolayers. J_{B-A} also showed no significant change in magnitude when T_3 was present in the apical membrane, but J_{B-A} decreased significantly from 66.12 ± 6.71 pmol/cm^2/hr to 14.53 ± 2.39 pmol/cm^2/hr when T_3 was in the basolateral membrane, a 78.0 % decrease ($P < 0.01$, n = 9, N = 3, Figure 6.7B).

There was no statistical significant difference in the uptake of digoxin across the apical membrane between the different conditions ($P > 0.05$, n = 10, N = 3, Figure 6.8A), but uptake across the basolateral membrane of the human PTC monolayers was significantly decreased when 10 μM T_3 was present in the basolateral membrane (1.29 ± 0.47 pmol/cm^2/hr, $P < 0.05$, n = 9, N = 3, Figure 6.8B).

A
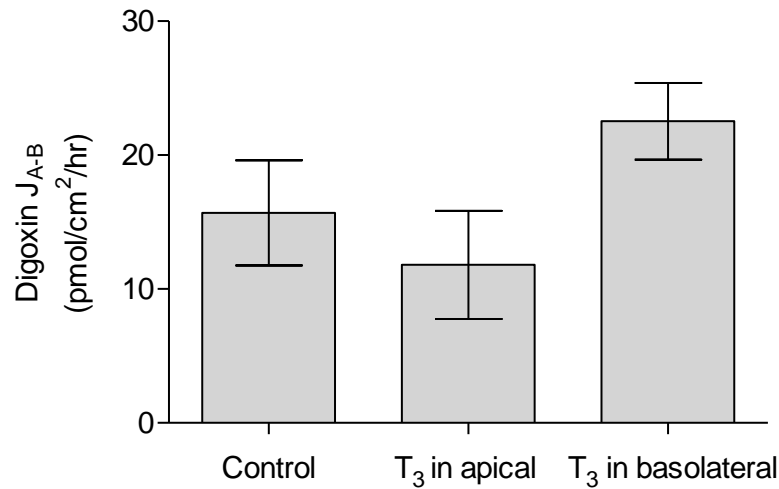
B
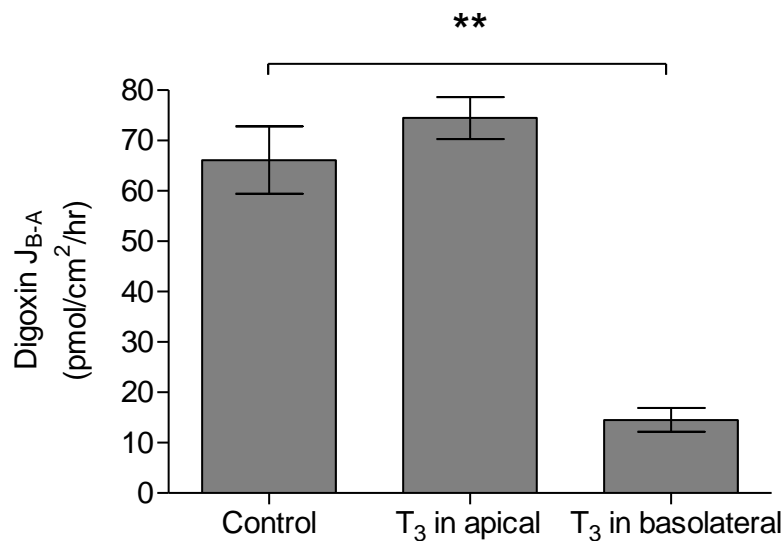
Figure 6.7: Unidirectional digoxin fluxes by human PTC monolayers in the presence of 10 μM T₃.

(A) Digoxin J_{A-B} was 11.81 ± 4.04 pmol/cm²/hr when T_3 was present in the apical membrane, which was not significantly different to the control (15.68 ± 3.92 pmol/cm²/hr). No statistically significant change was also observed in J_{A-B} when T_3 was present in the basolateral membrane of the human PTC monolayers. (B) J_{B-A} also showed no significant change in magnitude when T_3 was present in the apical membrane, but J_{B-A} decreased significantly from 66.12 ± 6.71 pmol/cm²/hr to 14.53 ± 2.39 pmol/cm²/hr when T_3 was in the basolateral membrane, a 78.0 % decrease. Each bar represents the mean ± SEM of 9-10 replicates from three separate experiments. Two-way ANOVA was performed to assess statistical significance. *, $P < 0.05$, **, $P < 0.01$.

A
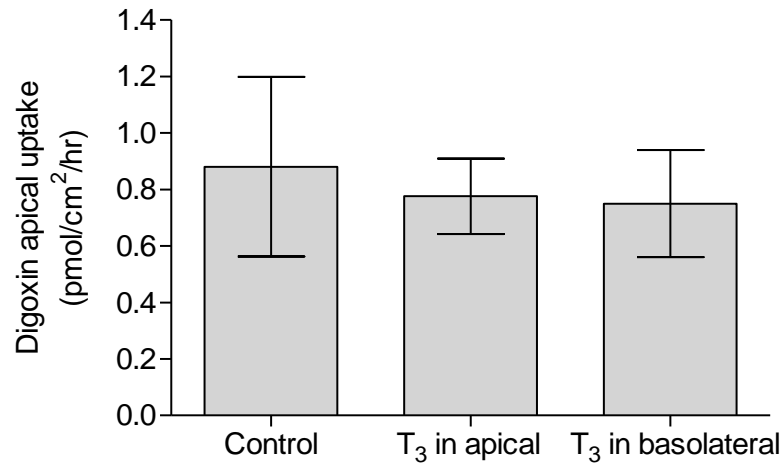
B
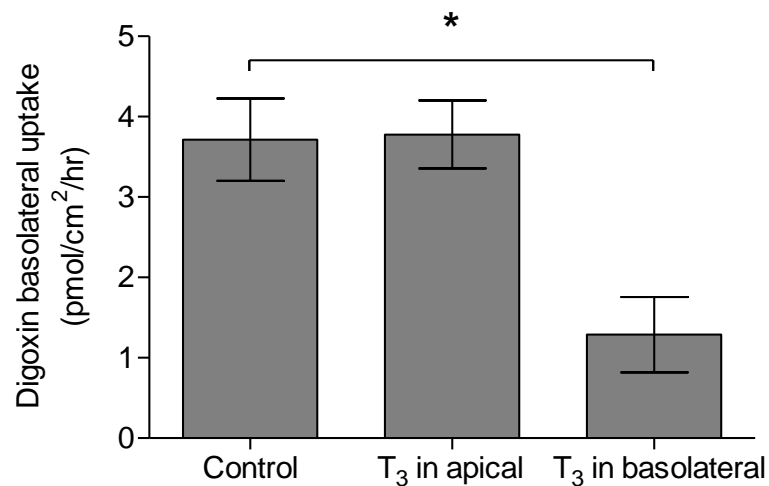
Figure 6.8: Uptake of digoxin by human PTC monolayers in the presence of 10 μM T₃.

*(**A**) There was no statistical significant difference in the uptake of digoxin across the apical membrane between the different conditions, (**B**) but uptake across the basolateral membrane of the human PTC monolayers was significantly decreased when 10 μM T₃ was present in the basolateral membrane (1.29 ± 0.47 pmol/cm²/hr). Each bar represents the mean ± SEM of 9-10 replicates from three separate experiments. Two-way ANOVA was performed to assess statistical significance. *, P < 0.05.*

6.8 Drug-drug interactions using digoxin as the substrate in human PTC monolayer

A series of experiments were carried out to determine 1 µM digoxin J_{B-A} by human PTC monolayers in the presence of known human MDR1 inhibitors. The inhibitors were carvedilol, diltiazem, isradipine, ketoconazole, mibefradil, nicardipine, quinidine, ranolazine and verapamil. These experiments provided a measure of the inhibitors' MDR1 inhibitory potency via their IC_{50}. Figure shows the apparent permeability of digoxin (P_{app}) against the concentration range of the inhibitor used. In all the figures, the data point in the extreme left represents digoxin P_{app} in the absence of the inhibitor. For the purpose of statistical analysis, a concentration 10-fold less than the lowest inhibitor concentration had been assigned as the minimum inhibitor concentration. The data point in the extreme right represents digoxin P_{app} in the presence of the positive control (2 µM GF120918), and a concentration 10-fold more than the highest inhibitor concentration was assigned as the maximum inhibitor concentration.

Human PTC monolayers exhibited digoxin P_{app} of around 45 nm/s in the absence of inhibitors. Digoxin P_{app} decreased to around 6 nm/s in the presence of the positive control. All inhibitors exhibited a dose-dependent relationship with digoxin P_{app}; the higher the concentration of the inhibitor, the lower the P_{app}. IC_{50} of the inhibitor was calculated by performing non-linear regression analysis on the data set. At 160.1 µM, isradipine exhibited the highest IC_{50} (Figure 6.11). Carvedilol gave the lowest IC_{50} at 0.13 µM (Figure 6.9). The other inhibitor's IC_{50} values were as follows: diltiazem was 102.9 µM (Figure 6.10), ketoconazole was 53.1 µM (Figure 6.12), mibefradil was 2.53 µM (Figure 6.13), nicardipine was 0.91 µM (Figure 6.14), quinidine was 5.0 µM (Figure 6.15), ranolazine was 34.8 µM (Figure 6.16) and verapamil was 1.23 µM (Figure 6.17). Table 6.1 summarises the data.
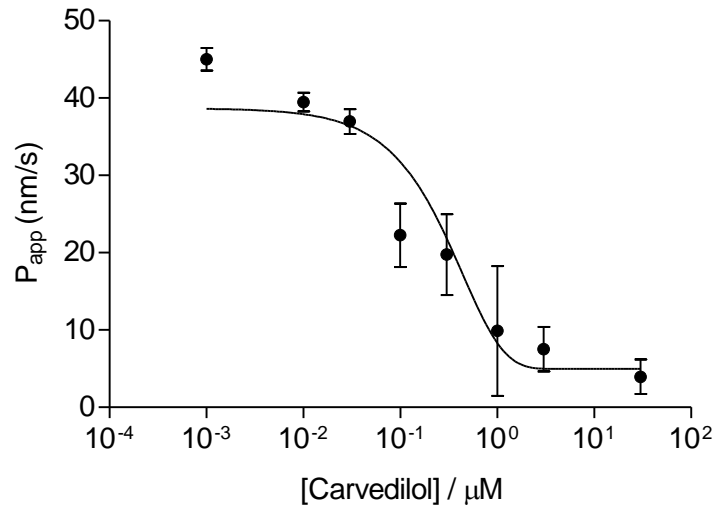
Figure 6.9: P_{app} in the basolateral to apical direction of 1 µM digoxin by human PTC monolayers in the presence of carvedilol.

Digoxin P_{app} exhibited a concentration-dependent relationship with carvedilol, and an apparent IC_{50} of 0.13 µM was calculated. Each data point represents the mean ± SEM of 9-12 replicates from three separate experiments. Non-linear regression analysis was used to fit the data points and calculate the IC_{50}, which lies within the 95 % confidence intervals.
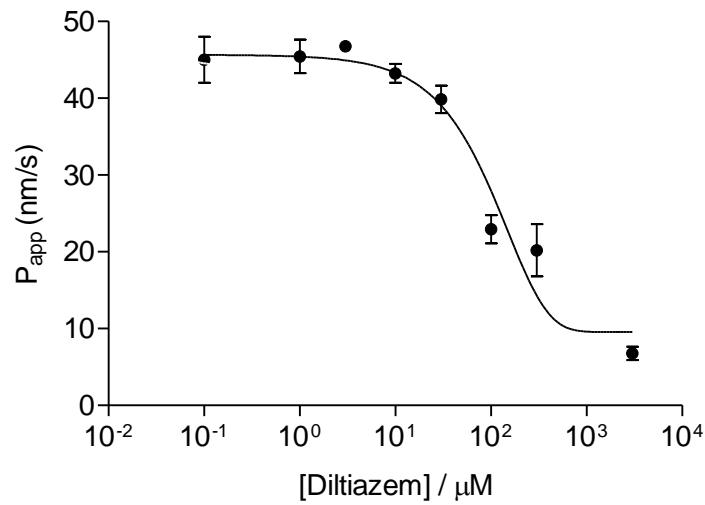
Figure 6.10: P_{app} in the basolateral to apical direction of 1 μM digoxin by human PTC monolayers in the presence of diltiazem.

An apparent IC_{50} of 102.9 μM was calculated from the digoxin P_{app} using a range of diltiazem concentrations. The P_{app} exhibited a concentration-dependent relationship. Each data point represents the mean ± SEM of 8 replicates from two separate experiments. Non-linear regression analysis was used to fit the data points and calculate the IC_{50}, which lies within the 95 % confidence intervals.
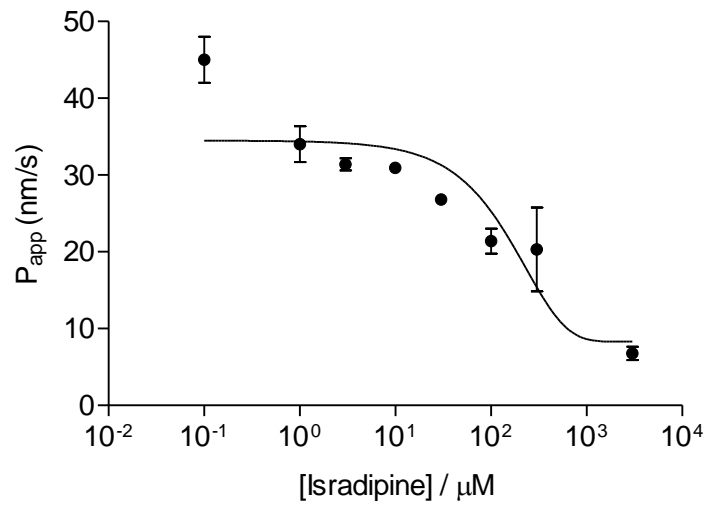
Figure 6.11: P_app in the basolateral to apical direction of 1 μM digoxin by human PTC monolayers in the presence of isradipine.

Digoxin P_{app} exhibited a concentration-dependent relationship with isradipine. Non-linear regression analysis was performed to obtain an apparent IC_{50} of 160.1 μM. Each data point represents the mean ± SEM of 9-12 replicates from three separate experiments. The non-linear regression analysis lies within the 95 % confidence intervals.
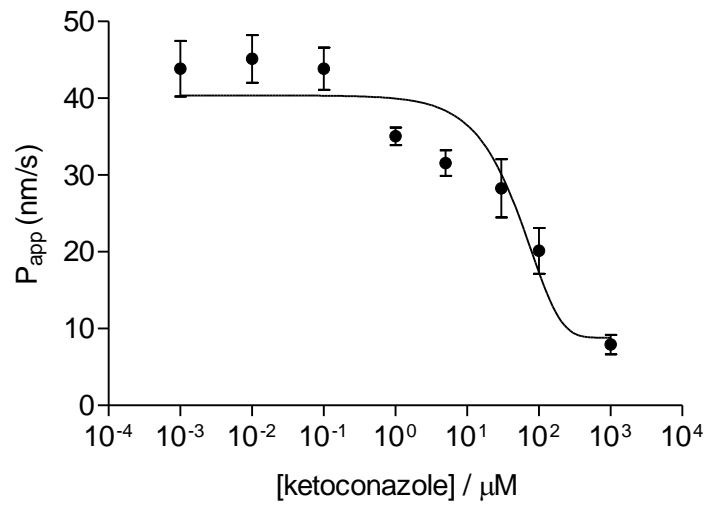
Figure 6.12: P_{app} in the basolateral to apical direction of 1 μM digoxin by human PTC monolayers in the presence of ketoconazole.

Digoxin P_{app} exhibited a concentration-dependent relationship with ketoconazole, and an apparent IC_{50} of 53.1 μM was calculated. Each data point represents the mean ± SEM of 8 replicates from two separate experiments. Non-linear regression analysis was used to fit the data points and calculate the IC_{50}, which lies within the 95 % confidence intervals.
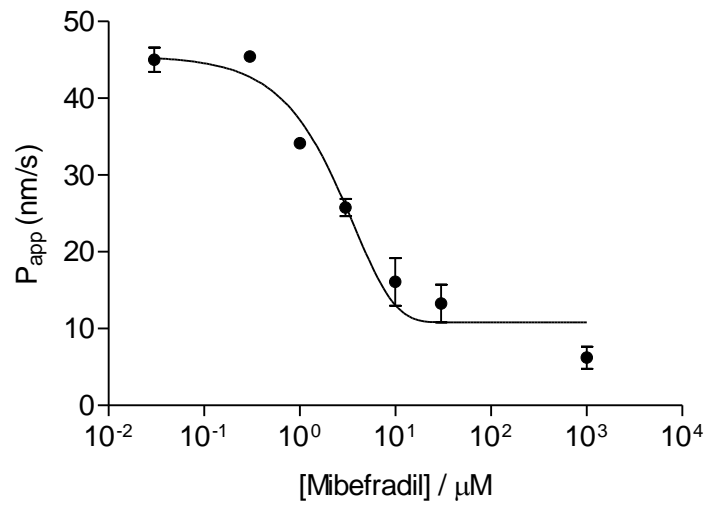
Figure 6.13: P_{app} in the basolateral to apical direction of 1 μM digoxin by human PTC monolayers in the presence of mibefradil.

An apparent IC_{50} of 2.53 μM was calculated from digoxin P_{app} in the presence of a range of mibefradil concentrations. Each data point represents the mean ± SEM of 8 replicates from two separate experiments. Non-linear regression analysis was used to fit the data points and calculate the IC_{50}, which lies within the 95 % confidence intervals.

Figure 6.14: P_{app} in the basolateral to apical direction of 1 µM digoxin by human
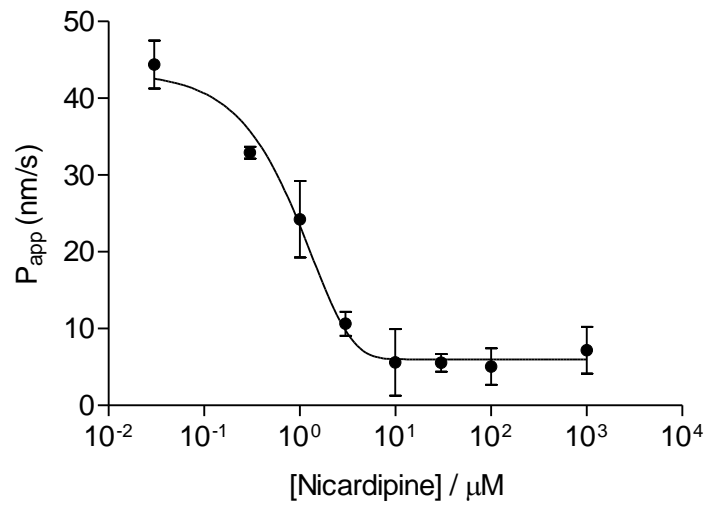
Figure 6.14: P_{app} in the basolateral to apical direction of 1 µM digoxin by human PTC monolayers in the presence of nicardipine.

Digoxin P_{app} exhibited a concentration-dependent relationship with nicardipine, and an apparent IC_{50} of 0.91 µM was calculated. Each data point represents the mean ± SEM of 8 replicates from two separate experiments. Non-linear regression analysis was used to fit the data points and calculate the IC_{50}, which lies within the 95 % confidence intervals.
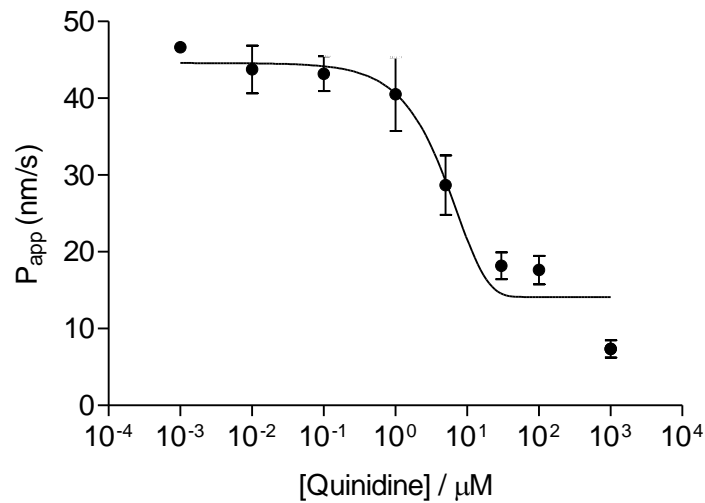
Figure 6.15: P_{app} in the basolateral to apical direction of 1 μM digoxin by human PTC monolayers in the presence of quinidine.

A range of quinidine concentrations were treated on human PTC monolayers and corresponding changes in digoxin P_{app} shown. An apparent IC_{50} of 5.0 μM was calculated from the concentration-dependent relationship. Each data point represents the mean ± SEM of 8 replicates two separate experiments. Non-linear regression analysis was used to fit the data points and calculate the IC_{50}, which lies within the 95 % confidence intervals.
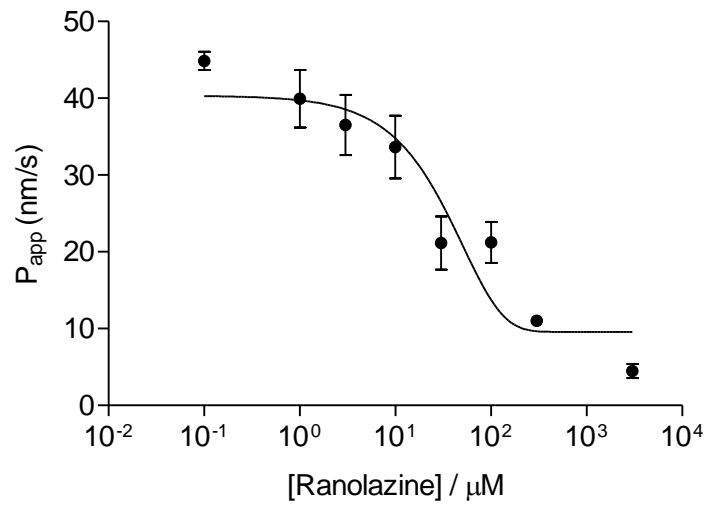
Figure 6.16: P_{app} in the basolateral to apical direction of 1 μM digoxin by human PTC monolayers in the presence of ranolazine.

Digoxin P_{app} exhibited a concentration-dependent relationship with ranolazine. An apparent IC_{50} of 34.8 μM was calculated. Each data point represents the mean ± SEM of 8 replicates from two separate experiments. Non-linear regression analysis was used to fit the data points and calculate the IC_{50}, which lies within the 95 % confidence intervals.
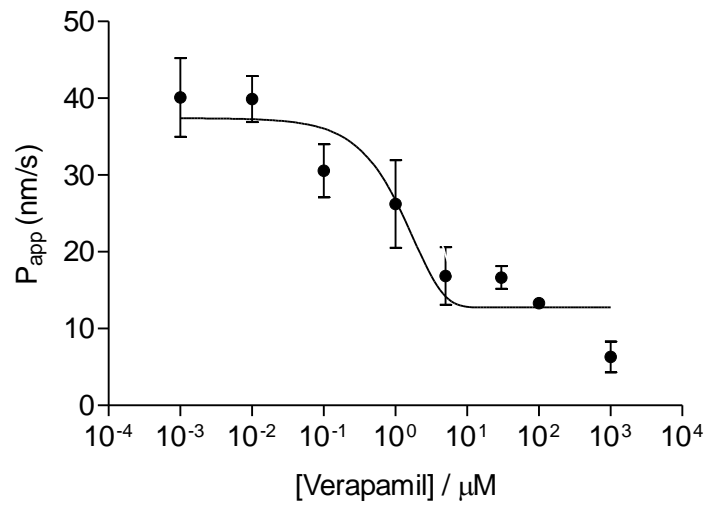
Figure 6.17: P_{app} in the basolateral to apical direction of 1 μM digoxin by human PTC monolayers in the presence of verapamil.

Verapamil IC_{50} determined from inhibition of MDR1-mediated digoxin P_{app} was 1.23 μM. Each data point represents the mean ± SEM of 8 replicates from two separate experiments. Non-linear regression analysis was used to fit the data points and calculate the IC_{50}, which lies within the 95 % confidence intervals.

Compound	IC$_{50}$ (µM)
Carvedilol	0.13
Diltiazem	102.9
Ketoconazole	53.1
Isradipine	160.1
Mibefradil	2.53
Nicardipine	0.91
Quinidine	5.0
Ranolazine	34.8
Verapamil	1.23

Table 6.1: Summary of the MDR1 inhibitor IC$_{50}$ generated in human PTC monolayers.

6.9 Discussion

The ability of the rat PTC monolayers developed in this project to handle the array of compounds a normal kidney is exposed to is paramount. In Chapter 5, urate reabsorption was demonstrated in rat PTC monolayers. They also showed good correlation with the human PTC monolayers in urate handling. Both species displayed the potential as *in vitro* models for drug transporter studies as they replicated the handling of urate *in vivo*. In this chapter, rat and human PTC monolayers handling of digoxin was investigated to further substantiate their utility as *in vitro* models. Digoxin is a prototypic drug usually eliminated unchanged in the kidneys of healthy humans (Lacarelle *et al.*, 1991), which makes it an ideal substrate for drug transporter studies. Furthermore, as digoxin has a narrow therapeutic range and one of the most widely prescribed concomitant drugs (Fenner *et al.*, 2008), its use in the presence of other drugs would provide an indication of the PTC monolayers' suitability as digoxin-drug interaction models.

6.9.1 Digoxin handling by human PTC monolayers

Glomerular filtration of digoxin was initially believed to be the sole method of renal excretion of the drug in humans (Lacarelle *et al.*, 1991). However, it has since been discovered that the renal excretion of digoxin involves both glomerular filtration and active tubular secretion, with the latter responsible for more than 50 % of excreted digoxin (Ohnhaus *et al.*, 1972; Steiness, 1974; Steiness *et al.*, 1982). Through various digoxin-drug interaction studies, it was discovered that digoxin is a substrate of MDR1 and it acts as an efflux pump that extrude digoxin from the proximal tubule cells into the urine for excretion (Woodland *et al.*, 1998).

The digoxin secretory pathway was illustrated in this project by human PTC monolayers. Unidirectional fluxes showed that digoxin J_{B-A} was significantly higher than J_{A-B}, which resulted in net secretion of the drug (Figure 6.5A). In the presence of MDR1-specific inhibitor, GF120918 (Tan *et al.*, 2000), J_{B-A} was significantly decreased whereas no difference was observed in J_{A-B} (Figure 6.6). The decrease in J_{B-A} can be explained by the inhibition of MDR1 by GF120918, which resulted in less digoxin being transported out of the human PTCs across the apical membrane. As there was no GF120918-sensitive component on the

basolateral side of the monolayer that could affect digoxin transport, J_{A-B} was not changed. This secretory pathway of digoxin transport was also evident from the increase in amount of intracellular digoxin in the presence of GF120918; more digoxin was retained in the cells as its apical exit was impeded by GF12918. MDR1 was thus shown to be a functional efflux transporter of digoxin in the human PTC monolayers.

An inherent difference between the amount of digoxin taken up across the apical and basolateral membranes was also detected in the human PTC monolayers. The uptake of digoxin was almost four times higher across the basolateral membrane (Figure 6.5B). This marked discrepancy of uptake signified the expression of a protein on the basolateral membrane that aided the uptake of digoxin. The transporter was most likely OATP4C1 as its expression in the human proximal tubule and substrate specificity has previously been verified (Mikkaichi *et al.*, 2004; Yamaguchi *et al.*, 2010). To demonstrate OATP4C1-dependent digoxin transport in the human PTC monolayer, digoxin fluxes were carried out in monolayers treated apically or basolaterally with triiodothyronine (T_3), a substrate of OATP4C1 (Chu *et al.*, 2007). The results showed significantly less uptake of digoxin across the basolateral membrane when T_3 was present on the basolateral surface of the monolayer, which resulted in the decrease in digoxin J_{B-A} (Figure 6.7 and Figure 6.8). No other parameters were significantly altered. The mechanism of digoxin transport in human PTC monolayer is thus assumed as follows: OATP4C1 takes up digoxin from the basolateral surface before MDR1-mediated efflux on the apical surface. This hypothesis is in agreement with previously published data (Steiness, 1974; Steiness *et al.*, 1982; Mikkaichi *et al.*, 2004; Yamaguchi *et al.*, 2010), confirming the use of digoxin transporter studies in this *in vitro* renal model.

6.9.2 Digoxin handling by rat PTC monolayers

In contrast to the human monolayers, rat PTC monolayers showed higher digoxin J_{A-B} than J_{B-A}, which resulted in the net absorption of digoxin (Figure 6.1A). In addition, the uptake of digoxin across the basolateral and apical membrane was not significantly different (Figure 6.1B). Since rat Mdr1 transcript had been detected along with its functional expression in the rat PTCs (Chapter 4), it was proposed that this transporter was also involved in the handling of digoxin (Hori

et al., 1993). Indeed, the presence of GF120918 caused a significant decrease in magnitude of digoxin J_{B-A} (Figure 6.2A), proving Mdr1-mediated transport of digoxin in the basolateral to apical direction. That was further substantiated by the increase in intracellular digoxin when uptake was across the basolateral membrane of the monolayer in the presence of GF120918 (Figure 6.2B).

T_3 was then treated on the apical or basolateral side of the monolayer during digoxin flux. When T_3 was treated only on the apical side, J_{A-B} was decreased while J_{B-A} was increased when compared to their respective controls (Figure 6.3). The uptake of digoxin across the apical membrane was also significantly lowered in apically T_3-treated monolayers. It was deduced that there was a T_3-sensitive component of digoxin transport in the apical membrane of rat PTC monolayers. The transporter was taking up digoxin across the apical membrane but was inhibited by T_3. This resulted in the decrease in apical uptake of digoxin and J_{A-B}. The inhibition of apical uptake of digoxin by T_3 also meant digoxin that had already been transported in the basolateral to apical direction was unable to be reabsorbed, which caused the increase in J_{B-A}.

Similarly, a T_3-sensitive component was also detected in the basolateral membrane. When T_3 was present only on the basolateral side of the rat PTC monolayer, J_{A-B} was significantly increased while J_{B-A} was decreased (Figure 6.3). The decrease in J_{B-A} could be ascribed to the inhibition of digoxin uptake across the basolateral membrane of the monolayer, which also resulted in less intracellular digoxin (Figure 6.4). Without the activity of the basolateral digoxin uptake transporter, digoxin that was reabsorbed would be unable to be transported in the basolateral to apical direction, and hence the observed increase in J_{A-B}.

This series of experiments was able to demonstrate the functional expression of T_3-sensitive transporters of digoxin on both sides of the polarised rat PTC monolayers. The most likely candidates were members of the Oatp family of transporters as they are known to express in rat kidneys and their substrates include digoxin and T_3 (Masuda *et al.*, 1997b; Masuda *et al.*, 1999a; Masuda *et al.*, 1999b; Mikkaichi *et al.*, 2004). Members such as Oatp1a3v1 and v2 (formerly known as OAT-K1 and OAT-K2, respectively) are expressed on the apical membrane of rat proximal tubule (Masuda *et al.*, 1997b; Masuda *et al.*, 1999a),

which coincided with the apical uptake of digoxin by the rat PTC monolayers seen in the experiments. Analogous with digoxin handling in human PTC monolayers, rat Oatp4c1 was then thought to be responsible for the movement of digoxin across the basolateral membrane of the rat PTC monolayer before efflux by Mdr1 across the apical membrane. After all, it is also a member of the Oatp family and its mRNA was detected in the rat PTCs (Chapter 4). However, a recent publication on the localisation of Oatp4c1 in rat proximal tubule refutes this view.

Oapt4c1 was initially shown to localise at the basolateral membrane in the rat proximal tubule (Mikkaichi *et al.*, 2004). Contradictorily, Kuo *et al.* managed to clone and transfect rat Oatp4c1 in MDCKII cells and found the expression of the transporter on the apical membrane of the polarised cells. In addition, the authors were also able to generate their own anti-Oatp4c1 antibody with which they used to discover expression of Oatp4c1 solely on the apical membrane of freshly isolated rat proximal tubules (Kuo *et al.*, 2012). This led the authors to conclude that rat Oatp4c1 was involved in the renal reabsorption of compounds, and this theory fitted with the data generated in this project. It is very likely that Oatp4c1, along with Oatp1a3v1 and Oatp1a3v2 expressed on the apical membrane of the rat PTC monolayers, brought about the dominance of digoxin transport in the apical to basolateral direction.

While tubular reabsorption of glomerular filtered digoxin has not been documented in human kidneys, this pathway has been detected in various species such as rats (Rasmussen *et al.*, 1975; Roman and Kauker, 1976). For example, Roman *et al.* (1976) found micropunctured rat kidneys were reabsorbing up to 35 % of glomerular filtered digoxin from the proximal tubule (Roman and Kauker, 1976). This discovery was made before the identification of Oatps in rat kidneys, which has since been implicated in the transport of digoxin (Hori *et al.*, 1993; Mikkaichi *et al.*, 2004). The in-depth mechanism of digoxin transport in rat kidney, however, remains unresolved to this date; the identity of the basolateral uptake transporter of digoxin is still unknown, nor is the mechanism of basolateral efflux of digoxin. This is compounded by the ambiguity of the localisation of rat Oatp4c1, and perhaps a lack of suitable *in vitro* model for such studies.

The use of the rat PTC monolayer in this project has generated the first report on the possible contribution of Oatp4c1 on the absorptive pathway of digoxin in rat. For this reason, the rat PTC monolayer remains an attractive model to further investigate the mechanisms of digoxin handling in rat kidneys. Assays such as immunocytochemistry could be performed on the rat PTC monolayers to identify the localisation of the individual components involved, which would provide better understanding of how rat kidneys handle digoxin.

6.9.3 Digoxin-drug interactions

Digoxin is a cardiac glycoside prescribed to patients suffering from chronic heart failure (Fenner *et al.*, 2008). Patients suffering from the disease usually are also given other heart medications such as verapamil and quinidine (Woodland *et al.*, 1998; Hunt, 2005). It was noticed that the co-administration of these drugs lowered the renal clearance of digoxin, which was later attributed to the inhibition of MDR1-mediated efflux of digoxin by the other drugs (Woodland *et al.*, 1998). Digoxin and has a narrow therapeutic window and slight changes in its plasma concentration can cause digitalis toxicity (Koren, 1987). Unfortunately, the change in digoxin plasma concentration can be brought about by the digoxin-drug interaction (DDI) as it causes less digoxin to be excreted from the body. It is therefore necessary to evaluate the risks of drugs taken with digoxin in inducing DDIs via the inhibition of MDR1 activity.

There are various platforms for the study of DDI. The pharmaceutical industry has been using MDR1 expressing or transfected polarised cell lines such as Caco-2 and MDCKII to assess DDIs (Bentz *et al.*, 2013). As digoxin handling by the human PTC monolayer has been shown to replicate the *in vivo* in this project, its role in drug interaction studies may also be appreciated. A series of experiments were carried out in human PTC monolayers where the digoxin apparent permeability (P_{app}) in the basolateral to the apical direction was measured. P_{app} is the ratio of the flow rate of a compound from a compartment into the opposite, to the surface area that the compound crosses (Jung *et al.*, 2006). It is generally recognised as a unit of measure of the movement of a compound (Palumbo *et al.*, 2008). Due to the lack of replication of digoxin handling in human kidneys, rat PTC monolayers were deemed unsuitable for this study and were not used.

Figure 6.9 to Figure 6.17 shows the relationship between digoxin P_{app} and the concentration ranges of nine different drugs. These drugs are common medicines patients take with digoxin that have been shown to induce DDIs (Bentz *et al.*, 2013). A large range of IC_{50} values between the different drugs was observed. This was expected as the drugs had different affinities for MDR1 (Acharya *et al.*, 2008; Bentz *et al.*, 2013). Some of the IC_{50}s calculated in this project were also noticed to be different to the ones reported in the literature. For instance, quinidine and verapamil IC_{50} in the experiment was calculated as 5 µM and 1.23 µM, respectively. The former was different to the IC_{50} determined by Kakumoto *et al.* (2002), which was 9.25 µM (Kakumoto *et al.*, 2002). Similarly, Rautio *et al.* (2006) showed verapamil IC_{50} of MDR1-mediated digoxin transport was 10.7 µM in their experimental model, an almost 9-fold change in magnitude when compared to the present study (Rautio *et al.*, 2006). The variation in MDR1 inhibitory potency is not uncommon. Bentz *et al.* (2013) analysed several inhibitor IC_{50}s of MDR1-mediated digoxin transport produced in different laboratories and found vast discrepancies in the values even though the laboratories were using the same inhibitors. Amongst the tested inhibitors, they found verapamil had the most variability in IC_{50}, which gave 20- and 790-fold difference between the lowest and highest values, respectively (Bentz *et al.*, 2013).

While the reason behind the inconsistency was not defined, Bentz *et al.* (2013) reckoned the differences could be due to the MDR1 model upon which the study was carried out (Bentz *et al.*, 2013). Different laboratories used different MDR1 expression systems that ranged from Caco-2 cells to MDR1 containing membrane vesicles (Bentz *et al.*, 2013; Ellens *et al.*, 2013). Each of this system would no doubt be handling digoxin uniquely to it. Difference within the same system could also be an inherent problem. The phenomenon known as phenotypic drift, a term more commonly used to describe the dedifferentiation of cancer cells (Zavyalova *et al.*, 2013), has also been used to described the changes in immortalised cell line after a period of time (Kwatra *et al.*, 2014). Phenotypic drift occurs in Caco-2 and MCDKII cells whereby their protein expressions change over several passages (Chandler *et al.*, 1993; Cassio, 2013). This would inevitably affect their ability to model digoxin transport and produce variable data. A robust *in vitro* model for DDIs is therefore needed.

The robustness of the human PTC monolayer makes it an ideal candidate for drug interaction studies. The advantage this model has over other cell-base models is that it is derived from healthy native tissue. The primary cells has been verified as an excellent model for renal xenobiotic handling (Brown *et al.*, 2008), and their competency in delivering consistent results in DDIs have been demonstrated in the present study. The use of this model also allows the influence of OATP4C1 on DDI to be examined, which is often overlooked in other systems. By the same token, rat PTC monolayers would also be a suitable candidate of drug interactions, albeit not in all substrates are applicable. Further investigations into rat PTC monolayer use in this setting are thus essential.

6.10 Summary

A summary of the mechanisms of digoxin transport by the human and rat PTC monolayer is shown in Figure 6.18. Rat PTC monolayers exhibited a predominant absorption pathway of digoxin, whereas human PTC monolayers were more representative of the digoxin secretory pathway *in vivo*. Human PTC monolayers were thus deemed a better model for use in digoxin-drug interaction studies. Digoxin P_{app} in the presence of a range of concentrations of several MDR1-inhibtors was performed and the subsequent IC_{50} of the inhibitors calculated. The human PTC monolayers demonstrated robustness that is ideal for such studies. Whilst the mechanism of digoxin transport in rat PTC monolayers was not fully elucidated, this was the first study to report the association of Oatp4c1 on the absorption pathway in rat proximal tubules. Further investigations into the transporters involved in digoxin handling are thus needed.
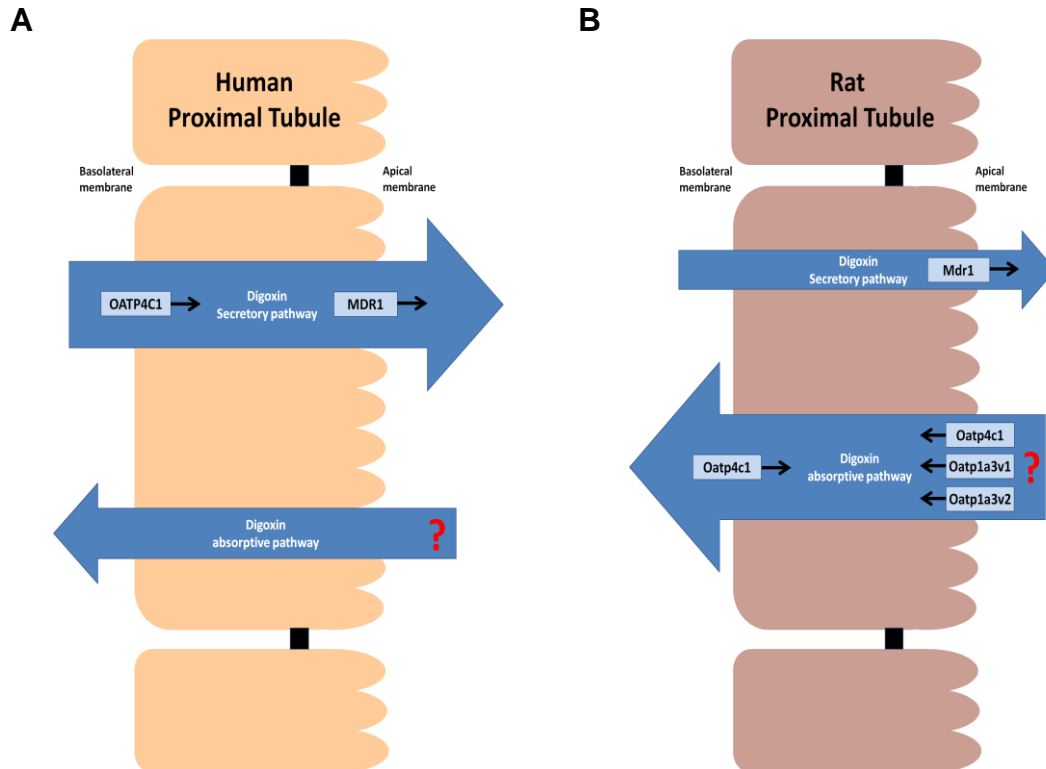
Figure 6.18: The mechanisms of digoxin transport in rat and human PTC monolayers.

*(**A**) Human PTC monolayers exhibited a dominant digoxin secretory pathway. It was shown that this pathway involved OATP4C1-mediated uptake of digoxin across the basolateral membrane and MDR1-mediated efflux across the apical membrane. Digoxin reabsorption in human proximal tubule has not been documented, although it was demonstrated in the human PTC monolayer. (**B**) In contrast, rat PTC monolayers exhibited a dominant absorptive pathway, which involved T₃-sensitive components. Oatps such as Oatp4c1, Oatp1a3v1 and Oatp1a3v2 were the most likely candidates of apical absorption of digoxin. Digoxin secretory pathway of digoxin was also detected. Mdr1 was found to be responsible for the apical efflux of digoxin. Further investigation is required to fully elucidate the mechanism of digoxin transport in both models.*

Chapter 7

Final Discussion and Conclusion

7.1 Final discussion

The kidney plays a vital role in the elimination of many endogenous metabolites and xenobiotics. Drug transporters expressed on the proximal tubule cells have been identified as one of the key factors on the ability of the organ to successfully carry out its function (Inui *et al.*, 2000; Beringer and Slaughter, 2005; Fagerholm, 2007; Consortium, 2010; König *et al.*, 2013). There are various *in vitro* models of renal drug transport, but many do not fully express the array of transporters to establish good *in vitro-in vivo* correlations (Brown *et al.*, 2008; Jenkinson *et al.*, 2012). Indeed, Lam *et al.* (2014) recently published a paper showcasing cells differentiated from human pluripotent stem cells (hPSCs) as potential *in vitro* proximal tubule cell model, but they have yet to shown the utility of this model in the context of drug transport and nehptoxicity. Whilst the group has shown evidence of the differentiated hPSCs expressing kidney markers (including N-cadherin), drug transporters have not been validated (Lam *et al.,* 2014). Primary human proximal tubule cells (PTCs), on the other hand, has been shown as a good model to address this issue (Lash *et al.*, 2006; Brown *et al.*, 2008). Brown et al. (2008) showed explicitly the functional expression of key drug transporters, including MDR1 and BCRP, with which factors to promote their expression in the differentiated hPSCs would be need. The corollary of this discovery is to develop a rat version of the model. This is because the extrapolation of drug transport data from animals to humans is still a challenge due to unpredictable species differences in drug handling (Rasmussen, 1983; Lin, 1995; Bass *et al.*, 2009). With the rat and human PTC models in place, the data from the handling of the same molecules by both species can be compared and any difference the two may have will be apparent. This project was therefore set out to develop and characterise the primary rat PTC as a model for drug transporter and drug interaction studies, and compare the handling of candidate molecules with that of the human PTC model.

The results from the isolation and development of the rat PTC model are shown in Chapter 3 and 4 of this thesis. Rat PTCs were successfully isolated and cultured. More importantly, the mRNA and functional expressions of the multitude of drug transporters, such as Mdr1, Mrp2, Oat1, Oct2, Urat1 and Slc2a9, found in the native tissue were retained in the cells. This was important as these

transporters influence renal drug disposition (Consortium, 2010), and their expression would enhance the utility of the rat PTC as an *in vitro* model of renal drug transport.

Further characterisation of the rat PTC model was also performed. Chapter 5 and 6 show the results of the handling of an endogenous compound (urate) and a xenobiotic (digoxin) by the rat PTC monolayer. The monolayer was able to replicate the absorptive pathway of urate, as did the human PTC monolayer. This indicated the suitability of both species as models for renal urate transport. In addition, direct inference of the workings of urate transporters can be made between the species as both models handled urate in similar fashion.

However, unlike the human, the rat PTC monolayer was unable to reproduce the secretory pathway of digoxin. The difference in the handling of digoxin reiterated the need for renal drug transporter models from different species. This allows the mechanisms with which a species handle the same drug to be ascertained. As illustrated in the urate transport experiments, both models demonstrated the same route of urate absorption. In the case of digoxin transport, rat PTC monolayer showed Oatps dominance that led to more digoxin moving in the apical to basolateral direction, whereas human PTC monolayer showed MDR1-mediatated efflux of digoxin across the apical membrane. This difference also meant only human PTC monolayer was suitable for use in experiments to showcase its application in digoxin-drug interaction studies.

Rat and human PTC are not limited to only drug transporter and drug interaction studies. Indeed, rat PTC had been used as an *in vitro* model to study the mechanisms of nephrotoxicity. Boogaard *et al.* had isolated and cultured rat PTCs similar to the method described in this project (Boogaard *et al.*, 1989; Boogaard *et al.*, 1990a; Boogaard *et al.*, 1990b). They found cultured rat PTCs retained expression of enzyme activities such as that of γ-glutamyltranspeptidase, and showed that these enzymes could be used as parameters of toxicity; nephrotoxin would affect the enzyme activity and correlate to the severity of toxicity (Boogaard *et al.*, 1990b). More recently, rat and human PTCs have been used to elucidate the mechanism of nephrotoxicity induced by anti-viral drugs by Brown *et al.* Yet to be published data show anti-viral drugs such as tenofovir, adefovir and cidofovir were transported via the same pathway in both rat and human PTC. It

is hoped that further work on this would provide information on the molecular mechanisms of disposition and nephrotoxicity of these compounds.

Despite the differences in handling of certain molecules, the robustness of both models is evident from the experiments performed. For instance, the kinetics of several ABC transporters were determined from cells isolated from at least three different rats. The K_m produced was similar in magnitude in all experiments. The fluxes of the urate and digoxin were also similar in magnitude, indicating the lack of variability in transporter expression between individuals, although there are studies that showed variations in serum urate level between different rodent strains (Dan *et al.*, 1990; Preitner *et al.*, 2009).

As discussed in Chapter 4, the mimic of *in vivo* condition greatly improves the mRNA expression of many drug transporters. There are increasing interests to culture cells in a 3D environment, and that has been considered in the culture of rat and human PTCs. This involves the introduction of flowing media to recreate the movement of basolateral and apical fluids *in vivo*. Initial data produced in our laboratory show cells cultured under the "flow" environment produced higher transepithelial resistance and enhanced functional activities of several ABC transporters. While the reason behind this is yet to be discovered, this offer an improvement of the model on which more drug transporter and drug interaction studies can be carried out.

7.2 Conclusion

Rat PTCs can be successfully isolated and cultured. These cells show expression of several classes of drug transporters considered important in drug development studies. Rat PTCs are also able to be cultured as monolayers with epithelial cobberstone-like morphology and be used to perform transepithelial fluxes.

The handling of endogenous metabolite, urate, by rat PTC monolayers is remarkably similar to the handling of urate by human PTC monolayers; both species replicate the reabsorption pathway of urate *in vivo*. However, only human PTC monolayers are able to replicate the secretory pathway of digoxin, whereas rat PTC monolayers demonstrate a dominant reabsorption pathway. Rat PTC monolayers, therefore, are unable to be used as an *in vitro* model for the renal handling of digoxin in humans. A species difference in the handling of a key molecule is thus highlighted.

The aims of this project are to isolate and characterise the rat PTC monolayers, and to investigate their suitability as an *in vitro* drug transporter model. The aims have been achieved on both counts.

Chapter 8

References

Acharya, P., O'Connor, M.P., Polli, J.W., Ayrton, A., Ellens, H. and Bentz, J. (2008) 'Kinetic Identification of Membrane Transporters That Assist P-glycoprotein-Mediated Transport of Digoxin and Loperamide through a Confluent Monolayer of MDCKII-hMDR1 Cells', *Drug Metabolism and Disposition*, 36(2), pp. 452-460.

Alexandre, E., Viollon-Abadie, C., David, P., Gandillet, A., Coassolo, P., Heyd, B., Mantion, G., Wolf, P., Bachellier, P., Jaeck, D. and Richert, L. (2002) 'Cryopreservation of adult human hepatocytes obtained from resected liver biopsies', *Cryobiology*, 44(2), pp. 103-113.

Allikmets, R., Schriml, L.M., Hutchinson, A., Romano-Spica, V. and Dean, M. (1998) 'A human placenta-specific ATP-binding cassette gene (ABCP) on chromosome 4q22 that is involved in multidrug resistance', *Cancer Research*, 58(23), pp. 5337-5339.

Anzai, N., Ichida, K., Jutabha, P., Kimura, T., Babu, E., Jin, C.J., Srivastava, S., Kitamura, K., Hisatome, I., Endou, H. and Sakurai, H. (2008) 'Plasma Urate Level Is Directly Regulated by a Voltage-driven Urate Efflux Transporter URATv1 (SLC2A9) in Humans', *Journal of Biological Chemistry*, 283(40), pp. 26834-26838.

Anzai, N., Jutabha, P., Enomoto, A., Yokoyama, H., Nonoguchi, H., Hirata, T., Shiraya, K., He, X., Cha, S.H., Takeda, M., Miyazaki, H., Sakata, T., Tomita, K., Igarashi, T., Kanai, Y. and Endou, H. (2005) 'Functional Characterization of Rat Organic Anion Transporter 5 (Slc22a19) at the Apical Membrane of Renal Proximal Tubules', *Journal of Pharmacology and Experimental Therapeutics*, 315(2), pp. 534-544.

Augustin, R., Carayannopoulos, M.O., Dowd, L.O., Phay, J.E., Moley, J.F. and Moley, K.H. (2004) 'Identification and Characterization of Human Glucose Transporter-like Protein-9 (GLUT9): Alternative Splicing Alters Trafficking', *Journal of Biological Chemistry*, 279(16), pp. 16229-16236.

Babu, E., Takeda, M., Narikawa, S., Kobayashi, Y., Enomoto, A., Tojo, A., Cha, S.H., Sekine, T., Sakthisekaran, D. and Endou, H. (2002) 'Role of human organic anion transporter 4 in the transport of ochratoxin A', *Biochim Biophys Acta*, 1590(1-3), pp. 64-75.

Badagnani, I., Castro, R.A., Taylor, T.R., Brett, C.M., Huang, C.C., Stryke, D., Kawamoto, M., Johns, S.J., Ferrin, T.E., Carlson, E.J., Burchard, E.G. and Giacomini, K.M. (2006) 'Interaction of methotrexate with organic-anion transporting polypeptide 1A2 and its genetic variants', *Journal of Pharmacology and Experimental Therapeutics*, 318(2), pp. 521-9.

Badolo, L., Trancart, M.M., Gustavsson, L. and Chesné, C. (2011) 'Effect of cryopreservation on the activity of OATP1B1/3 and OCT1 in isolated human hepatocytes', *Chemico-Biological Interactions*, 190(2–3), pp. 165-170.

Baer, P.C., Nockher, W.A., Haase, W. and Scherberich, J.E. (1997) 'Isolation of proximal and distal tubule cells from human kidney by immunomagnetic separation: Technical Note', *Kidney International*, 52(5), pp. 1321-1331.

Bakhiya, N., Bahn, A., Burckhardt, G. and Wolff, N.A. (2003) 'Human Organic Anion Transporter 3 (hOAT3) can Operate as an Exchanger and Mediate Secretory Urate Flux', *Cellular Physiology and Biochemistry*, 13(5), pp. 249-256.

Bass, A.S., Cartwright, M.E., Mahon, C., Morrison, R., Snyder, R., McNamara, P., Bradley, P., Zhou, Y.-Y. and Hunter, J. (2009) 'Exploratory drug safety: A discovery strategy to reduce attrition in development', *Journal of Pharmacological and Toxicological Methods*, 60(1), pp. 69-78.

Be, Eacute, Ry, E., eacute, bet, Rajnai, Z., Abonyi, T., Makai, I., oacute, Aacute, Ns, Aacute, Ghi, S., aacute, va, Erd, x, Franciska, Szir, Aacute, Ki, I., aacute, Her, Eacute, Di, S., Oacute, Krisztina, Kis, E., Jani, M., aacute, rton, Aacute, Rki-Zay, J., aacute, nos, Oacute, Th K, G., aacute, bor, Krajcsi, P., eacute and ter (2012) 'ABCG2 Modulates Chlorothiazide Permeability *In Vitro*;characterization of Its Interactions', *Drug Metabolism and Pharmacokinetics*, 27(3), pp. 349-353.

Belinsky, M.G., Chen, Z.-S., Shchaveleva, I., Zeng, H. and Kruh, G.D. (2002) 'Characterization of the Drug Resistance and Transport Properties of Multidrug Resistance Protein 6 (MRP6, ABCC6)', *Cancer Research*, 62(21), pp. 6172-6177.

Belinsky, M.G. and Kruh, G.D. (1999) 'MOAT-E (ARA) is a full-length MRP cMOAT subfamily transporter expressed in kidney and liver', *British Journal of Cancer*, 80(9), pp. 1342-1349.

Bello-Reuss, E. (1986) 'Cell membranes and paracellular resistances in isolated renal proximal tubules from rabbit and Ambystoma', *The Journal of Physiology*, 370(1), pp. 25-38.

Bens, M. and Vandewalle, A. (2008) 'Cell models for studying renal physiology', *Pflügers Archiv - European Journal of Physiology*, 457(1), pp. 1-15.

Bentz, J., O'Connor, M.P., Bednarczyk, D., Coleman, J., Lee, C., Palm, J., Pak, Y.A., Perloff, E.S., Reyner, E., Balimane, P., Brännström, M., Chu, X., Funk, C., Guo, A., Hanna, I., Herédi-Szabó, K., Hillgren, K., Li, L., Hollnack-Pusch, E., Jamei, M., Lin, X., Mason, A.K., Neuhoff, S., Patel, A., Podila, L., Plise, E., Rajaraman, G., Salphati, L., Sands, E., Taub, M.E., Taur, J.-S., Weitz, D., Wortelboer, H.M., Xia, C.Q., Xiao, G., Yabut, J., Yamagata, T., Zhang, L. and Ellens, H. (2013) 'Variability in P-Glycoprotein Inhibitory Potency (IC50) Using Various in Vitro Experimental Systems: Implications for Universal Digoxin Drug-Drug Interaction Risk Assessment Decision Criteria', *Drug Metabolism and Disposition*, 41(7), pp. 1347-1366.

Bergwerk, A.J., Shi, X., Ford, A.C., Kanai, N., Jacquemin, E., Burk, R.D., Bai, S., Novikoff, P.M., Stieger, B., Meier, P.J., Schuster, V.L. and Wolkoff, A.W. (1996) 'Immunologic distribution of an organic anion transport protein in rat liver and kidney', *Am J Physiol*, 271(2 Pt 1), pp. G231-8.

Beringer, P.M. and Slaughter, R.L. (2005) 'Transporters and Their Impact on Drug Disposition', *The Annals of Pharmacotherapy*, 39(6), pp. 1097-1108.

Bobulescu, I.A. and Moe, O.W. (2012) 'Renal Transport of Uric Acid: Evolving Concepts and Uncertainties', *Advances in Chronic Kidney Disease*, 19(6), pp. 358-371.

Bonate, P.L., Reith, K. and Weir, S. (1998) 'Drug interactions at the renal level - Implications for drug development', *Clinical Pharmacokinetics*, 34(5), pp. 375-404.

Bonsdorff, C.-H.v., Fuller, S.D. and Simons, K. (1985) 'Apical and basolateral endocytosis in Dadin-Darby canine kidney (MDCK) cells grown in nitrocellulose filters', *The EMBO Journal*, 4(11), pp. 2781-2792.

Bonventre, J.V. (2003) 'Dedifferentiation and Proliferation of Surviving Epithelial Cells in Acute Renal Failure', *Journal of the American Society of Nephrology*, 14(suppl 1), pp. S55-S61.

Boogaard, P.J., Mulder, G.J. and Nagelkerke, J.F. (1989) 'Isolated Proximal Tubular Cells from Rat Kidney as an in Vitro Model for Studies for Nephrotoxicity: I. An Improved Method for Preparation of Proximal Tubular Cells and Their Functional Characterization by α-Methylglucose Uptake', *Toxicology and Applied Pharmacology*, 101, pp. 135-143.

Boogaard, P.J., Nagelkerke, J.F. and Mulder, G.J. (1990a) 'Renal Proximal Tubular Cells in Suspension or in Primary Culture as Invitro Models to Study Nephrotoxicity', *Chemico-Biological Interactions*, 76(3), pp. 251-292.

Boogaard, P.J., Zoeteweij, J.P., Van Berkel, T.J.C., Van't Noordende, J.M., Mulder, G.J. and Nagelkerke, J.F. (1990b) 'Primary culture of proximal tubular cells from normal rat kidney as an in vitro model to study mechanisms of nephrotoxicity: Toxicity of nephrotoxicants at low concentrations during prolonged exposure', *Biochemical Pharmacology*, 39(8), pp. 1335-1345.

Brown, C.D.A., Sayer, R., Windass, A.S., Haslam, I.S., De Broe, M.E., D'Haese, P.C. and Verhulst, A. (2008) 'Characterisation of human tubular cell monolayers as a model of proximal tubular xenobiotic handling', *Toxicology and Applied Pharmacology*, 233(3), pp. 428-438.

Bulger, R.E. (1965) 'The shape of rat kidney tubular cells', *American Journal of Anatomy*, 116(1), pp. 237-255.

Cano, M.M., Calonge, M.L. and Ilundain, A.A. (2010) 'Expression of OCTN2 and OCTN3 in the apical membrane of rat renal cortex and medulla', *J Cell Physiol*, 223(2), pp. 451-9.

Cassio, D. (2013) 'Long term culture of MDCK strains alters chromosome content', *BMC Research Notes*, 6(1), pp. 1-7.

Caulfield, M.J., Munroe, P.B., O'Neill, D., Witkowska, K., Charchar, F.J., Doblado, M., Evans, S., Eyheramendy, S., Onipinla, A., Howard, P., Shaw-Hawkins, S.,

Dobson, R.J., Wallace, C., Newhouse, S.J., Brown, M., Connell, J.M., Dominiczak, A., Farrall, M., Lathrop, G.M., Samani, N.J., Kumari, M., Marmot, M., Brunner, E., Chambers, J., Elliott, P., Kooner, J., Laan, M., Org, E., Veldre, G., Viigimaa, M., Cappuccio, F.P., Ji, C., Iacone, R., Strazzullo, P., Moley, K.H. and Cheeseman, C. (2008) 'SLC2A9 Is a High-Capacity Urate Transporter in Humans', *Plos Medicine*, 5(10), pp. 1509-1523.

Cha, S.H., Sekine, T., Fukushima, J.I., Kanai, Y., Kobayashi, Y., Goya, T. and Endou, H. (2001) 'Identification and characterization of human organic anion transporter 3 expressing predominantly in the kidney', *Mol Pharmacol*, 59(5), pp. 1277-86.

Chandler, C.E., Zaccaro, L.M. and Moberly, J.B. (1993) 'Transepithelial transport of cholytaurine by Caco-2 cell monolayers is sodium dependent', *American Journal of Physiology*, 264, pp. G1118-G1125.

Chen, C.-j., Chin, J.E., Ueda, K., Clark, D.P., Pastan, I., Gottesman, M.M. and Roninson, I.B. (1986) 'Internal duplication and homology with bacterial transport proteins in the mdr1 (P-glycoprotein) gene from multidrug-resistant human cells', *Cell*, 47(3), pp. 381-389.

Chen, C. and Klaassen, C.D. (2004) 'Rat multidrug resistance protein 4 (Mrp4, Abcc4): molecular cloning, organ distribution, postnatal renal expression, and chemical inducibility', *Biochemical and Biophysical Research Communications*, 317(1), pp. 46-53.

Chen, Y., S. Li, Brown, C., Cheatham, S., Castro, R.A., Leabman, M.K., Urban, T.J., Chen, L., Yee, S.W., Choi, J.H., Huang, Y., Brett, C.M., Burchard, E.G. and Giacomini, K.M. (2009) 'Effect of Genetic Variation in the Organic Cation Transporter 2, OCT2, on the Renal Elimination of Metformin', *Pharmacogenetics and Genomics.*, 19, pp. 497–504.

Chen, Z.-S., Lee, K. and Kruh, G.D. (2001) 'Transport of Cyclic Nucleotides and Estradiol 17-β-d-Glucuronide by Multidrug Resistance Protein 4: RESISTANCE TO 6-MERCAPTOPURINE AND 6-THIOGUANINE', *Journal of Biological Chemistry*, 276(36), pp. 33747-33754.

Cherrington, N.J., Hartley, D.P., Li, N., Johnson, D.R. and Klaassen, C.D. (2002) 'Organ Distribution of Multidrug Resistance Proteins 1, 2, and 3 (Mrp1, 2, and 3) mRNA and Hepatic Induction of Mrp3 by Constitutive Androstane Receptor Activators in Rats', *Journal of Pharmacology and Experimental Therapeutics*, 300(1), pp. 97-104.

Chu, X.Y., Bleasby, K., Yabut, J., Cai, X., Chan, G.H., Hafey, M.J., Xu, S., Bergman, A.J., Braun, M.P., Dean, D.C. and Evers, R. (2007) 'Transport of the dipeptidyl peptidase-4 inhibitor sitagliptin by human organic anion transporter 3, organic anion transporting polypeptide 4C1, and multidrug resistance P-glycoprotein', *J Pharmacol Exp Ther*, 321(2), pp. 673-83.

Chun, J.K., M. Piquette-Miller, L. Zhang, and K. M. Giacomini (1997) 'Expression of Human Polyspecific Renal Organic Cation Transport Activity in Xenopus laevis Oocytes', *J. Pharm. Sci.*, 86(6), pp. 753-755.

Cole, S.P., Bhardwaj, G., Gerlach, J.H., Mackie, J.E., Grant, C.E., Almquist, K.C., Stewart, A.J., Kurz, E.U., Duncan, A.M. and Deeley, R.G. (1992) 'Overexpression of a transporter gene in a multidrug-resistant human lung cancer cell line', *Science*, 258(5088), pp. 1650-4.

Consortium, T.I.T. (2010) 'Membrane transporters in drug development', *Nat Rev Drug Discov*, 9(3), pp. 215-236.

Courjault-Gautier, F., Chevalier, J., Abbou, C.C., Chopin, D.K. and Toutain, H.J. (1995) 'Consecutive use of hormonally defined serum-free media to establish highly differentiated human renal proximal tubule cells in primary culture', *Journal of the American Society of Nephrology*, 5(11), pp. 1949-63.

Croop, J.M., Raymond, M., Haber, D., Devault, A., Arceci, R.J., Gros, P. and Housman, D.E. (1989) 'The three mouse multidrug resistance (mdr) genes are expressed in a tissue-specific manner in normal mouse tissues', *Mol Cell Biol*, 9(3), pp. 1346-50.

Curthoys, N.P. and Bellemann, P. (1979) 'Renal cortical cells in primary monolayer culture: Enzymatic changes and morphological observations', *Experimental Cell Research*, 121(1), pp. 31-45.

Dan, T., Tanaka, H. and Koga, H. (1990) 'Mechanism of uricosuric action of AA-193 in DBA/2N mice', *Journal of Pharmacology and Experimental Therapeutics*, 253(2), pp. 437-443.

Deguchi, T., Kusuhara, H., Takadate, A., Endou, H., Otagiri, M. and Sugiyama, Y. (2004) 'Characterization of uremic toxin transport by organic anion transporters in the kidney', *Kidney Int*, 65(1), pp. 162-174.

Deuchars, K.L., Duthie, M. and Ling, V. (1992) 'Identification of distinct P-glycoprotein gene sequences in rat', *Biochim Biophys Acta*, 1130(2), pp. 157-65.

Devault, A. and Gros, P. (1990) 'Two members of the mouse mdr gene family confer multidrug resistance with overlapping but distinct drug specificities', *Molecular and Cellular Biology*, 10(4), pp. 1652-1663.

Diestra, J.E., Scheffer, G.L., Catala, I., Maliepaard, M., Schellens, J.H., Scheper, R.J., Germa-Lluch, J.R. and Izquierdo, M.A. (2002) 'Frequent expression of the multi-drug resistance-associated protein BCRP/MXR/ABCP/ABCG2 in human tumours detected by the BXP-21 monoclonal antibody in paraffin-embedded material', *J Pathol*, 198(2), pp. 213-9.

Dinour, D., Gray, N.K., Campbell, S., Shu, X., Sawyer, L., Richardson, W., Rechavi, G., Amariglio, N., Ganon, L., Sela, B.-A., Bahat, H., Goldman, M., Weissgarten, J., Millar, M.R., Wright, A.F. and Holtzman, E.J. (2010) 'Homozygous SLC2A9 Mutations Cause Severe Renal Hypouricemia', *Journal of the American Society of Nephrology*, 21(1), pp. 64-72.

Dinour, D., Gray, N.K., Ganon, L., Knox, A.J.S., Shalev, H., Sela, B.-A., Campbell, S., Sawyer, L., Shu, X., Valsamidou, E., Landau, D., Wright, A.F. and Holtzman, E.J. (2012) 'Two novel homozygous SLC2A9 mutations cause renal hypouricemia type 2', *Nephrology Dialysis Transplantation*, 27(3), pp. 1035-1041.

Doyle, L.A., Yang, W., Abruzzo, L.V., Krogmann, T., Gao, Y., Rishi, A.K. and Ross, D.D. (1998) 'A multidrug resistance transporter from human MCF-7 breast cancer cells', *Proc Natl Acad Sci U S A*, 95(26), pp. 15665-70.

Ekaratanawong, S., Anzai, N., Jutabha, P., Miyazaki, H., Noshiro, R., Takeda, M., Kanai, Y., Sophasan, S. and Endou, H. (2004) 'Human organic anion transporter 4 is a renal apical organic anion/dicarboxylate exchanger in the proximal tubules', *Journal of Pharmacological Sciences*, 94(3), pp. 297-304.

Eladari, D., Chambrey, R., Irinopoulou, T., Leviel, F., Pezy, F., Bruneval, P., Paillard, M. and Podevin, R.-A. (1999) 'Polarized Expression of Different Monocarboxylate Transporters in Rat Medullary Thick Limbs of Henle', *Journal of Biological Chemistry*, 274(40), pp. 28420-28426.

Ellens, H., Deng, S., Coleman, J., Bentz, J., Taub, M.E., Ragueneau-Majlessi, I., Chung, S.P., Herédi-Szabó, K., Neuhoff, S., Palm, J., Balimane, P., Zhang, L., Jamei, M., Hanna, I., O'Connor, M., Bednarczyk, D., Forsgard, M., Chu, X., Funk, C., Guo, A., Hillgren, K.M., Li, L., Pak, A.Y., Perloff, E.S., Rajaraman, G., Salphati, L., Taur, J.-S., Weitz, D., Wortelboer, H.M., Xia, C.Q., Xiao, G., Yamagata, T. and Lee, C.A. (2013) 'Application of Receiver Operating Characteristic Analysis to Refine the Prediction of Potential Digoxin Drug Interactions', *Drug Metabolism and Disposition*, 41(7), pp. 1367-1374.

Enomoto, A., Kimura, H., Chairoungdua, A., Shigeta, Y., Jutabha, P., Ho Cha, S., Hosoyamada, M., Takeda, M., Sekine, T., Igarashi, T., Matsuo, H., Kikuchi, Y., Oda, T., Ichida, K., Hosoya, T., Shimokata, K., Niwa, T., Kanai, Y. and Endou, H. (2002) 'Molecular identification of a renal urate-anion exchanger that regulates blood urate levels', *Nature*, 417(6887), pp. 447-452.

Evers, R., Kool, M., van Deemter, L., Janssen, H., Calafat, J., Oomen, L.C., Paulusma, C.C., Oude Elferink, R.P., Baas, F., Schinkel, A.H. and Borst, P. (1998) 'Drug export activity of the human canalicular multispecific organic anion transporter in polarized kidney MDCK cells expressing cMOAT (MRP2) cDNA', *The Journal of Clinical Investigation*, 101(7), pp. 1310-1319.

Evers, R., Zaman, G.J., van Deemter, L., Jansen, H., Calafat, J., Oomen, L.C., Oude Elferink, R.P., Borst, P. and Schinkel, A.H. (1996) 'Basolateral localization and export activity of the human multidrug resistance-associated protein in polarized pig kidney cells', *J Clin Invest*, 97(5), pp. 1211-8.

Fagerholm, U. (2007) 'Prediction of human pharmacokinetics — renal metabolic and excretion clearance', *Journal of Pharmacy and Pharmacology*, 59(11), pp. 1463-1471.

Fauth, C., Rossier, B. and Roch-Ramel, F. (1988) Transport of tetraethylammonium by a kidney epithelial cell line (LLC-PK1).

Feng, B., LaPerle, J.L., Chang, G. and Varma, M.V. (2010) 'Renal clearance in drug discovery and development: molecular descriptors, drug transporters and disease state', *Expert Opinion on Drug Metabolism & Toxicology*, 6(8), pp. 939-952.

Fenner, K.S., Troutman, M.D., Kempshall, S., Cook, J.A., Ware, J.A., Smith, D.A. and Lee, C.A. (2008) 'Drug-Drug Interactions Mediated Through P-Glycoprotein: Clinical Relevance and In Vitro-In Vivo Correlation Using Digoxin as a Probe Drug', *Clin Pharmacol Ther*, 85(2), pp. 173-181.

Fox, I.H. and Sinclair, D.S. (1977) 'The Pharmacology of the Hypouricemic Effect of Benzbromarone', in Müller, M., Kaiser, E. and Seegmiller, J.E. (eds.) *Purine Metabolism in Man—II*. Springer US, pp. 328-333.

Fulcher, M.L., Gabriel, S., Burns, K.A., Yankaskas, J.R. and Randell, S.H. (2005) 'Well-differentiated human airway epithelial cell cultures', *Methods Mol Med*, 107, pp. 183-206.

Furuse, M., Sasaki, H. and Tsukita, S. (1999) 'Manner of Interaction of Heterogeneous Claudin Species within and between Tight Junction Strands', *The Journal of Cell Biology*, 147(4), pp. 891-903.

Garcia, C.K., Goldstein, J.L., Pathak, R.K., Anderson, R.G.W. and Brown, M.S. (1994) 'Molecular characterization of a membrane transporter for lactate, pyruvate, and other monocarboxylates: Implications for the Cori cycle', *Cell*, 76(5), pp. 865-873.

Gekeler, V., Ise, W., Sanders, K.H., Ulrich, W.R. and Beck, J. (1995) 'The leukotriene LTD4 receptor antagonist MK571 specifically modulates MRP

associated multidrug resistance', *Biochem Biophys Res Commun*, 208(1), pp. 345-52.

Gesek, F.A., Wolff, D.W. and Strandhoy, J.W. (1987) Improved separation method for rat proximal and distal renal tubules.

Glube, N., Closs, E. and Langguth, P. (2006) 'OCTN2-Mediated Carnitine Uptake in a Newly Discovered Human Proximal Tubule Cell Line (Caki-1)', *Molecular Pharmaceutics*, 4(1), pp. 160-168.

Gochoco, C.H., Ryan, F.M., Miller, J., Smith, P.L. and Hidalgo, I.J. (1994) 'Uptake and transepithelial transport of the orally absorbed cephalosporin cephalexin, in the human intestinal cell line, Caco-2', *International Journal of Pharmaceutics*, 104(3), pp. 187-202.

Goldin, A.L. (1992) 'Maintenance of Xenopus laevis and oocyte injection', in Bernardo, R. (ed.) *Methods in Enzymology*. Academic Press, pp. 266-279.

Gorboulev, V., Ulzheimer, J., Akhoundova, A., Ulzheimer-Teuber, I., Karbach, U., Quester, S., Baumann, C., Lang, F., Busch, A.E. and Koepsell, H. (1997) 'Cloning and characterization of two human polyspecific organic cation transporters', *DNA Cell Biology*, 16(7), pp. 871-81.

Gros, P., Ben-Neriah, Y., Croop, J.M. and Housman, D.E. (1986) 'Isolation and Expression of a Complementary-DNA That Confers Multidrug Resistance', *Nature*, 323(6090), pp. 728-731.

Gründemann, D., Babin-Ebell, J., Martel, F., Örding, N., Schmidt, A. and Schömig, E. (1997) 'Primary Structure and Functional Expression of the Apical Organic Cation Transporter from Kidney Epithelial LLC-PK1Cells', *Journal of Biological Chemistry*, 272(16), pp. 10408-10413.

Grundemann, D., Gorboulev, V., Gambaryan, S., Veyhl, M. and Koepsell, H. (1994) 'Drug excretion mediated by a new prototype of polyspecific transporter', *Nature*, 372(6506), pp. 549-552.

Guggino, S.E. and Aronson, P.S. (1985) 'Paradoxical effects of pyrazinoate and nicotinate on urate transport in dog renal microvillus membranes', *The Journal of Clinical Investigation*, 76(2), pp. 543-547.

Gupta, A., Dai, Y., Vethanayagam, R., Hebert, M., Thummel, K., Unadkat, J., Ross, D. and Mao, Q. (2006) 'Cyclosporin A, tacrolimus and sirolimus are potent inhibitors of the human breast cancer resistance protein (ABCG2) and reverse resistance to mitoxantrone and topotecan', *Cancer Chemotherapy and Pharmacology*, 58(3), pp. 374-383.

Gurdon, J.B., Lane, C.D., Woodland, H.R. and Marbaix, G. (1971) 'Use of frog eggs and oocytes for the study of messenger RNA and its translation in living cells', *Nature*, 233(5316), pp. 177-182.

Gutmann, H., Fricker, G., Török, M., Michael, S., Beglinger, C. and Drewe, J. (1999) 'Evidence for Different ABC-Transporters in Caco-2 Cells Modulating Drug Uptake', *Pharmaceutical Research*, 16(3), pp. 402-407.

Hagos, Y., Krick, W., Braulke, T., Muhlhausen, C., Burckhardt, G. and Burckhardt, B.C. (2008) 'Organic anion transporters OAT1 and OAT4 mediate the high affinity transport of glutarate derivatives accumulating in patients with glutaric acidurias', *Pflugers Archiv : European journal of physiology*, 457(1), pp. 223-31.

Hagos, Y., Stein, D., Ugele, B., Burckhardt, G. and Bahn, A. (2007) 'Human renal organic anion transporter 4 operates as an asymmetric urate transporter', *Journal of the American Society of Nephrology*, 18(2), pp. 430-439.

Haley, D.P. and Bulger, R.E. (1983) 'The aging male rat: Structure and function of the kidney', *American Journal of Anatomy*, 167(1), pp. 1-13.

Hasegawa, M., Kusuhara, H., Sugiyama, D., Ito, K., Ueda, S., Endou, H. and Sugiyama, Y. (2002) 'Functional involvement of rat organic anion transporter 3 (rOat3; Slc22a8) in the renal uptake of organic anions', *J Pharmacol Exp Ther*, 300(3), pp. 746-53.

Haslam, I.S., Wright, J.A., O'Reilly, D.A., Sherlock, D.J., Coleman, T. and Simmons, N.L. (2011) 'Intestinal Ciprofloxacin Efflux: The Role of Breast Cancer

Resistance Protein (ABCG2)', *Drug Metabolism and Disposition*, 39(12), pp. 2321-2328.

Hediger, M.A., Johnson, R.J., Miyazaki, H. and Endou, H. (2005) 'Molecular Physiology of Urate Transport', *Physiology*, 20(2), pp. 125-133.

Helbert, M.J., Dauwe, S.E., Van der Biest, I., Nouwen, E.J. and De Broe, M.E. (1997) 'Immunodissection of the human proximal nephron: flow sorting of S1S2S3, S1S2 and S3 proximal tubular cells', *Kidney international*, 52(2), pp. 414-428.

Herrmann, H., Strelkov, S.V., Burkhard, P. and Aebi, U. (2009) 'Intermediate filaments: primary determinants of cell architecture and plasticity', *The Journal of Clinical Investigation*, 119(7), pp. 1772-1783.

Hilgendorf, C., Ahlin, G., Seithel, A., Artursson, P., Ungell, A.-L. and Karlsson, J. (2007) 'Expression of Thirty-six Drug Transporter Genes in Human Intestine, Liver, Kidney, and Organotypic Cell Lines', *Drug Metabolism and Disposition*, 35(8), pp. 1333-1340.

Hirsch, M. and Noske, W. (1993) 'The tight junction: Structure and function', *Micron*, 24(3), pp. 325-352.

Hopper, E., Belinsky, M.G., Zeng, H., Tosolini, A., Testa, J.R. and Kruh, G.D. (2001) 'Analysis of the structure and expression pattern of MRP7 (ABCC10), a new member of the MRP subfamily', *Cancer Lett*, 162(2), pp. 181-91.

Hori, R., Okamura, N., Aiba, T. and Tanigawara, Y. (1993) 'Role of P-glycoprotein in renal tubular secretion of digoxin in the isolated perfused rat kidney', *Journal of Pharmacology and Experimental Therapeutics*, 266(3), pp. 1620-1625.

Hosoyamada, M., Ichida, K., Enomoto, A., Hosoya, T. and Endou, H. (2004) 'Function and localization of urate transporter 1 in mouse kidney', *J Am Soc Nephrol*, 15(2), pp. 261-8.

Hu, E., Chen, Z., Fredrickson, T.A., Spurr, N., Gentle, S., Sims, M., Zhu, Y., Halsey, W., Van Horn, S., Mao, J., Sathe, G.M. and Brooks, D.P. (2001) 'Rapid isolation of tissue-specific genes from rat kidney', *Exp Nephrol*, 9(2), pp. 156-64.

Huisman, M.T., Smit, J.W., Crommentuyn, K.M.L., Zelcer, N., Wiltshire, H.R., Beijnen, J.H. and Schinkel, A.H. (2002) 'Multidrug resistance protein 2 (MRP2) transports HIV protease inhibitors, and transport can be enhanced by other drugs', *Aids*, 16(17), pp. 2295-2301.

Huls, M., Brown, C.D.A., Windass, A.S., Sayer, R., van den Heuvel, J.J.M.W., Heemskerk, S., Russel, F.G.M. and Masereeuw, R. (2008) 'The breast cancer resistance protein transporter ABCG2 is expressed in the human kidney proximal tubule apical membrane', *Kidney International*, 73(2), pp. 220-225.

Huls, M., van den Heuvel, J.J., Dijkman, H.B., Russel, F.G. and Masereeuw, R. (2006) 'ABC transporter expression profiling after ischemic reperfusion injury in mouse kidney', *Kidney Int*, 69(12), pp. 2186-93.

Hunt, S.A. (2005) 'ACC/AHA 2005 Guideline Update for the Diagnosis and Management of Chronic Heart Failure in the Adult: A Report of the American College of Cardiology/American Heart Association Task Force on Practice Guidelines (Writing Committee to Update the 2001 Guidelines for the Evaluation and Management of Heart Failure)', *Journal of the American College of Cardiology*, 46(6), pp. e1-e82.

Hynes, R.O. (1987) 'Integrins: A family of cell surface receptors', *Cell*, 48(4), pp. 549-554.

Imaoka, T., H. Kusuhara, M. Adachi, J. D. Schuetz, K. Takeuchi, and Y. Sugiyama (2007) 'Functional Involvement of Multidrug Resistance-Associated Protein 4 (MRP4/ABCC4) in the Renal Elimination of the Antiviral Drugs Adefovir and Tenofovir', *Mol. Pharmacol.*, 71, pp. 619–627.

Inui, K.-I., Masuda, S. and Saito, H. (2000) 'Cellular and molecular aspects of drug transport in the kidney', *Kidney International*, 58(3), pp. 944-958.

Isern, J., Hagenbuch, B., Stieger, B., Meier, P.J. and Meseguer, A. (2001) 'Functional analysis and androgen-regulated expression of mouse organic anion transporting polypeptide 1 (Oatp1) in the kidney', *Biochim Biophys Acta*, 1518(1-2), pp. 73-8.

Ito, S., Kusuhara, H., Yokochi, M., Toyoshima, J., Inoue, K., Yuasa, H. and Sugiyama, Y. (2012) 'Competitive Inhibition of the Luminal Efflux by Multidrug and Toxin Extrusions, but Not Basolateral Uptake by Organic Cation Transporter 2, Is the Likely Mechanism Underlying the Pharmacokinetic Drug-Drug Interactions Caused by Cimetidine in the Kidney', *Journal of Pharmacology and Experimental Therapeutics*, 340(2), pp. 393-403.

Jackson, V.N. and Halestrap, A.P. (1996) 'The Kinetics, Substrate, and Inhibitor Specificity of the Monocarboxylate (Lactate) Transporter of Rat Liver Cells Determined Using the Fluorescent Intracellular pH Indicator, 2′,7′-Bis(carboxyethyl)-5(6)-carboxyfluorescein', *Journal of Biological Chemistry*, 271(2), pp. 861-868.

Jacquemin, E., Hagenbuch, B., Stieger, B., Wolkoff, A.W. and Meier, P.J. (1994) 'Expression cloning of a rat liver Na$^+$-independent organic anion transporter', *Proc Natl Acad Sci U S A*, 91(1), pp. 133-7.

Jani, M., Szabó, P., Kis, E., Molnár, É., Glavinas, H. and Krajcsi, P. (2009) 'Kinetic Characterization of Sulfasalazine Transport by Human ATP-Binding Cassette G2', *Biological and Pharmaceutical Bulletin*, 32(3), pp. 497-499.

Jansen, J., Schophuizen, C.M.S., Wilmer, M.J., Lahham, S.H.M., Mutsaers, H.A.M., Wetzels, J.F.M., Bank, R.A., van den Heuvel, L.P., Hoenderop, J.G. and Masereeuw, R. (2014) 'A morphological and functional comparison of proximal tubule cell lines established from human urine and kidney tissue', *Experimental Cell Research*, 323(1), pp. 87-99.

Jedlitschky, G., Burchell, B. and Keppler, D. (2000) 'The multidrug resistance protein 5 functions as an ATP-dependent export pump for cyclic nucleotides', *Journal of Biological Chemistry*, 275(39), pp. 30069-30074.

Jenkinson, S., Chung, G., van Loon, E., Bakar, N., Dalzell, A. and Brown, C. (2012) 'The limitations of renal epithelial cell line HK-2 as a model of drug transporter expression and function in the proximal tubule', *Pflügers Archiv European Journal of Physiology*, 464(6), pp. 601-611.

Jung, S.J., Choi, S.O., Um, S.Y., Kim, J.I., Choo, H.Y.P., Choi, S.Y. and Chung, S.Y. (2006) 'Prediction of the permeability of drugs through study on quantitative structure–permeability relationship', *Journal of Pharmaceutical and Biomedical Analysis*, 41(2), pp. 469-475.

Jutabha, P., Anzai, N., Kitamura, K., Taniguchi, A., Kaneko, S., Yan, K., Yamada, H., Shimada, H., Kimura, T., Katada, T., Fukutomi, T., Tomita, K., Urano, W., Yamanaka, H., Seki, G., Fujita, T., Moriyama, Y., Yamada, A., Uchida, S., Wempe, M.F., Endou, H. and Sakurai, H. (2010) 'Human Sodium Phosphate Transporter 4 (hNPT4/SLC17A3) as a Common Renal Secretory Pathway for Drugs and Urate', *Journal of Biological Chemistry*, 285(45), pp. 35123-35132.

Kakumoto, M., Takara, K., Sakaeda, T., Tanigawara, Y., Kita, T. and Okumura, K. (2002) 'MDR1-Mediated Interaction of Digoxin with Antiarrhythmic or Antianginal Drugs', *Biological and Pharmaceutical Bulletin*, 25(12), pp. 1604-1607.

Karbach, U., Kricke, J., Meyer-Wentrup, F., Gorboulev, V., Volk, C., Loffing-Cueni, D., Kaissling, B., Bachmann, S. and Koepsell, H. (2000) 'Localization of organic cation transporters OCT1 and OCT2 in rat kidney', *Am J Physiol Renal Physiol*, 279(4), pp. F679-87.

Kawamura, Y., Matsuo, H., Chiba, T., Nagamori, S., Nakayama, A., Inoue, H., Utsumi, Y., Oda, T., Nishiyama, J., Kanai, Y. and Shinomiya, N. (2011) 'Pathogenic GLUT9 Mutations Causing Renal Hypouricemia Type 2 (RHUC2)', *Nucleosides, Nucleotides and Nucleic Acids*, 30(12), pp. 1105-1111.

Keppler, D. (2011) 'Multidrug Resistance Proteins (MRPs, ABCCs): Importance for Pathophysiology and Drug Therapy and Drug Transporters', in Fromm, M.F. and Kim, R.B. (eds.) Springer Berlin Heidelberg, pp. 299-323.

Kimura, N., Masuda, S., Tanihara, Y., Ueo, H., Okuda, M., Katsura, T. and Inui, K.-i. (2005) 'Metformin is a Superior Substrate for Renal Organic Cation Transporter OCT2 rather than Hepatic OCT1', *Drug Metabolism and Pharmacokinetics*, 20(5), pp. 379-386.

Kis, E., Nagy, T., Jani, M., Molnár, É., Jánossy, J., Ujhellyi, O., Német, K., Herédi-Szabó, K. and Krajcsi, P. (2009) 'Leflunomide and its metabolite A771726 are high affinity substrates of BCRP: implications for drug resistance', *Annals of the Rheumatic Diseases*, 68(7), pp. 1201-1207.

Knaggs, H. (1992) 'The cell biology of the extracellular matrix', *Biochemical Education*, 20(3), pp. 187-187.

Kojima, R., Sekine, T., Kawachi, M., Cha, S.H., Suzuki, Y. and Endou, H. (2002) 'Immunolocalization of Multispecific Organic Anion Transporters, OAT1, OAT2, and OAT3, in Rat Kidney', *Journal of the American Society of Nephrology*, 13(4), pp. 848-857.

Komatsu, T., Hiasa, M., Miyaji, T., Kanamoto, T., Matsumoto, T., Otsuka, M., Moriyama, Y. and Omote, H. (2011) 'Characterization of the human MATE2 proton-coupled polyspecific organic cation exporter', *International Journal of Biochemistry and Cell Biology*, 43(6), pp. 913-8.

König, J. (2011) 'Uptake Transporters of the Human OATP Family Drug Transporters', in Fromm, M.F. and Kim, R.B. (eds.) *Drug Transporters, Handbook of Experimental Pharmacology*. Springer Berlin Heidelberg, pp. 1-28.

König, J., Müller, F. and Fromm, M.F. (2013) 'Transporters and Drug-Drug Interactions: Important Determinants of Drug Disposition and Effects', *Pharmacological Reviews*, 65(3), pp. 944-966.

König, J., Nies, A.T., Cui, Y., Leier, I. and Keppler, D. (1999) 'Conjugate export pumps of the multidrug resistance protein (MRP) family: localization, substrate specificity, and MRP2-mediated drug resistance', *Biochimica et Biophysica Acta (BBA) - Biomembranes*, 1461(2), pp. 377-394.

Konig, J., Zolk, O., Singer, K., Hoffmann, C. and Fromm, M.F. (2011) 'Double-transfected MDCK cells expressing human OCT1/MATE1 or OCT2/MATE1: determinants of uptake and transcellular translocation of organic cations', *British Journal of Pharmacology*, 163(3), pp. 546-55.

Kool, M., de Haas, M., Scheffer, G.L., Scheper, R.J., van Eijk, M.J., Juijn, J.A., Baas, F. and Borst, P. (1997) 'Analysis of expression of cMOAT (MRP2), MRP3, MRP4, and MRP5, homologues of the multidrug resistance-associated protein gene (MRP1), in human cancer cell lines', *Cancer Research*, 57(16), pp. 3537-47.

Kool, M., van der Linden, M., de Haas, M., Baas, F. and Borst, P. (1999) 'Expression of human MRP6, a homologue of the multidrug resistance protein gene MRP1, in tissues and cancer cells', *Cancer Research*, 59(1), pp. 175-82.

Koren, G. (1987) 'Clinical Pharmacokinetic Significance of the Renal Tubular Secretion of Digoxin', *Clinical Pharmacokinetics*, 13(5), pp. 334-343.

Kuo, K.-L., Zhu, H., McNamara, P.J. and Leggas, M. (2012) 'Localization and Functional Characterization of the Rat Oatp4c1 Transporter in an *In Vitro* Cell System and Rat Tissues', *PLoS ONE*, 7(6), p. e39641.

Kusuhara, H., Sekine, T., Utsunomiya-Tate, N., Tsuda, M., Kojima, R., Cha, S.H., Sugiyama, Y., Kanai, Y. and Endou, H. (1999) 'Molecular cloning and characterization of a new multispecific organic anion transporter from rat brain', *J Biol Chem*, 274(19), pp. 13675-80.

Kuteykin-Teplyakov, K., Luna-Tortós, C., Ambroziak, K. and Löscher, W. (2010) 'Differences in the expression of endogenous efflux transporters in MDR1-transfected versus wildtype cell lines affect P-glycoprotein mediated drug transport', *British Journal of Pharmacology*, 160(6), pp. 1453-1463.

Kuze, K., Graves, P., Leahy, A., Wilson, P., Stuhlmann, H. and You, G. (1999) 'Heterologous expression and functional characterization of a mouse renal organic anion transporter in mammalian cells', *J Biol Chem*, 274(3), pp. 1519-24.

Kwatra, D., Khurana, V. and Mitra, A.K. (2014) 'In vitro models in drug discovery and delivery', in Mitra, A.K., Kwatra, D. and Vadlapudi, A.D. (eds.) *Drug Delivery*. 1 edn. Boston: Jones & Bartlett Publishers.

Lacarelle, B., Rahmani, R., de Sousa, G., Durand, A., Placidi, M. and Cano, J.P. (1991) 'Metabolism of digoxin, digoxigenin digitoxosides and digoxigenin in human hepatocytes and liver microsomes', *Fundamental & Clinical Pharmacology*, 5(7), pp. 567-582.

Lalande, M.E., Ling, V. and Miller, R.G. (1981) 'Hoechst 33342 Dye Uptake as a Probe of Membrane-Permeability Changes in Mammalian-Cells', *Proceedings of the National Academy of Sciences of the United States of America-Biological Sciences*, 78(1), pp. 363-367.

Lam, A.Q., Freedman, B.S., Morizane, R., Lerou, P.H., Valerius, M.T. and Bonventre, J.V. (2014) 'Rapid and Efficient Differentiation of Human Pluripotent Stem Cells into Intermediate Mesoderm That Forms Tubules Expressing Kidney Proximal Tubular Markers', *Journal of the American Society of Nephrology*, 25(6), pp. 1211-1255.

Lash, L.H. (2006) 'Mitochondrial glutathione transport: Physiological, pathological and toxicological implications', *Chemico-Biological Interactions*, 163(1–2), pp. 54-67.

Lash, L.H., Putt, D.A. and Cai, H. (2006) 'Membrane transport function in primary cultures of human proximal tubular cells', *Toxicology*, 228(2–3), pp. 200-218.

Leabman, M.K., Huang, C.C., Kawamoto, M., Johns, S.J., Stryke, D., Ferrin, T.E., DeYoung, J., Taylor, T., Clark, A.G., Herskowitz, I., Giacomini, K.M. and Pharmacogenetics of Membrane Transporters, I. (2002) 'Polymorphisms in a human kidney xenobiotic transporter, OCT2, exhibit altered function', *Pharmacogenetics*, 12(5), pp. 395-405.

Lee, M.H., Graham, G.G., Williams, K.M. and Day, R.O. (2008) 'A benefit-risk assessment of benzbromarone in the treatment of gout. Was its withdrawal from the market in the best interest of patients', *Drug Safety*, 31(8), pp. 643-65.

Lee, W., Glaeser, H., Smith, L.H., Roberts, R.L., Moeckel, G.W., Gervasini, G., Leake, B.F. and Kim, R.B. (2005) 'Polymorphisms in human organic anion-transporting polypeptide 1A2 (OATP1A2): implications for altered drug disposition and central nervous system drug entry', *Journal of Biological Chemistry*, 280(10), pp. 9610-7.

Li, S., Sanna, S., Maschio, A., Busonero, F., Usala, G., Mulas, A., Lai, S., Dei, M., Orrù, M., Albai, G., Bandinelli, S., Schlessinger, D., Lakatta, E., Scuteri, A., Najjar, S.S., Guralnik, J., Naitza, S., Crisponi, L., Cao, A., Abecasis, G., Ferrucci, L., Uda, M., Chen, W.-M. and Nagaraja, R. (2007) 'The GLUT9 Gene Is Associated with Serum Uric Acid Levels in Sardinia and Chianti Cohorts', *PLoS Genetics*, 3(11), p. e194.

Lickteig, A.J., Cheng, X., Augustine, L.M., Klaassen, C.D. and Cherrington, N.J. (2008) 'Tissue distribution, ontogeny and induction of the transporters Multidrug and toxin extrusion (MATE) 1 and MATE2 mRNA expression levels in mice', *Life Sci*, 83(1-2), pp. 59-64.

Lin, J.H. (1995) 'Species similarities and differences in pharmacokinetics', *Drug Metabolism and Disposition*, 23(10), pp. 1008-1021.

Lipkowitz, M. (2012) 'Regulation of Uric Acid Excretion by the Kidney', *Current Rheumatology Reports*, 14(2), pp. 179-188.

Liu, Y. (2004) 'Epithelial to Mesenchymal Transition in Renal Fibrogenesis: Pathologic Significance, Molecular Mechanism, and Therapeutic Intervention', *Journal of the American Society of Nephrology*, 15(1), pp. 1-12.

Ltd, L.G. (2014) *Renal Cell Growth Medium* [Webpage]. Available at: http://www.lonza.com/products-services/bio-research/primary-and-stem-cells/human-cells-and-media/renal-cells-and-media/renal-cell-growth-medium.aspx (Accessed: 21/07/2014).

MacLean, C., Moenning, U., Reichel, A. and Fricker, G. (2008) 'Closing the Gaps: A Full Scan of the Intestinal Expression of P-Glycoprotein, Breast Cancer Resistance Protein, and Multidrug Resistance-Associated Protein 2 in Male and Female Rats', *Drug Metabolism and Disposition*, 36(7), pp. 1249-1254.

Madsen, K.M. and Tisher, C.C. (1976) 'Anatomy of the kidney', in Brenner, B.M. (ed.) *The Kidney*. 7 edn. Philadelphia: Elsevier, pp. 3-72.

Maeda, K., Tian, Y., Fujita, T., Ikeda, Y., Kumagai, Y., Kondo, T., Tanabe, K., Nakayama, H., Horita, S., Kusuhara, H. and Sugiyama, Y. (2014) 'Inhibitory effects of p-aminohippurate and probenecid on the renal clearance of adefovir and benzylpenicillin as probe drugs for organic anion transporter (OAT) 1 and OAT3 in humans', *European Journal of Pharmaceutical Sciences*, 59(0), pp. 94-103.

Maliepaard, M., Scheffer, G.L., Faneyte, I.F., van Gastelen, M.A., Pijnenborg, A.C.L.M., Schinkel, A.H., van de Vijver, M.J., Scheper, R.J. and Schellens, J.H.M. (2001) 'Subcellular Localization and Distribution of the Breast Cancer Resistance Protein Transporter in Normal Human Tissues', *Cancer Research*, 61(8), pp. 3458-3464.

Masuda, S., Ibaramoto, K., Takeuchi, A., Saito, H., Hashimoto, Y. and Inui, K.-I. (1999a) 'Cloning and Functional Characterization of a New Multispecific Organic Anion Transporter, OAT-K2, in Rat Kidney', *Molecular Pharmacology*, 55(4), pp. 743-752.

Masuda, S., Saito, H. and Inui, K.I. (1997a) 'Interactions of nonsteroidal anti-inflammatory drugs with rat renal organic anion transporter, OAT-K1', *Journal of Pharmacology and Experimental Therapeutics*, 283(3), pp. 1039-42.

Masuda, S., Saito, H., Nonoguchi, H., Tomita, K. and Inui, K.-i. (1997b) 'mRNA distribution and membrane localization of the OAT-K1 organic anion transporter in rat renal tubules', *FEBS Letters*, 407(2), pp. 127-131.

Masuda, S., Takeuchi, A., Saito, H., Hashimoto, Y. and Inui, K. (1999b) 'Functional analysis of rat renal organic anion transporter OAT-K1: bidirectional methotrexate transport in apical membrane', *FEBS Letters*, 459(1), pp. 128-32.

Masuda, S., Terada, T., Yonezawa, A., Tanihara, Y., Kishimoto, K., Katsura, T., Ogawa, O. and Inui, K. (2006) 'Identification and functional characterization of a new human kidney-specific H$^+$/organic cation antiporter, kidney-specific multidrug

and toxin extrusion 2', *Journal of the American Society of Nephrology*, 17(8), pp. 2127-35.

Matsuo, H., Chiba, T., Nagamori, S., Nakayama, A., Domoto, H., Phetdee, K., Wiriyasermkul, P., Kikuchi, Y., Oda, T., Nishiyama, J., Nakamura, T., Morimoto, Y., Kamakura, K., Sakurai, Y., Nonoyama, S., Kanai, Y. and Shinomiya, N. (2008) 'Mutations in Glucose Transporter 9 Gene SLC2A9 Cause Renal Hypouricemia', *The American Journal of Human Genetics*, 83(6), pp. 744-751.

Maunsbach, A.B. (1966) 'Observations on the segmentation of the proximal tubule in the rat kidney: Comparison of results from phase contrast, fluorescence and electron microscopy', *Journal of Ultrastructure Research*, 16(3–4), pp. 239-258.

Mendrick, D.L., Chung, D.C. and Rennke, H.G. (1990) 'Heymann antigen gp330 demonstrates affinity for fibronectin, laminin, and type I collagen and mediates rat proximal tubule epithelial cell adherence to such matrices in vitro', *Experimental Cell Research*, 188(1), pp. 23-35.

Mikkaichi, T., Suzuki, T., Onogawa, T., Tanemoto, M., Mizutamari, H., Okada, M., Chaki, T., Masuda, S., Tokui, T., Eto, N., Abe, M., Satoh, F., Unno, M., Hishinuma, T., Inui, K., Ito, S., Goto, J. and Abe, T. (2004) 'Isolation and characterization of a digoxin transporter and its rat homologue expressed in the kidney', *Proceedings of the National Academy of Sciences of the United States of America*, 101(10), pp. 3569-3574.

Miura, D., Anzai, N., Jutabha, P., Chanluang, S., He, X., Fukutomi, T. and Endou, H. (2011) 'Human urate transporter 1 (hURAT1) mediates the transport of orotate', *Journal of Physiological Sciences*, 61(3), pp. 253-7.

Moe, O.W., Baum, M., Berry, C.A. and Rector, F.C. (2004) 'Renal transport of glucose, amino acids, sodium, chloride and water', in Brenner, B.M. (ed.) *The Kidney*. Philadelphia: Elsevier, pp. 413-452.

Mukherjee, T., Squillantea, E., Gillespieb, M. and Shao, J. (2004) 'Transepithelial Electrical Resistance is Not a Reliable Measurement of the Caco-2 Monolayer Integrity in Transwell', *Drug Delivery*, 11(1), pp. 11-18.

Müller, H., Klinkhammer, W., Globisch, C., Kassack, M.U., Pajeva, I.K. and Wiese, M. (2007) 'New functional assay of P-glycoprotein activity using Hoechst 33342', *Bioorganic & Medicinal Chemistry*, 15(23), pp. 7470-7479.

Nakanishi, T., Fukushi, A., Sato, M., Yoshifuji, M., Gose, T., Shirasaka, Y., Ohe, K., Kobayashi, M., Kawai, K. and Tamai, I. (2011) 'Functional Characterization of Apical Transporters Expressed in Rat Proximal Tubular Cells (PTCs) in Primary Culture', *Molecular Pharmaceutics*, 8(6), pp. 2142-2150.

Nakanishi, T., Ohya, K., Shimada, S., Anzai, N. and Tamai, I. (2013) 'Functional cooperation of URAT1 (SLC22A12) and URATv1 (SLC2A9) in renal reabsorption of urate', *Nephrology Dialysis Transplantation*, 28(3), pp. 603-611.

Nelson, J.A., Santos, G. and Herbert, B.H. (1984) 'Mechanisms for the renal secretion of cisplatin', *Cancer Treat Rep*, 68(6), pp. 849-853.

Nyengaard, J.R. and Bendtsen, T.F. (1992) 'Glomerular number and size in relation to age, kidney weight, and body surface in normal man', *The Anatomical Record*, 232(2), pp. 194-201.

Ohashi, R., Tamai, I., Yabuuchi, H., Nezu, J.-I., Oku, A., Sai, Y., Shimane, M. and Tsuji, A. (1999) 'Na$^+$-Dependent Carnitine Transport by Organic Cation Transporter (OCTN2): Its Pharmacological and Toxicological Relevance', *Journal of Pharmacology and Experimental Therapeutics*, 291(2), pp. 778-784.

Ohnhaus, E.E., Sprung, P. and Dettli, L. (1972) 'Protein binding of digoxin in human serum', *Eurpoean Journal of Clinical Pharmacology*, 5, p. 34.

Ohta, K.-y., Inoue, K., Hayashi, Y. and Yuasa, H. (2006) 'Molecular Identification and Functional Characterization of Rat Multidrug and Toxin Extrusion Type Transporter 1 as an Organic Cation/H$^+$ Antiporter in the Kidney', *Drug Metabolism and Disposition*, 34(11), pp. 1868-1874.

Ohtomo, T., Saito, H., Inotsume, N., Yasuhara, M. and Inui, K.I. (1996) 'Transport of levofloxacin in a kidney epithelial cell line, LLC-PK1: interaction with organic cation transporters in apical and basolateral membranes', *Journal of Pharmacology and Experimental Therapeutics*, 276(3), pp. 1143-1148.

Okuda, M., Saito, H., Urakami, Y., Takano, M. and Inui, K.-i. (1996) 'cDNA Cloning and Functional Expression of a Novel Rat Kidney Organic Cation Transporter, OCT2', *Biochemical and Biophysical Research Communications*, 224(2), pp. 500-507.

Omote, H., Hiasa, M., Matsumoto, T., Otsuka, M. and Moriyama, Y. (2006) 'The MATE proteins as fundamental transporters of metabolic and xenobiotic organic cations', *Trends in Pharmacological Sciences*, 27(11), pp. 587-593.

Otsuka, M., Matsumoto, T., Morimoto, R., Arioka, S., Omote, H. and Moriyama, Y. (2005) 'A human transporter protein that mediates the final excretion step for toxic organic cations', *Proceedings of the National Academy of Sciences of the United States of America*, 102(50), pp. 17923-17928.

Palmgren, A.-P., Fihn, B.-M., Bird, J., Courtney, P. and Grime, K. (2013) 'A novel matrix for the short-term storage of cells: utility in drug metabolism and drug transporter studies with rat, dog and human hepatocytes', *Xenobiotica*, 43(6), pp. 487-497.

Palumbo, P., Picchini, U., Beck, B., van Gelder, J., Delbar, N. and DeGaetano, A. (2008) 'A general approach to the apparent permeability index', *Journal of Pharmacokinetics and Pharmacodynamics*, 35(2), pp. 235-248.

Pan, G., Giri, N. and Elmquist, W.F. (2007) 'Abcg2/Bcrp1 Mediates the Polarized Transport of Antiretroviral Nucleosides Abacavir and Zidovudine', *Drug Metabolism and Disposition*, 35(7), pp. 1165-1173.

Peitruck, F. and Ullrich, K.J. (1995) 'Transport interactions of different organic cations during their excretion by the intact rat kidney', *Kidney Int*, 47(6), pp. 1647-1657.

Peng, K.C., Cluzeaud, F., Bens, M., Duong Van Huyen, J.P., Wioland, M.A., Lacave, R. and Vandewalle, A. (1999) 'Tissue and cell distribution of the multidrug resistance-associated protein (MRP) in mouse intestine and kidney', *J Histochem Cytochem*, 47(6), pp. 757-68.

Pertoft, H., Rubin, K., Kjellén, L., Laurent, T.C. and Klingeborn, B. (1977) 'The viability of cells grown or centrifuged in a new density gradient medium, Percoll(TM)', *Experimental Cell Research*, 110(2), pp. 449-457.

Pochini, L., Scalise, M., Galluccio, M. and Indiveri, C. (2013) 'OCTN Cation Transporters in Health and Disease: Role as Drug Targets and Assay Development', *Journal of Biomolecular Screening*.

Preitner, F., Bonny, O., Laverrière, A., Rotman, S., Firsov, D., Costa, A.D., Metref, S., Thorens, B. and (2009) 'Glut9 is a major regulator of urate homeostasis and its genetic inactivation induces hyperuricosuria and urate nephropathy', *Proc Natl Acad Sci U S A*, 106(36), pp. 15501-15506.

Randell, S.H., Fulcher, M.L., O'Neal, W. and Olsen, J.C. (2011) 'Primary epithelial cell models for cystic fibrosis research', *Methods in Molecular Biology*, 742(3), pp. 285-310.

Rasmussen, F. (1983) 'Renal clearance: Species differences and similarities', *Veterinary Research Communications*, 7(1), pp. 301-306.

Rasmussen, F., Nawaz, M. and Steiness, E. (1975) 'Renal excretion of digoxin in swine and goats', *Acta Vet Scand*, 16(4), pp. 525-536.

Rautio, J., Humphreys, J.E., Webster, L.O., Balakrishnan, A., Keogh, J.P., Kunta, J.R., Serabjit-Singh, C.J. and Polli, J.W. (2006) '*In vitro* P-glycoprotein inhibition assays for assessment of clinical drug interaction protential of new drug candidates: A recommendation for probe substrates', *Drug Metabolism and Disposition*, 34(5), pp. 786-792.

Rider, T.G. and Jordan, K.M. (2010) 'The modern management of gout', *Rheumatology*, 49(1), pp. 5-14.

Roch-Ramel, F. and Guisan, B. (1999) 'Renal Transport of Urate in Humans', Physiology, 14(2), pp. 80-84.

Roman, R.J. and Kauker, M.L. (1976) 'Renal tubular transport of ^{3}H-digoxin in saline diuresis in rats', *Circulation Research*, 38(3), pp. 185-91.

Romiti, N., Tramonti, G. and Chieli, E. (2002) 'Influence of Different Chemicals on MDR-1 P-Glycoprotein Expression and Activity in the HK-2 Proximal Tubular Cell Line', *Toxicology and Applied Pharmacology*, 183(2), pp. 83-91.

Russ, H.A., Ravassard, P., Kerr-Conte, J., Pattou, F. and Efrat, S. (2009) 'Epithelial-Mesenchymal Transition in Cells Expanded *In Vitro* from Lineage-Traced Adult Human Pancreatic Beta Cells', *PLoS ONE*, 4(7), p. e6417.

Russell, W. and Burch, R. (1959) *The Principles of Humane Experimental Technique*. 1st edn. Methuen.

Ryan, M.J., Johnson, G., Kirk, J., Fuerstenberg, S.M., Zager, R.A. and Torok-Storb, B. (1994) 'HK-2: An immortalized proximal tubule epithelial cell line from normal adult human kidney', *Kidney International*, 45(1), pp. 48-57.

Saito, H., Masuda, S. and Inui, K.-i. (1996) 'Cloning and Functional Characterization of a Novel Rat Organic Anion Transporter Mediating Basolateral Uptake of Methotrexate in the Kidney', *Journal of Biological Chemistry*, 271(34), pp. 20719-20725.

Salomon, J.J., Endter, S., Tachon, G., Falson, F., Buckley, S.T. and Ehrhardt, C. (2012) 'Transport of the fluorescent organic cation 4-(4-(dimethylamino)styryl)-N-methylpyridinium iodide (ASP$^+$) in human respiratory epithelial cells', *European Journal of Pharmaceutics and Biopharmaceutics*, 81(2), pp. 351-359.

Sato, M., Wakayama, T., Mamada, H., Shirasaka, Y., Nakanishi, T. and Tamai, I. (2011) 'Identification and functional characterization of uric acid transporter Urat1 (Slc22a12) in rats', *Biochim Biophys Acta*, 1808(6), pp. 1441-7.

Schaub, T.P., Kartenbeck, J., Konig, J., Spring, H., Dorsam, J., Staehler, G., Storkel, S., Thon, W.F. and Keppler, D. (1999) 'Expression of the MRP2 gene-encoded conjugate export pump in human kidney proximal tubules and in renal cell carcinoma', *J Am Soc Nephrol*, 10(6), pp. 1159-69.

Schaub, T.P., Kartenbeck, J., König, J., Vogel, O., Witzgall, R., Kriz, W. and Keppler, D. (1997) 'Expression of the conjugate export pump encoded by the

Mrp2 gene in the apical membrane of kidney proximal tubules', *Journal of the American Society of Nephrology*, 8(8), pp. 1213-21.

Scheffer, G.L., Hu, X., Pijnenborg, A.C., Wijnholds, J., Bergen, A.A. and Scheper, R.J. (2002) 'MRP6 (ABCC6) detection in normal human tissues and tumors', *Lab Investigation*, 82(4), pp. 515-8.

Schinkel, A.H. and Jonker, J.W. (2003) 'Mammalian drug efflux transporters of the ATP binding cassette (ABC) family: an overview', *Advanced Drug Delivery Reviews*, 55(1), pp. 3-29.

Schroeder, A., Mueller, O., Stocker, S., Salowsky, R., Leiber, M., Gassmann, M., Lightfoot, S., Menzel, W., Granzow, M. and Ragg, T. (2006) 'The RIN: an RNA integrity number for assigning integrity values to RNA measurements', *BMC Molecular Biology*, 7(1), p. 3.

Seely, J.F. (1973) Variation in electrical resistance along length of rat proximal convoluted tubule.

Sekine, T., Cha, S.H., Tsuda, M., Apiwattanakul, N., Nakajima, N., Kanai, Y. and Endou, H. (1998) 'Identification of multispecific organic anion transporter 2 expressed predominantly in the liver', *FEBS Letters*, 429(2), pp. 179-182.

Sekine, T., Watanabe, N., Hosoyamada, M., Kanai, Y. and Endou, H. (1997) 'Expression Cloning and Characterization of a Novel Multispecific Organic Anion Transporter', *Journal of Biological Chemistry*, 272(30), pp. 18526-18529.

Sharpe, P.T. (1988) *Methods of cell separation*. Elsevier.

Shin, H.J., Takeda, M., Enomoto, A., Fujimura, M., Miyazaki, H., Anzai, N. and Endou, H. (2011) 'Interactions of urate transporter URAT1 in human kidney with uricosuric drugs', *Nephrology*, 16(2), pp. 156-162.

Slitt, A.L., Cherrington, N.J., Hartley, D.P., Leazer, T.M. and Klaassen, C.D. (2002) 'Tissue Distribution and Renal Developmental Changes in Rat Organic Cation Transporter mRNA levels', *Drug Metabolism and Disposition*, 30(2), pp. 212-219.

Smeets, P.H.E., Van Aubel, R.A.M.H., Wouterse, A.C., Van Den Heuvel, J.J.M.W. and Russel, F.G.M. (2004) 'Contribution of multidrug resistance protein 2 (MRP2/ABCC2) to the renal excretion of p-aminohippurate (PAH) and identification of MRP4 (ABCC4) as a novel PAH transporter', *Journal of the American Society of Nephrology*, 15(11), pp. 2828-2835.

So, A. and Thorens, B. (2010) 'Uric acid transport and disease', *The Journal of Clinical Investigation*, 120(6), pp. 1791-1799.

Stavric, B. and Nera, E.A. (1978) 'Use of the Uricase-Inhibited Rat as an Animal Model in Toxicology', *Clinical Toxicology*, 13(1), pp. 47-74.

Steiness, E. (1974) 'Renal tubular secretion of digoxin', *Circulation*, 50, pp. 103-107.

Steiness, E., Waldorff, S. and Hansen, P.B. (1982) 'Renal digoxin clearance: Dependence on plasma digoxin and diuresis', *European Journal of Clinical Pharmacology*, 23(2), pp. 151-154.

Sun, W., Wu, R.R., van Poelje, P.D. and Erion, M.D. (2001) 'Isolation of a Family of Organic Anion Transporters from Human Liver and Kidney', *Biochemical and Biophysical Research Communications*, 283(2), pp. 417-422.

Suzuyama, N., Katoh, M., Takeuchi, T., Yoshitomi, S., Higuchi, T., Asashi, S. and Yokoi, T. (2007) 'Species differences of inhibitory effects on P-glycoprotein-mediated drug transport', *Journal of Pharmaceutical Sciences*, 96(6), pp. 1609-1618.

Sweet, D.H., Chan, L.M.S., Walden, R., Yang, X.-P., Miller, D.S. and Pritchard, J.B. (2003) 'Organic anion transporter 3 (Slc22a8) is a dicarboxylate exchanger indirectly coupled to the Na+gradient', *American Journal of Physiology - Renal Physiology*, 284, pp. F763–F769.

Sweet, D.H., Wolff, N.A. and Pritchard, J.B. (1997) 'Expression cloning and characterization of ROAT1. The basolateral organic anion transporter in rat kidney', *Journal of Biological Chemistry*, 272(48), pp. 30088-95.

Takeuchi, A., Masuda, S., Saito, H., Abe, T. and Inui, K. (2001) 'Multispecific substrate recognition of kidney-specific organic anion transporters OAT-K1 and OAT-K2', *Journal of Pharmacology and Experimental Therapeutics*, 299(1), pp. 261-7.

Takeuchi, A., Masuda, S., Saito, H., Hashimoto, Y. and Inui, K. (2000) 'Trans-stimulation effects of folic acid derivatives on methotrexate transport by rat renal organic anion transporter, OAT-K1', *Journal of Pharmacology and Experimental Therapeutics*, 293(3), pp. 1034-9.

Tamai, I., China, K., Sai, Y., Kobayashi, D., Nezu, J.-i., Kawahara, E. and Tsuji, A. (2001) 'Na$^+$-coupled transport of l-carnitine via high-affinity carnitine transporter OCTN2 and its subcellular localization in kidney', *Biochimica et Biophysica Acta (BBA) - Biomembranes*, 1512(2), pp. 273-284.

Tamai, I., Nakanishi, T., Kobayashi, D., China, K., Kosugi, Y., Nezu, J.-i., Sai, Y. and Tsuji, A. (2003) 'Involvement of OCTN1 (SLC22A4) in pH-Dependent Transport of Organic Cations', *Molecular Pharmaceutics*, 1(1), pp. 57-66.

Tamai, I., Ohashi, R., Nezu, J., Yabuuchi, H., Oku, A., Shimane, M., Sai, Y. and Tsuji, A. (1998) 'Molecular and functional identification of sodium ion-dependent, high affinity human carnitine transporter OCTN2', *Journal of Biological Chemistry*, 273(32), pp. 20378-82.

Tamai, I., Ohashi, R., Nezu, J.I., Sai, Y., Kobayashi, D., Oku, A., Shimane, M. and Tsuji, A. (2000) 'Molecular and functional characterization of organic cation/carnitine transporter family in mice', *Journal of Biological Chemistry*, 275(51), pp. 40064-72.

Tamai, I., Yabuuchi, H., Nezu, J., Sai, Y., Oku, A., Shimane, M. and Tsuji, A. (1997) 'Cloning and characterization of a novel human pH-dependent organic cation transporter, OCTN1', *Febs Letters*, 419(1), pp. 107-111.

Tan, B., Piwnica-Worms, D. and Ratner, L. (2000) 'Multidrug resistance transporters and modulation', *Current Opinion in Oncology*, 12(5), pp. 450-458.

Tanaka, M., Itoh, K., Matsushita, K., Matsushita, K., Wakita, N., Adachi, M., Nonoguchi, H., Kitamura, K., Hosoyamada, M., Endou, H. and Tomita, K. (2003) 'Two male siblings with hereditary renal hypouricemia and exercise-induced ARF', *American Journal of Kidney Diseases*, 42(6), pp. 1287-1292.

Tanaka, Y., Slitt, A.L., Leazer, T.M., Maher, J.M. and Klaassen, C.D. (2005) 'Tissue distribution and hormonal regulation of the breast cancer resistance protein (Bcrp/Abcg2) in rats and mice', *Biochemical Biophysical Research Communications*, 326(1), pp. 181-7.

Tanihara, Y., Masuda, S., Sato, T., Katsura, T., Ogawa, O. and Inui, K. (2007) 'Substrate specificity of MATE1 and MATE2-K, human multidrug and toxin extrusions/H^+-organic cation antiporters', *Biochemical Pharmacology*, 74(2), pp. 359-71.

Taub, M., Suk Yang, I.L. and Wang, Y. (1989) 'Primary rabbit kidney proximal tubule cell cultures maintain differentiated functions when cultured in a hormonally defined serum-free medium', *In Vitro Cellular & Developmental Biology*, 25(9), pp. 770-775.

Terada, T., Masuda, S., Asaka, J., Tsuda, M., Katsura, T. and Inui, K. (2006) 'Molecular cloning, functional characterization and tissue distribution of rat H^+/organic cation antiporter MATE1', *Pharmaceutical Research*, 23(8), pp. 1696-701.

Terryn, S., Jouret, F., Vandenabeele, F., Smolders, I., Moreels, M., Devuyst, O., Steels, P. and Kerkhove, E.V. (2007) *A primary culture of mouse proximal tubular cells, established on collagen-coated membranes.*

Thiebaut, F., T. Tsuruo, H. Hamada, M. M. Gottesman, I. Pastan, and M. C. Willingham (1987) 'Cellular localization of the multidrug-resistance gene product P-glycoprotein in normal human tissues', *Proc. Nati. Acad. Sci. USA*, 84, pp. 7735-7738.

Tramonti, G., Romiti, N., Norpoth, M. and Chieli, E. (2001) 'P-glycoprotein in HK-2 proximal tubule cell line', *Renal Failure*, 23(3-4), pp. 331-337.

Tsuda, M., Terada, T., Ueba, M., Sato, T., Masuda, S., Katsura, T. and Inui, K. (2009) 'Involvement of Human Multidrug and Toxin Extrusion 1 in the Drug Interaction between Cimetidine and Metformin in Renal Epithelial Cells', *Journal of Pharmacology and Experimental Therapeutics*, 329(1), pp. 185-191.

Ueda, K., Cornwell, M.M., Gottesman, M.M., Pastan, I., Roninson, I.B., Ling, V. and Riordan, J.R. (1986) 'The mdr1 gene, responsible for multidrug-resistance, codes for P-glycoprotein', *Biochemical and Biophysical Research Communications*, 141(3), pp. 956-962.

Urakami, Y., Okuda, M., Masuda, S., Akazawa, M., Saito, H. and Inui, K. (2001) 'Distinct characteristics of organic cation transporters, OCT1 and OCT2, in the basolateral membrane of renal tubules', *Pharmaceutical Research*, 18(11), pp. 1528-34.

Urakami, Y., Okuda, M., Masuda, S., Saito, H. and Inui, K.I. (1998) 'Functional characteristics and membrane localization of rat multispecific organic cation transporters, OCT1 and OCT2, mediating tubular secretion of cationic drugs', *Journal of Pharmacology and Experimental Therapeutics*, 287(2), pp. 800-5.

Van Aubel, R.A., Peters, J.G., Masereeuw, R., Van Os, C.H. and Russel, F.G. (2000) 'Multidrug resistance protein mrp2 mediates ATP-dependent transport of classic renal organic anion p-aminohippurate', *American Journal of Physiology. Renal Physiology*, 279(4), pp. F713-7.

van Aubel, R.A.M.H., Smeets, P.H.E., Peters, J.G.P., Bindels, R.J.M. and Russel, F.G.M. (2002) 'The MRP4/ABCC4 Gene Encodes a Novel Apical Organic Anion Transporter in Human Kidney Proximal Tubules: Putative Efflux Pump for Urinary cAMP and cGMP', *Journal of the American Society of Nephrology*, 13(3), pp. 595-603.

Van Aubel, R.A.M.H., Smeets, P.H.E., van den Heuvel, J.J.M.W. and Russel, F.G.M. (2005) Human organic anion transporter MRP4 (ABCC4) is an efflux pump for the purine end metabolite urate with multiple allosteric substrate binding sites.

van de Water, F.M., Boleij, J.M., Peters, J.G., Russel, F.G. and Masereeuw, R. (2007) 'Characterization of P-glycoprotein and multidrug resistance proteins in rat kidney and intestinal cell lines', *European Journal of Pharmaceutical Sciences*, 30(1), pp. 36-44.

van den Berg van Saparoea, H.B., Lubelski, J., van Merkerk, R., Mazurkiewicz, P.S. and Driessen, A.J.M. (2005) 'Proton Motive Force-Dependent Hoechst 33342 Transport by the ABC Transporter LmrA of *Lactococcus lactis*', *Biochemistry*, 44(51), pp. 16931-16938.

Verhulst, A., Sayer, R., De Broe, M.E., D'Haese, P.C. and Brown, C.D.A. (2008) 'Human Proximal Tubular Epithelium Actively Secretes but Does Not Retain Rosuvastatin', *Molecular Pharmacology*, 74(4), pp. 1084-1091.

Vickers, A.E.M., Rose, K., Fisher, R., Saulnier, M., Sahota, P. and Bentley, P. (2004) 'Kidney Slices of Human and Rat to Characterize Cisplatin-Induced Injury on Cellular Pathways and Morphology', *Toxicologic Pathology*, 32(5), pp. 577-590.

Vitart, V., Rudan, I., Hayward, C., Gray, N.K., Floyd, J., Palmer, C.N.A., Knott, S.A., Kolcic, I., Polasek, O., Graessler, J., Wilson, J.F., Marinaki, A., Riches, P.L., Shu, X., Janicijevic, B., Smolej-Narancic, N., Gorgoni, B., Morgan, J., Campbell, S., Biloglav, Z., Barac-Lauc, L., Pericic, M., Klaric, I.M., Zgaga, L., Skaric-Juric, T., Wild, S.H., Richardson, W.A., Hohenstein, P., Kimber, C.H., Tenesa, A., Donnelly, L.A., Fairbanks, L.D., Aringer, M., McKeigue, P.M., Ralston, S.H., Morris, A.D., Rudan, P., Hastie, N.D., Campbell, H. and Wright, A.F. (2008) 'SLC2A9 is a newly identified urate transporter influencing serum urate concentration, urate excretion and gout', *Nature Genetics*, 40(4), pp. 437-442.

Wang, L., Leggas, M., Goswami, M., Empey, P.E. and McNamara, P.J. (2008a) 'N-(4-[2-(1,2,3,4-Tetrahydro-6,7-dimethoxy-2-isoquinolinyl)ethyl]-phenyl)-9,10-dihydro-5-methoxy-9-oxo-4-acridine Carboxamide (GF120918) As a Chemical ATP-Binding Cassette Transporter Family G Member 2 (Abcg2) Knockout Model to Study Nitrofurantoin Transfer into Milk', *Drug Metabolism and Disposition*, 36(12), pp. 2591-2596.

Wang, Q., Darling, I.M. and Morris, M.E. (2006) 'Transport of γ-Hydroxybutyrate in Rat Kidney Membrane Vesicles: Role of Monocarboxylate Transporters', *Journal of Pharmacology and Experimental Therapeutics*, 318(2), pp. 751-761.

Wang, Q., Strab, R., Kardos, P., Ferguson, C., Li, J., Owen, A. and Hidalgo, I.J. (2008b) 'Application and limitation of inhibitors in drug–transporter interactions studies', *International Journal of Pharmaceutics*, 356(1–2), pp. 12-18.

Wielinga, P.R., Reid, G., Challa, E.E., van der Heijden, I., van Deemter, L., de Haas, M., Mol, C., Kuil, A.J., Groeneveld, E., Schuetz, J.D., Brouwer, C., De Abreu, R.A., Wijnholds, J., Beijnen, J.H. and Borst, P. (2002) 'Thiopurine metabolism and identification of the thiopurine metabolites transported by MRP4 and MRP5 overexpressed in human embryonic kidney cells', *Molecular Pharmacology*, 62(6), pp. 1321-31.

Wielinga, P.R., van der Heijden, I., Reid, G., Beijnen, J.H., Wijnholds, J. and Borst, P. (2003) 'Characterization of the MRP4- and MRP5-mediated transport of cyclic nucleotides from intact cells', *Journal of Biological Chemistry*, 278(20), pp. 17664-71.

Wieser, M., Stadler, G., Jennings, P., Streubel, B., Pfaller, W., Ambros, P., Riedl, C., Katinger, H., Grillari, J., Grillari-Voglauer, R. (2008) 'hTERT alone immortalizes epithelial cells of renal proximal tubules without changing their functional characteristics', *American Journal of Physiology Renal Physiology*, 295, pp. F1365-F1375.

Wijnholds, J., Mol, C.A.A.M., van Deemter, L., de Haas, M., Scheffer, G.L., Baas, F., Beijnen, J.H., Scheper, R.J., Hatse, S., De Clercq, E., Balzarini, J. and Borst, P. (2000) 'Multidrug-resistance protein 5 is a multispecific organic anion transporter able to transport nucleotide analogs', *Proceedings of the National Academy of Sciences of the United States of America*, 97(13), pp. 7476-7481.

Witkowska, K., Smith, K.M., Yao, S.Y.M., Ng, A.M.L., O'Neill, D., Karpinski, E., Young, J.D. and Cheeseman, C.I. (2012) 'Human SLC2A9a and SLC2A9b isoforms mediate electrogenic transport of urate with different characteristics in the presence of hexoses', *American Journal of Physiology - Renal Physiology*, 303(4), pp. F527-F539.

Witzgall, R., Brown, D., Schwarz, C. and Bonventre, J.V. (1994) 'Localization of proliferating cell nuclear antigen, vimentin, c-Fos, and clusterin in the postischemic kidney. Evidence for a heterogenous genetic response among nephron segments, and a large pool of mitotically active and dedifferentiated cells', *The Journal of Clinical Investigation*, 93(5), pp. 2175-2188.

Woodland, C., Ito, S. and Koren, G. (1998) 'A Model for the Prediction of Digoxin-Drug Interactions at the Renal Tubular Cell Level', *Therapeutic Drug Monitoring*, 20(2), pp. 134-138.

Woodward, O.M., Köttgen, A., Coresh, J., Boerwinkle, E., Guggino, W.B. and Köttgen, M. (2009) 'Identification of a urate transporter, ABCG2, with a common functional polymorphism causing gout', *Proceedings of the National Academy of Sciences*, 106(25), pp. 10338-10342.

Wright, S.H. and Dantzler, W.H. (2004) 'Molecular and Cellular Physiology of Renal Organic Cation and Anion Transport', *Physiological Reviews*, 84(3), pp. 987-1049.

Wu, X., George, R.L., Huang, W., Wang, H., Conway, S.J., Leibach, F.H. and Ganapathy, V. (2000a) 'Structural and functional characteristics and tissue distribution pattern of rat OCTN1, an organic cation transporter, cloned from placenta', *Biochimica et Biophysica Acta (BBA) - Biomembranes*, 1466(1–2), pp. 315-327.

Wu, X., Huang, W., Ganapathy, M.E., Wang, H., Kekuda, R., Conway, S.J., Leibach, F.H. and Ganapathy, V. (2000b) 'Structure, function, and regional distribution of the organic cation transporter OCT3 in the kidney', *American Journal of Physiology*, 279(3), pp. F449-58.

Wu, X., Huang, W., Prasad, P.D., Seth, P., Rajan, D.P., Leibach, F.H., Chen, J., Conway, S.J. and Ganapathy, V. (1999) 'Functional characteristics and tissue distribution pattern of organic cation transporter 2 (OCTN2), an organic cation/carnitine transporter', *Journal of Pharmacology and Experimental Therapeutics*, 290(3), pp. 1482-92.

Wu, X., Prasad, P.D., Leibach, F.H. and Ganapathy, V. (1998) 'cDNA sequence, transport function, and genomic organization of human OCTN2, a new member of the organic cation transporter family', *Biochemical and Biophysical Research Communications*, 246(3), pp. 589-95.

Wu, X., Wakamiya, M., Vaishnav, S., Geske, R., Montgomery, C., Jones, P., Bradley, A. and Caskey, C.T. (1994) 'Hyperuricemia and urate nephropathy in urate oxidase-deficient mice', *Proceedings of the National Academy of Sciences*, 91(2), pp. 742-746.

Yabuuchi, H., Shimizu, H., Takayanagi, S. and Ishikawa, T. (2001) 'Multiple splicing variants of two new human ATP-binding cassette transporters, ABCC11 and ABCC12', *Biochemical and Biophysical Research Communications*, 288(4), pp. 933-9.

Yabuuchi, H., Tamai, I., Nezu, J., Sakamoto, K., Oku, A., Shimane, M., Sai, Y. and Tsuji, A. (1999) 'Novel membrane transporter OCTN1 mediates multispecific, bidirectional, and pH-dependent transport of organic cations', *Journal of Pharmacology and Experimental Therapeutics*, 289(2), pp. 768-73.

Yamaguchi, H., Sugie, M., Okada, M., Mikkaichi, T., Toyohara, T., Abe, T., Goto, J., Hishinuma, T., Shimada, M. and Mano, N. (2010) 'Transport of estrone 3-sulfate mediated by organic anion transporter OATP4C1: estrone 3-sulfate binds to the different recognition site for digoxin in OATP4C1', *Drug Metabolism and Disposition*, 25(3), pp. 314-7.

Youngblood, G.L. and Sweet, D.H. (2004) 'Identification and functional assessment of the novel murine organic anion transporter Oat5 (Slc22a19) expressed in kidney', *American Journal of Physiology*, 287(2), pp. F236-44.

Zavyalova, M.V., Denisov, E.V., Tashireva, L.A., Gerashchenko, T.S., Litviakov, N.V., Skryabin, N.A., Vtorushin, S.V., Telegina, N.S., Slonimskaya, E.M., Cherdyntseva, N.V. and Perelmuter, V.M. (2013) 'Phenotypic Drift as a Cause for Intratumoral Morphological Heterogeneity of Invasive Ductal Breast Carcinoma Not Otherwise Specified', *Bioresearch Open Access*, 2(2), pp. 148-154.

Zhuang, S., Duan, M. and Yan, Y. (2012) 'Src family kinases regulate renal epithelial dedifferentiation through activation of EGFR/PI3K signaling', *Journal of Cellular Physiology*, 227(5), pp. 2138-2144.